

AD-A268 012

DOCUMENTATION PAGE

Form Approved
OMB No. 0704-0188

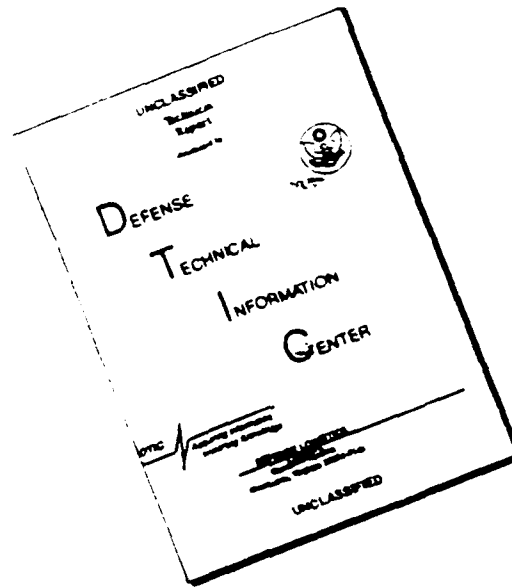
This document is a report of work performed for the Department of the Air Force. It contains information that may be classified as "Secret" or "Confidential" under the provisions of the Espionage Laws of the United States. It is to be controlled, stored, handled, transmitted, and disposed of in accordance with the provisions of the Espionage Laws of the United States. It is to be controlled, stored, handled, transmitted, and disposed of in accordance with the provisions of the Espionage Laws of the United States. It is to be controlled, stored, handled, transmitted, and disposed of in accordance with the provisions of the Espionage Laws of the United States.

1. AGENCY USE ONLY (Leave blank)		2. REPORT DATE May 1993		3. REPORT TYPE AND DATES COVERED THESIS/DISSERTATION	
4. TITLE AND SUBTITLE Flow Instability Tests for a Particle Bed Reactor Nuclear Thermal Rocket Fuel Element				5. FUNDING NUMBERS	
6. AUTHOR(S) Timothy James Lawrence					
7. PERFORMING ORGANIZATION NAME(S) AND ADDRESS(ES) AFIT Student Attending: U.S. Air Force Academy				8. PERFORMING ORGANIZATION REPORT NUMBER AFIT/CI/CIA-93-079	
9. SPONSORING/MONITORING AGENCY NAME(S) AND ADDRESS(ES) DEPARTMENT OF THE AIR FORCE AFIT/CI 2950 P STREET WRIGHT-PATTERSON AFB OH 45433-7765				10. SPONSORING/MONITORING AGENCY REPORT NUMBER	
11. SUPPLEMENTARY NOTES					
12a. DISTRIBUTION/AVAILABILITY STATEMENT Approved for Public Release IAW 190-1 Distribution Unlimited MICHAEL M. BRICKER, SMSgt, USAF Chief Administration				12b. DISTRIBUTION CODE	
13. ABSTRACT (Maximum 200 words)					
14. SUBJECT TERMS					
				15. NUMBER OF PAGES 339	
				16. PRICE CODE	
17. SECURITY CLASSIFICATION OF REPORT		18. SECURITY CLASSIFICATION OF THIS PAGE		19. SECURITY CLASSIFICATION OF ABSTRACT	
				20. LIMITATION OF ABSTRACT	

DTIC
ELECTE
AUG 17 1993
S E D

93-18982

DISCLAIMER NOTICE



THIS DOCUMENT IS BEST
QUALITY AVAILABLE. THE COPY
FURNISHED TO DTIC CONTAINED
A SIGNIFICANT NUMBER OF
PAGES WHICH DO NOT
REPRODUCE LEGIBLY.

FLOW INSTABILITY TESTS FOR A PARTICLE BED REACTOR NUCLEAR THERMAL ROCKET FUEL ELEMENT

by

TIMOTHY JAMES LAWRENCE , CAPT, USAF

Submitted to the Department of Nuclear Engineering on May 7, 1993, in partial fulfillment of the requirements for the degree of Master of Science in Nuclear Engineering.

ABSTRACT

Recent analyses have focused on the flow stability characteristics of a particle bed reactor (PBR). These laminar flow instabilities may exist in reactors with parallel paths and are caused by the heating of the gas at low Reynolds numbers. This phenomena can be described as follows: several parallel channels are connected at the plenum regions and are stabilized by some inlet temperature and pressure; a perturbation in one channel causes the temperature to rise and increases the gas viscosity and reduces the gas density; the pressure drop is fixed by the plenum regions, therefore the mass flow rate in the channel would decrease; the decrease in flow reduces the ability to remove the energy added and therefore the temperature increases; and finally, this process could continue until the fuel element fails. Several analyses based on different methods have derived similar curves to show that these instabilities may exist at low Reynolds numbers and high ϕ 's ($(T_{final} - T_{initial})/T_{initial}$). These analyses need to be experimentally verified.

An insulated, stainless steel screen bed was designed to simulate the internal heat generation similar to the nuclear heating of the fuel in the PBR. A screen mesh was found with the wire diameter and spacing to give the element a porosity of 0.37 once the insulated coating was placed on the mesh. The hot and cold frit were made of stainless steel and were sintered to a porosity of 0.3. Other equipment items needed in addition to the screen and frits are as follows: containment vessel, power supply, gas flow system, chill down tank, instrumentation, and a data acquisition system.

The final design used a copper electroplated coating on the edges and tabs of the screen in order to carry the current into the bed and prevent hot spots on the edges. A painted alumina adhesive was painted onto the screen and cured in order to provide an insulated coating that could handle the rigors of assembly.

Six tests were performed that generated results useful to the flow stability phenomena. Three of the tests were at low ϕ 's and showed constant

temperatures with constant power. Three of the tests were at higher phi's (~3) and showed that several temperatures in the bed decreased, while several temperatures in the bed increased while the mixed mean outlet remained constant. The time steps for these divergences were slow enough that they could be controlled.

The bed thermocouples showed asymmetries in temperature existed in the bed. Analysis of the bed using a 2D SIMBED steady state code revealed that the welding seams (non porous) on the frits and random porosities in the bed caused by overlap and alignment of the wrapped wires may have been the cause to these asymmetries. A more detailed transient analysis may further explain these results. However, even though there were asymmetries in the bed, the temperatures remained constant at constant power for low phi's and diverged at higher phi's.

The results of these experiments showed that flow instabilities may exist in the PBR. Even though the screen bed was not completely prototypic, analysis of the temperatures showed that the points where the divergences occurred were very close to the predicted analyses. These temperature divergences were observed in a bed with a higher lateral thermal conductivity which should mitigate the development of these instabilities. This phenomena was evidenced in the repeated number of tests performed.

Flow instability is not a "show stopper" for the PBR. More tests should be conducted using other "out of pile" and later "in pile" tests to better characterize and define the flow instability region so control strategies can be developed to mitigate operation in these regions.

This research was conducted at Brookhaven National Laboratory and was sponsored by Brookhaven National Laboratory, MIT, and the U.S. Air Force.

Thesis Supervisor: Dr. David D. Lanning
 Title: Professor, Nuclear Engineering
 Thesis Reader: Dr. John E. Meyer
 Title: Professor, Nuclear Engineering

Accession For	
NTIS CRA&I	<input checked="checked" type="checkbox"/>
DTIC TAB	<input type="checkbox"/>
Unannounced	<input type="checkbox"/>
Justification	
By	
Distribution /	
Availability Codes	
Dist	Avail and/or Special
A-1	

DTIC QUALITY INSPECTED 3

REFERENCES

- B-1 R.W. Bussard and R.D. DeLauer, Fundamental of Nuclear Flight, McGraw - Hill, New York, 1965.
- B-2 J. R. Powell et al, "Particle Bed Reactor Orbit Transfer Vehicle Concept," AFAL-TR-88-014, Air Force Astronautics Laboratory, July 1988.
- B-3 S. K. Borowski, "The Rational Benefits of Nuclear Thermal Propulsion for NASA's Lunar Space Transportation System," AIAA/SAE/ASME/ASEE 27th Joint Propulsion Conference, June 24 - 26, 1991, Sacramento, CA.
- C-1 R. J. Cerbone and T. J. Lawrence, "Nuclear Heating in the Upperstage of a Particle Bed Driven Nuclear Propulsion System," AIAA/SAE/ASME/ASEE 27th Joint Propulsion Conference, June 24-26, 1991, Sacramento, CA.
- C-2 Cotronics Corporation, Adhesives Ceramics and High Temperature Materials Handbook, Cotronics Corporation, 1992.
- C-3 CRC Handbook of Chemistry an Physics, The Chemical Rubber Company, 1969.
- C-4 W.E. Casey, "Thermal-Hydraulic Transient Analysis of a Packed Particle Bed Reactor Fuel Element," SM and Naval Engineer Thesis, Department of Nuclear Engineering, Massachusetts Institute of Technology, May 1990.
- C-5 M. Charmchi, "Heat Transfer and Fluid Flow Characteristics of the Hydrogen-Cooled Small Particle Bed Reactor (PBR)," UL-MEE-89[05-5012]-F, Brookhaven National Laboratory, October 1989.
- E-1 Enerpac Basic Pressure Gauge, Model DGB Technical Manual, Enerpac, 1988.
- H-1 P.G. Hill and C. R. Peterson, Mechanics and Thermodynamics of Propulsion, Addison-Wesley, New York 1992.
- H-2 D.E. Hastings, Course 16.53 Rocket Propulsion Class Notes, Massachusetts Institute of Technology, September 1992.
- H-3 H. Herman, "Plasma-Sprayed Coatings," Scientific American, September 1988.

- K-1 J. L. Kerrebrock, "Flow Instability in Particle-Bed Nuclear Reactors," Massachusetts Institute of Technology Informal Report, November 1992.
- K-2 J. Kalamas, "Particle Bed Reactor Stability Analysis," SM Thesis, Department of Aeronautics and Astronautics, Massachusetts Institute of Technology, May 1993.
- M-1 G. Maise, "Flow Stability in the Particle Bed Reactor," Informal Report BNL/RSD-91-002, Brookhaven National Laboratory, January 1991.
- M-2 Matheson, "Mass Flowmeters - Linear Mass Flowmeter - Series 8100 Technical Data Sheet," Matheson, 1988.
- M-3 Metals Handbook, 9th Edition, Volume 5, Surface Cleaning, Finishing, and Coating, American Society for Metals, Metals Park, OH, 1982.
- O-1 Omega Engineering Inc., "The Temperature Handbook," Omega Engineering Inc., Stamford, Ct, 1992.
- O-2 Omega Engineering Inc., "PX100 Low - Level Pressure Transducer Data Sheet," Omega Engineering Inc., Stamford, Ct, 1988.
- O-3 Omega Engineering Inc., "Omega WB-ASC Card Technical Manual," Omega Engineering Inc., Stamford, Ct, 1988.
- P-1 Private Communication, D. R. Perkins, Astronautics Laboratory, Edwards AFB, CA, 1990.
- P-2 W H. Press, et al, Numerical Recipes in FORTRAN, The Art of Scientific Computing, 2nd Edition, Cambridge University Press, Port Chester, NY, 1992.
- R-1 Rapid Power Technologies Inc., "Thyristor (SCR) Power Supplies - for High Quality dc Power Supply Applications", Rapid Power Technologies Inc., 1990.
- S-1 V. V. Sychev, et al, Thermodynamic Properties of Helium, Hemisphere Publishing, New York, 1987.
- S-2 A. E. Sheidegger, Physics of Flow Through Porous Media, Toronto University, Toronto, 1963.
- S-3 Stafford (Chairman), "America's Space Exploration Initiative: America at the Threshold," The Report of the Stafford Committee to the President of the United States, May 1991.

- S-4 D.E. Suzuki, "Development and Analysis of Startup Strategies for a Particle Bed Nuclear Rocket Engine," SM Thesis, Department of Aeronautics and Astronautics and Nuclear Engineering, Massachusetts Institute of Technology, May 1993.
- U-1 H. H. Uhlig, Corrosion and Corrosion Control: An Introduction to Corrosion Science and Engineering, Wiley, New York, 1971.
- V-1 M. E. Vernon, "PIPE Series Experiment Plan," Sandia National Laboratory, Albuquerque, NM 1988.
- V-2 Vahalla Scientific, " Model 4100 ATC Digital Ohmmeter Technical Data Sheet", Vahalla Scientific, 1992.
- W-1 J. K. Witter, D. D. Lanning, J.E. Meyer, "Flow Stability Analysis of A Particle Bed Reactor Fuel Element," in Proceedings of Tenth Symposium on Space Nuclear Power and Propulsion, CONF-930103,M.S. El-Genk and M.D. Hoover, eds, American Institute of Physics, New York, 1993 1541.
- W-2 J. T. Watson, Viscosity of Gases in Metric Units, Her Majesty's Stationary Office, Edinburgh, England, 1972.
- W-3 J. K. Witter, "Modeling for the Simulation and Control of Nuclear Reactor Rocket Systems," Ph.D. Thesis, Department of Nuclear Engineering, Massachusetts Institute of Technology, June, 1993.

FLOW INSTABILITY TESTS FOR A PARTICLE BED REACTOR NUCLEAR THERMAL ROCKET FUEL ELEMENT

by
TIMOTHY JAMES LAWRENCE

B.S., Mathematical Sciences
U.S. Air Force Academy, Colorado Springs, CO
(1988)

SUBMITTED TO THE DEPARTMENT OF NUCLEAR ENGINEERING IN
PARTIAL FULFILLMENT OF THE REQUIREMENT FOR THE DEGREE OF

MASTER OF SCIENCE IN NUCLEAR ENGINEERING

at the
MASSACHUSETTS INSTITUTE OF TECHNOLOGY
May, 1993

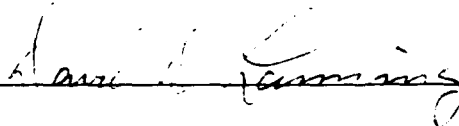
© Timothy James Lawrence, 1993. All rights reserved. The author hereby
grants to M.I.T. and to the U.S. Government permission to reproduce and
distribute copies of this thesis in whole or in part.

Signature of Author



Department of Nuclear Engineering
May, 1993

Certified by



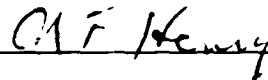
David D. Lanning
Thesis Supervisor
Professor, Department of Nuclear Engineering

Certified by



John E. Meyer
Thesis Reader
Professor, Department of Nuclear Engineering

Accepted by



Allan F. Henry, Chairman
Department of Nuclear Engineering Graduate Committee

FLOW INSTABILITY TESTS FOR A PARTICLE BED REACTOR NUCLEAR THERMAL ROCKET FUEL ELEMENT

by

TIMOTHY JAMES LAWRENCE

Submitted to the Department of Nuclear Engineering on May 7, 1993, in partial fulfillment of the requirements for the degree of Master of Science in Nuclear Engineering.

ABSTRACT

Recent analyses have focused on the flow stability characteristics of a particle bed reactor (PBR). These laminar flow instabilities may exist in reactors with parallel paths and are caused by the heating of the gas at low Reynolds numbers. This phenomena can be described as follows: several parallel channels are connected at the plenum regions and are stabilized by some inlet temperature and pressure; a perturbation in one channel causes the temperature to rise and increases the gas viscosity and reduces the gas density; the pressure drop is fixed by the plenum regions, therefore the mass flow rate in the channel would decrease; the decrease in flow reduces the ability to remove the energy added and therefore the temperature increases; and finally, this process could continue until the fuel element fails. Several analyses based on different methods have derived similar curves to show that these instabilities may exist at low Reynolds numbers and high ϕ 's ($(T_{final} - T_{initial})/T_{initial}$). These analyses need to be experimentally verified.

An insulated, stainless steel screen bed was designed to simulate the internal heat generation similar to the nuclear heating of the fuel in the PBR. A screen mesh was found with the wire diameter and spacing to give the element a porosity of 0.37 once the insulated coating was placed on the mesh. The hot and cold frit were made of stainless steel and were sintered to a porosity of 0.3. Other equipment items needed in addition to the screen and frits are as follows: containment vessel, power supply, gas flow system, chill down tank, instrumentation, and a data acquisition system.

The final design used a copper electroplated coating on the edges and tabs of the screen in order to carry the current into the bed and prevent hot spots on the edges. A painted alumina adhesive was painted onto the screen and cured in order to provide an insulated coating that could handle the rigors of assembly.

Six tests were performed that generated results useful to the flow stability phenomena. Three of the tests were at low ϕ 's and showed constant

temperatures with constant power. Three of the tests were at higher ϕ 's (~ 3) and showed that several temperatures in the bed decreased, while several temperatures in the bed increased while the mixed mean outlet remained constant. The time steps for these divergences were slow enough that they could be controlled.

The bed thermocouples showed asymmetries in temperature existed in the bed. Analysis of the bed using a 2D SIMBED steady state code revealed that the welding seams (non porous) on the frits and random porosities in the bed caused by overlap and alignment of the wrapped wires may have been the cause to these asymmetries. A more detailed transient analysis may further explain these results. However, even though there were asymmetries in the bed, the temperatures remained constant at constant power for low ϕ 's and diverged at higher ϕ 's.

The results of these experiments showed that flow instabilities may exist in the PBR. Even though the screen bed was not completely prototypic, analysis of the temperatures showed that the points where the divergences occurred were very close to the predicted analyses. These temperature divergences were observed in a bed with a higher lateral thermal conductivity which should mitigate the development of these instabilities. This phenomena was evidenced in the repeated number of tests performed.

Flow instability is not a "show stopper" for the PBR. More tests should be conducted using other "out of pile" and later "in pile" tests to better characterize and define the flow instability region so control strategies can be developed to mitigate operation in these regions.

This research was conducted at Brookhaven National Laboratory and was sponsored by Brookhaven National Laboratory, MIT, and the U.S. Air Force.

Thesis Supervisor: Dr. David D. Lanning
Title: Professor, Nuclear Engineering
Thesis Reader: Dr. John E. Meyer
Title: Professor, Nuclear Engineering

ACKNOWLEDGEMENTS

It is hard for me to express all the gratitude for all of the individuals that have helped me to grow mentally and socially at MIT for the past two years. Hopefully in the next couple of pages I can share some of the appreciation for the individuals that had an impact on my life.

I would like to thank Professor Lanning for his supervision and patience on this project. Professor Lanning allowed a lot of freedom for research, but supplied enough supervision to keep the project on task. I also learned a lot about nuclear power plants and operations in his classes.

I would also like to thank Professor John Meyer for his guidance, especially in thermal hydraulic discussions of the PBR and how to write a professional technical report. Hopefully some day Professor Meyer, we will have "Star Trek" technology.

I also appreciate the financial support I received from the Nuclear Engineering Department at MIT.

A special thanks to the personnel at Brookhaven National Laboratory, the sponsors of this research. Thanks to Dr. Walt Kato, Dr. Jim Powell, and Dr. Hans Ludewig for their support of this research, even when it looked like the apparatus would never work and funding was tight.. A lot of thanks and appreciation to the technical staff, Dr. George Maise and Dr. Dan Van Rooyan, who allowed me to pursue my ideas for this research project, no matter how crazy they were. I also appreciate the support they gave me when it looked like the experiment would never succeed, thanks for the faith guys. I also appreciate the golf lessons I learned from Dan. I hope to see you on the Senior Tour soon Dan!

I would like to express warm regards to the technical crew in 528. I really learned the intricacies of putting a piece of hardware together from Joe Savino and Bob Sick. Without your support and assistance, the project would never have been completed. Thanks a lot Joe for your support when I had to come back to Cambridge and required further coordination for finishing my thesis.

I would also like to thank the Air Force for allowing me to come to MIT to pursue a Master's Degree. I hope the knowledge I have gained here will help the Air Force in the development of future technology.

I would like to thank the following individuals for the following reasons:

-Dr. Jonathan Witter for his technical expertise, friendship, and reinforcing political views to know there is hope for this world.

-Professor Jack Kerrebrock and Jim Kalamas for enlightening discussions on flow stability and analyses run to compare with the data of the experiment.

-Lt Lorin Selby for his assistance in problem sets and his friendship, even though he joined the wrong service. Hopefully you will forget this comment when you become an admiral.

-Andrew and Vera Barritt for the excellent meals, hospitality, work outs, sharing Swiss culture, and friendship. I know that "Butch" is going to have wonderful parents.

-David Suzuki for his friendship, and work in keeping the apartment clean.

-Bronislav "Spetsnaz" Guimpleson for his friendship and sharing of Russian culture. Holodryga my friend!

-Renee DuBord and Jenn Uhle for converting me from "kind of" conservative to "pseudo" conservative.

-Dr. Anthony, Shelly, and Madison Woodrich for the friendship, work outs, and excellent Thai food. I really enjoyed going up to your place to blow off steam.

-Dave Jablonski for showing me that fusion guys could drink beer.

-Anthony Brinkley and Dan Doney for constant entertainment just describing their lifestyles.

-My out of town friends for always being there for support.

-The ANS basketball team for allowing a pathetic basketball player to be their coach.

-The MIT rugby team for allowing me to play, even when I did not have enough time to be a dedicated player.

-The AF Astronautics Laboratory personnel: Dr. Frank Mead, Dave Perkins, Dr. Ralph Cerbone, Capt J.C. Coleman, and Lt Col Michael Heil for laying the foundation and giving me the freedom to pursue my goals.

I would finally like to thank my Mom, Dad, and John for our strong Christian family that gave me the character development to pursue my dreams. It is always nice to know I have an ear to turn to. I would also like to thank my Aunt Bev, Uncle Bill, and Cousin Adrienne in Tucson. I appreciate all of your support through the good and bad times for the past two years.

FLOW INSTABILITY TESTS FOR A PARTICLE BED REACTOR NUCLEAR THERMAL ROCKET FUEL ELEMENT

by

TIMOTHY JAMES LAWRENCE , CAPT, USAF

Submitted to the Department of Nuclear Engineering on May 7, 1993, in partial fulfillment of the requirements for the degree of Master of Science in Nuclear Engineering.

ABSTRACT

Recent analyses have focused on the flow stability characteristics of a particle bed reactor (PBR). These laminar flow instabilities may exist in reactors with parallel paths and are caused by the heating of the gas at low Reynolds numbers. This phenomena can be described as follows: several parallel channels are connected at the plenum regions and are stabilized by some inlet temperature and pressure; a perturbation in one channel causes the temperature to rise and increases the gas viscosity and reduces the gas density; the pressure drop is fixed by the plenum regions, therefore the mass flow rate in the channel would decrease; the decrease in flow reduces the ability to remove the energy added and therefore the temperature increases; and finally, this process could continue until the fuel element fails. Several analyses based on different methods have derived similar curves to show that these instabilities may exist at low Reynolds numbers and high ϕ 's ($(T_{final} - T_{initial})/T_{initial}$). These analyses need to be experimentally verified.

An insulated, stainless steel screen bed was designed to simulate the internal heat generation similar to the nuclear heating of the fuel in the PBR. A screen mesh was found with the wire diameter and spacing to give the element a porosity of 0.37 once the insulated coating was placed on the mesh. The hot and cold frit were made of stainless steel and were sintered to a porosity of 0.3. Other equipment items needed in addition to the screen and frits are as follows: containment vessel, power supply, gas flow system, chill down tank, instrumentation, and a data acquisition system.

The final design used a copper electroplated coating on the edges and tabs of the screen in order to carry the current into the bed and prevent hot spots on the edges. A painted alumina adhesive was painted onto the screen and cured in order to provide an insulated coating that could handle the rigors of assembly.

Six tests were performed that generated results useful to the flow stability phenomena. Three of the tests were at low ϕ 's and showed constant

temperatures with constant power. Three of the tests were at higher ϕ 's (~ 3) and showed that several temperatures in the bed decreased, while several temperatures in the bed increased while the mixed mean outlet remained constant. The time steps for these divergences were slow enough that they could be controlled.

The bed thermocouples showed asymmetries in temperature existed in the bed. Analysis of the bed using a 2D SIMBED steady state code revealed that the welding seams (non porous) on the frits and random porosities in the bed caused by overlap and alignment of the wrapped wires may have been the cause to these asymmetries. A more detailed transient analysis may further explain these results. However, even though there were asymmetries in the bed, the temperatures remained constant at constant power for low ϕ 's and diverged at higher ϕ 's.

The results of these experiments showed that flow instabilities may exist in the PBR. Even though the screen bed was not completely prototypic, analysis of the temperatures showed that the points where the divergences occurred were very close to the predicted analyses. These temperature divergences were observed in a bed with a higher lateral thermal conductivity which should mitigate the development of these instabilities. This phenomena was evidenced in the repeated number of tests performed.

Flow instability is not a "show stopper" for the PBR. More tests should be conducted using other "out of pile" and later "in pile" tests to better characterize and define the flow instability region so control strategies can be developed to mitigate operation in these regions.

This research was conducted at Brookhaven National Laboratory and was sponsored by Brookhaven National Laboratory, MIT, and the U.S. Air Force.

Thesis Supervisor: Dr. David D. Lanning
Title: Professor, Nuclear Engineering
Thesis Reader: Dr. John E. Meyer
Title: Professor, Nuclear Engineering

REFERENCES

- B-1 R.W. Bussard and R.D. DeLauer, Fundamental of Nuclear Flight, McGraw - Hill, New York, 1965.
- B-2 J. R. Powell et al, "Particle Bed Reactor Orbit Transfer Vehicle Concept," AFAL-TR-88-014, Air Force Astronautics Laboratory, July 1988.
- B-3 S. K. Borowski, "The Rational Benefits of Nuclear Thermal Propulsion for NASA's Lunar Space Transportation System," AIAA/SAE/ASME/ASEE 27th Joint Propulsion Conference, June 24 - 26, 1991, Sacramento, CA.
- C-1 R. J. Cerbone and T. J. Lawrence, "Nuclear Heating in the Upperstage of a Particle Bed Driven Nuclear Propulsion System," AIAA/SAE/ASME/ASEE 27th Joint Propulsion Conference, June 24-26, 1991, Sacramento, CA.
- C-2 Cotronics Corporation, Adhesives Ceramics and High Temperature Materials Handbook, Cotronics Corporation, 1992.
- C-3 CRC Handbook of Chemistry and Physics, The Chemical Rubber Company, 1969.
- C-4 W.E. Casey, "Thermal-Hydraulic Transient Analysis of a Packed Particle Bed Reactor Fuel Element," SM and Naval Engineer Thesis, Department of Nuclear Engineering, Massachusetts Institute of Technology, May 1990.
- C-5 M. Charmchi, "Heat Transfer and Fluid Flow Characteristics of the Hydrogen-Cooled Small Particle Bed Reactor (PBR)," UL-MEE-89[05-5012]-F, Brookhaven National Laboratory, October 1989.
- E-1 Enerpac Basic Pressure Gauge, Model DGB Technical Manual, Enerpac, 1988.
- H-1 P.G. Hill and C. R. Peterson, Mechanics and Thermodynamics of Propulsion, Addison-Wesley, New York 1992.
- H-2 D.E. Hastings, Course 16.53 Rocket Propulsion Class Notes, Massachusetts Institute of Technology, September 1992.
- H-3 H. Herman, "Plasma-Sprayed Coatings," Scientific American, September 1988.

- K-1 J. L. Kerrebrock, "Flow Instability in Particle-Bed Nuclear Reactors," Massachusetts Institute of Technology Informal Report, November 1992.
- K-2 J. Kalamas, "Particle Bed Reactor Stability Analysis," SM Thesis, Department of Aeronautics and Astronautics, Massachusetts Institute of Technology, May 1993.
- M-1 G. Maise, "Flow Stability in the Particle Bed Reactor," Informal Report BNL/RSD-91-002, Brookhaven National Laboratory, January 1991.
- M-2 Matheson, "Mass Flowmeters - Linear Mass Flowmeter - Series 8100 Technical Data Sheet," Matheson, 1988.
- M-3 Metals Handbook, 9th Edition, Volume 5, Surface Cleaning, Finishing, and Coating, American Society for Metals, Metals Park, OH, 1982.
- O-1 Omega Engineering Inc., "The Temperature Handbook," Omega Engineering Inc., Stamford, Ct, 1992.
- O-2 Omega Engineering Inc., "PX100 Low - Level Pressure Transducer Data Sheet," Omega Engineering Inc., Stamford, Ct, 1988.
- O-3 Omega Engineering Inc., "Omega WB-ASC Card Technical Manual," Omega Engineering Inc., Stamford, Ct, 1988.
- P-1 Private Communication, D. R. Perkins, Astronautics Laboratory, Edwards AFB, CA, 1990.
- P-2 W H. Press, et al, Numerical Recipes in FORTRAN, The Art of Scientific Computing, 2nd Edition, Cambridge University Press, Port Chester, NY, 1992.
- R-1 Rapid Power Technologies Inc., "Thyristor (SCR) Power Supplies - for High Quality dc Power Supply Applications", Rapid Power Technologies Inc., 1990.
- S-1 V. V. Sychev, et al, Thermodynamic Properties of Helium, Hemisphere Publishing, New York, 1987.
- S-2 A. E. Sheidegger, Physics of Flow Through Porous Media, Toronto University, Toronto, 1963.
- S-3 Stafford (Chairman), "America's Space Exploration Initiative: America at the Threshold," The Report of the Stafford Committee to the President of the United States, May 1991.

- S-4 D.E. Suzuki, "Development and Analysis of Start-up Strategies for a Particle Bed Nuclear Rocket Engine," SM Thesis, Department of Aeronautics and Astronautics and Nuclear Engineering, Massachusetts Institute of Technology, May 1993.
- U-1 H. H. Uhlig, Corrosion and Corrosion Control: An Introduction to Corrosion Science and Engineering, Wiley, New York, 1971.
- V-1 M. E. Vernon, "PIPE Series Experiment Plan," Sandia National Laboratory, Albuquerque, NM 1988.
- V-2 Vahalla Scientific, " Model 4100 ATC Digital Ohmmeter Technical Data Sheet", Vahalla Scientific, 1992.
- W-1 J. K. Witter, D. D. Lanning, J.E. Meyer, "Flow Stability Analysis of A Particle Bed Reactor Fuel Element," in Proceedings of Tenth Symposium on Space Nuclear Power and Propulsion, CONF-930103,M.S. El-Genk and M.D. Hoover, eds, American Institute of Physics, New York, 1993 1541.
- W-2 J. T. Watson, Viscosity of Gases in Metric Units, Her Majesty's Stationary Office, Edinburgh, England, 1972.
- W-3 J. K. Witter, "Modeling for the Simulation and Control of Nuclear Reactor Rocket Systems," Ph.D. Thesis, Department of Nuclear Engineering, Massachusetts Institute of Technology, June, 1993.

Table of Contents

ABSTRACT	2
ACKNOWLEDGEMENTS	4
TABLE OF CONTENTS	7
LIST OF TABLES	10
LIST OF FIGURES	11
CHAPTER 1 INTRODUCTION	20
1.1 STATEMENT OF PROBLEM	20
1.2 APPROACH	21
CHAPTER 2 BACKGROUND	24
2.1 PARTICLE BED REACTORS (PBR)	24
2.1.1 Applications	24
2.1.2 Particle Bed Reactor Design.....	30
2.2 FLOW INSTABILITIES OF PBR'S	34
2.2.1 Bussard and DeLauer Analysis for Parallel Channels	34
2.2.2 PBR Analyses	38
2.3 TESTING APPROACHES	44
2.3.1 Screen Bed	44
2.3.2 Other Experiments	45
CHAPTER 3 EXPERIMENT DESIGN	47
3.1 SCREEN BED	47
3.1.1 Frits	47
3.1.2 Screen	50
3.2 SCREEN BED SUPPORT STRUCTURE	56
3.2.1 Inner Vessel and Seals/Insulators	56
3.2.2 Outer Pressure Vessel and Seals	61
3.3 FLOW CONTROL SYSTEM	63
3.3.1 Inlet/Outlet Flow Control.....	63
3.3.2 Tank Farm	65
3.3.3 Chill-Down Tank	67
3.3.4 Piping	69
3.3.5 Flowmeter	69
3.4 POWER SUPPLY	72

3.4.1 System and Leads	72
3.4.2 Console	73
3.4.3 Copper Electrode Blocks	75
3.5 INSTRUMENTATION	75
3.5.1 Thermocouples	75
3.5.2 Pressure Transducer	78
3.5.3 Data Acquisition System	79
3.5.4 Ohmmeter	80
CHAPTER 4 TESTING	82
4.1 TESTING PROCEDURE	82
4.2 ALUMINA PAINTED SCREEN TEST (OCT 92)	85
4.3 8 ALUMINA PAINTED SCREEN TESTS (JAN 93)	92
CHAPTER 5 ANALYSES	115
5.1 INTERPRETATION OF ASYMMETRIES IN TEMPERATURES	115
5.2 TEMPERATURE AND PRESSURE DROP ANALYSES	116
5.2.1 Energy Balance	116
5.2.2 2D SIMBED	120
5.3 PHI VS REYNOLDS NUMBER CALCULATIONS	126
5.3.1 Description of Stability Curves	126
5.3.2 Description of Phi and Re Points	128
5.4 UNCERTAINTY IN DATA ANALYSIS	139
5.4.1 Seams in Frits	139
5.4.2 Variable Porosity	142
5.4.3 Variable Porosity and Seams	145
CHAPTER 6 CONCLUSIONS AND RECOMMENDATIONS	149
6.1 CONCLUSIONS	149
6.2 RECOMMENDATIONS FOR FURTHER STUDY	154
REFERENCES	157
APPENDIX A DESIGN EVOLUTION	160
A.1 COPPER COATINGS	160
A.1.1 Need for Copper Coatings at Ends and Tabs	160
A.1.2 Plasma Sprayed Copper Coating	164
A.1.3 Electroplated Copper Coating	170

A.2 ALUMINA COATINGS	179
A.2.1 Plasma Sprayed Alumina	179
A.2.2 Plasma Sprayed Spinel	181
A.2.3 Ceramic Paper Insulator	184
A.2.4 Ceramic Tapes	186
A.2.5 Zirconia Balls	187
A.2.6 Oxidized Screen	188
A.2.7 Glossy Coatings	191
A.2.8 Painted Alumina	191
A.3 SINGLE SCREEN	194
A.4 SEALS	196
A.5 THERMOCOUPLES	198
A.6 ASSEMBLY ISSUES	201
APPENDIX B PRELIMINARY TESTS	202
B.1 INITIAL FAILURES	202
B.2 7 SCREEN WITH PAPER INSULATOR TESTS (JULY 92)	207
B.3 4 OXIDIZED SCREEN TESTS (AUG 92)	220
APPENDIX C SUPPORT EXPERIMENTS	228
C.1 POROSITY	228
C.2 PRESSURE DROP	234
C.3 POWER SUPPLY CORRECTION	235
C.4 FLOWMETER CORRECTION	239
APPENDIX D TESTING DATA SHEETS.....	244
APPENDIX E EQUIPMENT CALIBRATION SHEETS	255
APPENDIX F TEMPERATURE DATA FROM JAN 93 EXPERIMENTS	263
APPENDIX G EXTRA MODELING RESULTS	296
G.1 1D PRESSURE DROP	296
G.2 1D TRANSIENT	298
G.3 OTHER RESULTS	303
APPENDIX H GLOSSARY	336

List of Tables

Table 2.1.1.1 Assumptions for Cases Plotted in Figure 2.1.1.1.....	28
Table 2.1.2.2 Comparison of Different Reactors	33
Table 3.1.2.1 Materials Considered for the Screen Mesh	51
Table 4.1.1 Operating Instructions for Screen Bed Experiments	82
Table 5.2.2.1 SIMBED Input	121
Table A.1.3.1 Chemicals Used for Electroplating	172
Table A.2.2.1 Impact of Wrapping on Resistance	183
Table A.2.8.1 Ceramic Adhesives	192
Table A.3.1 Original Screen Calculations	196
Table C.3.1 Power Readings	236
Table C.3.2 Ohmmeter Test	237
Table C.3.3 Power Supply Test #2 Results.....	238
Table C.4.1 Helium and Nitrogen Flowmeter Test #1	240
Table C.4.2 Results of Flowmeters in Series Tests	241
Table G.2.1 Input for TRITRAN Runs and Pictures of Element Layouts	298
Table H.1 Table of Acronyms	336
Table H.2 Table of Symbols	337

List of Figures

Figure 2.1.1.1 Mission Capability of Single Stage Propulsion Systems	27
Figure 2.1.2.1 PBR Engine	32
Figure 2.1.2.2 PBR Element and Core	32
Figure 2.2.1.1 Φ vs Reynolds Number for Hydrogen	37
Figure 2.2.1.2 Φ vs Reynolds Number for Various Gases and Bed Porosities	38
Figure 2.2.2.1 Witter's 1D Φ vs Reynolds Number for Hydrogen	40
Figure 2.2.2.2 1D Φ vs Reynolds Number for Experiments	40
Figure 2.2.2.3 Impact of Inlet Conditions on Stability Curve	41
Figure 2.2.2.4 Parallel Stream Stability Map	43
Figure 3.1.1.1 Engineering Drawing of the Element Assembly	48
Figure 3.1.1.2 Picture of Screen Bed Element	49
Figure 3.1.2.1 Stainless Steel Screen	50
Figure 3.1.2.2 Carbon Tube	52
Figure 3.1.2.3 Final Screen Design	54
Figure 3.1.2.4 Wrapped Screen Bed Inside Element	55
Figure 3.2.1.1 Picture of Screen Element Connected to Manifold	59
Figure 3.2.1.2 Picture of Element Assembly	60
Figure 3.2.2.1 Outer Pressure Vessel	62
Figure 3.3.1.1 Gas Flow System	64
Figure 3.3.1.2 Pipes for Inlet Flow to the Bed	65
Figure 3.3.2.1 Helium Tanks	66
Figure 3.3.2.2 1A Cylinder	67

Figure 3.3.3.1 Chill Down Calculations	68
Figure 3.3.3.2 Chill Down Calculations	68
Figure 3.3.5.1 Chill Down / Heat Addition System for Flowmeter	71
Figure 3.4.1.1 Entire Experimental Apparatus	74
Figure 3.5.1.1 Thermocouple Placement	76
Figure 4.2.1 Thermocouple Arrangements	87
Figure 4.2.2 Power vs Time for Test	87
Figure 4.2.3 Thermocouple Results for 14 Oct 93 Experiment	88
Figure 4.2.4 Melted Frits	90
Figure 4.3.1 Thermocouple Placement for Experiment	95
Figure 4.3.2 Flow Through Manifold Pipes	96
Figure 4.3.3 Bed Test at Low Phi	97
Figure 4.3.4 Bed Test with No Flow	98
Figure 4.3.5 Thermocouple Placement After Rotation	100
Figure 4.3.6 Rotated Bed Test with No Flow	101
Figure 4.3.7 Rotated Bed Test with Flow	102
Figure 4.3.8 High Phi Run	104
Figure 4.3.9 High Phi Lower Pressure Test	106
Figure 4.3.10 Repeat Test at Low Phi	108
Figure 4.3.11 High Phi Retest	110
Figure 4.3.12 Melted Bed and Hot Frit	112
Figure 4.3.13 Charred Bed	113
Figure 5.2.1.1 Energy Balance for Test #1	117

Figure 5.2.1.2 Energy Balance for Test #4	117
Figure 5.2.1.3 Energy Balance for Test #5	118
Figure 5.2.1.4 Energy Balance for Test #6	118
Figure 5.2.1.5 Energy Balance for Test #7	119
Figure 5.2.1.6 Energy Balance for Test #8	119
Figure 5.2.2.1 Temperature Profile for Test #5	123
Figure 5.2.2.2 Pressure Drop for Test #5	123
Figure 5.2.2.3 Test #5 Velocity Profile	124
Figure 5.3.1.1 Phi vs Reynolds Number for the Experimental Apparatus	128
Figure 5.3.2.1 Phi vs Reynolds Number for Test #1	131
Figure 5.3.2.2 Phi vs Reynolds Number for Test #4	131
Figure 5.3.2.3 Phi vs Reynolds Number for Test #5	132
Figure 5.3.2.4 Phi vs Reynolds Number for Test #6	132
Figure 5.3.2.5 Phi vs Reynolds Number for Test #8	133
Figure 5.3.2.6 Phi vs Reynolds Number Test #1	134
Figure 5.3.2.7 Phi vs Reynolds Number Test #4	135
Figure 5.3.2.8 Phi vs Reynolds Number Test #5	135
Figure 5.3.2.9 Phi vs Reynolds Number Test #6	136
Figure 5.3.2.10 Phi vs Reynolds Number Test #7	136
Figure 5.3.2.11 Phi vs Reynolds Number Test #8	137
Figure 5.3.2.12 Phi vs Reynolds Number (Temperature Divergences) Test #5	138
Figure 5.3.2.13 Phi vs Reynolds Number (Temperature Divergences) Test #6	138

Figure 5.3.2.14 Phi vs Reynolds Number (Temperature Divergences) Test #8	139
Figure 5.4.1.1 High Phi Run T=5 minutes Temperature Distribution	140
Figure 5.4.1.2 High Phi Run T=5 minutes Pressure Drop	141
Figure 5.4.1.3 High Phi Run T= 5 minutes Velocity Profile	141
Figure 5.4.1.4 High Phi Run T= 5 minutes Velocity Profile (Rotated)	142
Figure 5.4.2.1 Heat Generation within the Bed for a Random Porosity	143
Figure 5.4.2.2 Random Porosity Temperature Distribution	144
Figure 5.4.2.3 Random Porosity Velocity Profile	144
Figure 5.4.3.1 High Phi Run Variable Porosity and Seams Temperature Distribution	145
Figure 5.4.3.2 Variable Porosity and Seams Velocity Profile	146
Figure 5.4.3.3 High Phi Run Variable Porosity and Seams Velocity Profile (Rotated)	146
Figure 5.4.3.4 Phi versus Reynolds Number Showing SIMBED Point	147
Figure A.1.1.1 Hot Spot Development on Screen	160
Figure A.1.1.2 Copper Piece on Screen	161
Figure A.1.1.3 Wider Copper Piece	161
Figure A.1.1.4 Waterline Effect in Etching	163
Figure A.1.1.5 Coated Tabs vs Welded Tabs	164
Figure A.1.2.1 Hot Spots on Screen Bed	167
Figure A.1.2.2 Plasma Sprayed Copper Coated Pieces	168
Figure A.1.2.3 Solid Copper Clamped on Pieces Retest	169
Figure A.1.3.1 Electroplating System	173
Figure A.1.3.2 Copper Electroplated Test Screen	175

Figure A.1.3.3 Copper Plated Screen Used in Experiments	177
Figure A.2.1.1 Coating After Being Rolled	181
Figure A.2.3.1 Test for Pressure Drop Across Ceramic Paper	185
Figure A.2.3.2 Holes Put in Paper to Minimize Pressure Drop	186
Figure A.2.5.1 Zirconia Balls as an Insulator	187
Figure A.2.6.1 Resistance Test and In-Situ Oxidation of the Screen Bed	189
Figure A.2.6.2 Flow Effect of Round Wires vs Flat Wires	191
Figure A.2.8.1 Alumina Coating Test	193
Figure A.4.1 Leaks at Ends of Bed	197
Figure A.5.1 Thermocouple Insulation.....	199
Figure B.1.1 Thermocouple Positions	203
Figure B.1.2 Ohmmeter Tests on Apparatus	204
Figure B.1.3 Bed Inspection after Test	207
Figure B.2.1 Hot Frit Insulation	208
Figure B.2.2 Test #1	210
Figure B.2.3 Test #2	211
Figure B.2.4 Test #3	212
Figure B.2.5 Test #4	213
Figure B.2.6 Test #5	214
Figure B.2.7 Test #6	215
Figure B.2.8 Test #7	216
Figure B.3.1 Test #8 (Oxidized Test #1)	222
Figure B.3.2 Test #9	223

Figure B.3.3 Test #10	224
Figure B.3.4 Test #11	225
Figure C.1.1 Volume Displacement with Water	229
Figure C.1.2 Pressure Drop Porosity Test	230
Figure C.2.1 Pressure Drop Experiments	234
Figure C.3.1 Power Supply Test #1	235
Figure C.3.2 Ohmmeter Test	236
Figure C.3.3 Power Supply Test #2	238
Figure C.4.1 Flowmeter Calibration Test #2 (Meters in Series)	241
Figure D.1 Data Sheet From 14 Oct 92 Experiment	245
Figure D.2 Data Sheet From 20 Jan 93 Test #1	246
Figure D.3 Data Sheet From 20 Jan 93 Test #2	247
Figure D.4 Data Sheet From 22 Jan 93 Test #3	248
Figure D.5 Data Sheet From 22 Jan 93 Test #4	249
Figure D.6 Data Sheet From 22 Jan 93 Test #5	250
Figure D.7 Data Sheet From 22 Jan 93 Test #6	251
Figure D.8 Data Sheet From 25 Jan 93 Test #7	252
Figure D.9 Data Sheet From 26 Jan 93 Test #8.....	253
Figure D.10 Data Sheet That Showed Bed Was Damaged 26 Jan 93	254
Figure E.1 Calibration Sheet for Ohmmeter	256
Figure E.2 Calibration Sheet for Flowmeter	257
Figure F.1 Bed Test at Low Phi 20 Jan 93	264
Figure F.2 Bed Test with No Flow 20 Jan 93	270

Figure F.3 Rotated Bed Test with No Flow 22 Jan 93	272
Figure F.4 Rotated Bed Test with Flow 22 Jan 93	276
Figure F.5 High Phi Run 22 Jan 93	280
Figure F.6 High Phi Lower Pressure Test 22 Jan 93	284
Figure F.7 Repeat Low Phi Test 25 Jan 93	288
Figure F.8 High Phi Retest 26 Jan 93	292
Figure G.1.1 1D SS Pressure Drop	297
Figure G.2.1 Bed Test at Low Phi Transient	300
Figure G.2.2 Repeat Test at Low Phi Transient Analysis	301
Figure G.2.3 High Phi Lower Pressure Test (Test #6) Transient Analysis	301
Figure G.2.4 High Phi Lower Pressure Test Different Transient	302
Figure G.3.1 Phi versus Reynolds Number Shoeing 1DSS Result Test #8 ...	304
Figure G.3.2 Phi versus Reynolds Number Showing 1DSS Result Test #5 ..	305
Figure G.3.3 Phi versus Reynolds Number Showing 1DSS Result Test #6 ..	306
Figure G.3.4 Phi versus Reynolds Number for Energy Balance Mdot and Flowmeter Mdot Test #5	307
Figure G.3.5 Phi versus Reynolds Number for Energy Balance Mdot and Flowmeter Mdot Test #8	308
Figure G.3.6 Phi versus Reynolds Number for Energy Balance Mdot and Flowmeter Mdot Test #6	309
Figure G.3.7 TRITRAN Run for Test #4 (Power Ramps)	310
Figure G.3.8 TRITRAN Run for Test #4 (Temperatures)	311
Figure G.3.9 TRITRAN Run for Test #1 (Power Ramps)	312
Figure G.3.10 TRITRAN Run for Test #1 (Temperatures)	313

Figure G.3.11 TRITRAN Run for Test #4 - Different Time (Power Ramps)	314
Figure G.3.12 TRITRAN Run for Test #4 - Different Time (Temperatures).....	315
Figure G.3.13 TRITRAN Run for Test #5 (Power Ramps).....	316
Figure G.3.14 TRITRAN Run for Test #5 (Temperatures)	317
Figure G.3.15 TRITRAN Run for Test #5 - Different Time (Power Ramps)	318
Figure G.3.16 TRITRAN Run for Test #5 - Different Time (Temperatures).	319
Figure G.3.17 TRITRAN Run Bigger Particle Size (Power Ramps)	320
Figure G.3.18 TRITRAN Run Bigger Particle Size (Temperatures)	321
Figure G.3.19 SIMBED Run with One Node In Bed Blocked	322
Figure G.3.20 SIMBED Run with One Node In Bed Blocked - More Iterations	323
Figure G.3.21 SIMBED Run with Bed Porosity =0.3 (Pressure Drop)	324
Figure G.3.22 SIMBED Run with Bed Porosity =0.3 (Temperatures)	325
Figure G.3.23 SIMBED Run with Bed Porosity =0.4 (Pressure Drop)	326
Figure G.3.24 SIMBED Run with Bed Porosity =0.4 (Temperatures)	327
Figure G.3.25 SIMBED Run with Bed Porosity =0.5 (Pressure Drop)	328
Figure G.3.26 SIMBED Run with Bed Porosity =0.5 (Temperatures)	329
Figure G.3.27 SIMBED Run with Bed Porosity =0.6 (Pressure Drop)	330
Figure G.3.28 SIMBED Run with Bed Porosity =0.6 (Temperatures)	331
Figure G.3.29 SIMBED Run with 0.0464 cm Particle Diameter (Temperatures)	332
Figure G.3.30 SIMBED Run with 0.0464 cm Particle Diameter (Pressure Drop)	333
Figure G.3.31 SIMBED Run with 0.04318 cm Particle Diameter (Temperatures)	334

Figure G.3.32 SIMBED Run with 0.04318 cm Particle Diameter (Pressure Drop)	335
---	-----

CHAPTER 1

INTRODUCTION

1.1 STATEMENT OF PROBLEM

Brookhaven National Laboratory has proposed a particle bed reactor (PBR) nuclear thermal rocket engine for space missions. The concept was chosen because of the high power density that is made possible by the large heat transfer area per unit fuel volume and because of the availability of high exit gas temperatures. Its distinguishing feature is the direct cooling of small (350 - 500 μm diameter) coated spheres (U235 surrounded by pyrolytic graphite and zirconium carbide) by hydrogen propellant. The fuel is packed between two concentric porous cylinders, called frits, which contain the fuel and allow coolant passage. Nineteen of these small annular fuel elements would be arrayed in a cylindrical moderator block (candidate materials are beryllium or lithium hydride) to form a 500 MW PBR core (this type of design would be typical for an orbital transfer vehicle). Coolant flow is directed radially inward, through the packed bed and hot frit, and axially out the inner annular channel to be expanded out the nozzle to produce thrust.

Several models have been developed and experiments conducted to try to characterize the thermal hydraulics of a PBR fuel element. Most of the early experiments have shown the capability to operate at a high power density (20 to 40 MW/L). More recent experiments were designed to operate at lower power densities in the ACRR (Annular Core Research Reactor) at Sandia National Laboratory. These Packed Bed Element experiments (PIPE) set out to verify computer analysis of flow through the element and create an environment to measure the thermal loads and material behavior of the

packed bed and element [V-1]. Analysis of these data has led to investigations of flow stability through the PBR fuel element.

A viscosity induced stability criterion was first investigated for nuclear thermal rockets by Bussard and DeLauer in 1958 and 1965 [B-1]. Their analyses predicted that a system with multiple heated channels cooled by flowing gas has a possibility for viscosity induced temperature and flow instabilities. These instabilities can be described as follows: several parallel channels are connected at the plenum regions and are operating at some inlet temperature and pressure; a perturbation by flow decrease in one channel causes the temperature to rise and increases the gas viscosity and reduces the gas density; the pressure drop is fixed by the plenum regions, therefore the mass flow rate in the channel would decrease; the decrease in flow reduces the ability to remove the energy added and therefore the temperature increases; and finally, this process could continue until the fuel element fails [W-1].

The instability usually occurs at low flow rates and high temperatures. This is a key issue for the PBR since these conditions might occur during start-up and shutdown. It is important to try to determine and characterize these instabilities (if they exist) for the given reactor geometry so a design and operation strategy can be developed to avoid instabilities of the element.

1.2 APPROACH

The major emphasis of this investigation is to conduct experiments to try to characterize the flow stability criterion of a PBR fuel element. Existing analyses are used and modified for the geometry of the experimental bed to determine calculated stable/unstable regions. These regions then are used to plan ranges for experimental study. The tests operate in these stable and

unstable regions and use temperature, pressure, and flow readings to characterize the flow stability for a particular operating point. Post - experiment analyses are conducted to minimize uncertainties in the experimental data. A brief description of the entire investigation follows.

Chapter 2 contains background information on PBR's and other computational flow stability analyses conducted to date. A discussion on the reasons for choosing the experimental design is also presented.

Chapter 3 gives a detailed description of the experimental design.

Chapter 4 discusses the testing procedure and the tests conducted during this investigation.

Chapter 5 contains analyses conducted after the experiments to analyze the test data and gives predictions for the corresponding flow stability criteria.

Chapter 6 gives conclusions and recommendations for further study.

Appendix A discusses the design evolution in coatings, seals, and thermocouples.

Appendix B describes early tests conducted and why their results are not very useful.

Appendix C gives porosity, pressure drop, power supply, and flowmeter tests performed to help minimize uncertainties in the results.

Appendix D is a supply of all test data sheets used for the experiments described in Chapter 4.

Appendix E contains equipment calibration sheets.

Appendix F is a listing in spreadsheet format of the temperature results for the 8 Tests conducted in Jan 93.

Appendix G describes more analyses run to study the experiment.

Finally, Appendix H is a glossary of terms discussed in this report.

The important facts about this investigation are that it was a timely and relatively inexpensive approach to try to characterize a phenomena that had never been observed before for PBR's or other similar devices.

CHAPTER 2

BACKGROUND

2.1 PARTICLE BED REACTORS

2.1.1 Applications

The PBR is proposed primarily for nuclear thermal propulsion. Nuclear thermal propulsion is a mission enabling technology. This can easily be seen from an observation of physics related to rocket propulsion. The conservation of momentum applied to a rocket is summarized by the rocket equation:

1. Apply conservation of momentum when no external forces are applied.

$$P_{\text{FINAL}} - P_{\text{INITIAL}} = [(M - \Delta M)(\vec{V} + \Delta \vec{V}) + \Delta M \vec{U}] - M \vec{V} = \Delta P = 0 \quad [2-1]$$

where P = momentum, M = mass, V , U = velocities

2. Apply Newton's second law for external forces acting on the system
(This is not the rocket thrust).

$$F_{\text{EXTERNAL}} = \lim_{\Delta t \rightarrow 0} \frac{\Delta P}{\Delta t}, \quad \frac{\Delta P}{\Delta t} = M \frac{\Delta \vec{V}}{\Delta t} - \vec{V} \frac{\Delta M}{\Delta t} - \frac{\Delta M \Delta \vec{V}}{\Delta t} + \vec{U} \frac{\Delta M}{\Delta t} \quad [2-2]$$

where t = time

$$\text{As } \Delta t \rightarrow 0, \frac{\vec{V}}{\Delta t} \rightarrow \frac{d\vec{V}}{dt}, \frac{\Delta M}{\Delta t} \rightarrow -\frac{dM}{dt}, \frac{\Delta M \Delta \vec{V}}{\Delta t} \rightarrow 0 \quad [2-3]$$

$$\boxed{F_{\text{EXTERNAL}} = M \frac{d\vec{V}}{dt} + (\vec{V} - \vec{U}) \frac{dM}{dt}} \quad [2-4]$$

3. Integrate for ΔV when external forces are set to zero.

$\vec{V} - \vec{U}$ = Relative ejection mass velocity = \vec{V}_{REL} = Constant for a given rocket design.

$$\int_{V_{\text{INITIAL}}}^{V_{\text{FINAL}}} d\vec{V} = -\vec{V}_{\text{REL}} \int_{M_{\text{INITIAL}}}^{M_{\text{FINAL}}} \frac{dM}{M} = \vec{V}_{\text{REL}} \ln \left(\frac{M_{\text{INITIAL}}}{M_{\text{FINAL}}} \right) \quad [2-5]$$

$$\text{Specific Impulse} \equiv \frac{F_{\text{ROCKET}}}{\left(\frac{dM}{dt} \right) g_0} = \frac{V_{\text{REL}}}{g_0} = I_{\text{SP}} \quad [2-6]$$

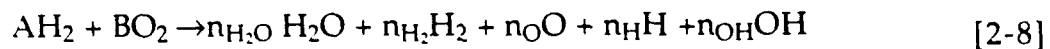
Therefore,

$$\boxed{\Delta \vec{V} = I_{\text{SP}} g_0 \ln \left(\frac{M_{\text{INITIAL}}}{M_{\text{FINAL}}} \right)} \quad [2-7]$$

The ΔV defined above is the velocity change capability of the rocket system. The specific impulse is defined as the rocket thrust divided by the mass flow

rate of propellants required to generate the rocket thrust. The g_0 term is a units conversion constant. M_{FINAL} is the rocket's inert mass plus the mass of any payload. M_{INITIAL} is the initial mass and is approximately equal to M_{INITIAL} plus the amount of mass (propellant) expended to deliver the ΔV .

The benefit of a PBR for nuclear thermal propulsion is the very high specific impulse at high thrust levels. Rockets are thermally driven gas dynamic devices whose specific impulse capability is proportional to $\sqrt{\frac{T_E}{M_G}}$ (For a derivation, see [H-1]), where T_E is the gas temperature and M_G is the mean molecular weight of the exhaust gases. Nuclear thermal rockets produce thrust by heating and ejecting a propellant just as chemical rockets do. However, in a chemical rocket the propellant releases energy through combustion. In a nuclear rocket, the propellant is heated by the controlled fission of uranium 235. Nuclear propulsion has the unique option of choosing low molecular weight exhaust gases with inherently high specific impulse. Chemical propulsion is limited to combustion products of inherently heavier molecular weight, than for example, hydrogen, which only has a molecular weight of 2.0 compared to the hydrogen oxygen reaction



which will have a higher molecular weight. Since the PBR can produce large quantities of thermal energy with low molecular weight gases, it has a specific impulse advantage of at least double that of chemical rockets. If a very high power density PBR were designed, it could result in a relatively compact configuration with thrust to weight ratios comparable to chemical rockets. The reactor mass at lower power densities resulted in past designs having thrust to weight ratios on the order of 5:1 compared to 50:1 ratios for chemical engines.

Figure 2.1.1.1 summarizes a simple first order analysis that shows the trade that exists between payload mass and ΔV that is inherent in the rocket equation. The comparison is made between nuclear propulsion (accounting for a range of expectations in performance and mass) and highly advanced cryogenic and storable chemical propulsion systems. Each system was constrained to a single stage configuration, and all payload support equipment was assumed to be part of the payload. Table 2.1.1.1 summarizes the assumptions of the cases plotted. All cases assumed a constrained initial mass of 35,000 kilograms. The propulsion inert masses were calculated as the sum of the fixed mass plus the product of the tank fraction and the propellant weight [P-1].

**Figure 2.1.1.1 Mission Capability of Single Stage Propulsion Systems From
Ref [P-1]**

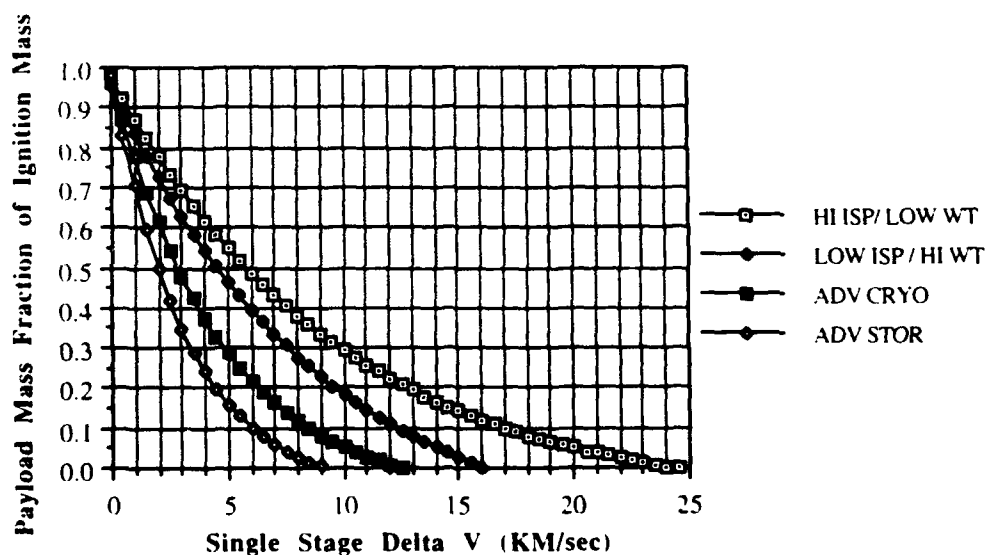


**Table 2.1.1.1 Assumptions for Cases Plotted In Figure 2.1.1.1 From
Ref [P-1]**

PROPULSION CONCEPT	ISP	TANK FRACTION	FIXED MASS
HI ISP LOW WT Nuclear Rocket	1000 s	0.06	1000 kg
LOW ISP HI WT Nuclear Rocket	900 s	0.14	1500 kg
Advanced LOX/H ₂ Cryogenic Rocket	475 s	0.05	750 kg
Advanced NTO/MMH Storable Rocket	325 s	0.04	600 kg

The different specific impulses from Table 2.1.1.1 for the nuclear rocket depend on an outlet gas temperature which depends on fuel temperature. The 1000 s engine assumes a 3000 K outlet gas temperature and the 900 s engine assumes a 2750 K outlet gas temperature. The low tank fractions represent composite tank technology and the higher ones represent today's metal technology. The 475 sec cryogenic rocket is the highest obtainable for the LOX/H₂ reaction, since the



has an maximum theoretical output energy of $1.5 \cdot 10^7$ J/kg (If all of the energy from the reaction could be converted to kinetic energy for thrust, the specific impulse would be 540 s). The 475 s engine will be very difficult to develop since it will require very high temperature and high pressure turbines. The Space Shuttle Main Engine produces a specific impulse of 452 s [H-2].

Launch vehicles require up to 10 kilometers per second ΔV capability to place payloads into Low Earth Orbit (LEO). The reason the ΔV requirement is high is due to the tremendous energy required to overcome the earth's gravitational pull as the vehicle accelerates from the surface. Since the above analysis represents a single stage, the nuclear single stage to orbit offers quite

an advantage compared to chemical systems (4 - 6 times higher payload capability).

Due to its high power density, the PBR could be used as an upper stage on existing launch vehicles e.g. Atlas, Delta, Titan, and ICBM's. The first stage of the existing launch vehicle would be used to boost the vehicle into a high altitude and then the nuclear stage would be used to carry the payload to LEO or to Geosynchronous Orbit (GEO). The ΔV required from the upper stage is around 7 km/s (depending on the first stage ΔV which is different for each launch vehicle). The payload increase would be 4 - 5 times higher for this mission class.

Orbital Transfer Vehicles (OTV) are designed to carry payloads (satellites) from LEO to GEO. A chemical launch vehicle would be used to carry the OTV to LEO (Most U.S. systems would use the Shuttle or Titan). The ΔV requirement for this mission class is ~4 - 5 km/sec (depending on if a plane change is made). The increased payload capability is ~2 times compared to the chemical system.

In 1988, Brookhaven National Laboratory conducted an OTV point design study using the Titan 34-D and Shuttle as launch vehicles [B-2]. For the Titan 34-D, the analysis assumed the total ignition mass at LEO was 28,310 kg. The PBR OTV delivered 11,727 kg to GEO compared to the Centaur G's (LOX/H₂ engine) 4545 kg. For the Shuttle analysis, the total ignition mass was 21,590 kg. The PBR OTV launched 9,090 kg to GEO compared to the Centaur G's 6000 kg [B-2].

There are various ΔV requirements for a manned mission to Mars. A long mission (100's of days) would require a ΔV ~6 km/s from LEO to Mars. A 40 day transfer from LEO to Mars would require 85 km/s [H-2]. Galactic radiation makes such space travel hazardous, and since man will suffer

physical and mental difficulties (~ 0 g) for long space travel, it is imperative that the shortest possible trip time be achieved. The Stafford Synthesis Group released a report in the spring of 1991 calling for the use of nuclear thermal rockets for the Mars mission [S-3].

There are other applications where the PBR is mission enabling. A ΔV of 12 - 20 km/s would allow direct propulsion of small, high velocity projectiles for the role as interceptors. Interceptors could be used to destroy incoming missiles or asteroids.

The above analyses show tremendous pay-offs for the use of nuclear thermal propulsion and PBR's. The payload savings alone could offer tremendous economic benefits which would justify the development costs. However, due to risk considerations with a new technology program, the first missions should be conducted in space to demonstrate the safe operation of the technology, then all missions should be considered.

2.1.2 Particle Bed Reactor Design

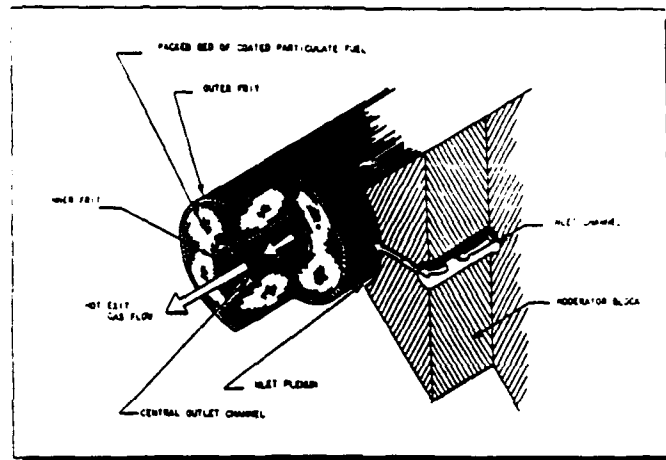
The design of a nuclear reactor core involves the linkage of three different disciplines : reactor physics, thermal-hydraulics, materials science/engineering and stress analysis. The linkage of these disciplines leads to a non-linear problem which can only be solved with iterations. Several computer codes have been developed/modified to design the PBR. Reference B-2 gives a conceptual design of the PBR.

A PBR for rocket applications usually consists of a coolant reservoir (tank), a coolant pump, a preheating stage, the reactor assembly, and the exhaust nozzle (see Fig 2.1.2.1). The turbopumps take propellant from the tank and

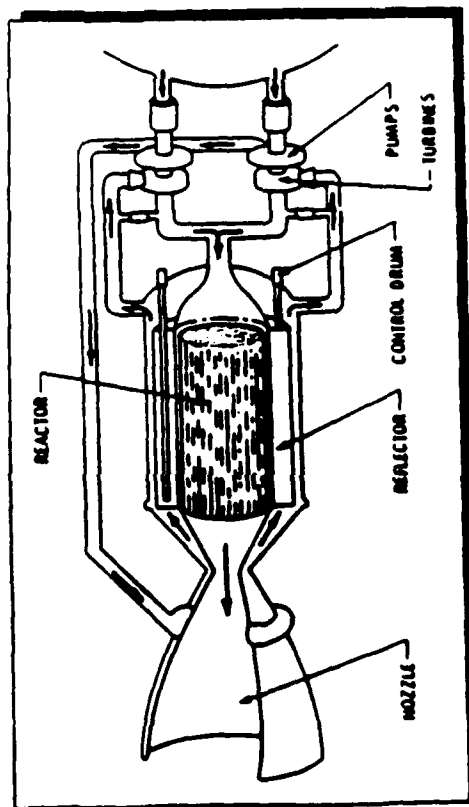
feed it into the reactor. The propellant is pressurized by means of pumps, which in turn are driven by turbines. The turbines derive their power from the expansion of hot gases. The nozzle flow is supersonic. The nozzle accelerates and ejects the propellant heated by the reactor, thereby imparting momentum to the system. The nozzle shown has a bell-shaped diverging contour, to permit the gas to expand without shock. This design allows the flow expansion losses to be small.

The PBR is a compact, high power density reactor concept. Its distinguishing feature is the direct cooling of small (500 μm diameter) coated particulate fuel spheres by the hydrogen propellant. Each sphere has a kernel of highly enriched uranium - 235 carbide surrounded by a pyrolytic graphite buffer coating to absorb the kinetic energy of fission. An inert external coating of zirconium carbide is next to the hot hydrogen. A representative fuel element and reactor are shown in Figure 2.1.2.2. The fuel is packed between two concentric porous cylinders, called "frits", which confine the fuel but allow coolant penetration. The inlet frit or cold frit is made of aluminum and is made porous through sintered holes or platelet technology (porosity ~ 0.64). The hot frit is made of coated carbon-carbon or rhenium (porosity ~ 0.5). Nineteen of these elements will form a 500 MW core (37 for a 2000 MW core). These elements are arrayed in a cylindrical moderator block (composed of beryllium or lithium-7 hydride) to form the core. Coolant flow is directed radially inward, through the packed bed (porosity ~ 0.35) and hot frit, and axially out the inner cylindrical channel. The frits are tapered at the outlet to lower the exit Mach number to ~ 0.2 in order to reduce vibrations in the core. Boron control rods outside the core bring the reactor up to power, stabilize power, and safely shut the reactor down [B-3].

Fig 2.1.2.1 PBR Engine

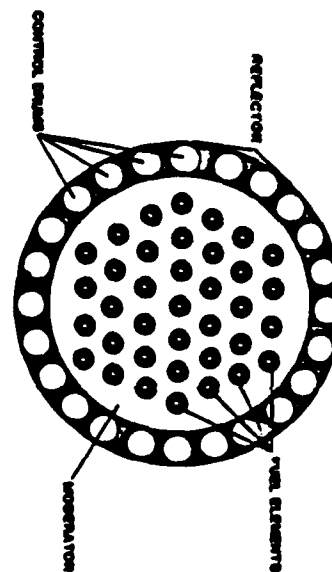


From Ref [B-3]



From Ref [B-3]

Fig 2.1.2.2 PBR Element and Core



From Ref [B-2]

Table 2.1.2.1 gives a comparison of the PBR to NERVA (Nuclear Engine for Rocket Vehicle Applications), and the Advanced NERVA (Enabler).

Table 2.1.2.1 Comparison of Different Reactors From Ref [C-1]

	NERVA	ADV. NERVA	PBR
Power (MW)	300	300	300
POWER DENSITY (MW/L)	1-2	1-2	20-40
PROPELLANT	H ₂	H ₂	H ₂
FUEL ELEMENT	SOLID ROD	SOLID ROD	POROUS BED
NUMBER OF ELEMENTS	380	380	19
MODERATOR TEMP (K)	2500	2500	400
FUEL TEMP (K)	2750	3000	3000
Isp (s)	835	925	1000
ENGINE WEIGHT (kg)	5100	2550	1200
THRUST / WEIGHT	5:1	12:1	50:1

The NERVA program had \$ 1.4 billion invested in it through the early '60's to early '70's [B-3]. The program built and static-tested 39 firings of nuclear thermal rockets in the Nevada desert [B-3]. Clearly, due to the large heat transfer area in the PBR element, the resultant higher power density makes the concept more favorable for propulsion missions. The system has had several "proof of concept" tests, but has not been tested at full scale like NERVA.

2.2.1 Bussard and DeLauer Analysis for Parallel Channels

Viscosity induced stability criterion was first investigated for nuclear thermal rockets by Bussard and DeLauer in 1958 and 1965 [B-1]. Their analysis predicted for a system with multiple heated channels cooled by flowing gas, there is a possibility for viscosity induced temperature and flow instabilities. Their analysis has since been extended for flow through a three dimensional bed, noting that the flow could become unstable as a result of localized heating due to variations in the local porosity. Lower porosity can increase the local heating rate and also increase the pressure drop gradient. Their method employs an integration across the flow length using approximate relations for density, viscosity, and heat input. A stability criterion was defined as the minimum point of pressure drop for a plot of pressure drop versus flow rate. A brief description of the methodology for the PBR follows.

Dr. George Maise of Brookhaven National Laboratory performed a one-dimensional heuristic analysis derived from Bussard and DeLauer and applied the Ergun correlation [M-1]. Bussard and DeLauer assumed that

$$p \propto T^{-1}, \mu \propto T^{0.5}, q''' \text{ is flat, and the pressure drop } \left(\frac{dp}{dx} \right) \propto Re^{-\beta} * \rho * V^2 \quad [2-10]$$

where Re is the Reynolds number at the bed inlet (just as the gas has passed through the cold frit):

$$Re = \frac{m D_p}{A_s \mu}$$

m = mass flow rate, D_p = particle or wire diameter, A_s =free stream area, or superficial area, μ = Gas viscosity [W-1].

However, over a broad range of temperatures, the hydrogen viscosity varied as $\mu \propto T^{2/3}$, so Maise needed to develop a new stability criterion. In order to develop the stability criterion, he applied the following inequality:

$$(1+\phi)^{(1+\frac{2\beta}{3})} < 1 - \left(\frac{5\beta-3}{9-3\beta} \right) \phi \quad [2-11]$$

where ϕ is a measure of the heat addition of the gas $(T_{\text{final}} - T_{\text{initial}})/T_{\text{initial}}$, and β is a measure of the flow regime ($\beta = 1$ for laminar flow and decreases to 0 for high Reynolds numbers). To define β , Maise needed to determine the pressure drop behavior. He applied the Ergun pressure drop for packed beds:

$$\frac{\Delta P}{L} = 150 \frac{(1-\epsilon)^2}{\epsilon^3} \mu \frac{U_M}{D_p^2} + 1.75 \frac{(1-\epsilon) U_M G}{\epsilon^3 D_p} \quad [2-12]$$

where ϵ is the porosity, D_p the particle diameter, μ the viscosity, U_M the superficial velocity and G the mass flow rate per unit total area. Since this equation does not contain a Reynolds number, the viscous and inertial terms which characterize the Reynolds number can be modified. In order to do this, Maise defined an effective friction factor f_E :

$$\Delta P = f_E \frac{L}{D_p} \frac{1}{2} \rho U_M^2 \quad [2-13]$$

This expression is similar to the conventional pipe pressure drop equation, except the diameter is the particle diameter and the velocity is the bed

superficial velocity. The above equation ΔP can be equated with the ΔP of the Ergun equation to find:

$$f_E = \left[\frac{300(1-\epsilon)^2}{\epsilon^3} \frac{1}{Re} + \frac{3.5(1-\epsilon)}{\epsilon^3} \right] \quad [2-14]$$

Maise than assumed that the porosity of the bed = 0.37. Then,

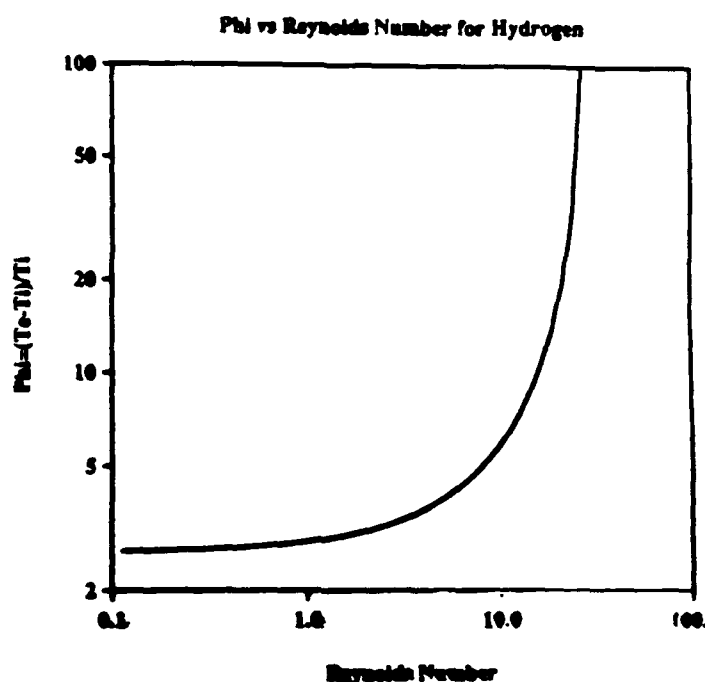
$$f_E = \frac{2350.7}{Re} + 43.5 \quad [2-15]$$

Therefore, when Re is low, the major contributor to the pressure drop is the first term ($\beta=1$).. When Re is large, the first term becomes negligible, and f_E approaches 43.5 and β approaches 0. The β term then can be defined as the negative slope of the $\log f_E$ versus $\log Re$ curve.

$$\beta = \frac{-d[\ln(f_E)]}{d[\ln(Re)]} = \left[\frac{1}{1 + 0.0185 Re} \right]^{-1} \quad [2-16]$$

The equations numbered [2-12] and [2-17] are used to determine the stability regime. For the Reynolds numbers and temperature ratios that lie above the line where the equality of the first equation is met, the flow is unstable. If β is less than 0.6, the inequality of equation [1-12] will be met, and the flow will be stable. If β is greater than 0.6 and the flow is large, the equation predicts an unstable condition. This equation showed that at each flow rate there may be a limiting temperature ratio indicating a flow instability. Figure 2.2.1.1 is a plot of Maise's ϕ vs Re number for hydrogen at a porosity of 0.37. All points above and to the right of the curve represent stable flow, while points below and to the left of the curve represent unstable flow.

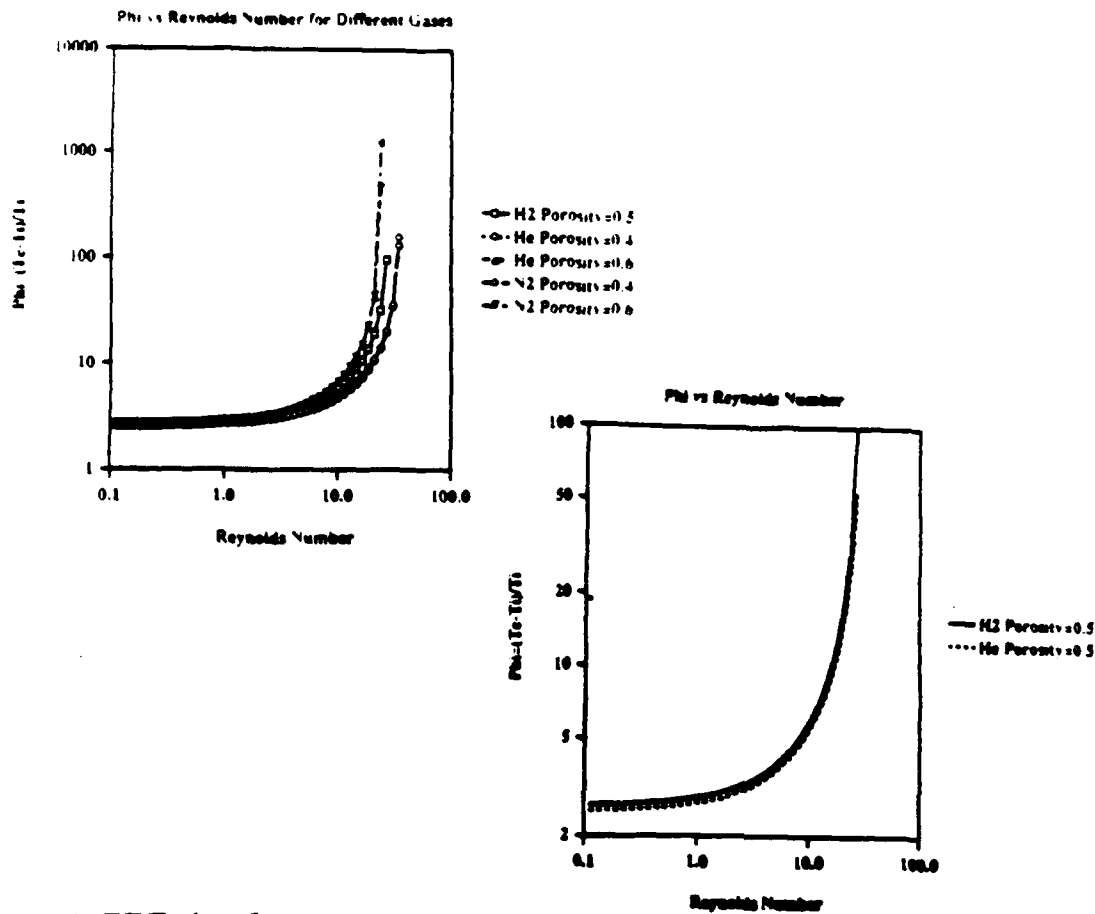
Figure 2.2.1.1 Phi vs Reynolds Number for Hydrogen



As seen from the above relations, the Bussard and DeLauer stability criterion is dependent on the gas properties and bed porosity.

Because of safety considerations, it was determined that nitrogen and helium would be better working fluids to use in the experiment than hydrogen. According to temperature dependent properties taken from W-2, the viscosity/temperature relation for helium and nitrogen are: $\mu \propto T^{0.7}$, and $\mu \propto T^{0.69}$, respectively. These numbers were used to modify the above analysis to find the stability criterion for different gases and bed porosities. Figure 2.2.1.2 shows the comparisons between He, H₂, and N₂ for different bed porosities. This analysis determined that the bed porosity and gas properties are important parameters for the experiment.

Figure 2.2.1.2 Phi vs Reynolds Number for Various Gases and Bed Porosities



2.2.2 PBR Analyses

Other analyses have been conducted to study flow stability in the PBR. Jonathan Witter of MIT expanded upon Maise's analysis [W-1]. He used actual element dimensions and tabulated hydrogen properties to generate a 1-D stability curve by using numerical integration methods. Witter determined at a given q''' and mass flow rate (inlet Re), the enthalpy rise =

$$w \, dh = q''' 2\pi r \, dz \Rightarrow h(r) = h(r_0) + q''' \pi (r_0^2 - r^2) dz/w \quad [2-17]$$

He then applied the Ergun relation for pressure drop with $\rho(p, h)$ and $\mu(p, h)$

to find the pressure:

$$dp(r) = F(r)w^2 dr \text{ and } p(r) = p(r_o) - \sum_{j=r_o}^{j=r} dp(r_j) \quad [2-18]$$

A stability line is then determined by an iteration scheme that increases the mass flow rate until the minimum converged pressure drop is found. The outlet pressure and enthalpy are then used to determine the temperature rise. A set of pressure drops and temperature rise factors can be determined by varying the mass flow rate at a particular heat deposition rate. This procedure was repeated for a series of bed power densities to create a data set of ϕ versus Re values.

Witter's curve is shown in Figure 2.2.2.1. using the fuel region pressure drop within the frits for the stability criterion. The curve is the same shape as Maise's, but higher flow rates are required for stability. It also shows the effect of the number of radial control volumes equal to 1, 5, and 10 (Lines 1R Zone, 5 R Zones, and 10 R Zones). The same methodology was used in this study for the experiment geometry and for He properties (He was used for the experiments of interest to be discussed later). Figure 2.2.2.2 shows the results of Witter's methodology applied to the experimental apparatus. Figure 2.2.2.3 shows the impact of varying inlet pressure and temperature on the stability curve for the methodology (Some inlet condition must be specified, and since the experiments had varying inlet conditions, it was important to show this factor did not have a big impact on the stability curve).

Figure 2.2.2.1 Witter's 1-D Phi vs Re for Hvdrogen From Ref W-1

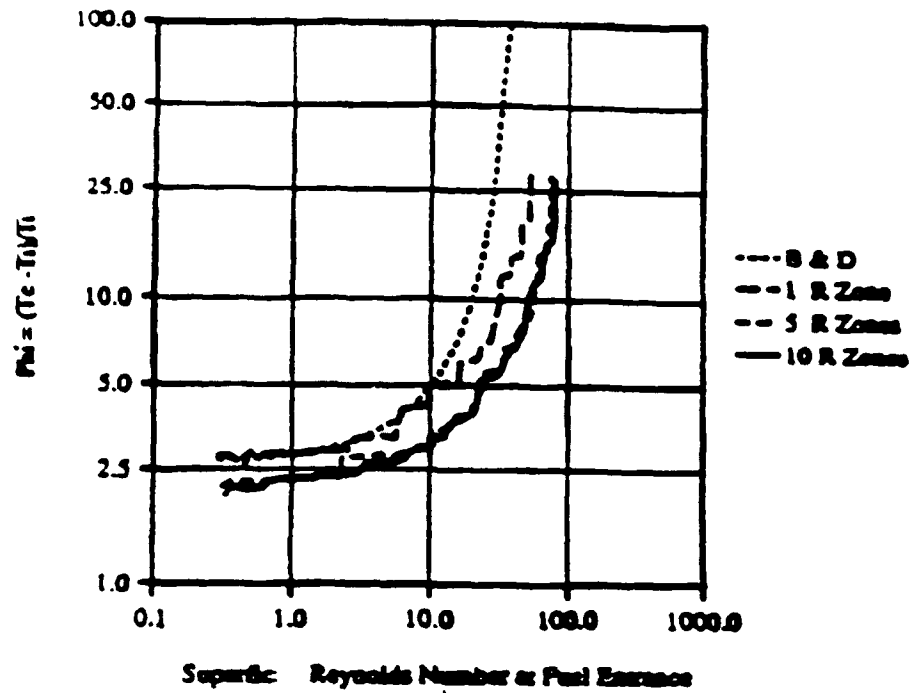


Figure 2.2.2.2 1-D Phi vs Reynolds Number for Experiments

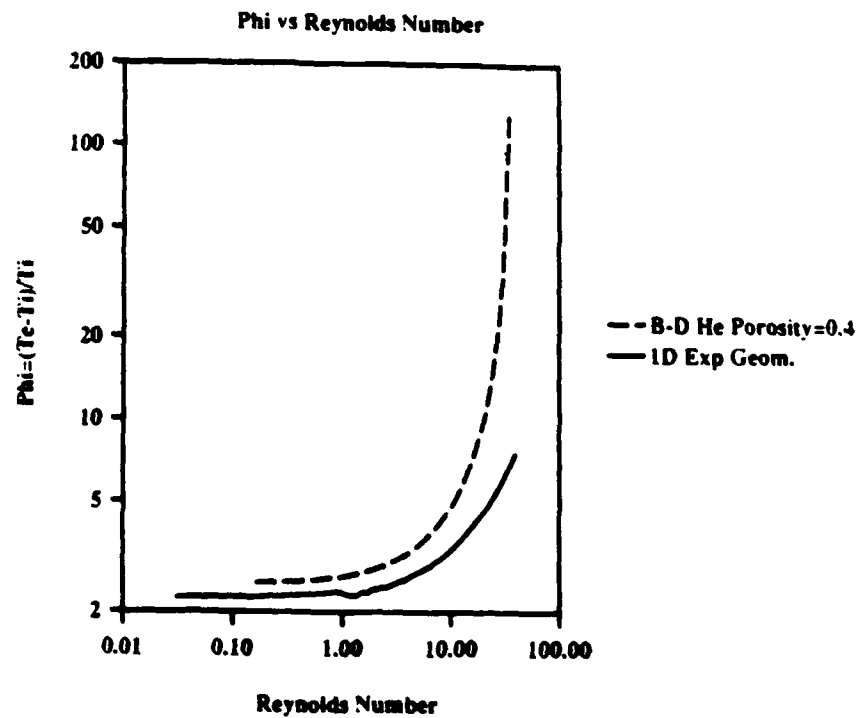
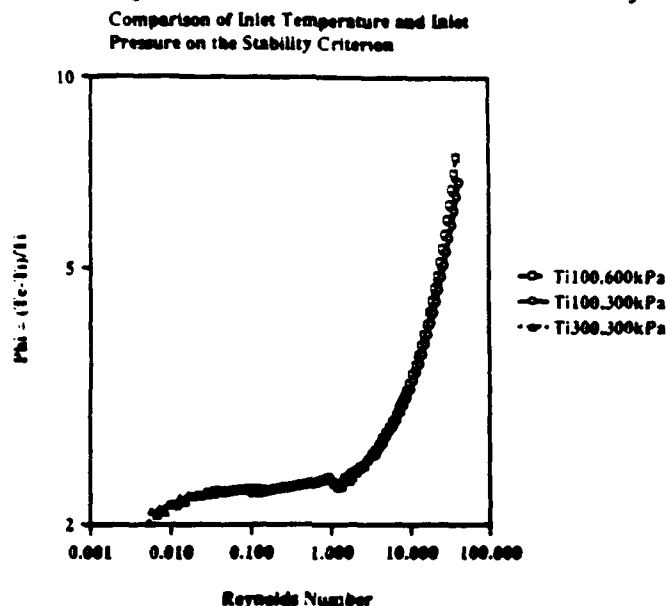


Figure 2.2.2.3 Impact of Inlet Conditions on Stability Curve



Witter also performed some other analyses which are explained in detail in W-1. His conclusions are as follows: (1) If the cold frit resistance is increased, the element stability increases with respect to the total core flow distribution among all fuel elements. This trend is due to the decreasing importance of the fuel region pressure drop as the pressure drop across the cold frit increases. However, this criterion does not provide a good prediction of stability once the flow has entered the bed. (2) Looking at the pressure drop in the bed as the stability criterion, higher flows are necessary to maintain stability. Two-dimensional calculations using different heat deposition rates also confirmed this calculation. (3) Finally, the one-dimensional analysis approach is adequate for defining the stability regions [W-1].

Professor J. Kerrebrock and Mr James Kalamas of MIT have developed a more general three dimensional model of the bed, in which the fluid has mobility in three directions [K-1]. They approached the flow stability issue in three levels : (1) a parallel flow instability; (2) a three-dimensional instability described locally - presents an instability locally as a disturbance harmonic in

space and exponential in time, and asks if such a disturbance will grow in time; and (3) a full three-dimensional instability analyzed with account for inflow and outflow boundary values for the zeroth order variation within the bed - the full stability analysis treats the disturbance as harmonic in distance parallel to the plane of the bed and exponential in time.

Kerrebrock's parallel stream stability was studied by calculating the pressure drop through the bed from the zeroth- order solution:

$$p^2_0 = 1 - \frac{2b_1}{(v+2)q} [(1+qx)^{v+2} - 1] - \frac{b_2}{q} [(1+qx)^2 - 1]. \quad [2-19]$$

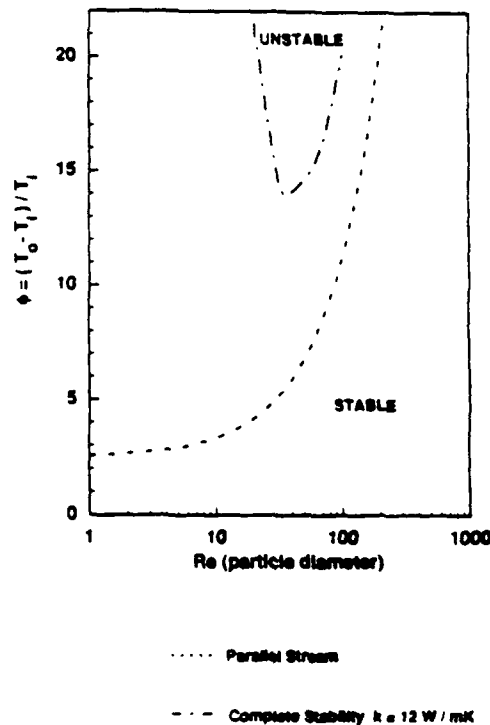
If the pressure drop decreased with increasing flow, for constant volumetric heat addition, this is an indication of possible instability (in a manner similar to the one's described above). Kerrebrock stated that this is not a firm criterion due to the fact that the flow can distribute laterally in the bed.

Jim Kalamas ran a case using the above methodology for the experiment geometry with He as the working fluid. His plot is shown in Figure 2.2.2.4. The differences in the curves is due to the effective thermal conductivity of the bed. The thermal conductivity curve shows much more stability than the parallel stream curve due to the higher thermal conductivity in the screen bed (higher thermal conductivity removes the heat to mitigate instabilities).

Figure 2.2.2.4 Parallel Stream Stability Map From Ref K-2

PARTICLE BED REACTOR STABILITY BOUNDARIES
COMPLETE STABILITY ANALYSIS
FIT TEST for He

$$k_y = k_z = 1 / \text{cm}; d^2T / dx^2 = 0; p_1 = 7.4 \text{ atm}$$



Kerrebrock's analysis is discussed fully in K-1. His analysis gives the following conclusions: (1) a PBR without a cold frit would be subject to instability if operated at the high temperatures desired for nuclear rockets, and at power densities below about 4 MW/L. Since the steady state power density is about 40 MW/L, operation at exit temperature and reduced power could cause difficulties. (2) An appropriate cold frit could cure the instability. (3) More definite conclusions must await calculations for specific designs [K-1].

2.3 TESTING APPROACHES

2.3.1 Screen Bed

The above analyses have shown that flow stability is a concern for the PBR, specifically at low flows and ϕ 's above 2 (depending on which analysis and which parameters are involved) until the Reynolds number is $> \sim 20$. These analyses have shown the need to conduct experiments to verify the analyses or to show that the instabilities do not exist. The goals of a flow instability experiment are to demonstrate unstable flow and establish the existence of points on the line of demarcation. The experimental apparatus chosen for this investigation was an electrically heated, insulated, stainless steel screen bed. It was decided to conduct these experiments at Brookhaven National Laboratory due to availability of lab space, equipment, and technical expertise.

The insulated stainless steel screen bed was chosen for its flexibility and relatively low cost. The electrical power could be put into the stainless steel mesh to generate internal heat similar to nuclear heating of the fuel in the PBR. A screen mesh was found with the wire diameter and spacing to give the element a porosity $\sim 0.35 - \sim 0.40$ once the insulated coating was placed on the mesh. The hot and cold frit were made of 304 stainless steel and were sintered to the desired porosity (~ 0.30). Other equipment items needed in addition to the screen and frits are as follows: containment vessel, power supply, gas flow system, chill down tank, instrumentation, and a data acquisition system. Thermocouples at the bed inlet, middle of the bed, and outlet would determine the temperature profile of the bed. Analyzing the temperature profile, mass flow, and pressure will determine if there is stable or unstable flow. The limitations of this approach are : (1) local electrical power fluctuations could occur in the bed and not be detected, (2) local

porosity variations could occur from non-uniformities in the insulation coating, (3) an insulation material is needed to prevent electrical shorts and allow enough heating in the bed, (4) and the higher thermal conductivity of the s.s screen may not allow instabilities to develop. The detailed description of the experimental apparatus is discussed in Chapter 3.

2.3.2 Other Experiments

Another approach to conduct flow instability tests would be to use an existing test reactor and not have to worry about "simulated" nuclear heat generation. The ACRR at Sandia National Laboratory would be a candidate facility. The problems with this approach for the first test series is that the facility would be expensive. Nuclear tests are needed, but not for the first generation of experiments. Every successful reactor development program has had a series of "in pile" and "out of pile" experiments. The approach has been to conduct the "out of pile" experiments first, in order to learn as much information as possible (since "out of pile" experiments are cheaper due to less stringent safety requirements, easier access to the test apparatus and facility, and no need for elaborate fuel design and post-experiment handling) and then use the knowledge (thermal-hydraulics, materials, etc) to proceed to the "in pile" experiments and full-scale design. This same testing approach is described in B-1.

There are other methods to generate internal heat. Microwave heating is one such approach. The problem with this approach is finding materials with the proper thermal conductivities. High thermal conductivity materials arc and do not get enough power into the gas; low thermal conductivity particles may melt before reaching the desired power level. Professor Kerrebrock has a

student working on this type of experiment. Their approach has been to use silicon carbide balls packed in a bed with a chill down system for the inlet gas in a 1 kW oven. The gas is passed in and expands through a tube packed with a solid bed of silicon carbide balls. An infrared camera is used to study fluid flow/heat transfer. The latest results showed there may be an issue with non-uniform heating in the oven. The research is still ongoing.

Another approach planned at Brookhaven National Laboratory is to use big (2 cm diameter) copper or other high conducting material balls with small electrical heaters connected together with wire. Electrical power has been supplied to one of the balls, and the temperature drop across the ball is minimal. The experiment is still in the conceptual stage (investigating the proper configuration for the placement of the balls, developing insulators for the balls touching the containment vessel, obtaining cold frit designs for the inlet to the bed, determining thermocouple placement, and establishing hot wire placement for flow velocity profiles). This approach is planned as a next generation experiment after the experiment conducted under this investigation.

This Chapter discussed the benefits of using a PBR for a broad range of space missions. It also described the design of the system, which lead to the introduction of the flow stability issue. Several different flow stability analyses were discussed. These analyses were then applied to the experimental geometry, and porosity with the use of helium properties. These analyses generated stable / unstable regions based on the Reynolds number and ϕ . The regions were used as input for setting test variables. The screen bed was compared to other designs and it was shown that the design was a good first generation experiment.

CHAPTER 3

EXPERIMENT DESIGN

3.1 SCREEN BED

3.1.1 Frits

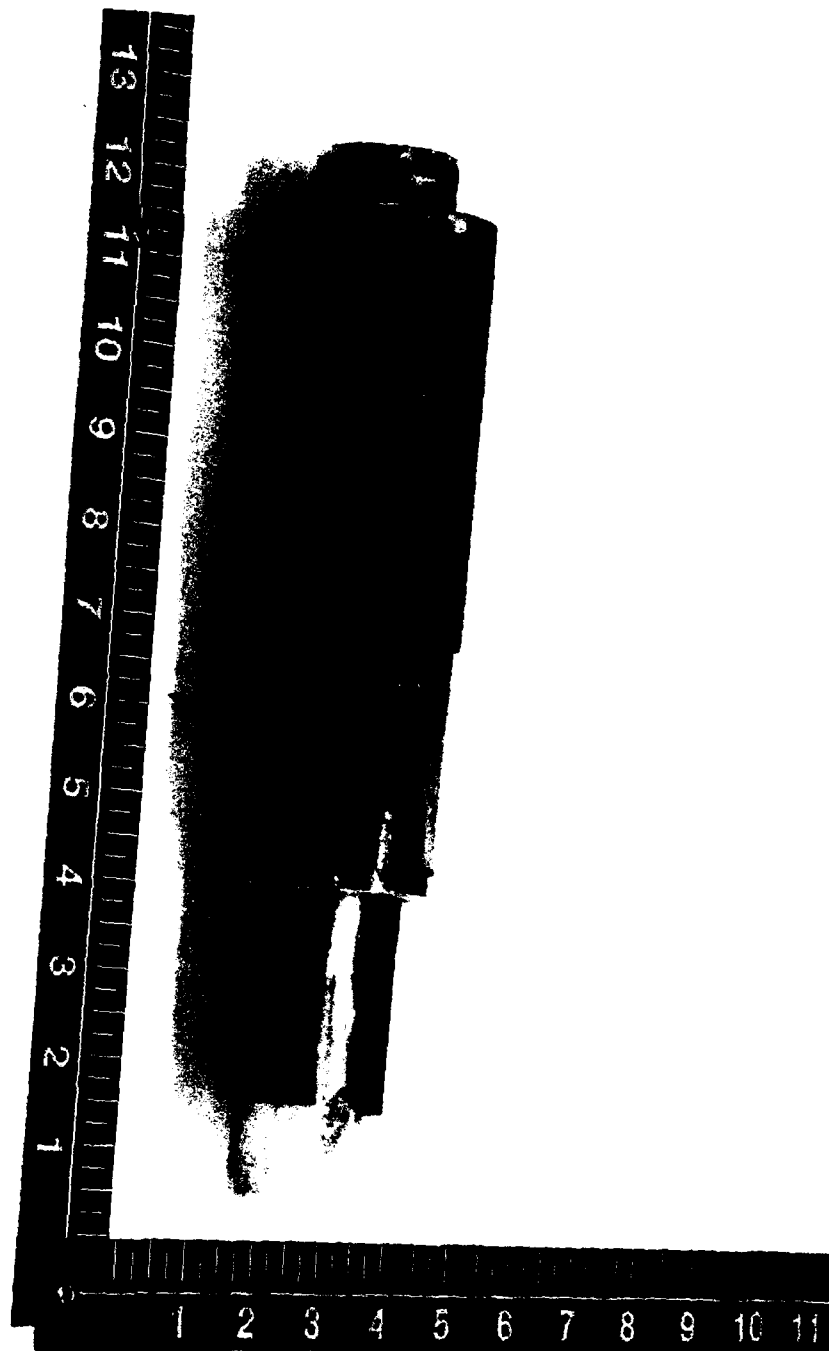
The cold frit is a porous cylinder made of 304 stainless steel. Its dimensions are 10 cm long, with a 6.3 cm outer diameter by 6.0 cm inner diameter (see Fig 3.1.1.1 for a detailed drawing of the element assembly). The porosity of the frit is ~ 0.30 . The frit is made porous by sintered metal technology. It is laid flat and hot pressed as part of the sintering process. The frit then is welded together to form a cylinder. The seam created from the weld is not porous. The seam extends down the middle of the cylinder for the entire length, and is approximately 0.3 cm wide (see Fig 3.1.1.2, for a picture of the element).

The hot frit is a porous cylinder also made of 304 stainless steel. Its dimensions are 30.5 cm long, with a 3.8 cm outer diameter by 3.5 cm inner diameter. The porosity of the hot frit is also ~ 0.30 and is manufactured the same way as the cold frit with a 0.01 cm wide seam.

Drawn by Bob Sick at BNL

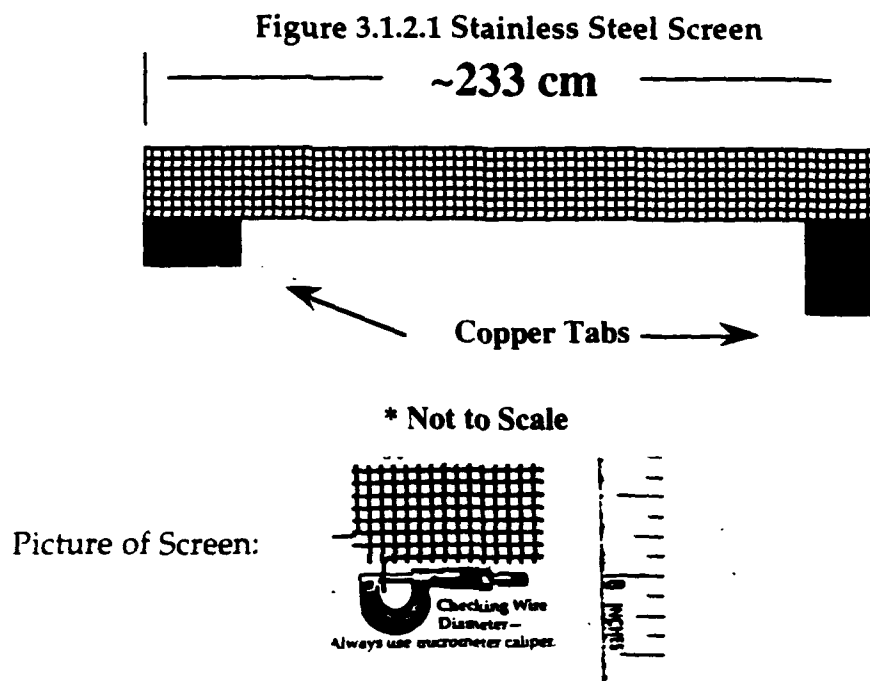


Figure 3.1.1.2 Picture of Screen Bed Element



3.1.2 Screen

The 316 stainless steel screen is shown in Figure 3.1.2.1. The screen is approximately 233 cm in length. It is designed to fill the volume between the hot and cold frits at a porosity ~ 0.35 to ~ 0.40 .



The copper tabs shown were designed in two fashions. First, solid copper was cut out and welded to the screen. Second, the screen was cut to include the tabs and a copper coating was applied (The later procedure was used on a majority of the experiments and the coating is shown in Fig 3.1.1.2). The copper tabs were needed to carry the current to the bed by way of the electrode blocks connected to the power supply .

There were several candidate materials considered for the screen. The major requirement was that the screen mesh be made of conducting material (Table 3.1.2.1 shows the materials considered).

Table 3.1.2.1 Materials Considered for the Screen Mesh

Property	.S.S	Graphite	Alloy 625 Hast. C.	Nichrome
Resistivity ($\mu\Omega$ cm)	70	800	130 -140	100
Available	Y	N	N	Y
Insulation Required	Y	N	Y	Y
Porosity	OK	NO	OK	OK
Reaction with Gas (He)	OK	OK	OK	OK
Cost	OK	High	High	High

As shown in Table 3.1.2.1, graphite offered the best resistivity, but after consultation with several vendors, could not be developed in a reasonable time and was cost prohibitive. Two vendors did send samples that were analyzed. One of the samples was woven into a grid similar to Figure 3.1.2.1, but was a cloth-like material (too flimsy - issues with packing into the frits and connecting to the electrodes). The other sample was a porous tube, with a density and material structure similar to Styrofoam (see Figure 3.1.2.2 for a sketch).

Figure 3.1.2.2 Graphite Tube



This tube was too porous and the wave-like orientation of the fibers would not create the desired flow effect. The sporadic orientation of the fibers also could cause current flow problems. The vendors said they would need time and money to make a screen that could be used, so graphite was not considered as a material option.

The alloy 625 (hastalloy carbon) offered the second highest resistivity of the materials considered, but could not be fabricated into a screen mesh by the vendors.

The Nichrome wire offered the next best resistivity, and could be fabricated by a vendor. The problem was that it was expensive and required time to fabricate. Therefore, it was determined that stainless steel would be the best material to pursue.

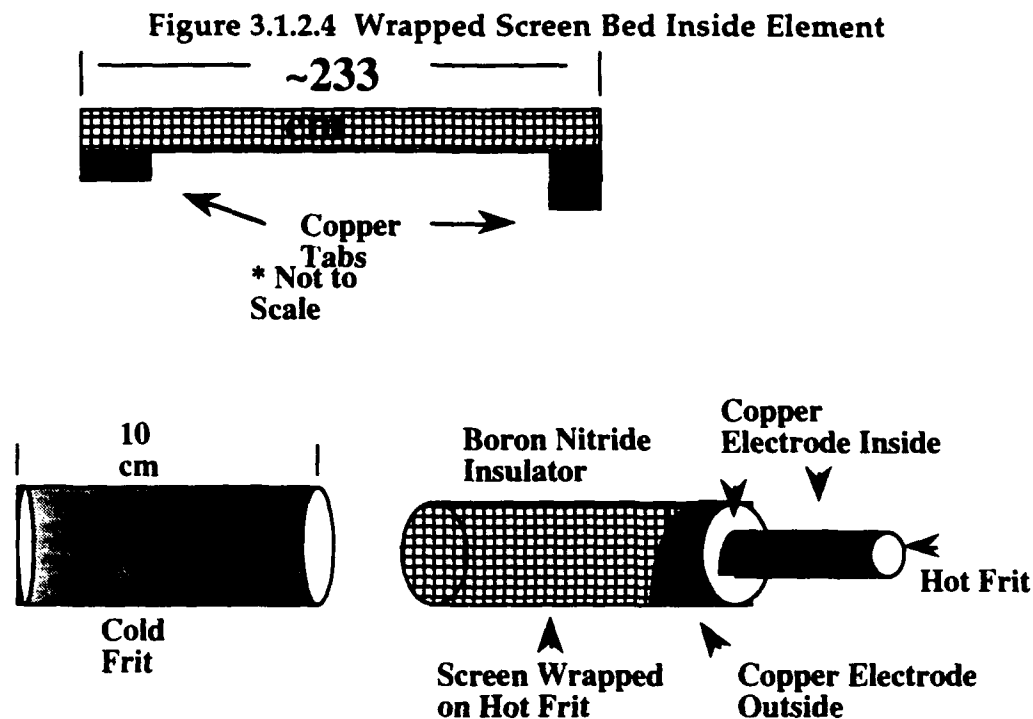
The 316 stainless steel was woven into a screen mesh by Newark Wire Inc. The mesh chosen specified a 30 mesh/inch (1.18 mesh/mm) with a wire diameter of 0.33 mm and a .52 mm width of opening between wires (see Figure 3.1.2.1 for an orientation of the wires). The porosity of this screen was ~ 50 %.

In order to get enough power into the gas while preventing the bed from shorting out, and also insulating the frits, an insulating coating was needed across the screen. All parts of the screen were coated with insulating material except the copper tabs. It was also discovered that a copper coating was needed on the screen ends in order to prevent hot spots on the edges of the screen. It was an arduous task to find a ceramic and copper coating that could prevent hot spots and properly insulate the screen. This subject is discussed in Appendix A. The final screen design chosen that achieved the best test results is shown in Figure 3.1.2.3. The ends were etched in aquaregia (in order to have an even coating on the screen, see Appendix A), ends and tabs copper electroplated, and the entire screen (except the tabs) insulated with a cured alumina adhesive that was painted onto the screen. Due to coating temperature limits (swelling - see Appendix A), the maximum temperature the screen could operate was 700 °C. This temperature would give a ϕ of ~8 which allowed the apparatus to go into the unstable region from some of the analyses mentioned in Chapter 2. The final porosity of the coated screen was ~0.37 for the tests (see Appendix C).

The diagram illustrates the experimental setup for the electroless deposition of copper on a wire. A cross-sectional view at the top shows a central **Wire** surrounded by a layer of **Painted Alumina**. The main view is a side cross-section of the assembly. A central horizontal tube, labeled **~233 cm** in length, is shown with a grid pattern representing the copper coating. This tube is flanked by two vertical end pieces. Dimensions are provided for the components: the central tube has an outer diameter of **5.08 cm** and an inner diameter of **18.4 cm**. The end pieces have a width of **12.1 cm** and a height of **25.4 cm**. A section of the central tube is indicated by a double-headed arrow and labeled **Cut to copper Coating** with a length of **185 cm**. A note at the bottom states *** Not to Scale**.

54

some of the assemblies (see Figure 3.1.2.4 for a drawing of the screen wrapped into the frits).



Several insulating materials were used very close to the assembled bed (see Fig 3.1.1.2). Ceramic paper was wrapped around the hot frit to prevent the hot frit from carrying current, especially in the upper region near the smaller tab. The tab was connected very tightly to the electrode blocks. A short was detected on the hot frit if the paper was not applied. A boron nitride cylinder was also placed close to the cold frit for insulation of the bigger tab. The cylinder was 7.6 cm long, and since boron nitride is a "chalky" substance, the diameter could be modified to fit snugly over the hot frit and other tab. The cylinder was inside the cold frit flush with the bed. This insulator had an

important role, it had to insulate the big tab from making extra contact with the bed and cold frit, and had to prevent interaction with the other tab.

Both ends of the bed array were sealed. The top end (top of Fig 3.1.1.2) was sealed with ceramic paper and the boron nitride cylinder on top of it. In order to prevent gas leaks, an RTV sealant (silicon sealant) mixed with Zircar boron nitride powder was applied between the ceramic paper and the boron nitride cylinder. The boron nitride powder was added to the RTV to increase the melting point / swelling properties. The optimum mixture was determined by mixing the materials and placing them under heat (propane torch) to monitor material degradation. The torch was placed on the material for several seconds in several passes lasting about a minute. The material showed no degradation and was used as a sealant. At the lower end of the bed, ceramic paper, Al temperature twine, and the above sealant were used between the end of the bed and another boron nitride plug (see Fig 3.1.1.1). Determining the proper sealing was an evolutionary process, and is discussed further in Appendix A.4. Other parts were connected to the screen bed and frits and will be discussed in other sections of this chapter.

3.2 SCREEN BED SUPPORT STRUCTURE

3.2.1 Inner Vessel and Seals/Insulators

A series of containment pieces were needed to minimize pressure losses through out the system. Pieces were also needed for sealing and insulation. The assembly can be broken down into the inner sealed region, and outer sealed region. The inner sealed region can be described through Figure 3.1.1.1.

The best way to describe the pieces will be to go across the assembly from bottom to top.

At the bed outlet, a boron nitride plug was sealed to the manifold. The bed rested against the boron nitride plug. It was not securely sealed (glued or welded) due to the need to remove the bed after assembly and the expected frequent use of the plug for new bed experiments. The plug attached to the manifold provided a seal to the bed and insulated the cold frit (see Figure 3.2.1.1 for a picture of the bed attached to the manifold).

Figure 3.2.1.1 shows some pipes surrounding the element. These pipes provided the inlet flow to the element and will be discussed in Section 3.3. Looking at the manifold, three holes can be seen at the bottom. These holes were used to mount the electrode blocks. The 4 mounts (one hole can not be seen) were long screws which extended from the two blocks and attached to the manifold. Figure 3.1.1.1 shows these mounts (tie rods).

The bed was surrounded by an inner vessel. The main purpose of this vessel was confinement if problems occurred in the bed. It also provided heat containment. It was not 100 % sealed, but did not have to be since the outer pressure vessel was 100 % sealed. The vessel was a cylinder made out of 304 s.s. with a diameter of 12 cm and was 14 cm long. The thickness of the cylinder was 0.6 cm. The bottom side of the vessel was attached to the manifold. A groove the same thickness as the vessel was used to secure it in this location (see Figure 3.2.1.1). The top of the vessel was more intricate. A lid was attached to the top of the vessel. The lid was attached to the vessel with a groove similar to the bottom attachment. The lid was made of s.s., with the middle section having four holes with boron nitride bushings in each hole for insulation. These holes were needed for the tie rods which mount the electrode blocks to the bottom manifold. The boron nitride

bushings were inserted to insulate the vessel from the electrode blocks. Two pieces of ceramic paper were used to rest on top of the lid. This paper was used to insulate the lid and vessel from the electrode block since the electrode block rested on it (see Figure 3.2.1.2 for a picture of the vessel attached to the assembly).

Other support structure shown in Figure 3.2.1.2 are the electrodes, an insulator ring, and inner connection tube. The inner connection tube is used to connect the hot frit to the outer pressure vessel. The connection to the hot frit included a boron nitride plug for insulation and to seal gases from escaping out of the bed (see Figure 3.1.1.1 for the end plug). This plug was located just past the top electrode. Figure 3.1.1.1 and 3.2.1.2 also show a boron nitride insulation ring which was used to insulate the two copper electrodes from each other. The inner connection tube (made of s.s.) then continues to the outer pressure vessel. It rests against the outlet pressure vessel and continues past the outer pressure vessel where a s.s. plug is used as a second seal to the gases. The threads of the screw were also coated with boron nitride liners for insulation. The outer pressure vessel will be discussed in the next section.

Figure 3.2.1.1 Picture of Screen Element Connected to Manifold

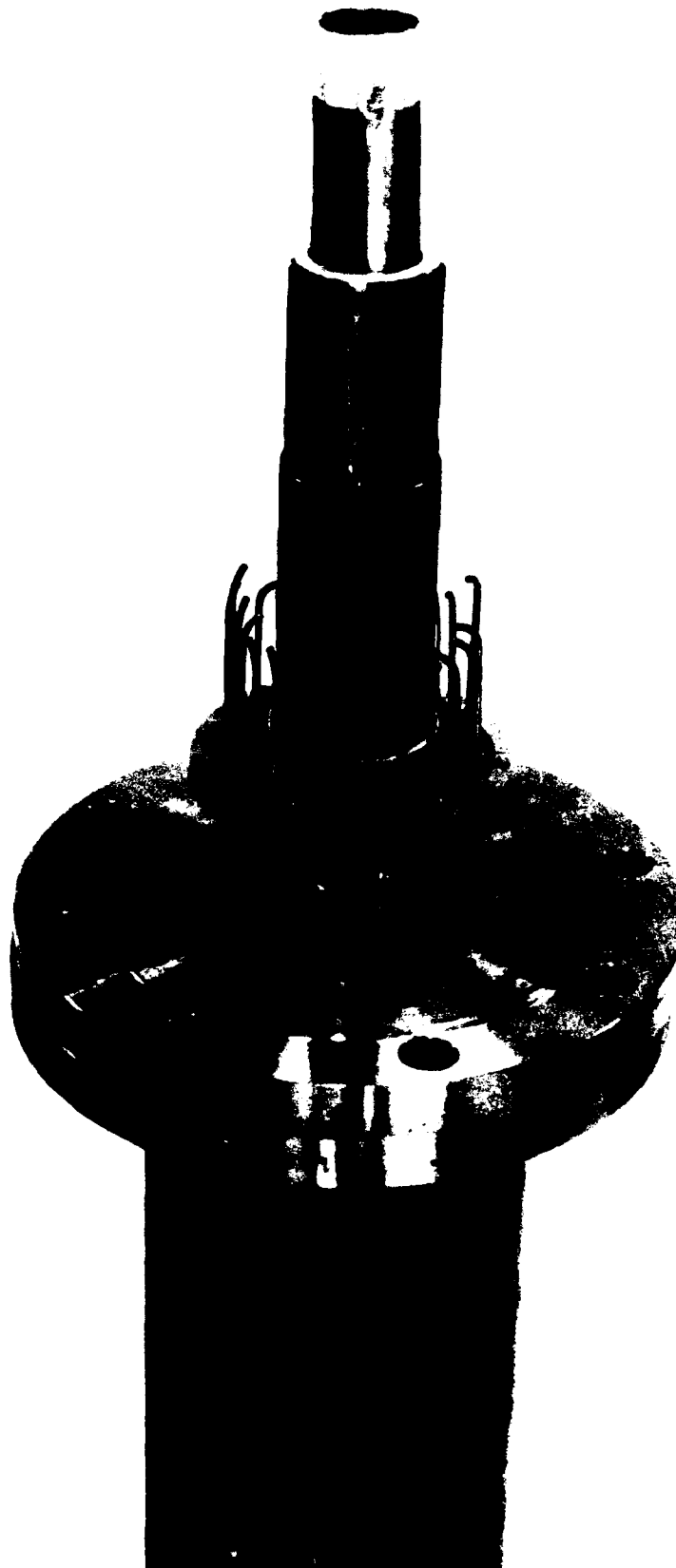
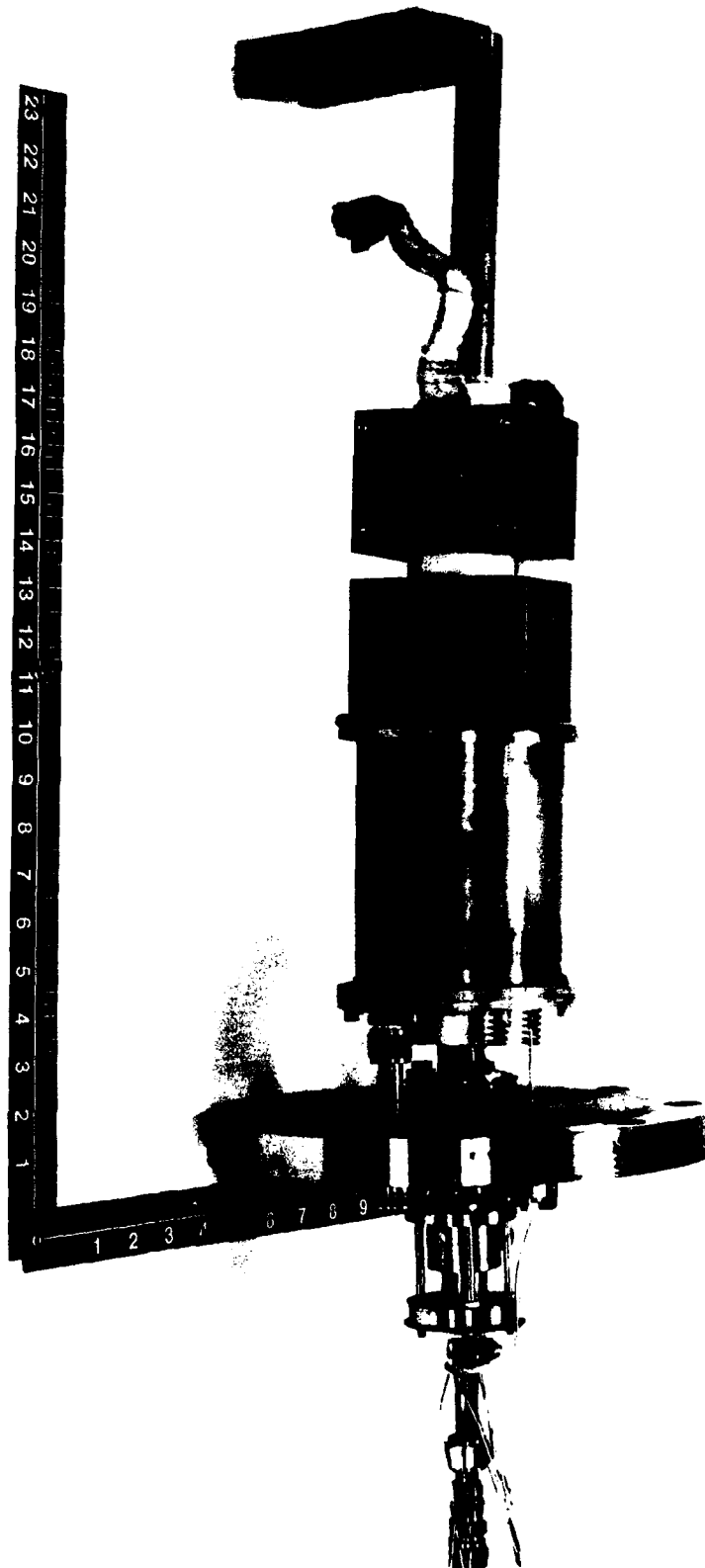


Figure 3.2.1.2 Picture of Element Assembly



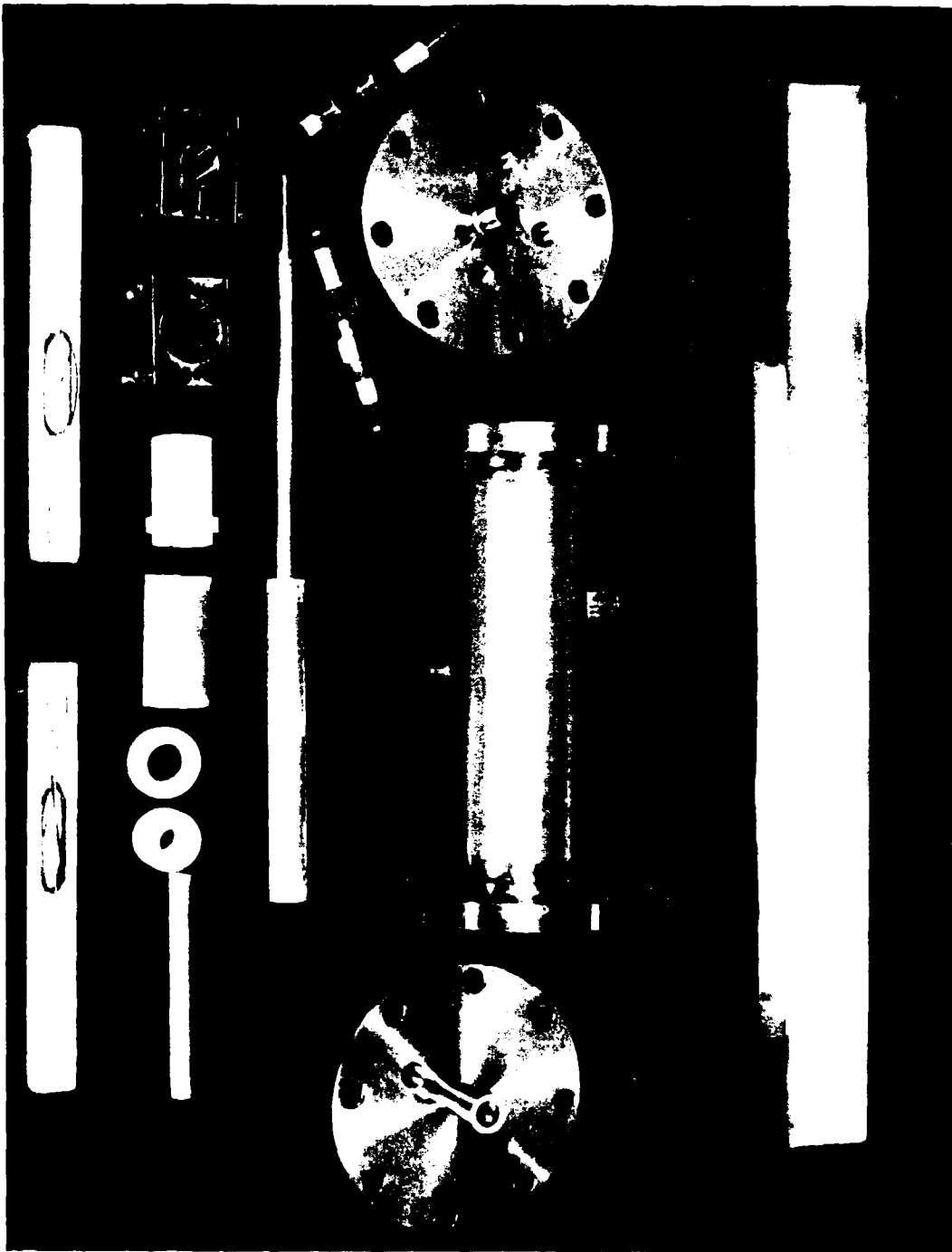
3.2.2 Outer Pressure Vessel and Seals

A picture of the outer vessel is shown in Figure 3.2.2.1 (in the middle of the picture). This vessel is used primarily for pressure confinement (100 % sealed). It is also used as a second defense if the inlet vessel can not contain problems in the bed. The vessel is made of stainless steel and was rated to 1020 kPa. The vessel dimensions are 53.34 cm long (including flanges), 10.16 cm diameter, and 0.635 cm thick. The flanges are 2.54 cm thick with a 13.34 cm diameter.

The flanges are used to seal the vessel. The left flange (Figure 3.2.2.1) is used at the bottom end of the bed assembly. The two holes in the middle of the flange are for the gas inlet and outlet. The right flange is used at the top of the bed for connections of the electrodes to the terminals. The two holes to the left and right of the middle are used for this requirement. The middle hole is used for support of the pipe connected to the bed. The fourth hole is used for a pressure relief valve. This valve is set for the max load to the pressure vessel of 1020 kPa. The eight outer holes on both flanges are used to connect the flanges to the vessel. The diameter of the bolts for these holes is 0.71 cm. A thin liner is placed between the flanges and vessel as an extra seal. The bolts are then torqued to 102 Nm, to complete the connection.

A pressure transducer was placed on the top of the vessel to measure vessel pressure. This pressure was used as the inlet pressure to the cold frit (see Figure 3.2.2.1).

Figure 3.2.2.1 Outer Pressure Vessel



3.3 FLOW CONTROL SYSTEM

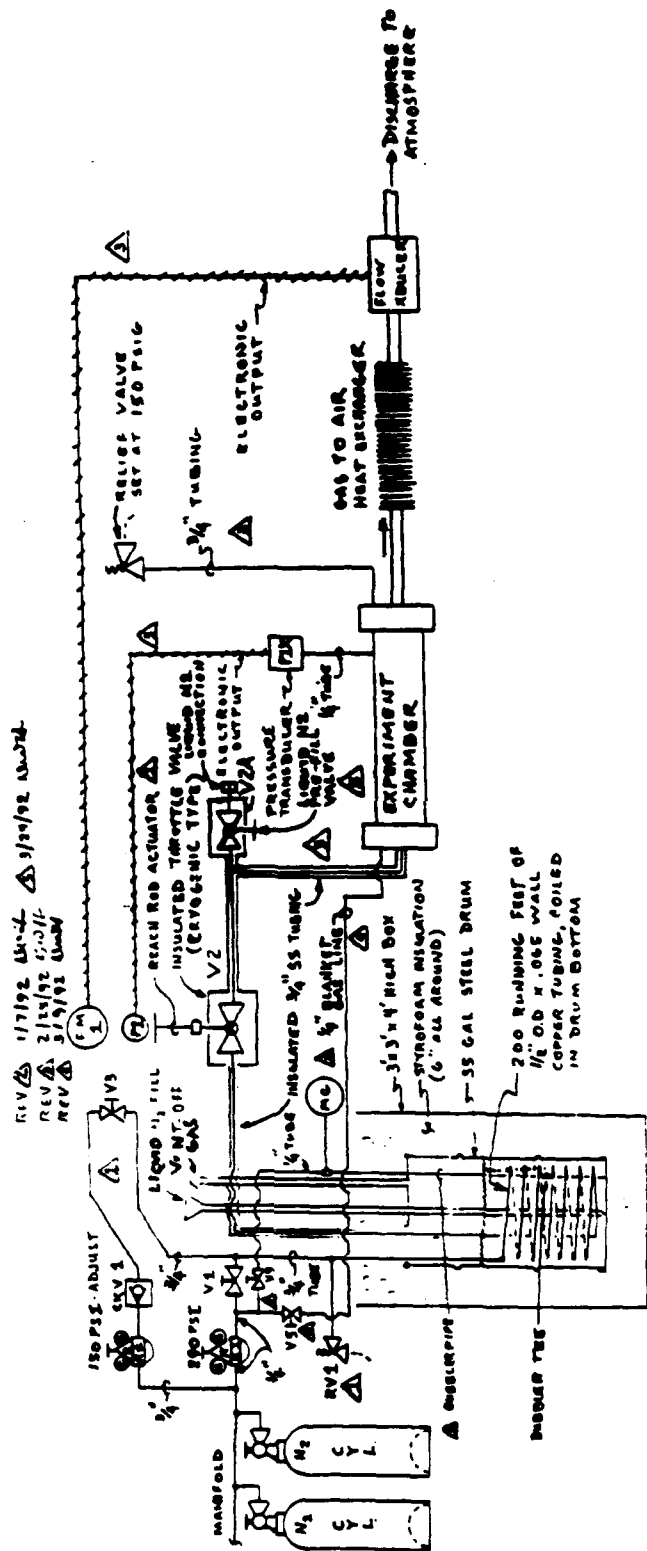
3.3.1 Inlet/Outlet Flow Control

Figure 3.3.1.1 shows a schematic for most of the flow system for the experiment. The gas enters the system from a manifold of cylinders or the tank farm (Depending on the working fluid, this system is discussed in the next section). The inlet flow is regulated at 1020 kPa. This is the max setting of the regulator and this pressure was set for every experiment. The flow then leaves the regulator and goes through the chill down refrigerator. It then enters the experimental apparatus, flows through the bed and is expanded out of the apparatus. The gas then goes through another chill down tank, through a heat exchanger, through the flowmeter, and then is discharged into the atmosphere.

The pressure transducer located at the outer pressure vessel was used as the indicator for bed inlet pressure. This pressure could be changed by adjusting a valve just aft of the assembly to create a higher back pressure in the vessel area.

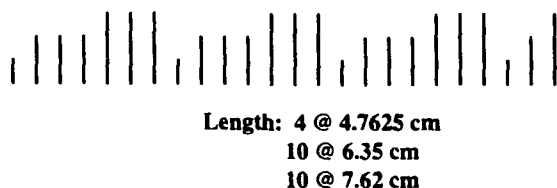
Figure 3.3.1.2 displays the 24 tubes attached to the bed inlet manifold. The diameter of each tube is 0.32 cm. Figure 3.3.1.2 shows a picture of the length of these tubes. The tubes were added to provide better flow to the bed. The tubes were added and pre-tested to determine the best configuration for providing flow across the element.

Figure 3.3.1.1 Gas Flow System Drawn by D. Huszagh



LEGEND	
R1	NITROGEN PRESSURE REGULATOR, SET AT 290 PSIG
R2	" " " " 150 PSIG
CV1	1/2" HIGH FLOW, BUBBLE TIGHT CHECK VALVE
V3	SYSTEM CHARGING STOP VALVE
V2/V2A	1" THROTTLING TYPE CRYOGENIC GLOBE VALVE (BUTTERFLY)
V1	1/2" GLOBE VALVE FOR STOP & THROTTLING SERVICE
PI	0 TO 300 PSI PRESSURE INDICATOR
FM1	REMOTE DIGITAL FLOW INDICATOR
RV1	1/2" ADJUSTABLE RELIEF VALVE - SET AT 300 PSIG
RV2	1/2" " " 150 PSIG
RV3	1/2" NEEDLE VALVE FOR BUBBLE CONTROL BLANKET GAS
MC	MACHINIC GAUGE - 0 TO 10" H ₂ O LL MEASUREMENT

Figure 3.3.1.2 Pipes for Inlet Flow to the Bed



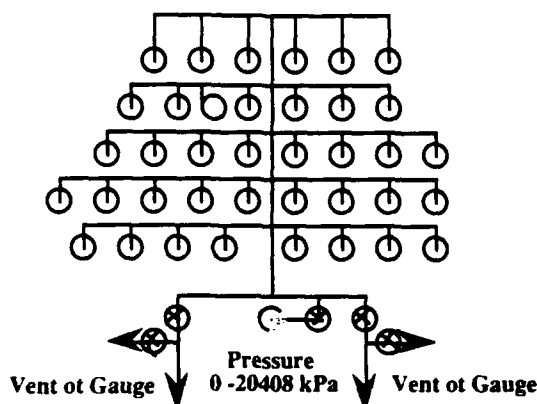
The flow control to the system was controlled by the inlet regulator and valve aft of the bed. The inlet regulator was opened fully and pressure was adjusted by the valve aft of the bed. The flow and pressure were then balanced to the desired setting using the flowmeter and pressure transducer.

3.3.2 Tank Farm

There were two cryogenic tanks filled with liquid nitrogen for the chill down system used to cool down the inlet gas to create a higher phi. The first tank used was a 1136 L LN₂ dewar. The tank was fastened to a small trailer so it could be picked up and filled quickly. This dewar was located ~ 30 m from the experiment apparatus. Its purpose was to fill the chill down tank and the other liquid nitrogen tank (A metal hose was used for this task). The other tank was located 1 m from the apparatus and had a 160 L LN₂ capacity. The purpose of this tank was to cool the bed with liquid nitrogen. After trial-and-error, it was determined that the bed achieved the lowest inlet temperature if liquid nitrogen was pumped directly into the apparatus for ~ 5 to 10 minutes, then was shut off, and the gas through the chill down tank was started.

The He gas tank farm is quite extensive. Figure 3.3.2.1 shows the tanks used for the experiments located on top of a flat bed truck.

Figure 3.3.2.1 Helium Tanks

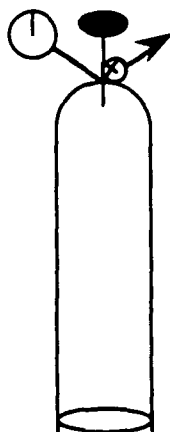


There are 38 tanks on top of the flat bed truck. The volume of each tank is 41,064 L. Usually two tanks would be opened for each run. The tank farm lines are opened to allow gas flow through the regulator (opened fully) and then through 1.905 cm diameter s.s. pipe to the inlet regulator to the experimental apparatus. The gas travels through ~ 25 m of pipe until it gets to the inlet regulator.

This tank system has been selected due to the expected need for long run times for flow stability tests, reduced handling cost, no interruptions, and greater control. The volume of a 1A cylinder is 7278.24 L (see Figure 3.3.2.2 for drawing of a 1A cylinder). If the system had 1A cylinders, a calculation shows $(41,064 \text{ L} \times 38) / 7278.24 \text{ L}$ that 214 1A cylinders would have to be used for the same volume.

In some of the early experiments, GN_2 and air were used as the working fluids. Several 1A cylinders were connected to a 1.905 cm diameter s.s. pipe that was connected to the inlet regulator to the apparatus for the gaseous nitrogen experiments. An air compressor was connected to the inlet regulator by a rubber hose (1.905 cm diameter) to provide air flow.

Figure 3.3.2.2 1A Cylinder



3.3.3 Chill Down Tank

The chill down tank was used as a refrigerator to lower the temperature of the gas to the bed. Figure 3.3.1.1 showed the design of the refrigerator. The key parameter in the design of this system was the use of existing/cheap materials. The 208.2 L drum was used as the volume for the liquid nitrogen since it was available from another experiment. The 1.27 diameter cm copper tubing came from a vendor in 1524 cm length coils. Calculations were performed to determine the volume of gas in the coils depending on the pressure for 20 °C and the volume of gas at reduced temperature (see Figure 3.3.3.1 and 3.3.3.2). The 4 - 1524 cm coils were determined as an adequate configuration. The amount of Styrofoam insulation added was enough to completely surround the drum and fit into a location in close proximity to the bed (to minimize losses in the lines). Evaporation losses were small enough that the tank would last all day for runs in the summer. A check out of this system revealed that it could maintain low inlet temperatures throughout an experiment.

Figure 3.3.3.1 Chill Down Calculations From D. Huszagh

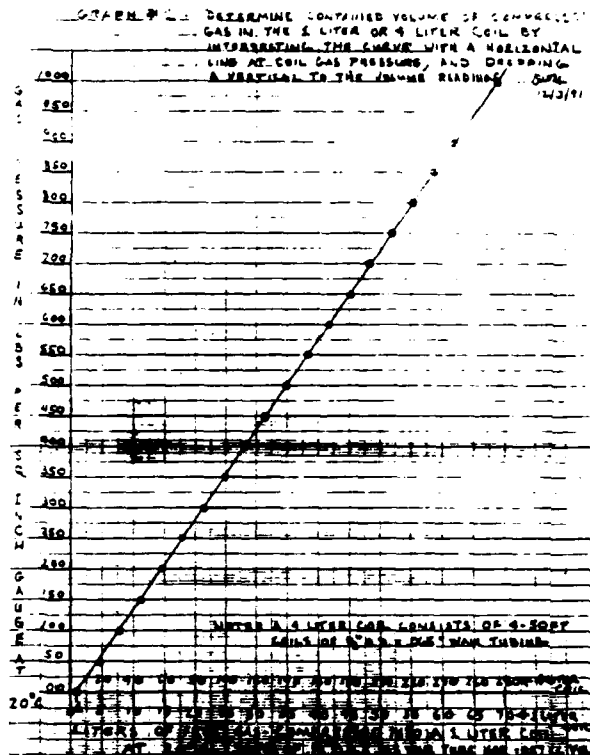
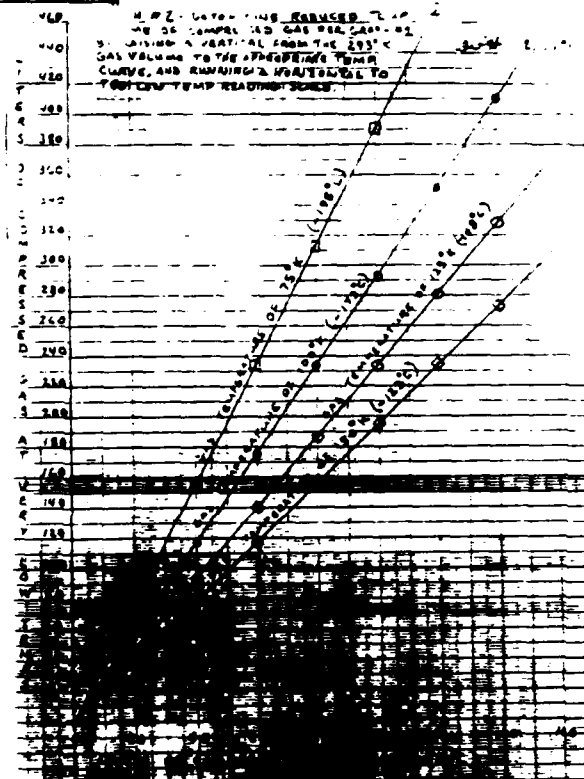


Figure 3.3.3.1 Chill Down Calculations From D. Huszagh



3.3.4 Piping

Most of the piping in the flow system was 1.905 diameter s.s. Insulation was wrapped around the piping coming out of the chill down tank and continued around the piping into the bed inlet (see Figure 3.3.1.1). Valves V2 and V2A were closed while the chill down tank was filled and when the liquid nitrogen was placed directly into the vessel from the 160 L LN₂ tank. The pipes were checked for leaks prior to each test.

3.3.5 Flowmeter

The mass flowmeter is a Matheson Model 8100 - 04XX Mass Flowmeter [M-2]. The flowmeter consists of a flow sensing transducer, a digital readout box containing a digital tube display, and the transducer-to-readout box connection cable. The technical specifications are as follows:

Material:	stainless steel 316
"O" ring seals:	vilton
Max. working pressure:	10000 kPa
Temperature range:	0-50 C
Accuracy:	+/- 1% per C
Temperature coefficient:	< 0.1 % per C
Response time:	6 sec to 90% of scale, 10 sec to 99% of scale
Flow capacity:	0.2 ccm to 1500 lpm

The mass flowmeter transducers consist of an electrically heated tube and an arrangement of thermocouples to measure the differential cooling caused by a gas passing through the tube. Thermoelectric elements generate a DC voltage which is approximately proportional to the rate of mass flow of gas through the tube. The reading depends only on the mass flow and heat capacity of a

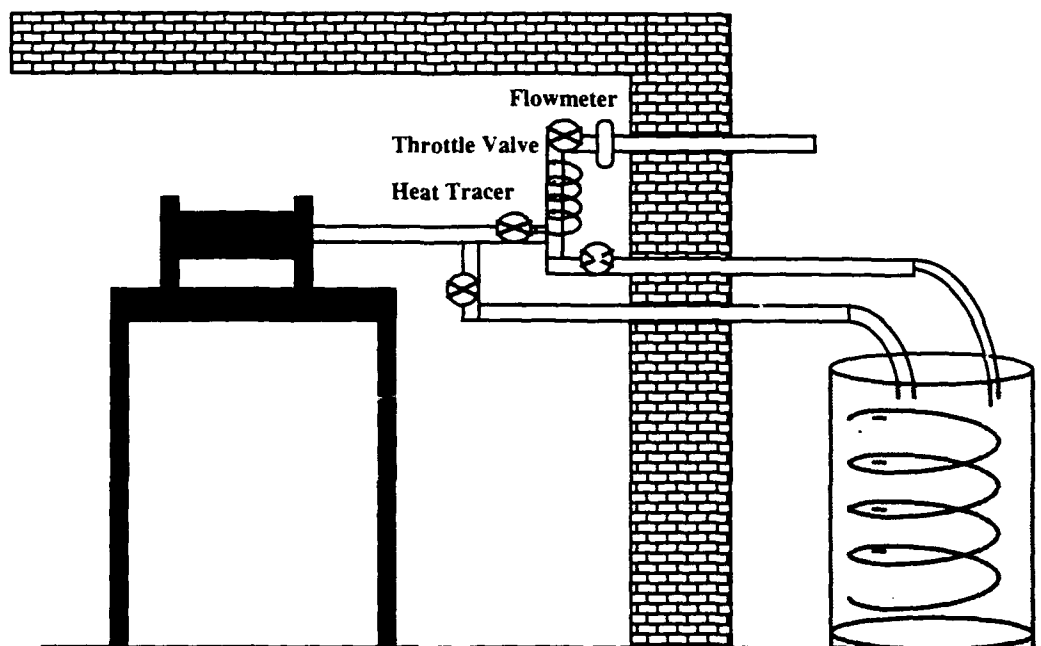
particular gas and is, therefore, almost insensitive to pressure and temperature changes (Therefore, the flow meter reading was used as the mass flow rate through the bed).

The flowmeter used for the test was calibrated for nitrogen. The flowmeter was read directly for the nitrogen tests. The conversion factor based on heat capacity for the He runs was 1.43 (calculated by the vendor). Each reading was multiplied by 1.43 for the He runs. The flowmeter display for the runs read in liters per minute. The flow was converted to kg/sec by multiplying by $(4\text{g/mole}) / (22.4\text{ L/mole} \cdot 60\text{ s} \cdot 1000)$. This reading had to be recorded by hand since a data channel was not available from the data acquisition system.

Since all of the runs could not exceed 1020 kPa due to the regulator, there was no problem with the pressure technical specification. However, since the inlet gas was around -170 - -180 °C and the outlet temperature was expected to reach 700 °C, a chill down/ heat addition system had to be designed at the exit to stay within the 0 - 50 °C temperature range for the flowmeter inlet.

Figure 3.3.5.1 shows a drawing of the chill down / heat addition system for the flowmeter.

Figure 3.3.5.1 Chill Down / Heat Addition System for Flowmeter



This drawing shows the flowmeter, throttle valve for pressure control of the bed pressure vessel, 208 L drum filled with water, 1.905 diameter copper tubing 1524 cm long, and a 800 watt heat tracer. This system is designed to use existing laboratory materials.

A series of check out runs at different outlet temperatures revealed that the system maintained a temperature range of 0 - 50 °C inlet temperature to the flowmeter. The heat tracer was turned on for all of these check out runs and for all of the experiments.

Some of the post experiment analysis speculated there may have been some problems with the flow meter calibration. Some of the experiments also were run beyond the 1500 lpm maximum (The display read to 2000 lpm). This will be discussed further in Chapter 5 and Appendix C.

3.4 POWER SUPPLY

3.4.1 System and Leads

The Rapid Model SCRA418C050 Power Supply provides 90 kW of DC power (0-60 V, 0-1500 Amperes) with an AC input [R-1]. The AC input requires 480 Volts + - 5% in 3 phase at 60 Hz , 130 Amps AC. The control uses a self contained SCR (thyristor). The supply has a AC contactor for starting and a circuit breaker for safety. The regulation is 0.1% for current and voltage. The ripple is 5% rms at full rated DC current and voltage. The dimensions for the supply are 165.1 cm high by 86.36 wide by 86.36 depth. A built in fan is provided for cooling.

Two copper leads extended from the power supply located inside the lab to the test assembly located outside (see Figure 3.4.1.1 for a picture of the complete assembly). The leads are connected by nut and bolt to copper tubes connected to flexible tinned copper leads extending from the copper electrode blocks attached to the apparatus.

The electrodes were rated up to 150 amperes of current. A water cooling system was installed to cool the electrode connections. Two rubber hoses were connected to the copper electrode tubes for water cooling. This cooling allowed the system to support 1500 amps of current flow for a long period of time with no material degradation (see Figure 3.4.1.1).

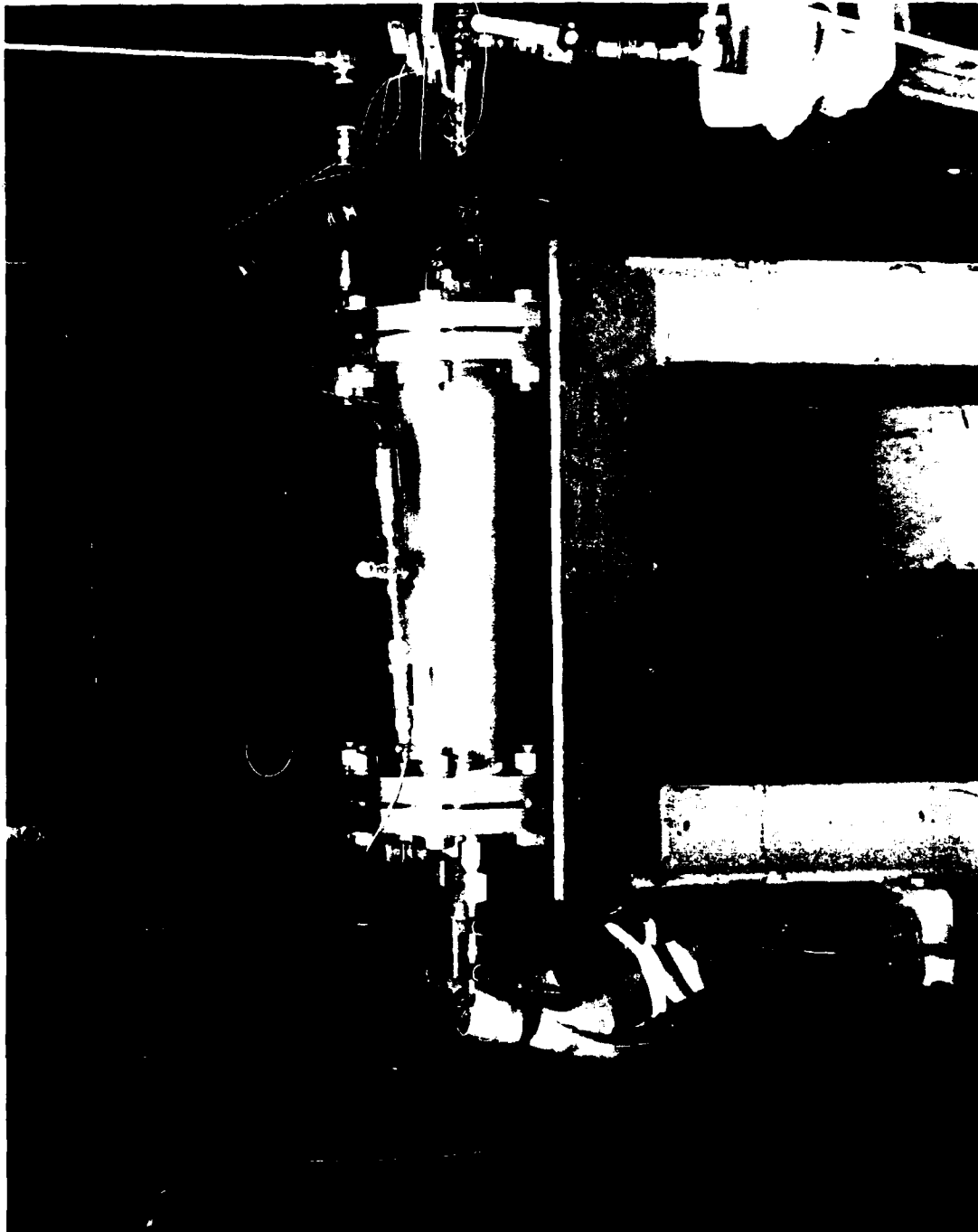
Three Lambda LES-F-01-0V power supplies were connected in parallel to provide power for electroplating , oxidizing, bed analysis, and material experiments. Each power supply provided 0 - 7.5 V and 100 amps at 40 °C ambient temperature (47.5 amps at 71 °C ambient temperature). The voltage regulation was 0.02 %. The ripple and noise for the system was 10 millivolts

rms, 50 millivolts peak-to-peak. The current regulation was 0.5% plus 50 mA. Each system required 105-132 V AC input at 47-63 Hz. Each system was convection cooled.

3.4.2 Console

The console gave digital display for voltage and current. The console had an on /off switch to the power supply. The power ramps were controlled by a dial. Due to the limited data channels, power readings for the experiments were recorded by hand. The console display of current and voltage was interrupted as the power supplied to the bed. Analysis of the experimental results revealed that there was an error in the console display and actual power supplied to the bed (more power into the bed). This is discussed further in Appendix C.

Figure 3.4.1.1 Entire Experimental Apparatus



3.4.3 Copper Electrode Blocks

Figure 3.1.1.1 and 3.2.1.2 show the copper electrode blocks that carry the power from the power supply to the bed. Each terminal block has a lead that is connected to the power supply leads. The blocks are 10.1 cm by 7.6 cm (each block consists of two pieces). Figure 3.2.1.2 shows that the top block is the anode and the bottom block is the cathode. Four screws and bolts are used on each block to connect them together around the copper tabs on the screen to carry power to the screen. Four tie rods are used on the bottom block to mount it to the bottom manifold. The tie rods and bolts to connect them are insulated with rubber in order to not carry current throughout the inner vessel and manifold. The leads were insulated with electric tape in the bed in order to not carry current to the outer pressure vessel.

3.5 INSTRUMENTATION

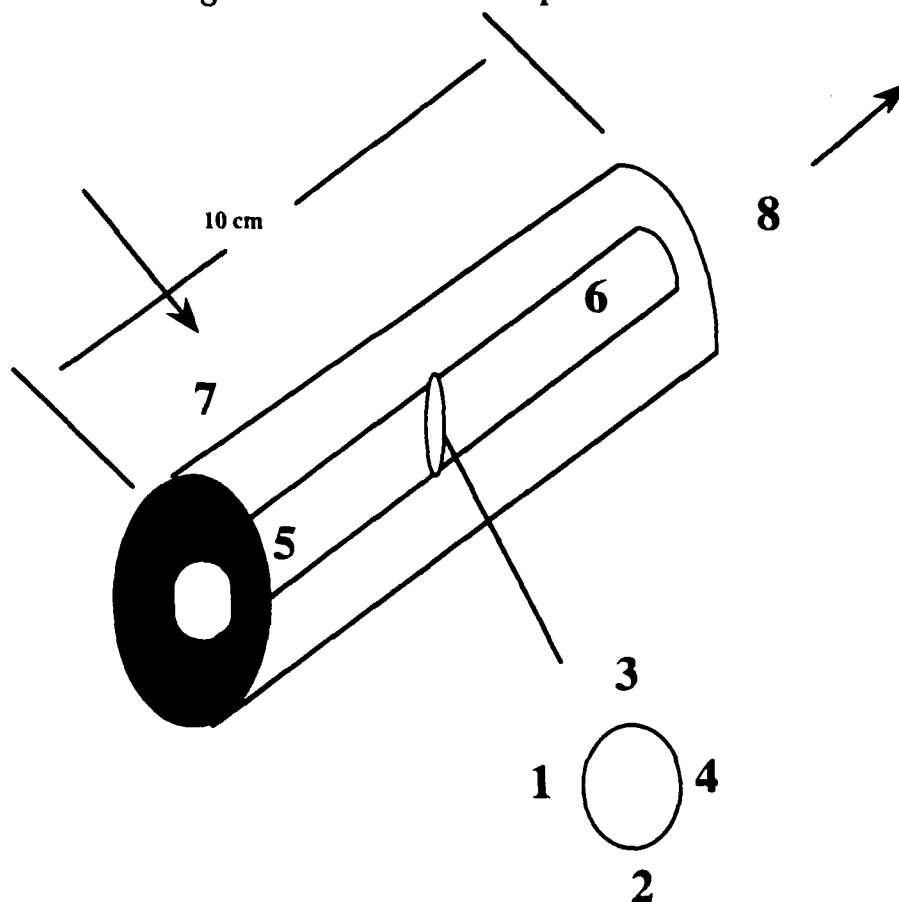
3.5.1 Thermocouples

The thermocouples used for temperature measurement were Omega Engineering Inc. KMQSS-0620-18 probes [O-1]. These type K (chromelTM-alumelTM) thermocouples were 0.15758 cm in diameter and 45.72 cm in length. Each thermocouple had a s.s. sheath. The recommended temperature range for the type K thermocouples was - 200 °C to 1260 °C which was in the desired testing temperature range. The thermocouples used had ungrounded junctions. The ungrounded junction was recommended for measurements in corrosive environments where it is desirable to have the thermocouples electronically isolated from and shielded by the sheath. The welded wire

thermocouple was physically insulated from the thermocouple sheath by MgO powder. This type of junction was needed since the thermocouples had to be insulated from the current being used to heat the bed.

The thermocouples are arranged in different configurations. The configurations changed as the tests evolved. Specific placement will be discussed in Chapter 4, Appendix A, and Appendix B, but the best configuration used in a majority of the runs is shown below.

Figure 3.5.1.1 Thermocouple Placement



The thermocouple placement is as follows: Middle of the bed (~ 5 cm) - #3 touches the hot frit and is at the top (0°), #4 touches the hot frit on the right side (90°), #1 touches the hot frit on the left side (270°), #2 touches the hot frit on the bottom (180°); Inlet - #7 touches the cold frit (~ 1 cm from the beginning of the bed), #5 touches the hot frit at the top (~ 2 cm from the beginning of the bed); Outlet - #6 touches the hot frit at the bottom (~ 9 cm from the beginning of the bed), #8 is in the middle of the gas stream (~1 cm aft of the bed). The thermocouples were slid into placement from the back of the apparatus. An insulated fitting was designed for the thermocouples to rest on in order to help fasten them into place. The bed was then slid into place over the thermocouples (except for #7). The thermocouples were oriented so that spring expansion would cause them to rest against the hot frit (#1-#6). All of the thermocouples were fitted tightly into place so gas velocities would not cause thermocouple movement. The male plugs to the thermocouples were connected to female plugs aft and above of the assembly. These wires were then connected to the data acquisition system (capable of supporting 8 data channels). The thermocouples were pre-tested using ice and a hot air gun for calibration prior to assembly (see Figure 3.2.1.2 for picture of thermocouples coming out of the bed assembly). Technical issues with the thermocouples are also discussed in Chapter 4, Appendix A, and Appendix B.

Several thermocouples were also placed throughout the piping of the flow system to determine other temperatures (e.g. at the exit of the chill down tank, at the entrance to the flowmeter). These thermocouples readings were sent to a digital display box and were periodically checked throughout the different tests.

3.5.2 Pressure Transducer

Two pressure transducers were used for pressure measurements inside the outer pressure vessel. An Omega Engineering PX100 and an Enerpac #SP97KFS were used. They were both located at the top of the outer pressure vessel (The two were used to check each other's reading). This pressure is interpreted as the inlet pressure to the cold frit. Due to space requirements, there was no way to place a transducer inside the bed or at the exit of the bed. Other pre-experiments were conducted to determine the pressure drop of the frits and bed (see Appendix C).

The PX 100 is a small, rugged pressure transducer which utilizes a silicone strain-gage bridge bonded to a flat diaphragm to measure low-level pressure-induced diaphragm deflections. The pressure cavity is manufactured from a solid machined piece of 17-4PH s.s. The all one piece construction helped to eliminate leaks. The full scale output is 100 mV for a 10 V bridge excitation (DC or AC). The transducer can measure absolute pressure from 0 - 5000 PSIA (0 - 34,014 kPa). The system can handle an overpressure of 200% . The pressure readings are recorded by hand during the experiments. The transducer is connected to a digital display gauge [O-2].

The operating temperature range for the transducer was - 54 °C - 124 °C [O-2]. Since the transducer read pressure in the outer pressure vessel, the temperature was ~ -170 °C - 180 °C. Several pre-tests revealed that the pressure readings were realistic based on the pressure at the inlet regulator.

The Enerpac #SP97KFS pressure transducer reads gauge pressure from 0 - 10,000 psi (0 - 68,027 kPa). The pressure transducer is connected to a digital display gauge with a 457 cm cord. A 115 V A.C. power transformer supplies

power to the system. The display reads from 0 - 10,000 psi in increments of 10 psi. The operating temperature range for this transducer is -1.1 °C to 54.4 °C. The readings of this gauge were very close to the Omega gauge [E-1].

3.5.3 Data Acquisition System

The Omega WB-ASC Card was used for the data acquisition system [O-3]. The system was installed on an IBM AT with 256 K RAM. The system offered the following hardware features: 8 differential analog inputs, software selectable resolution from 9 - 12 bits, acquisition speed up to 10 KHz, a low noise integrating converter, 6 software selected voltage ranges individually selectable on each input, cold junction compensation and linearization for thermocouples, input protection for 50 volts continuous, and one counter/timer for counting pulses or events [O-3].

The system was used in initial experiments for the flowmeter reading and seven thermocouple readings. It was then decided that eight thermocouple readings would give better results. The thermocouple readings were displayed every second on the computer monitor in degrees C. The readings were stored on disk/sent to the printer every 10 seconds. The system was just used for these thermocouple displays. All control of experimental parameters was done by hand.

The software for the system was written in BASIC and required DOS 2.0 with GWBASIC or higher (DOS 5.0 was installed on the machine). Since the source code was written in BASIC, it was easy to make modifications. Modifications were made to change the temperature readings from volts to degrees C, give a real-time plot of the temperatures or a columnar display of the thermocouples temperatures in order from #1 to #8 , and extraneous

read-outs were deleted (e.g. the system subtracted different temperatures from each other, which was not needed).

Another card could have been purchased for more data channels, but since the other information could be adequately recorded by hand, this was not necessary.

3.5.4 Ohmmeter

An ohmmeter was needed to check screen resistances for different coatings, voltage measurement for electroplating, and to insure that the apparatus was insulated from spurious current migration. Two ohmmeters were used, a Fluke 77 and a Valhalla 4100 ATC .

The battery operated Fluke 77 was used as a first check for the insulation of the apparatus and electroplating due to its portability. Its digital display was good to 3 decimal places which was appropriate for these applications. Its resistance range was from Ω to $M\Omega$. An overload indication would read "OL".

The Valhalla 4100 ATC ohmmeter had a resistance range from 200 $m\Omega$ to 20 $K\Omega$ [V-2]. This sensitive device was important for determining the resistance of the screen before it was assembled, during assembly, and after assembly to determine if parts were properly insulated and if the bed was good enough to use in a test (The ceramic coating tended to flake off in some cases which caused too low of a resistance and shorts in the bed. This phenomena will be discussed in Appendix A). Its display was 4.5 (19999) digit LED. Some of the technical specifications were as follows: voltage sensitivity - 200 mV full scale, accuracy + - 0.02% , reading + - 2 digits, overload indication - display flashes, maximum input - 10 amps peak,

terminal configuration - four wire Kelvin (used to eliminate lead wire and contact resistances in the current carrying leads), power - 115/230 VAC + - 10%, 50 - 60 Hz, size - 23 cm L x 35 cm W x 6.4 cm H, the operating temperature range - 0 °C to 50 °C (all of the measurements were performed at room temperature), and the range, resolution, and test current.

Range	200 mΩ	2 Ω	20 Ω	200 Ω	2 KΩ	20 KΩ
Resolution	10 μΩ	100 μΩ	1 mΩ	10mΩ	100 mΩ	1Ω
Test Current	1A	100mA	10mA	1mA	100μA	10μA

[V-2]

The ohmmeter was calibrated before use and read consistent with the Fluke ohmmeter.

This Chapter described the final design used for the tests conducted in Chapter 4. The key issue in the design was the coatings. It was discovered that the maximum temperature the coatings could handle was 700 °C (with margin for error). There were design evolutions leading up to the final design which are found in Appendix A. Equipment calibration tests (power supply and flowmeter) are listed in Appendix C.

CHAPTER 4

TESTING

4.1 TESTING PROCEDURE

The purpose of the experiments was to demonstrate stable or unstable flow through thermocouple, pressure, and flow measurements in the bed. The test plan called for running at low ϕ 's to demonstrate stable flow, and then try for high ϕ 's (unstable flow regions according to analyses shown in Chapter 2) for various Reynolds numbers. If there were no indications of unstable flow for high ϕ 's, a perturbation of porosity (small blockage) would be induced into a section of the screen. If no indications of unstable flow were found after this perturbation it could be concluded that this test apparatus did not show signs of unstable flow.

Table 4.1.1 gives a brief discussion on how operations in general were conducted for each experiment.

Table 4.1.1 Operating Instructions for Screen Bed Experiments

Section I Set up, System, and Equipment Checks

A. Test Section

- Test section is assembled and secured to test stand.

B. Piping

- Piping is installed per flow diagram and is free of leaks.
- Valves operate and are free of stem and seat leaks.

C. Electrical

- Electric supply cables are connected with proper polarities.
- System has continuity.
- System is free of shorts and grounds.

D. Instrumentation

- Instrument sensors are properly installed.
- Read-outs function as expected.
 - Power supply turned on to check there is no thermocouple feedback (learned for tests past Aug 92).

Section II Gas Refrigerator Filling & Testing (See Figure 18)

A. Transferring Liquid N₂ into Refrigerator Well (assumes N₂ is experiment working fluid)

- With all system valves closed, and gas pressure regulators in off position; open N₂ manifold valves and set regulator R1 to 1972 kPa and regulator R2 to 1020 kPa.
- Slightly open bubbler valve V4 to bleed a small flow of N₂ through the bubbler pipe (this will drive out trapped air and prevent internal icing of the bubbler when the well is filled with liquid N₂).
- Open throttle valve V2 one turn.
- Slightly open fill valve V1 to force trapped air out of the cooling coil insulated valve V2, body of V2, insulated line to the experiment chamber, and the experiment chamber.
- Slightly open blanket gas valve V5.
- Close valve V2, and quickly.
- Close valve V1 temporarily, if desired to shorten refrigerator cool down time. Note: Valve V5 remains open to supply blanket gas to the experiment chamber until an actual test run is started. Valve V4 remains open slightly to keep the bubbler air free.
- Insert the filling nozzle into the refrigerator fill pipe and slowly open the transfer valve on the liquid N₂ supply tank. Violent N₂ boil off will occur and persist until the refrigerator well and the cooling coil

approximately reach liquid N₂ temperature.

- When boiling subsides substantially, and the liquid N₂ level rises above 10 inches from the well floor, the MG bubbler gauge will begin to register. When the gauge pointer reaches 8, the transfer valve can be closed.
- Watch the gauge pointer fall, and crack open and adjust the transfer valve opening to maintain the MG gauge pointer slightly above 7 (if possible).
- Open N₂ gas charge valve V1 wide, observe the speed and amount by which the MG gauge pointer drops as the 1973 kPa charge of gaseous N₂ is cooled. Recharge refrigerator well until filled and gauge pointer exceeds 8.

Section III Test Operations

- Connect 160 L LN₂ tank directly to bed inlet pipe, flow ~ 10 min or until thermocouple readings are between -170 °C to ~ -180 °C then disconnect tank.
- Open Valve V2 wide open.
- Open up valves from Tank Farm.
- Open V1 fully for gas flow from Tank Farm.
- Use R1, Throttle Valve Aft of the Rig (Figure 3.3.5.1), the Pressure Transducer, and the Flowmeter to set desired flow rate and pressure.
- Insure Data Acquisition system is working.
- Set Power Supply, use control knob to set desired power setting.
- Continue to monitor thermocouples, flowmeter, pressure transducer, and power supply throughout test.

Section IV Shut Down

- Turn Power Supply off.
- Close Valves from Tank Farm.
- Let Remaining Gas flow through System (done when flowmeter reads 0).
- Close Valve V1.
- Close Valve V2.
- Put Plug over Gas Exit Pipe.
- Turn Data Acquisition System off.

4.2 1 Alumina Painted Screen Test (Oct 92)

The painted alumina screen showed promise in sample tests (see Appendix A). One 233 cm long screen was etched, copper electroplated, edge wires removed, and sent to the paint shop for alumina spraying. The painter had problems spraying a constantly even coating (did not have a problem with the smaller samples). Many of the holes got clogged, which was an unacceptable condition. The painter was given a sample and directed to spray a one pass coating and then stop (Not to keep spraying pass coats on until the visual build up could be seen). The coating on the other screen was removed by using a wire brush and hydrofluoric acid. The new technique worked and the proper coating was added to the screen. The screen was rolled, placed into the cold frit, and then the hot frit was added into the middle of the bed. The measured resistance was $0.2090\ \Omega$ (across the bed).

The thermocouples were insulated per Appendix A.5. Their arrangement was as shown in Figure 4.2.1 (no huge anomaly from the past experiments). Thermocouple #7 was in the same position. The bed was fully assembled.

The resistance was good through out the assembly. It was decided to go for a low inlet temperature for the first experiment since the coating looked good. During the chill down using LN₂ directly into the unit and monitoring the thermocouple temperatures, the power supply was turned on and it's effect on thermocouple readings was first discovered (this is also discussed in Appendix A.5). The temporary solution to the problem was to turn the power supply off and take the thermocouple readings by hand. The power was turned off at each minute mark of the experiment for ~2 sec for temperature measurements (They were taken by hand off of the data acquisition system computer). The test was started at a flow rate of 2145 lpm with helium at 952 kPa. The power vs time is shown in Figure 4.2.2.

Figure 4.2.1 Thermocouple Arrangements

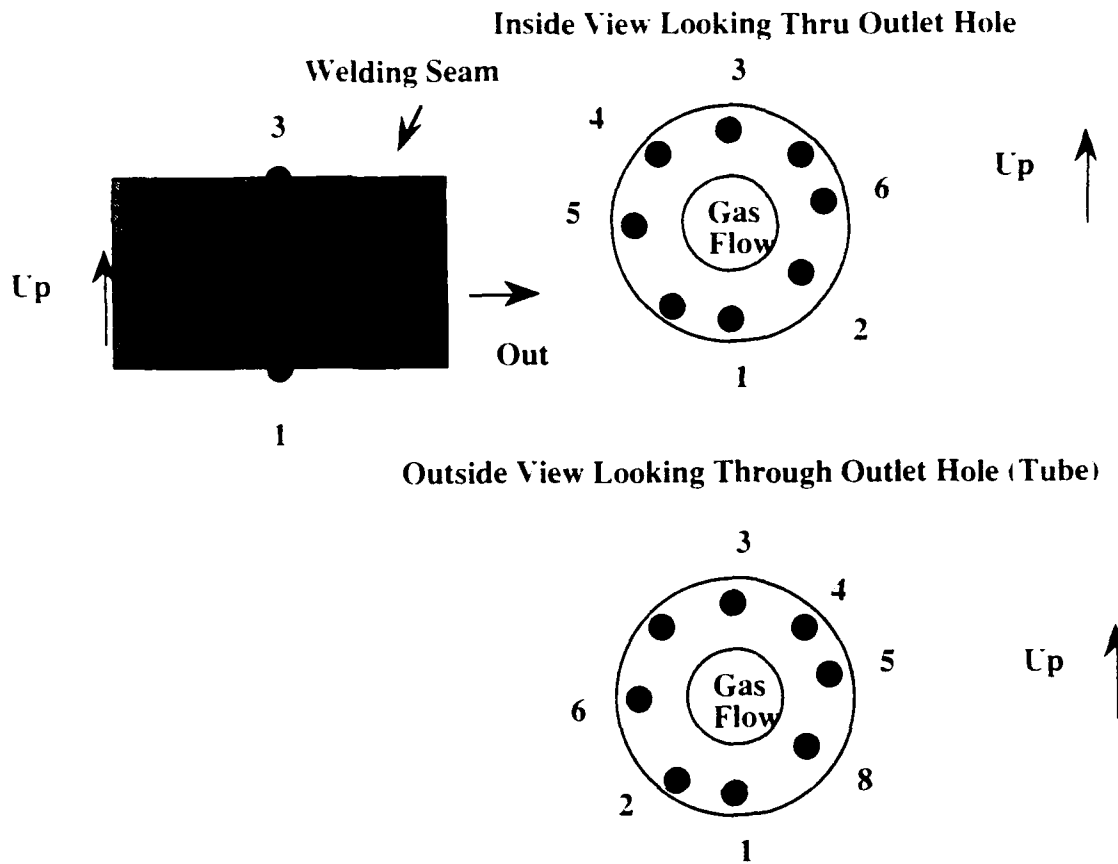
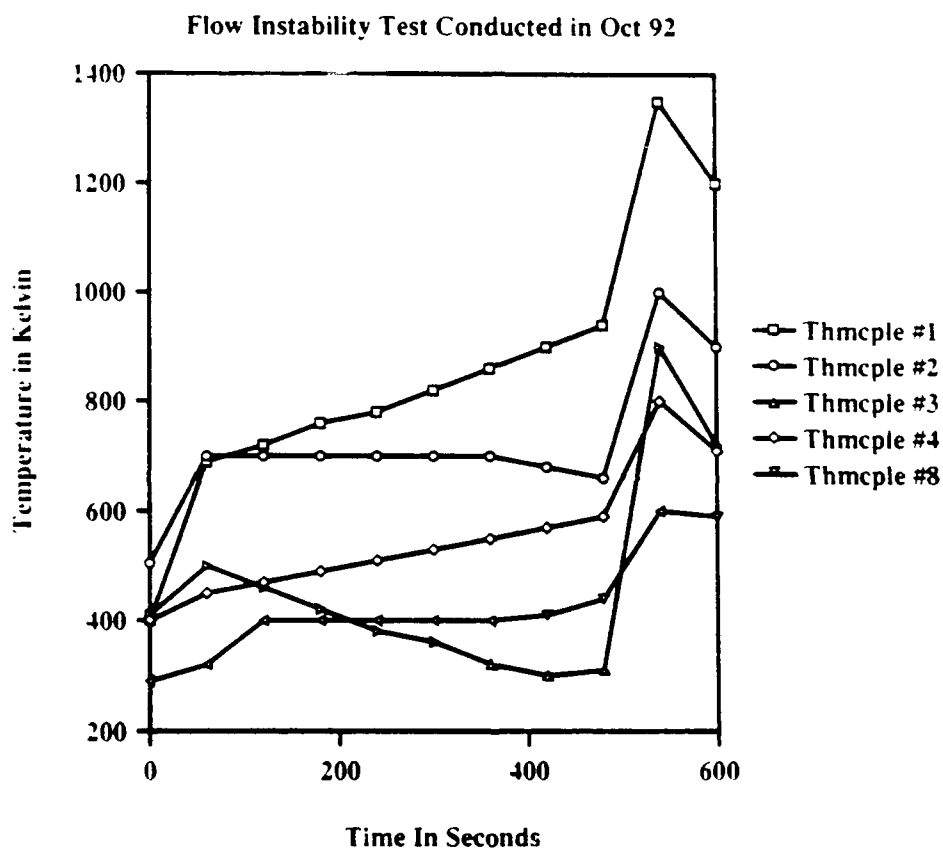


Figure 4.2.2 Power vs Time For Test

Time (min)	Volts	Amps
0	7	2
2	20	133
5	30	166
6	40	200
7	50	245
8	40	200
9	50	245
0	0	0

Figure 4.2.3 showed the temperature results of the experiment. Thermocouple #7 was not plotted, but its temperature was very near 100 K for the entire test.

Figure 4.2.3 Thermocouple Results for 14 Oct 93 Experiment



The results from Figure 4.2.3 show that the bed responded well to the power input. An energy balance for Time = 400 sec shows that the $T_{exit} = T_8 = 410\text{ K}$, $T_{inlet} = 100\text{ K}$, $c_p = 5.193\text{ kJ/kg K}$ at He Temp and Pressure, $\dot{m} = 2145\text{ lpm} = .00638\text{ kg/sec}$, therefore $Q = 10.27\text{ kW}$. At this point in the test the power is in the transient from 8 kW (6 minute mark) to 12.25 kW (7 minute mark). This is a much better match than previous tests (see Appendix B).

The power was continued in steps up to 12.25 kW. Between the 8 and 9 minute mark, all of the thermocouples spiked (It is not known when they actually spiked due to that readings were taken every minute). The current fluctuated at this point and between 9 and 10 minutes it no longer read on the power supply console. It was concluded that some parts of the bed melted. The experiment was stopped and it was decided to wait to the next day, since it was late in the afternoon, to inspect the bed in order to let any melted parts cool.

The bed assembly was disassembled and the melting was severe. The melting had occurred through out the entire bed. The bed melted through the hot frit and cold frit. The inner vessel held the molten mass of material. All of the thermocouples were lost and had to be replaced. The pipes from the manifold were damaged and had to be re-attached to the manifold (see Figure 4.2.4 for a picture and an enlarged drawing of the melted frits).

Figure 4.2.4 Melted Frits

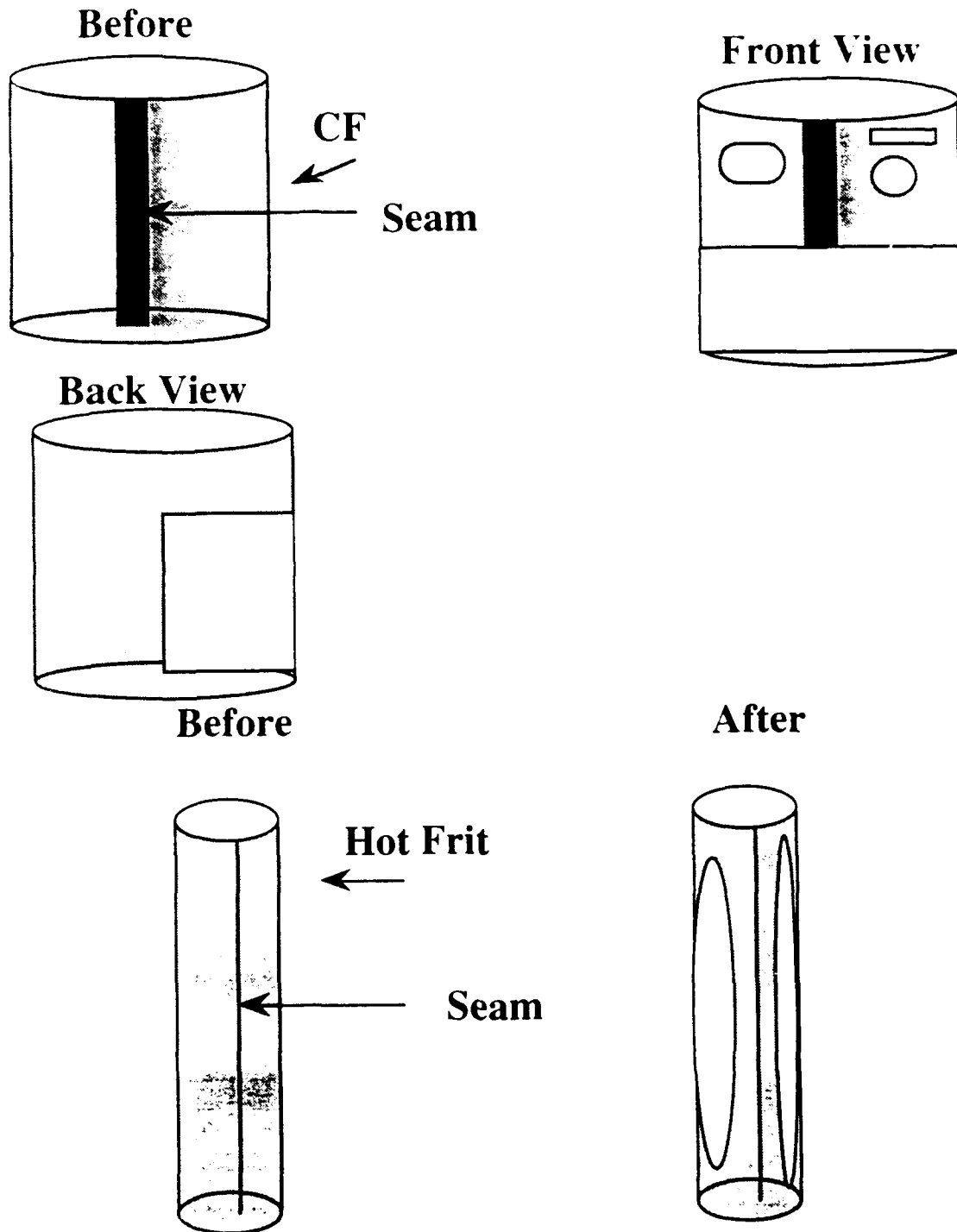
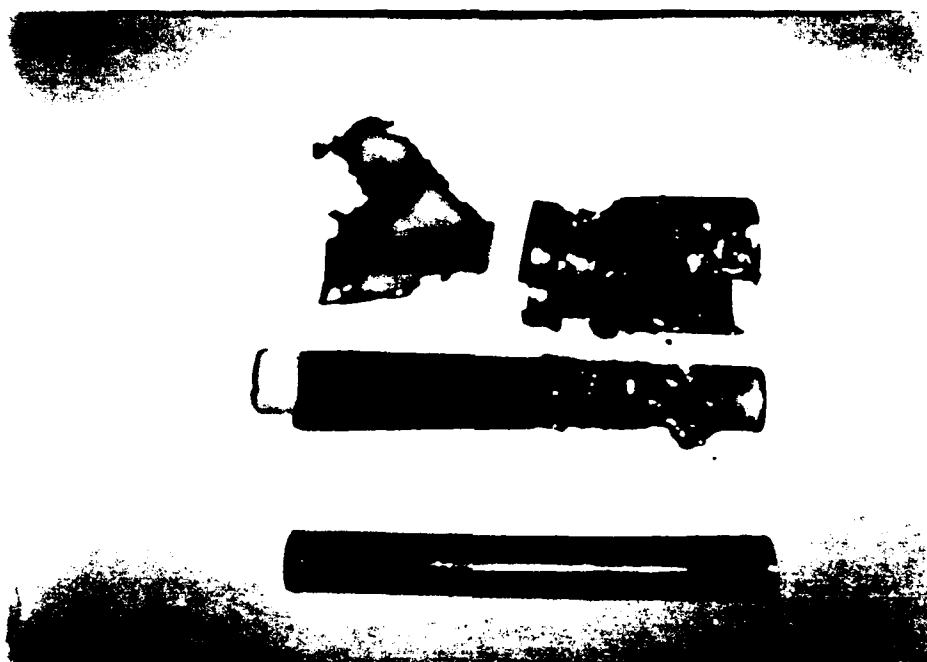


Figure 4.2.4 (Continued)



There was some concern that the frits melted due to the seams. The melting occurred mostly on the inlet part of the cold frit (upper region around thermocouple #5) with 3/4's of this area completely melted away. The outlet part of the cold frit had melting in spot . There was no melting on the seam in this region . The hot frit showed melting (bubbles) uniformly around the entire frit, except for the seam . It was the only area that did not show melting. The bed was severely melted and charred. The remaining coating that could be inspected had swollen. The coating had grown such that the holes in the screen were almost closed. It was not known whether this was due to the high temperatures at the spike or swelling at lower temperatures.

It was difficult to give conclusions regarding this experiment. Was the spike caused by flow instability or was it that the coating reached too high a temperature and flaked off causing a clogging in one area of the bed? Was the decrease in temperature in thermocouple #3 and the subsequent increase in the other thermocouples caused by flow instability ? If this was flow

instability, the runaway situation could have developed in seconds (definitely less than a minute). It was determined that there were too many uncertainties in the data to give any solid conclusions. However, this bed and coating showed a very strong potential of producing useful results.

The recommendations for future experiments were as follows : (1) conduct more tests on the coating to determine temperatures that swelling may occur to set an upper bound for future experiments so the coating can not be blamed for clogging of the bed; and (2) solve the thermocouple problem with the power supply so continuous temperature readings can be monitored.

4.3 8 Alumina Painted Screen Tests (Jan 93)

The first action item was to look at the coating temperatures. As stated in Appendix A.2.8, tests revealed the upper bound temperature of 700 °C should be set for the alumina coating. The thermocouple problem was solved by connecting the thermocouple cathode wire into the data acquisition system board which fed into the computer (Appendix A.5).

Many complications arose in putting coatings on the screen. The high-efficiency electroplating coating would not go on evenly onto the screen, so it was decided to use the strike coating for a longer period of time (Appendix A.1.3). Once the copper plating problem was solved, the screen was sent to the painter for alumina coating. The first coating was put on too thick and the screen would not fit between the frits (The painter had not done the job in awhile and forgot how to do the process ; there was a long delay from the last experiment due to having to wait for new thermocouples to arrive). The coating was removed and tried a second time. This time the painter was low on the 989 thinner, but decided to do the job anyway. The coating went on

unevenly and in big chunks. A microscope revealed that particles of paint covered the holes. The coating had to be removed and new thinner was ordered to mix with the 989 adhesive in the proper ratio to get the right consistency (Appendix A.2.8). Aquaregia was used to try to remove the previous coating and a bad reaction happened, melting the screen. A new screen was cut, etched, electroplated and the coating was painted again. The micrometer read that 0.0025 cm of coating was applied. The painter did not want to put too much coating onto the bed. It was decided to try to use this screen in the experiment.

It was decided in this experiment to have one 225 cm screen and a short 8 cm screen to wrap around it. The shorter screen would be used to insulate the cold frit, but could also insure that the bed had minimal loss of coating due to sliding the bed into the cold frit. The 225 cm screen was wrapped and then the 8 cm screen was wrapped around it. The starting bed resistance was 0.186 Ω . After assembling the screen into the frits, the resistance had dropped to 0.09 Ω - 0.07 Ω . This was an unacceptable reading, due to the thinner coating. It was decided to put the thicker coating on (~ 0.005 cm). Also in the heat of trying to get an experiment going, the coating that was applied to the screen was not cured before assembly.

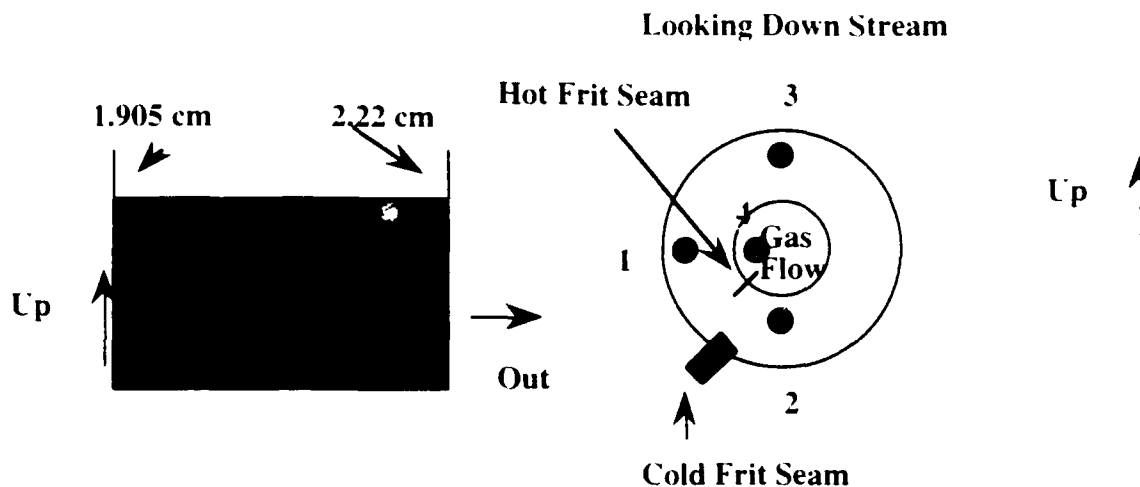
The coating was left on the screen and taken to the painter for another pass. The paint shop applied the coating in 3 short passes. The micrometer showed that the desired 0.005 cm of coating was applied to the wires. The 1x microscope showed that all of the wires were covered in a nice even fashion. The edge wires had a few open areas which were covered with the alumina adhesive with a small paint brush. The screen was then taken back to the lab and cured for 12 hours at 110 °C. The starting bed resistance was 0.1889 Ω . The screen was rolled around with a pipe and put into the cold frit. Due to

the thickness of the coating, the small 8 cm wrap could not fit into the cold frit and was not used. The resistance of the screen after it was installed into the bed was $0.166\ \Omega$. This was attributed to the scrapping of coating as the hot frit was installed into the bed. The final bed resistance was $0.15825\ \Omega$ (decreases a little since the readings include the leads and electrode blocks, while the previous readings read directly from the screen) with the entire apparatus assembled.

The assembly was connected to the inlet and outlet pipes and the boron nitride plug in the outlet pipe was broken (used to help seal the bed). This was replaced with a teflon gasket with thoria packed around it. The teflon was known to contract under temperature, but it was deduced that since it was aft of the bed the gas temperature would not be too extreme and the compression would help to seal the bed.

The thermocouples were placed in the configuration the same axially as Figure 3.5.1.1 but with some modifications shown in Figure 4.3.1. It was decided to have thermocouple #4 not touch the hot frit in the middle of the bed to get a feel for the gas temperature in the middle of the bed. It was determined to mark the thermocouples to determine their position relative to the two seams since it was important to get a feel for how large the seam temperature dependence was from the past experiment.

Figure 4.3.1 Thermocouple Placement for Experiment

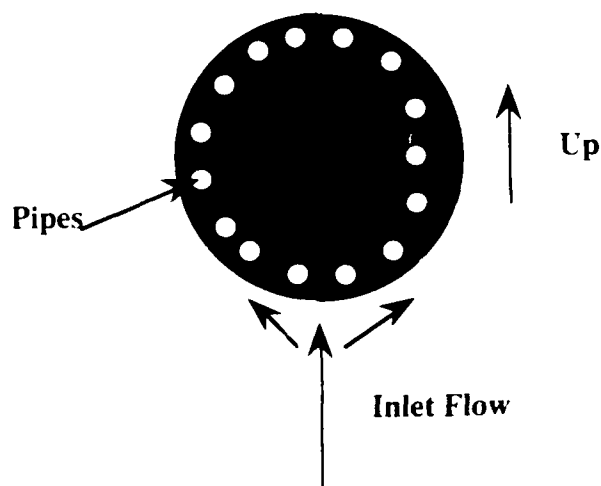


In order to check the temperature distribution for the first test, it was decided to test with an ambient temperature inlet. The gas was sent in through the He tank farm, and through the inlet regulator to the apparatus (the chill down system was not filled to insure an ambient inlet temperature). The power, flow, and temperature results for the experiment are shown in Figure 4.3.3. The pressure (before the gas passes through the cold frit) was at 272.1 kPa. The experiment was conducted at low flow and low power at first and then at higher power and flow. The flow rates shown in lpm in Figure 4.3.3 are the bed mass flow rates since the flow meter is pressure and temperature compensating (Section 3.3.4).

The results from the experiment indicated that there are asymmetries in the bed temperatures. Several options were discussed on the possible causes which are as follows: (1) seams, (2) porosity differences in the bed, and (3) flow non-uniformities. It was speculated that a pressure drop in the inlet manifold may be causing the flow non uniformities. However, since the gas enters the manifold at the bottom pipes and works it way upwards if there

was a pressure drop the highest temperatures should have been at the top of the bed (See Figure 4.3.2).

Figure 4.3.2 Flow Through Manifold Pipes

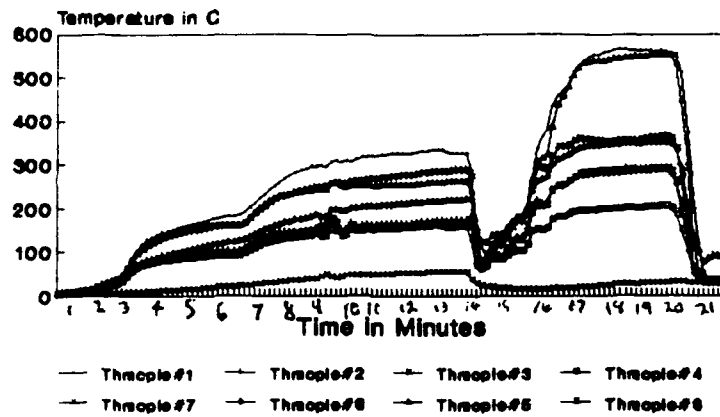


Thermocouple #3 read high throughout the experiment, so it was determined that this was not the cause of the flow non-uniformities.

Figure 4.3.3 Bed Test at Low Phi

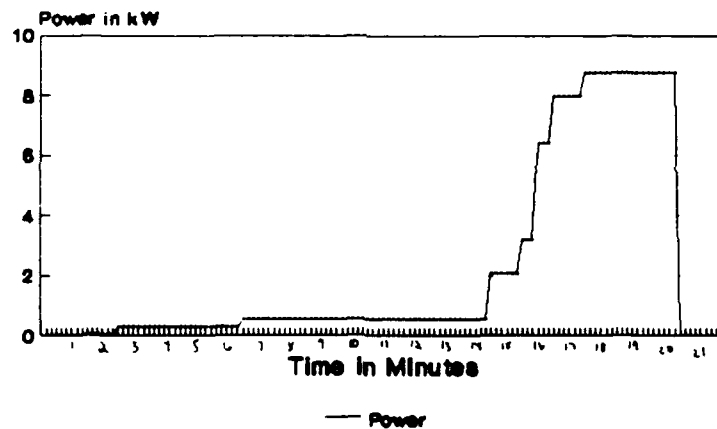
Bed Test at Low Phi

20 Jan 93 14:10



Power vs Time

20 Jan 93 14:10



Flow vs Time

20 Jan 93 14:10

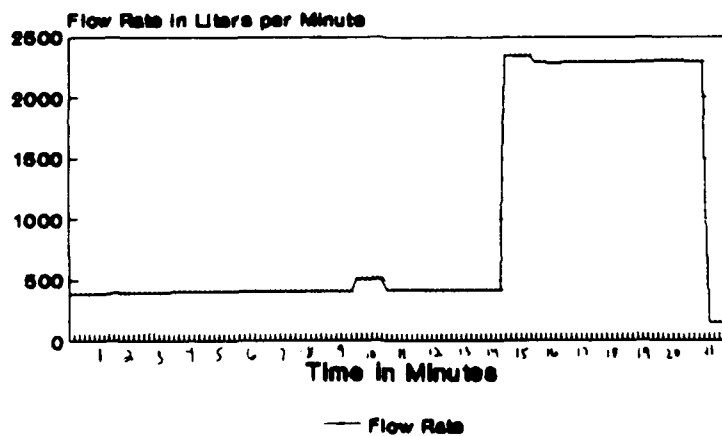
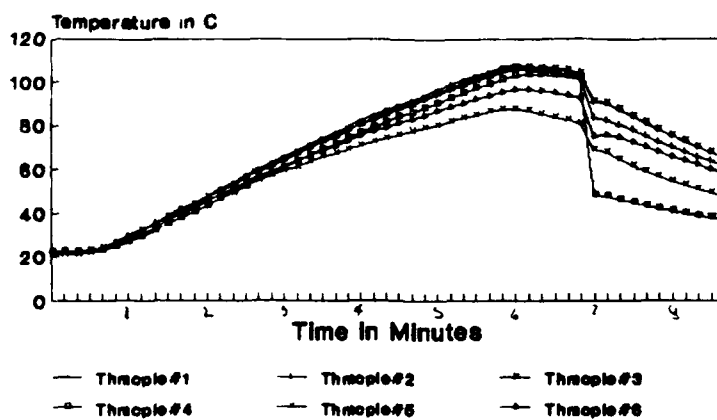


Figure 4.3.4 Bed Test with No Flow

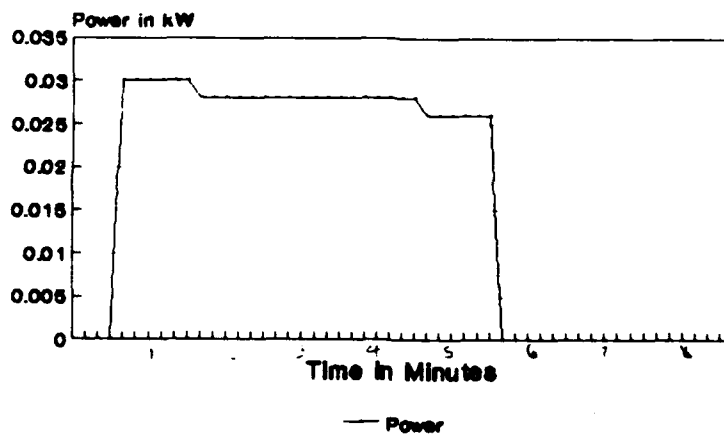
Bed Test with No Flow

20 Jan 93 1530



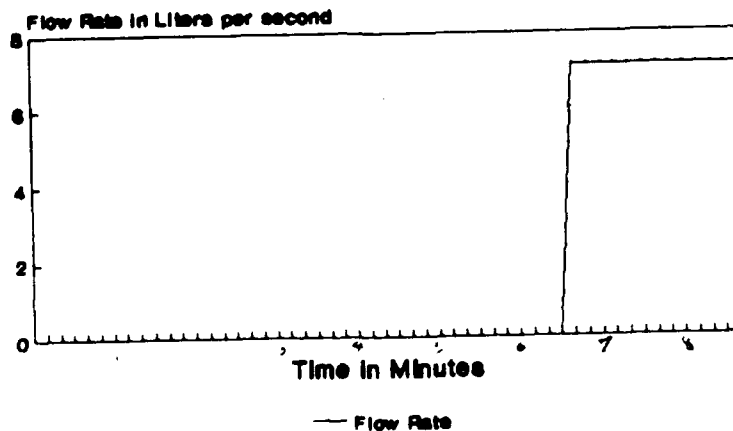
Power vs Time

20 Jan 93 1530



Flow vs Time

20 Jan 93 1530



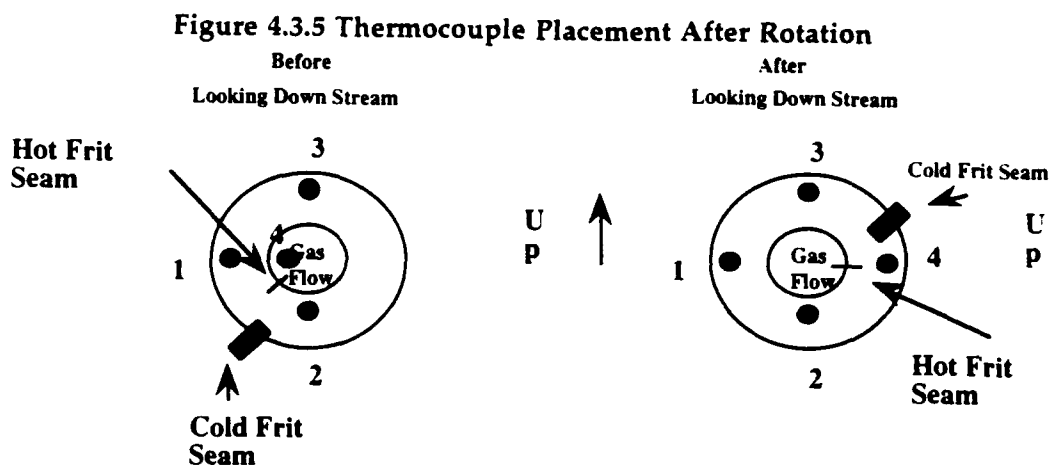
It is also shown in Figure 4.3.3 that thermocouple #6 was reading low (located at near the bed exit). It was speculated this difference could have been caused by that thermocouple #6 was not touching the bed, but was in the gas stream (similar temperature to #8).

Another test was performed with no flow at the start and then a little gas was added at the end (see Figure 4.3.4 for power, flow and temperature results). This experiment showed that there was good heating in the bed with no gas flow. The thermocouple readings were very similar. When the gas was entered near the end of the test, the thermocouples kept the same slope, except that #4 dropped a little faster, but this made sense since it was in the gas stream and the others were touching the bed.

Since the above test showed that the bed was heating evenly with no flow (no shorts or electrical problems in bed), the flow non-uniformities, seams, or porosities, may have caused the asymmetries. Therefore, it was decided to rotate the bed ~ 90 degrees (thermocouples remain in same place except that it was decided to have #4 touch the bed, so all bed thermocouples were touching, #8 still remained in the gas stream). The entire bed with frits was rotated (see Figure 4.3.5).

After disassembly, it was hard to tell if thermocouple #6 was touching the bed. It was extended a little bit more out to insure that it was touching the bed for the next experiment. Looking down at the top of the bed, a brownish color was discovered on the top edges of the ceramic coating. The discoloration was pretty much uniform throughout the bed, with a little more concentration in the area next to thermocouple #1. This confirmed the thermocouple readings with flow, #1 was the highest reading, but the no flow experiment showed even heating. Since, the resistance reading was still 0.15 Ω and the second run determined that the bed saw even heating, this

discoloration was not deemed a problem as long as the resistance did not drop too much in future tests.

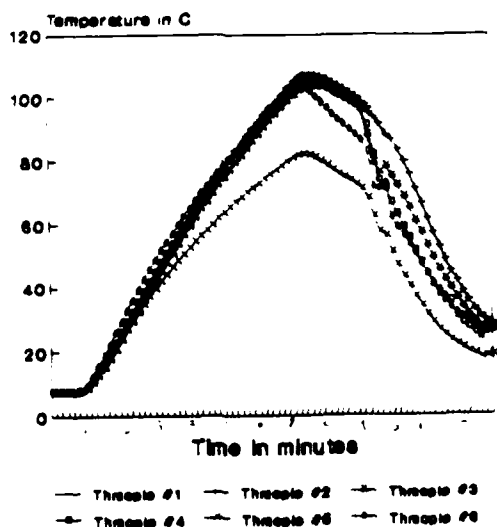


The next test performed looked at the bed heating with no flow. This test checked the bed heating to insure the bed was still performing adequately. He gas was added near the end of the run between 350 to 275 lpm for cooling and flow effects (see Figure 4.3.6). All of the thermocouples read evenly in the first part of the run with #5 and #6 dropping down a little as the run progressed. When the gas was added, #3 and #4 fell quicker in temperature compared to #1 and #2 in the middle of the bed. Since these thermocouples were located closer to the seam, it was hard to conclude that the seams had a significant impact on flow.

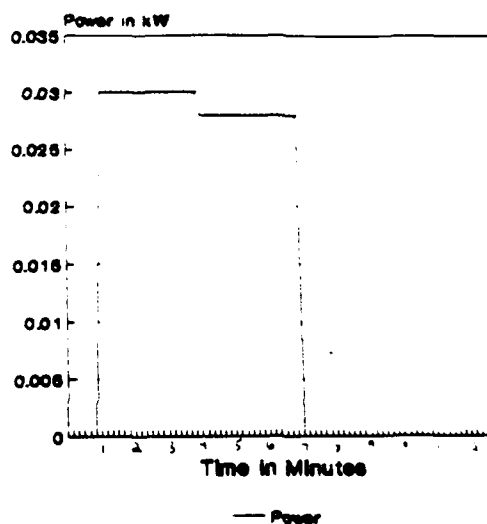
It was decided to proceed on with the next test with higher flow and power. The pressure held throughout the run at 340.14 kPa. The flow and power were varied per Figure 4.3.7. There was variation in the power and flow throughout the test in order to not exceed the coating temperature limits.

Figure 4.3.6 Rotated Bed Test with No Flow

Rotated Bed Test with No Flow
22 Jan 93 0900



Power vs Time
22 Jan 93 0900



Flow vs Time
22 Jan 93 0900

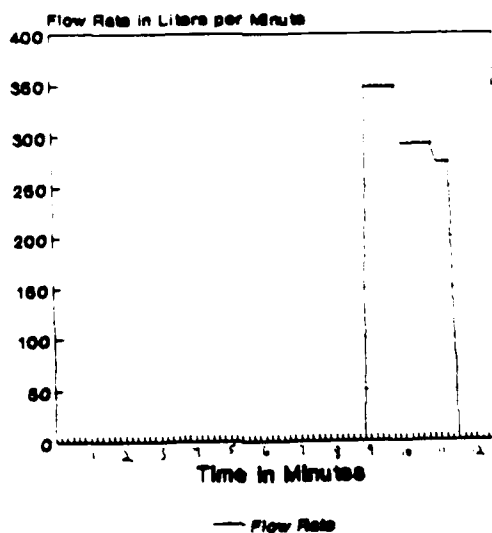
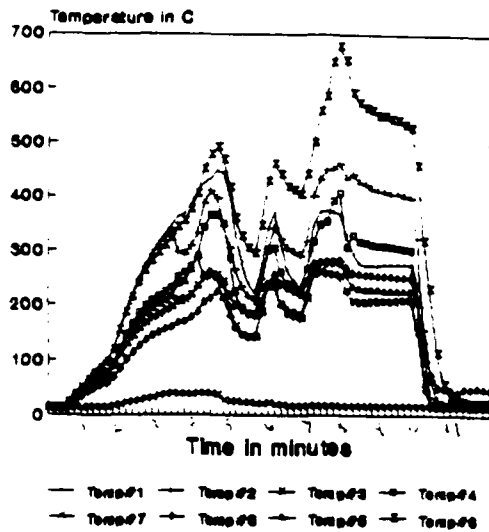
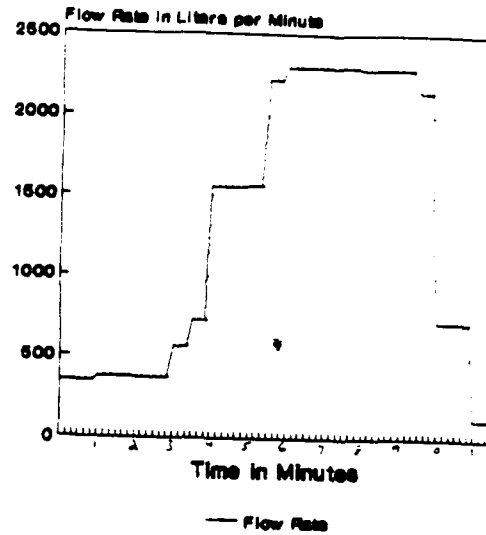


Figure 4.3.7 Rotated Bed Test with Flow

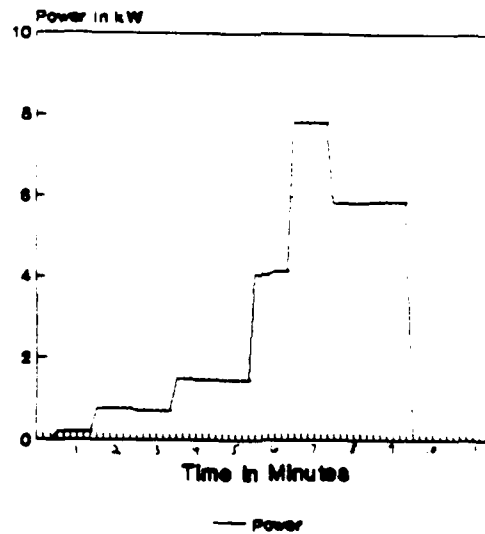
Rotated Bed Test with Flow
22 Jan 93 0945



Flow vs Time
22 Jan 93 0945



Power vs Time
22 Jan 93 0945



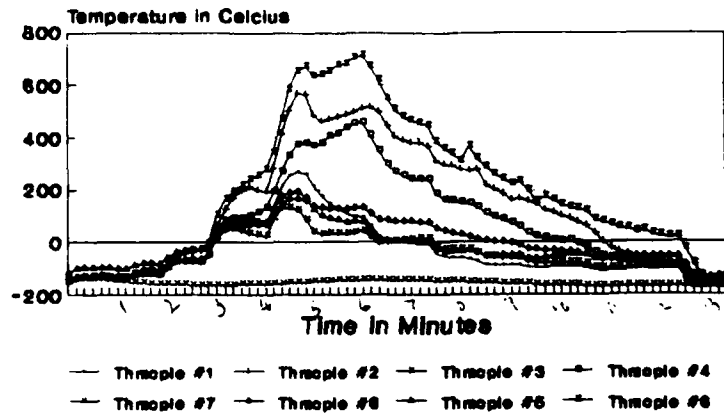
The test in Figure 4.3.7 used an ambient temperature inlet again to insure that bed temperatures could be checked in areas of definite flow stability. Once the higher power and flow was set, at time equals 8 minutes , the temperatures were relatively constant for all of the thermocouples. The readings tended to support what the temperature profile should be in the bed: #6 reading the highest at the bed outlet, #5 reading much lower than #6, and #8 reading low since it was in the gas stream aft of the bed. The middle of the bed temperatures could not be fully explained. It made sense to have #4 read higher than #1 since it was next to the seams. However, there was not that much of a difference between the two readings. Comparisons were hard to make to the experiment conducted on 20 Jan since #4 did not touch the bed on that experiment. There was at least a 300 °C difference between #2 and #3. In 20 Jan experiment, there was a 250 °C difference between #1 and #3. Since the bed was rotated, this showed that this region is warmer than other regions as far as the middle of the bed. This proved that the temperature change was not caused by the flow pipes, but the bed which could be due to a local power or porosity fluctuation in the bed.

Even though there were asymmetries in the bed temperatures, the temperatures held constant once they got to the desired power and flow which tended to support the belief that this experiment demonstrated stable flow. The chill down system would be used on the next test in order to create a higher ϕ to study this impact on the flow stability.

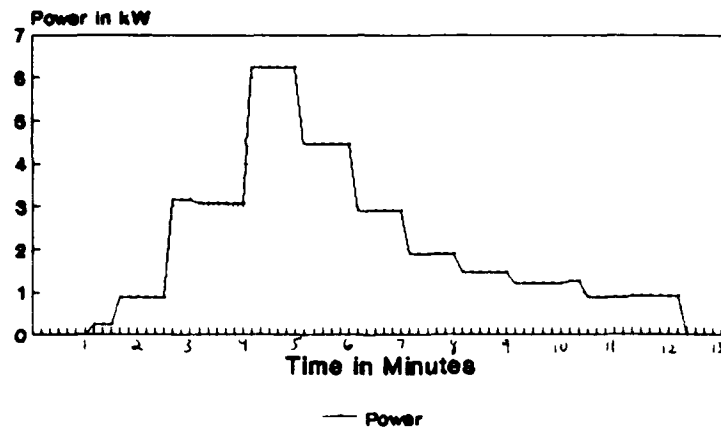
The test with high ϕ results are shown in Figure 4.3.8. The pressure for this experiment is 748.29 kPa. The inlet temperatures were around -180 °C which showed that the chill down system is effective and stayed very low throughout the run as shown by thermocouple #7 in Figure 4.3.8. The flow rate is set and then the power is increased to bring the bed up in temperature.

Figure 4.3.8 High Phi Run

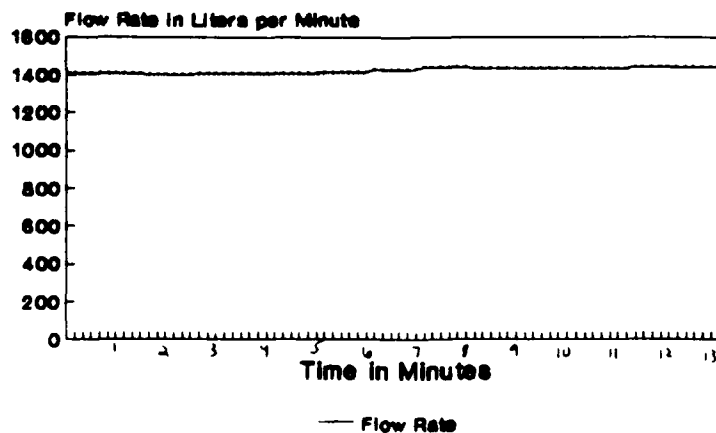
High Phi Run 22 Jan 93 1405



Power vs Time 22 Jan 93 1405



Flow vs Time 22 Jan 93 1405



As power is added, thermocouple #6, #2, 4 increased in temperature while #5, #1, and #3 decreased in temperature. Thermocouple #8 kept relatively constant in temperature for this time frame. Power is decreased at time equals 5 minutes since #2 is approaching the maximum temperature allowed for the coating. As power is increased the temperatures gradually converged and *all* thermocouples showed the same trends.

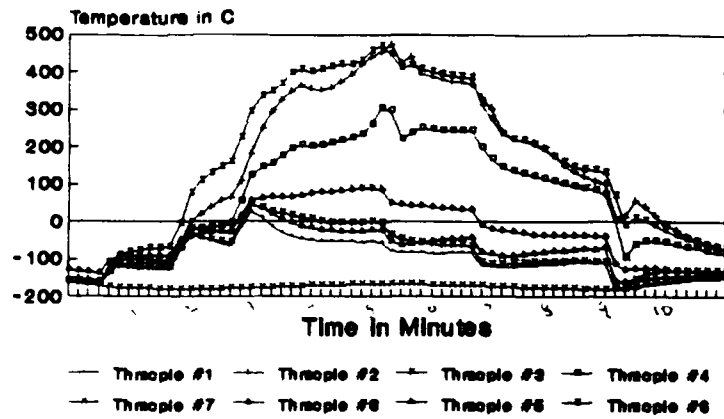
Based on past experiments, it was felt that the experiment demonstrated unstable flow. Three of the thermocouples increased in temperature, and three of the thermocouples diverged in temperature while the mixed mean outlet remained the same. This phenomena was very similar to the original Bussard and DeLauer viscosity based stability discussion, under certain conditions in parallel channels hot areas get hotter while cold areas get colder. The divergences in temperatures could not be completely blamed on the seams. The increase in temperature in thermocouple #4 could be justified by the seams and maybe #2 (distance between the seams and #2 and #3 is approximately equidistant), but in no way #6 since it was located on the bottom which is the opposite side of both seams. It was also noticed that the seams may have caused asymmetries in the low phi experiments, but the thermocouples read constant when power and flow were constant.

The resistance of the bed after the experiment was 0.11Ω . It was decided to perform another experiment at a higher flow rate. In order to increase the mass flow rate, the aft throttle valve was opened in order to get more mass flow, but bed pressure would decrease.

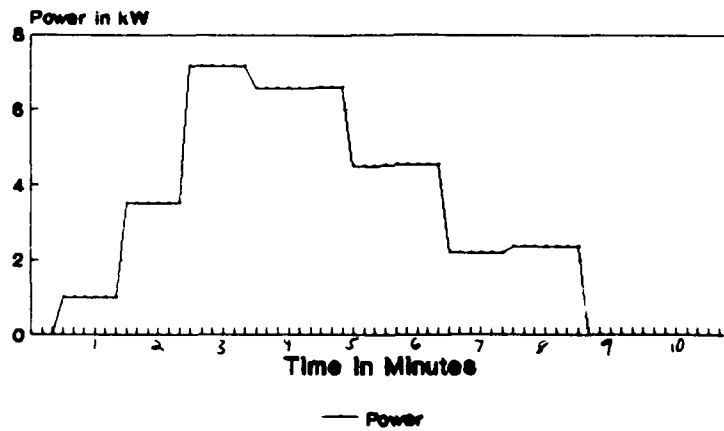
The flow rate for the next experiment was around 2300 lpm for the entire run at a vessel pressure of 408.16 kPa. As witnessed in Figure 4.3.9, the same phenomena occurred as in the past experiment and was easier to see.

Figure 4.3.9 High Phi Lower Pressure Test

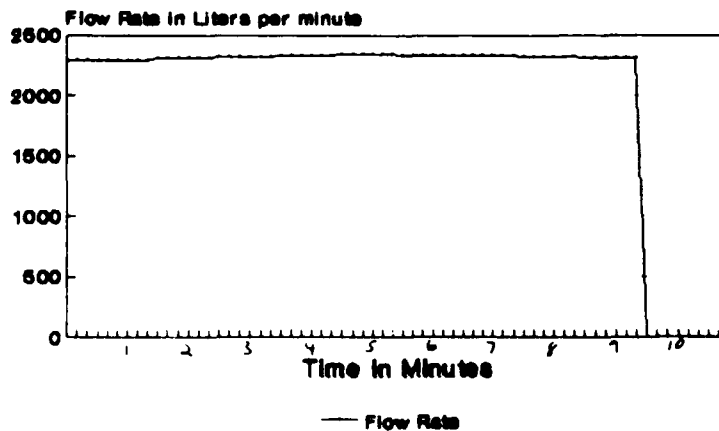
High Phi Lower Pressure Test 22 Jan 93 1445



Power vs Time 22 Jan 93 1445



Flow vs Time 22 Jan 93 1445



The figure showed that #6 and #2 have a sharper rise than #4 which was right next to the seam. It also was clearly shown that #8 remained constant while the thermocouples were diverging. The power was held higher for this experiment for a longer period of time than the previous run. In order to insure that the bed was saved, it was decided to lower the power and let the thermocouples flatten out and then eventually shut off the power.

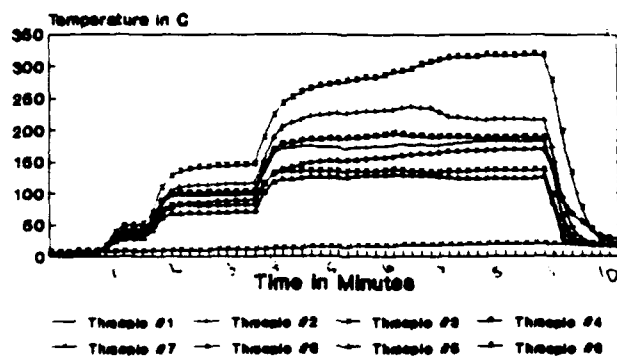
The resistance of the bed after the experiment was 0.116Ω . The proposed next test was to perform another low phi run with a room temperature inlet temperature to see if any of the same flow effects just observed might occur. The flow rate was set in the upper 1400's lpm at a pressure of 476.19 kPa. The results are shown in Figure 4.3.10. The results of the experiment showed that the temperatures remained *constant*. The asymmetries were not as severe as the fourth test. It was concluded that there was a definite difference between the low phi and high phi experiments.

The resistance of the bed dropped a little to 0.1034Ω . For the next experiment, it was proposed to operate at a high phi for a longer period of time. It was also decided to try to increase the flow rate and try to maintain a higher pressure. The throttle valve was tightened and the flow from the tank farm was fully opened. Since enough flow could not be generated with the 1020 kPa regulator, it was decided to put a 1A cylinder of He above the regulator to allow more flow into the bed (it had to go through the 1634 kPa regulator). The 1A bottle increased flow but pressure in the vessel rose drastically and the vessel pressure relief was actuated. It was a difficult task to match flow and pressure due to the throttle valve being aft of the bed and the flowmeter was located inside, so one person had to monitor flow and yell very loudly to the individual changing the valve position. Since the flow

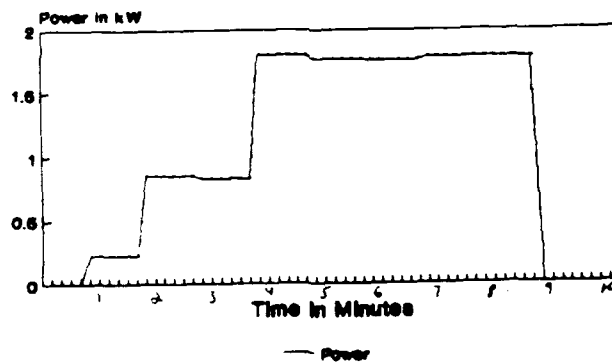
meter was not calibrated past 1500 lpm (not including the He 1.43 correction factor),

Figure 4.3.10 Repeat Test at Low Phi

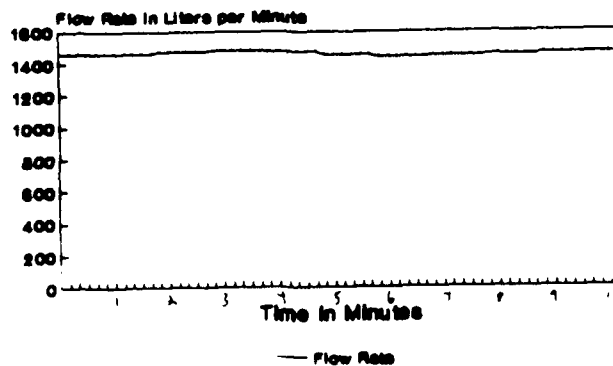
Repeat Test at Low Phi 25 Jan 93 15:22



Power vs Time 25 Jan 93 15:22



Flow vs Time 25 Jan 93 15:22



it was determined to not exceed this for too high of a value (see Appendix C.4 for flowmeter calibration). Since the 1A cylinder would also run out in a test (just above 7000 L in volume), it would not be worth to have to constantly change the bottles. The max flow was set for ~2570 lpm at 612.24 kPa.

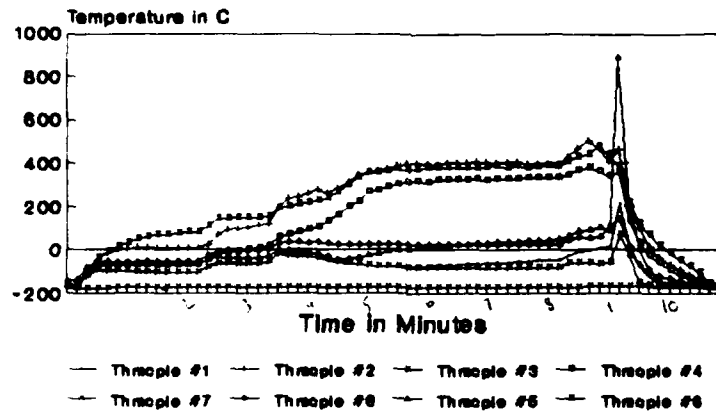
The results of the experiment are shown in Figure 4.3.11. The thermocouples followed the same trends as past experiments for the first two minutes of the power addition. Then for ~ the next three minutes, while power was held constant, the slope of the divergence decreased for all of the thermocouples except #5 which started to gradually increase in temperature. Since the divergence slope had decreased, it was decided to increase power again. Approximately 58 sec after the power addition, thermocouple #5 got very hot (screen display showed 1100 °C). Thermocouple #6, #4, and #2 increased for the first 30 sec of the power ramp, but then decreased for the next 20 seconds. The power was shut off and gas continued to cool the bed. The thermocouple's indicated - 170 °C temperatures which seemed to indicate they were still working. Power was added to the bed again, and there was no current indication which showed that there was problems with the bed.

The above experiment indicated that the temperature divergences did not run away in a short period of time (slow time step so corrections could be made, as past experiments). However, when the power was increased while maintaining flow, the bed was lost in a short period of time. Temperatures were below the 700 °C max for coating swelling, so it was believed that this was not the cause of the problem. The resistance of the bed did decrease gradually with each experiment, so it was suggested that using the bed for eight experiments may have been a cause. It was hoped that inspection of the bed would give some insight into this issue.

Figure 4.3.11 High Phi Retest

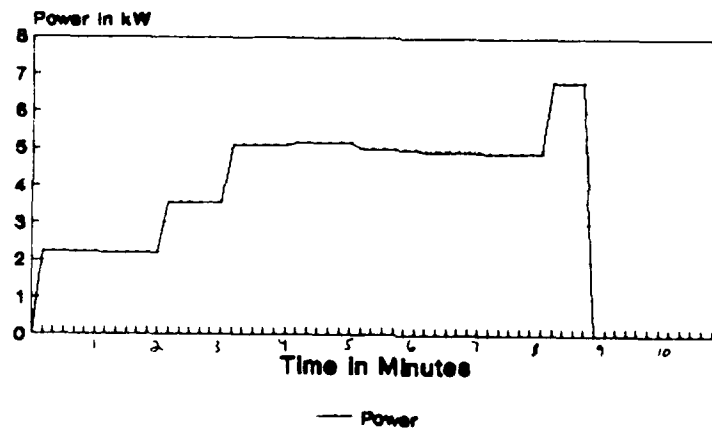
High Phi Retest

26 Jan 93 0940



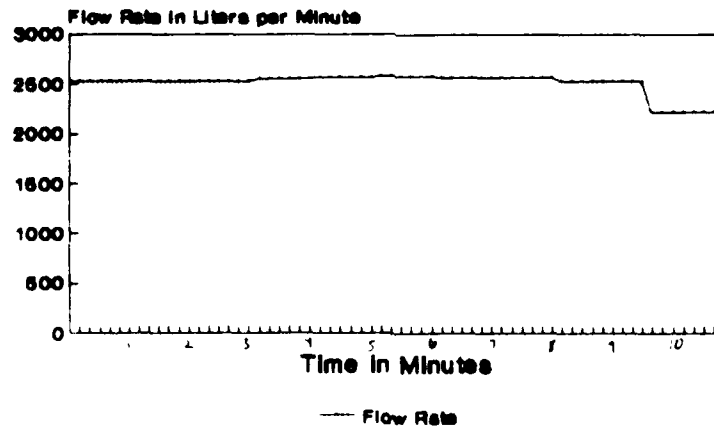
Power vs Time

26 Jan 93 0940



Flow vs Time

26 Jan 93 0940



Preliminary inspection of the bed was that it was not as bad a melt as the Oct 92 experiment. The cold frit and hot frit were still intact. An attempt was made to remove the bed from the manifold, but was unsuccessful since the thermocouples were fused to the bed. Shears were used to cut the thermocouples. Looking downwards on the bed, it had a char all around the circumference of the bed with more of a char in the region next to thermocouple #5 (bottom side - see Figure 4.3.13 for a view of the bed). The bed was removed from the frits. The bed was unrolled (hard to do since the screen was fused together) approximately 1/3 of its length until it could not be rolled any more due to melting. Inspection of the bed revealed that severe melting had occurred at the inlet side of the bed in the lower region near the hot frit. The hot frit was severely melted in this area. Looking downwards into the middle of the hot frit, a nice ring of bubbles had formed in the inside of the frit at the inlet end (see Figure 4.3.12 for a picture of the melted bed and hot frit).

The bed coating that was unraveled looked good in the middle, with black streaks occurring approximately at every wrap (see Figure 4.3.12). These black streaks probably came from the hot region, near thermocouple #5. The final conclusion from post inspection revealed that the melting occurred at the inlet side around thermocouple #5. Different causes were pondered. It was speculated that it could have been a bed problem since #5 spiked and the others did not increase as much compared to the Oct 92 experiment. This argument could also be supported by the fact that #5 started to increase in temperature before the additional power was put into the bed. If it was not a bed problem, even though the instabilities were relatively slow moving, (minutes) a power ramp (temperature increase) does rapidly increase the divergence and runaway in a shorter time (s).

Figure 4.3.12 Melted Bed and Hot Frit

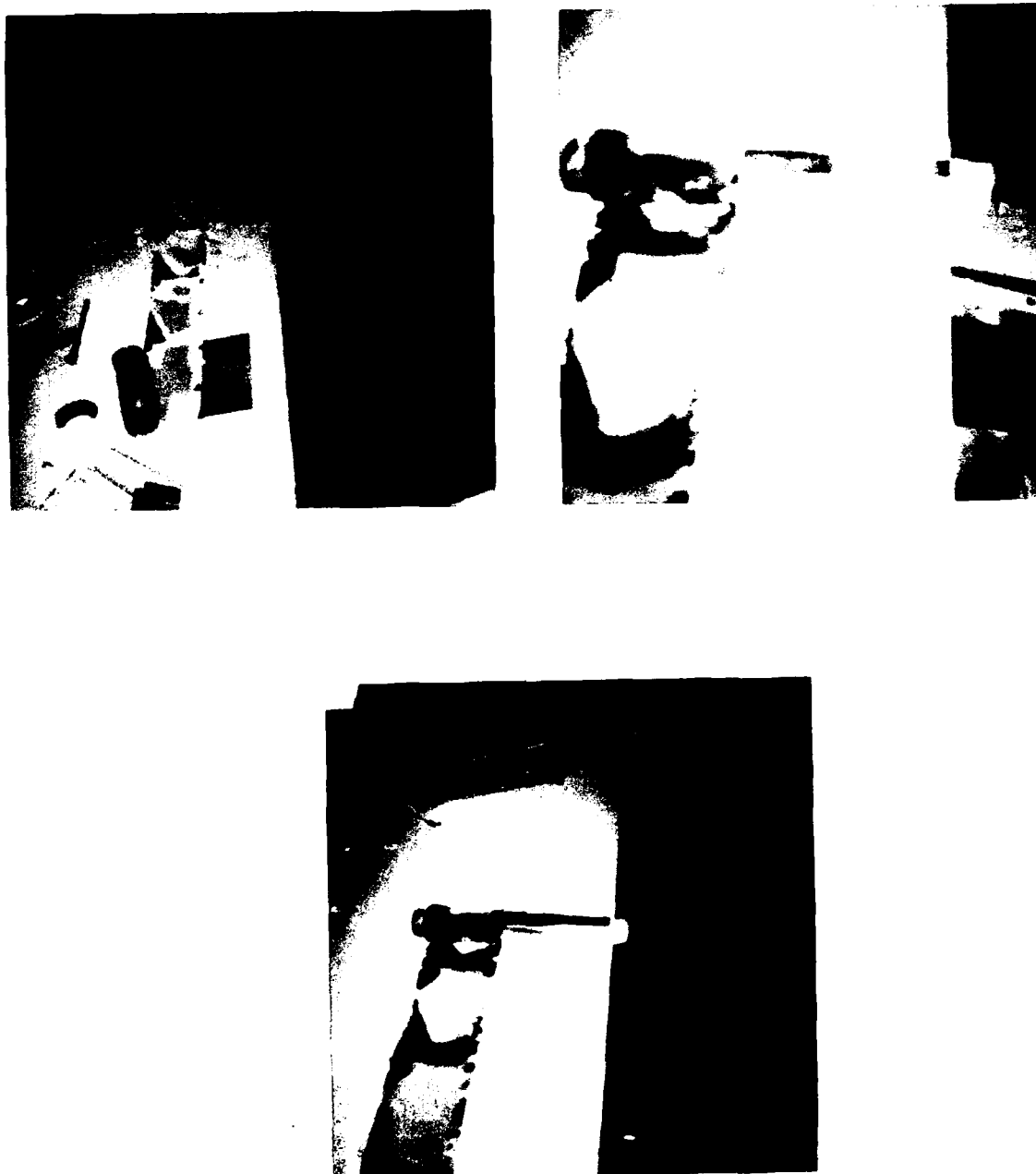


Figure 4.3.13 Charred Bed



The seams were not felt to be a cause since melting only occurred at the inlet side and not along the entire seam. The melting occurred close to the hot frit seam, but not directly upon it. There also was no melting at all on or around the cold frit seam (a bigger seam).

The above 8 experiments were deemed successful. Low ϕ (room temperature runs) showed constant temperature, while higher ϕ runs showed temperature divergence with no induced blockages in the bed. The high ϕ experiments also showed that when power was decreased after the thermocouples diverged, the higher thermocouples dropped sharply in temperature as the lower bed thermocouples started to slightly *increase* in temperature. Was this flow instability? The next chapter will compare the above experimental results with other's predictions of stable/unstable regions. Analytical tools will also be used to try to model the experiments in order to reduce uncertainties.

This Chapter discussed the test procedure and 9 tests conducted using the design described in Chapter 4. These experiments produced results that could be used for comparison to the analytical predictions mentioned in Chapter 2. Some other experiments were conducted that were unsuccessful, but were important in the evolution of the design. These tests are described in Appendix B.

CHAPTER 5

ANALYSES

5.1 INTERPRETATION OF ASYMMETRIES IN TEMPERATURES

The results from Chapter 4 showed that there are asymmetries in the temperatures in the bed. There are several qualitative observations that can describe these asymmetries and should be mentioned as a precursor to the analysis that lead to the investigation of uncertainties in the data.

Due to the wrapping of the screen, the flow passages in the element are highly irregular with branching. Since the screen is wrapped, the wires may line up in some areas and be off set in others. This effect on temperature should be moderated by areas that are hotter mixing with other areas that are cooler. Even though the screen was thoroughly inspected before assembly to insure that none of the holes were clogged, local porosity fluctuations could have occurred in the bed.

The seams could create a temperature spike in the bed area since they are non-porous. However, as described from the experiments, it was hard to draw conclusions from visual inspections of the bed. In the two meltdown experiments, melting in the bed could not be linked to the seams.

Local power fluctuations could also have caused asymmetries in the bed. There was no way of measuring these fluctuations in the runs except for temperature spikes from the thermocouples (e.g. #5 in the last run) or inspection of the screen after disassembly. Measuring the macro bed resistance (end to end) before and during assembly was the only way to insure that there were no electrical shorts in the bed.

The analysis of the experimental results consists of two parts. The first part is to analyze the data to try to minimize uncertainties (e.g. energy balance

checks, check measured temperatures versus analytical temperatures) in the data. The second part is to relate the data to the flow instability analysis done-to-date in Chapter 2 .

5.2 TEMPERATURE AND PRESSURE DROP ANALYSES

5.2.1 Energy Balance

In order to minimize the uncertainties in the data, several energy balance calculations were performed to check the experiment power versus calculated power (The true experiment power was determined in Appendix C). The equation for calculated power is :

$$Q = \dot{m} c_p \Delta T \quad [5-1]$$

where Q = calculated power, \dot{m} =flowmeter mass flow rate, c_p = specific heat for He taken from W-2, and ΔT the outlet - inlet temperatures (thermocouple #8 - thermocouple #7). The calculations were set-up using a spreadsheet. The temperatures and mass flows for each interval (every 10 sec) were multiplied by the specific heat (~5.193 - 5.197 kJ/kg K) to get the calculated power. Figures 5.2.1 - 5.2.6 show the results of this calculated power to the experiment power for six of the runs (The no flow runs were not applicable).

Figure 5.2.1.1 Energy Balance for Test #1

Energy Balance Calculations Bed Test at Low Phi 20 Jan 93

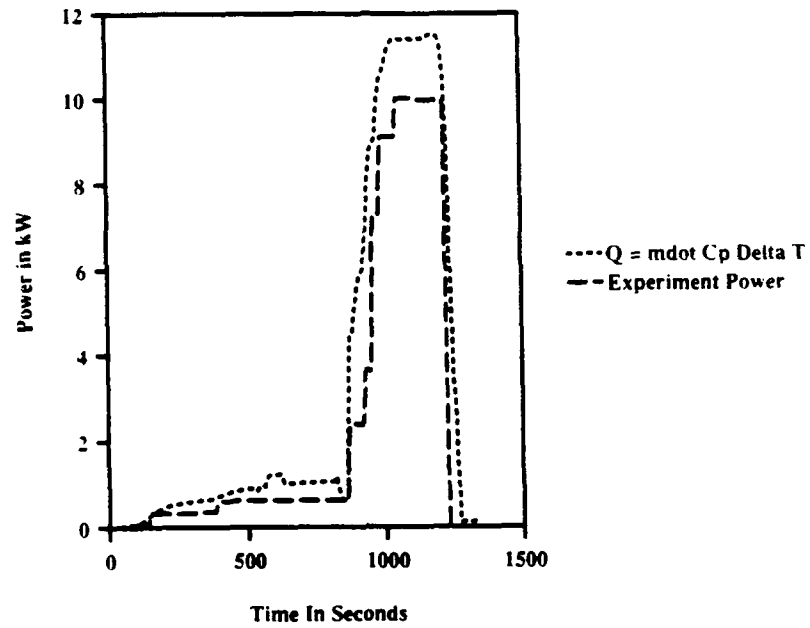


Figure 5.2.1.2 Energy Balance for Test #4

Energy Balance Calculation for Test on 22 Jan 93 0940

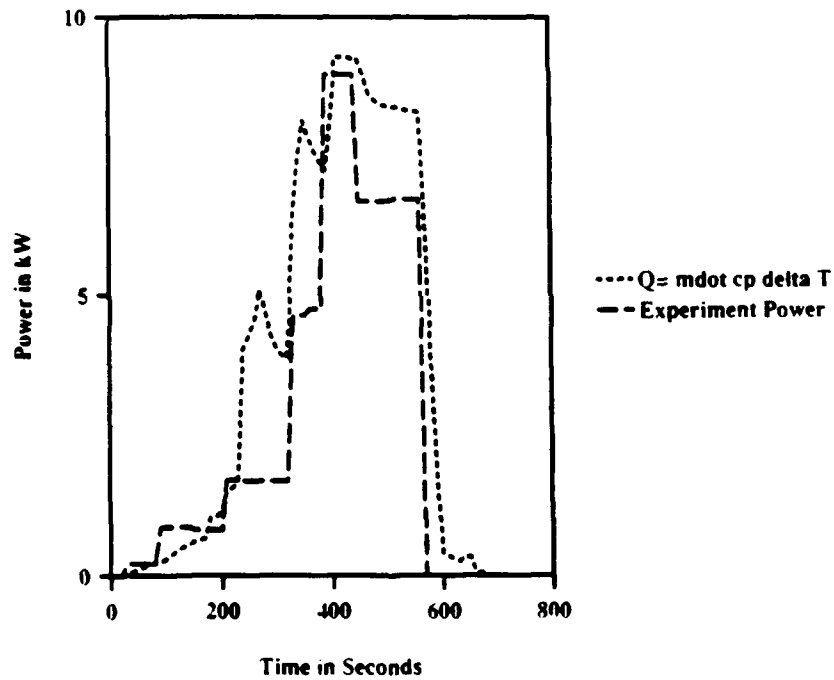


Figure 5.2.1.3 Energy Balance for Test #5

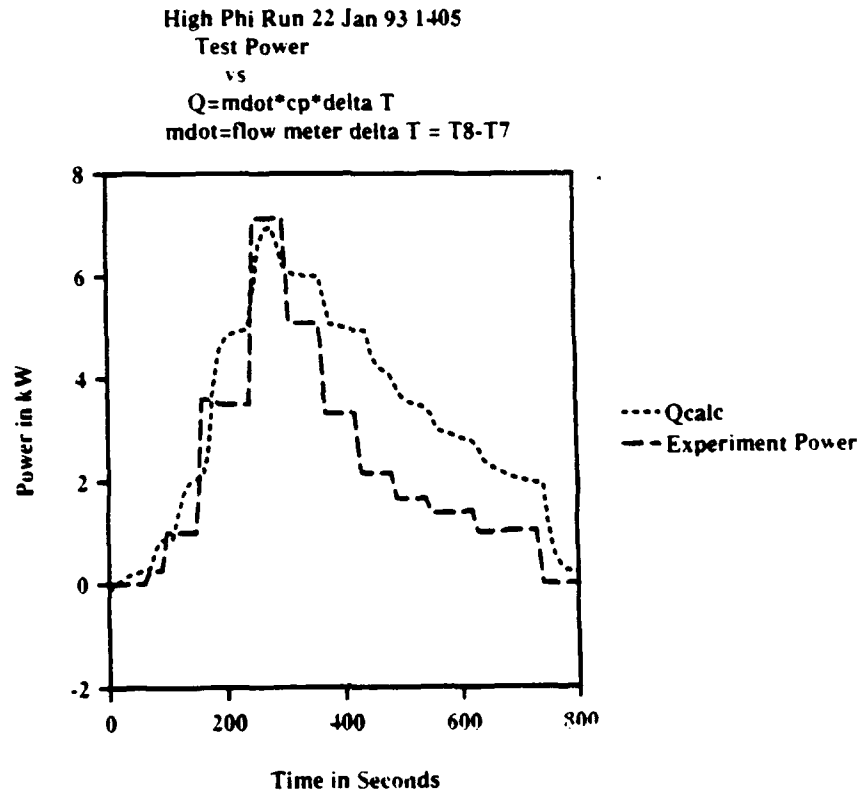


Figure 5.2.1.4 Energy Balance for Test #6

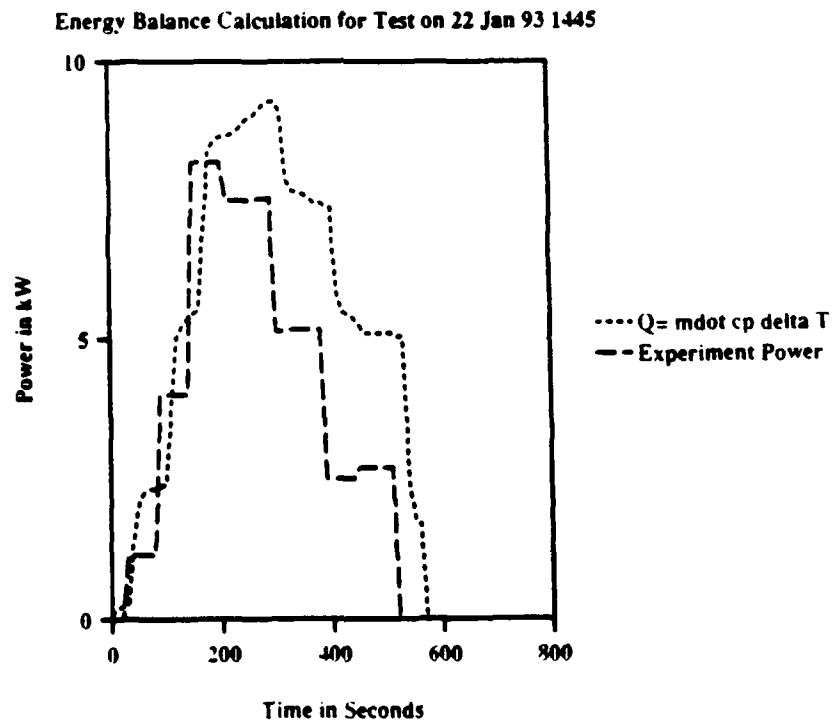


Figure 5.2.1.5 Energy Balance for Test #7

Energy Balance Calculation for Test on 25 Jan 93 1522

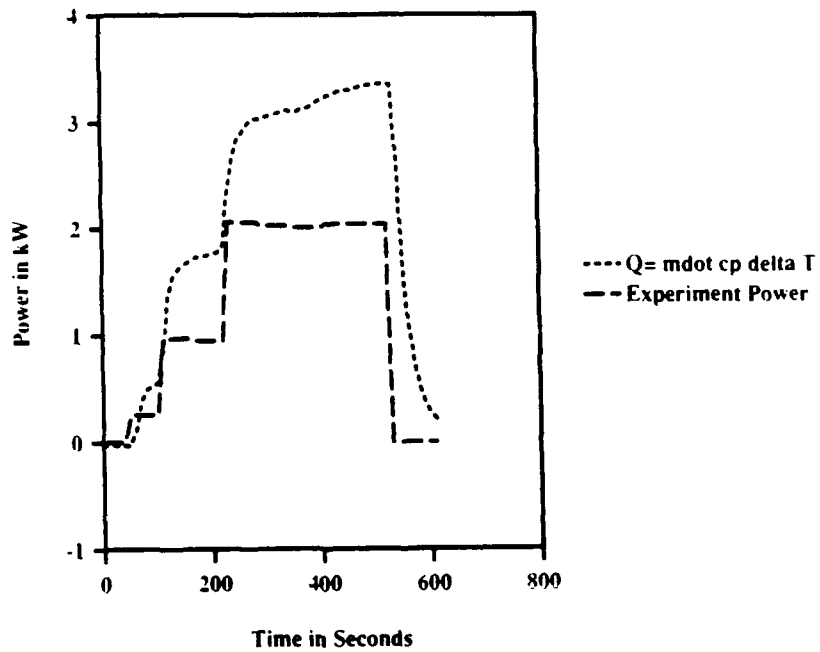
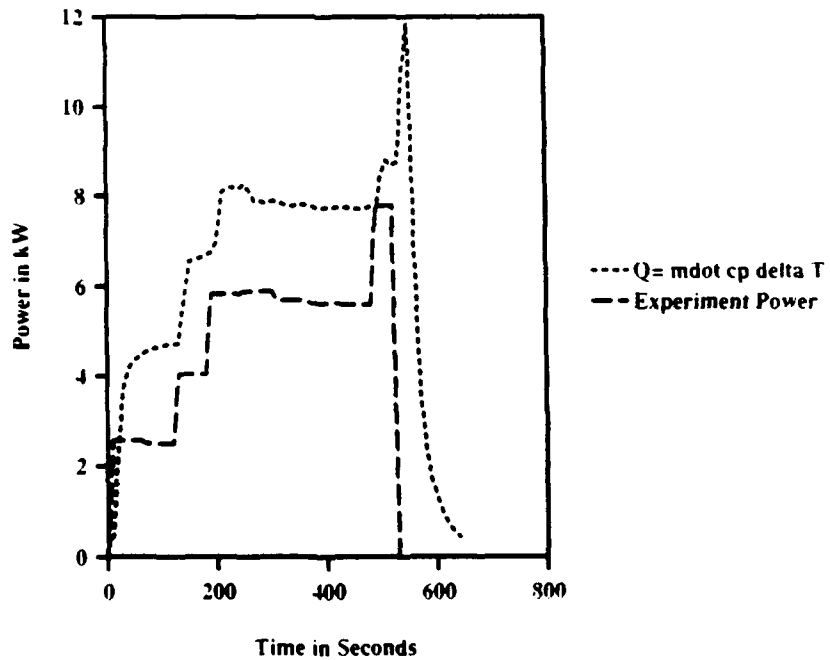


Figure 5.2.1.6 Energy Balance for Test #8

Energy Balance Calculation for Test on 26 Jan 93 0940



The results show that there was a slight imbalance in powers. It is interesting to note that the powers match the best at the highest powers for each experiment. The energy balance is also very close when the temperature divergences are occurring in the high phi runs. The slight off set on down ramps is attributed to the bed heat capacity.

Appendix C also mentions calibration tests for the flowmeter. Unfortunately, no conclusions regarding the calibration of the flowmeter could be interpreted for this analysis (Therefore, the flowmeter reading was used as the mass flow rate). Calibration tests after the experiment determined that the flowmeter was calibrated, but there was some uncertainty in the 1.43 correction factor.

5.2.2 2D SIMBED

The SIMBED code was developed by UMass Lowell for Brookhaven National Laboratory [C-5]. This two dimensional, finite element, steady-state code relaxes the common assumption of local thermal equilibrium between fluid and solid phases; instead two energy equations are developed, one for the solid phase and one for the fluid phase. These equations, together with the equations of motion, are solved simultaneously. The code used effective viscous and inertial terms for the cold and hot frit resistances. These terms are the A and B coefficients of the Ergun relation:

$$A = \frac{150 (1-\epsilon)^2}{D_p^2 \epsilon^3} \quad B = \frac{1.75 (1-\epsilon)}{D_p \epsilon^3} \quad [5-2]$$

where ε is the porosity (0.30 for both frits) and D_p the particle diameter (20 μm for both frits).

The element was modeled using 40 axial nodes and 30 radial nodes. The code used ten of the axial nodes for fine meshing of the wall channeling effects. The cold and hot frit nodes each used two radial nodes while the fuel region used 6 nodes. The outlet plenum used 14 nodes, six are used for fine meshing of the turning of the flow from a radial to an axial flow. The remaining 6 nodes are used for the inlet region. A sample of the input deck is shown in Table 5.2.2.1

Table 5.2.2.1 SIMBED INPUT

```

.....
Document File for
the case of

STEADY-STATE, 2-D, AND CONICAL GEOMETRY

VERSION 2DS_C-1

JANUARY 1992
.....

This sub-directory contains the latest version of the steady-state
2-D conical program for the Particle Bed Reactor model.
(Ver. 2DS_C-1.) In order to run this program, the files BNLS2S.D.FOR,
PBR2S_C.FOR, and PROP.FOR must be compiled and linked. The file
DATA_C.DAT contains the input parameters of the problem which are
described at the end of this document file. In this version, the
density correction terms are included in the pressure correction
equation.

The SIMPLEC procedure for pressure correction equation has been
employed in order to improve convergence.
-----
DEFINITION OF THE INPUT PARAMETERS (see file "DATA_C.DAT"):

LAST      = Total number of iterations to be performed in each run
NSTART    = Flag: 0 = Use initial guess; 1 = Read data from disk
NPRINT    = Flag: 0 = No printing; 1 = Print data field at end of run.
MSAVE     = Number of iterations at which the intermediate data is saved.
            recommended value = 50.
NSAVE     = Flag: 0 = Do not save the data at end of run; 1 = Save the data
RIP       = I index of the grid point at which the values of the variables
            are printed at selected iterations.
RJP       = J index of the grid point at which the values of the variables
            are printed at selected iterations.
LI        = Number of grid points in the Z-direction.
MI        = Number of grid points in the R-direction.
JR1       = J index for the last point in the inner tube.
JR2       = J index for the last point in the hot frit.
JR3       = J index for the last point in the bed.
JR4       = J index for the last point in the cold frit.
R1        = Inner radius of the Hot frit, @ X=0 (mm).
R2        = Outer radius of the Hot frit, @ X=0 (mm).
R3        = Inner radius of the Cold frit, @ X=0 (mm).
R4        = Outer radius of the Cold frit, @ X=0 (mm).
R5        = Outer radius of the inlet channel, @ X=0 (mm).
            (If the inlet channel does not exist, CASE 2, R5 = R4)
RR1       = Inner radius of the Hot frit, @ X=R (mm).
RR2       = Outer radius of the Hot frit, @ X=R (mm).
RR3       = Inner radius of the Cold frit, @ X=R (mm).
RR4       = Outer radius of the Cold frit, @ X=R (mm).
RR5       = Outer radius of the inlet channel, @ X=R (mm).
            (If the inlet channel does not exist, CASE 2, RR5 = RR4)
DP        = Diameter of the fuel particle (mm).
DCP       = Diameter of the Cold frit particle (mm).
DHP       = Diameter of the Hot frit particle (mm).
H         = Length of the system (mm).
EP30      = Porosity of the porous layer far from the walls.
RELKV     = Relaxation factor for velocity components; 0.5 is recommended
RELTY     = Relaxation factor for the temperatures; 1. is recommended
RELPRHO   = Relaxation factor for the fluid density (= 1. for most cases)

```

FLMASS - Total mass flow rate entering the system [Kg/sec].
 TIN - Temperature of the fluid entering the system [K].
 PIN - Pressure of the fluid entering the system [Pa].
 RHOS - Density of the solid phase in the porous layer [Kg/m3].
 CPS - Specific Heat of the solid phase in the porous layer [J/Kg-K].
 CONDS - Thermal conductivity of the solid phase in the porous layer [W/m-K].
 ALPHCF - Viscous Resistance Coefficient of the cold frit [1/m2].
 BETACF - Inertial Resistance Coefficient of the cold frit [1/m].
 RHOCF - Density of the solid phase in the cold frit [kg/m3].
 EMSCF - Emissivity of the solid phase in the cold frit.
 CPCF - Specific Heat of the solid phase in the cold frit [J/Kg-K].
 CONDCF - Thermal Conductivity of the solid phase in the cold frit [W/m-K].
 ALPHHF - Viscous Resistance Coefficient of the hot frit [1/m2].
 BETAHF - Inertial Resistance Coefficient of the hot frit [1/m].
 RHOHF - Density of the solid phase in the hot frit [Kg/m3].
 EMSHF - Emissivity of the solid phase in the hot frit.
 CPHF - Specific Heat of the solid phase in the hot frit [J/Kg-K].
 CONDNF - Thermal Conductivity of the solid phase in the hot frit [W/m-K].
 UHEAT - Power Density of the fuel bed [W/m3].
 GAMMA - Residual reduction factor used in SOLVE (use 0.01 to 0.2).
 DELTA - Relaxation parameter used in SOLVE (use 0.0 to 0.5).
 DATAFILE - Name of file from which to read and write data for the run.

The SIMBED code was used to check the experimental bed temperatures. Since the code required many iterations to converge (~2500 iterations - 15 hours of run time on a Vax 3100), time did not allow calculations to be made for more than two cases. The first test studied was Test #5 (High Phi Run 22 Jan 93) at time = 5 min, at an inlet temperature of 124 K, and an inlet pressure of 748.3 kPa. The second test studied was Test#1 (Bed Test at Low Phi 20 Jan 93) at time = 13 min 30 s, at an inlet temperature of 328.15 K, and an inlet pressure of 272.11 kPa. The code used a modified NASA Prop2ph2 properties routine for He [W-3]. The results of the temperature distribution, pressure drop, and radial velocity profile are shown in Figures 5.2.2.1., 5.2.2.2, and 5.2.2.3

Figure 5.2.2.1 Temperature Profile for Test #5

High Phi Run 22 Jan 93
Temperature Distribution
Time = 5 min

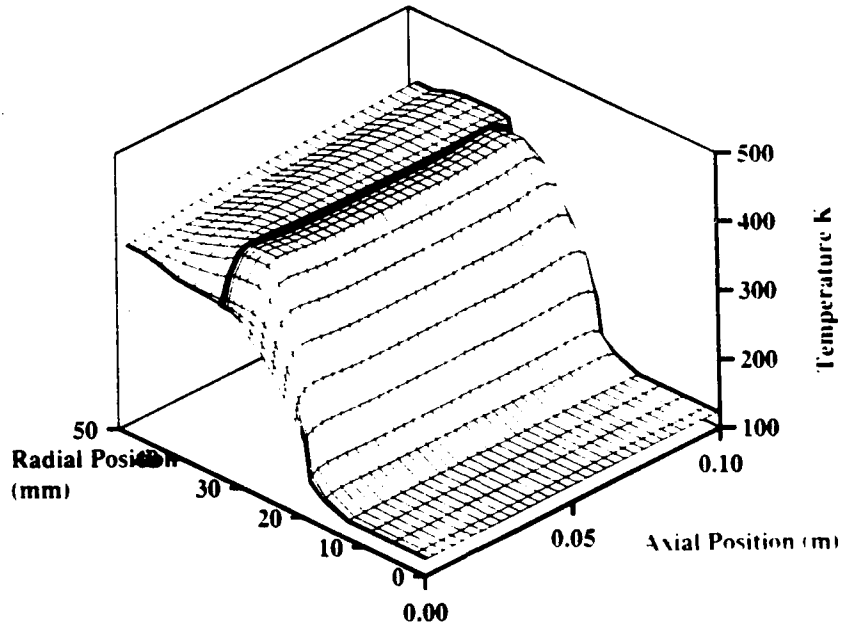


Figure 5.2.2.2 Pressure Drop For Test #5

High Phi Run 22 Jan 93
Pressure Drop
Time = 5 min

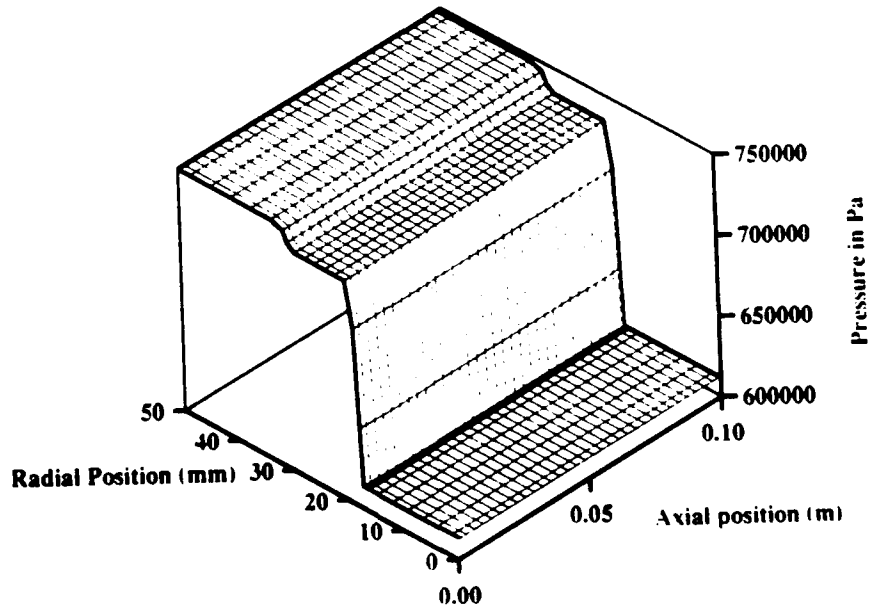
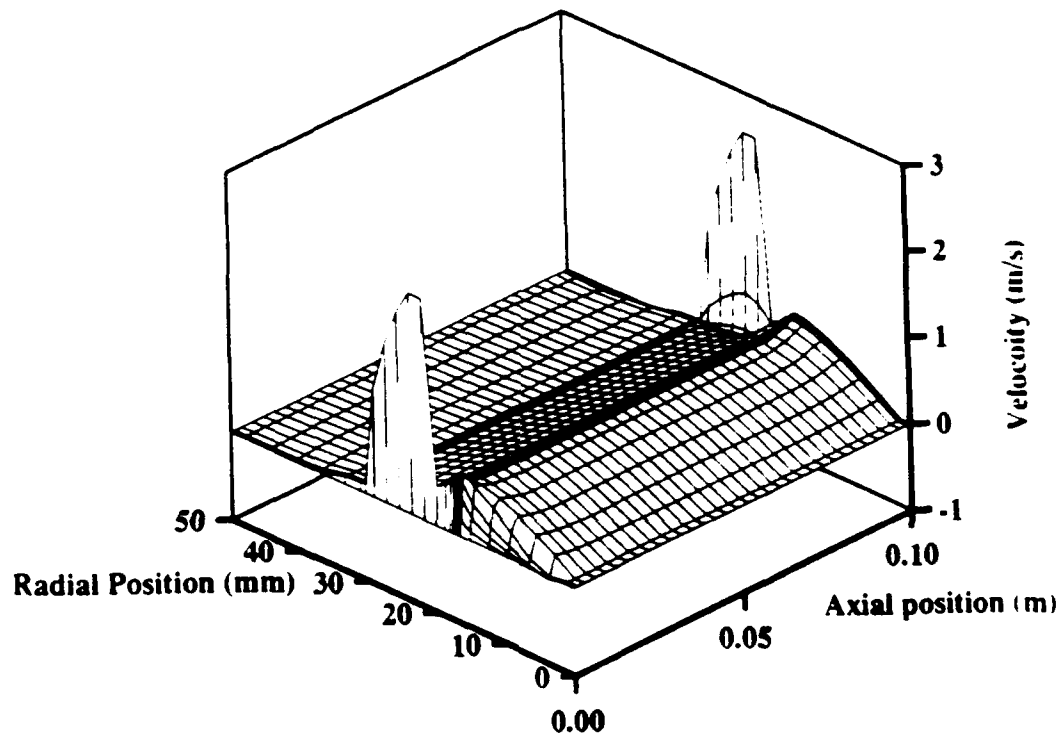


Figure 5.2.2.3 Test #5 Velocity Profile

High Phi Run 22 Jan 93
Radial Velocity Profile
Time = 5 min



The mixed mean outlet for the high phi run was very close to the experimental results. The mixed mean outlet temperature was 408 K for the SIMBED run and 410 K for the experimental results. This result was not surprising since the energy balance runs showed a close match for this time. The temperature profile for the SIMBED run was based on an uniform heat deposition shape and uniform cold frit resistance. There was a slight gradient in the temperature profile due to the higher pressure drop across the radial direction.

The pressure drop according to the following equation gave the following comparison:

$$\Delta P = R_{TOTAL} W^2 \quad [5-3]$$

$$\text{SIMBED: } \Delta P = 748.3 - 620 \text{ kPa} = 128.3 \text{ kPa}$$

$$m = .0041667 \text{ kg/sec}$$

$$R_{TOTAL} = 7.39 \cdot 10^9 \text{ Pa/kg}^2\text{s}^2 \text{ SIMBED}$$

$$R_{TOTAL} = 3.3769 \cdot 10^7 \text{ PA/kg}^2\text{s}^2 \text{ Appendix C}$$

Even though there was a huge difference in resistance factors between Appendix C and the SIMBED run, there was an explanation. First, the experiment in Appendix C had the gas exit through a tube three-fourth's into the bed, therefore it did not include the pressure drop through the cold frit. Second, since the gas flowed in through the hot frit, the gas would expand a little instead of contracting which would cause the pressure drop to be less in the experiment. Since the flows were so low, this effect should not be too substantial. Figure 5.2.2.2 showed that the biggest pressure drop occurs across the hot frit. This pressure gradient was caused by the cold frit and hot frit having the same resistances (same porosities), and the gas axial flow increased speed along the axial length as it picked up heat. Since there was not enough

time to perform a thorough pressure drop test, it was decided that the SIMBED pressure drop results were the most realistic for the tests.

The radial velocity profile shows in Figure 5.2.2.3 the edge channeling effects and the acceleration of the gas as it is heated by the screen and the area becomes smaller.

Figure 5.2.2.4 shows the temperature distribution for the Bed Test at Low Phi (Test #1) Experiment for 20 Jan 93. The outlet temperature matches better than the TRITRAN code (1D transient code discussed in Appendix G) for time = 13:30, (TRITRAN $T_{out}=380$ K, SIMBED $T_{out}=408$ K). However, the T_{out} according to thermocouple #8 was 494.5 K at this time. Section 5.4 will address the uncertainties in the data readings.

5.3 PHI VS REYNOLDS NUMBER CALCULATIONS

5.3.1 Description of Stability Curves

Three stability curves were used to compare with the experimental results. The first curve was for the Maise stability criterion (derived from Bussard and DeLauer) discussed in Chapter 2.. He viscosity properties $\mu \propto T^{0.7}$ and a bed porosity of 0.4 were applied to generate β 's (function of Reynolds number) and ϕ 's for a curve of the critical temperature ratio vs the critical Reynolds number.

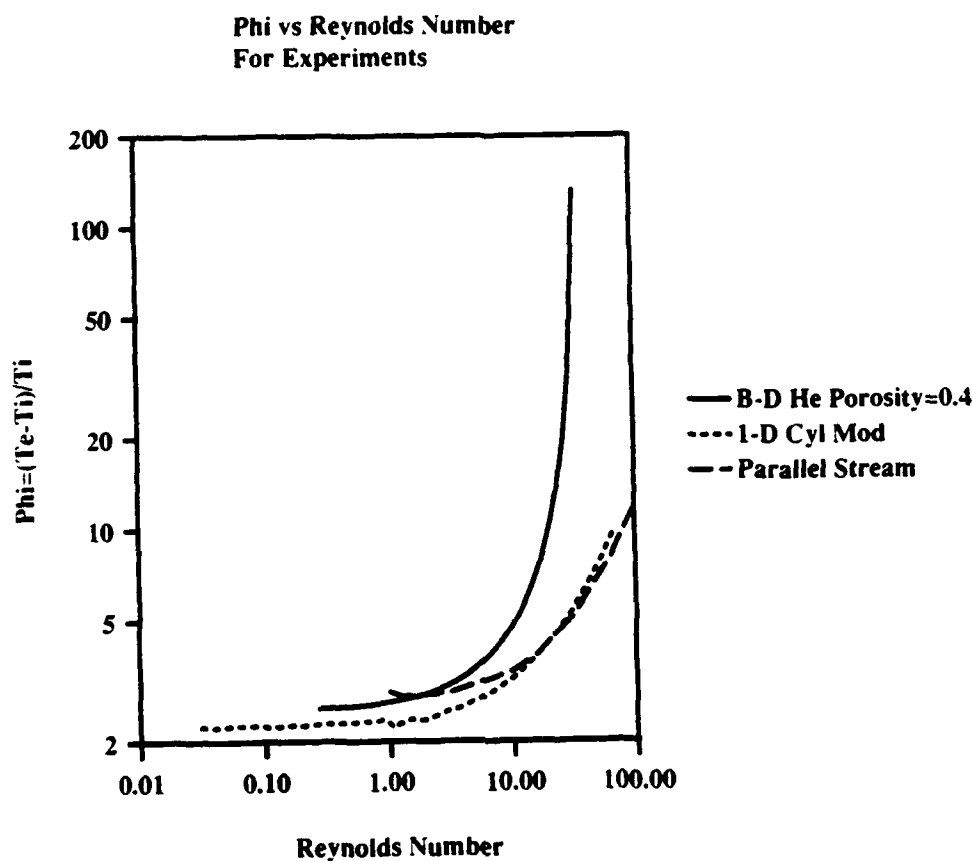
The second curve was a 1-D cylindrical model using numerical simulation derived from Jonathan Witter's approach [W-1]. The geometries of the screen bed, helium properties (prop2ph2 modified for He), and thermal hydraulic behavior (similar to the TRITRAN input deck, see Appendix G) were incorporated into a model. Using PBRFMP (PBR Find Mass Flow and

Pressure, see Appendix G), the minimum pressure drop can be determined through an iteration scheme. By the stepping up the mass flow rate (Reynolds number), the pressure drop can be compared to the last step's pressure drop. Once the current step pressure drop is greater than the previous step, the critical conditions have been determined. The inlet and outlet temperatures are used to find the temperature rise factor. Then the power is stepped to the next value and the iteration process for the minimum pressure drop is repeated [W-3].

As mentioned in Chapter 2, this analysis approach is conservative since it assumes that the fuel region pressure drop is the stability criterion. Witter showed in W-3 that the cold frit resistance is a stabilizing factor due to that the cold frit can act as a stabilizing orifice to help ensure that flow is directed in the radial direction to match the power profile. However, using the screen bed geometry and thermal hydraulic assumptions with He, Figure 5.3.1.1 shows that the stability region shifts to the right and upwards., compared to Bussard and DeLauer.

The work done by Kalamas and Kerrebrock was described in Chapter 2. Jim Kalamas performed a parallel stream analysis for the geometry and inlet conditions of the screen bed experiment [K-2]. His results are shown in Figure 5.3.1.1.

Figure 5.3.1.1 Phi vs Reynolds Number for the Experimental Apparatus



5.3.2 Description of Phi and Reynolds Number Points

The calculation of the Reynolds number is a very important parameter in comparison to the above stability curves. Since Reynolds number is defined as:

$$Re = \frac{\rho \bar{u} D}{\mu}$$

[5-4]

where

ρ = gas density, \bar{u} = average velocity, D = screen wire diameter, μ = gas viscosity
or

$$Re = \frac{\dot{m} D_p}{A_s \mu} \quad [5-5]$$

where m = mass flow rate, D_p = screen wire diameter, A_s = superficial flow area, μ = gas viscosity. It is important on how these variables are defined. The Reynolds number could be defined at the cold frit inlet, bed inlet, middle of the bed, or the bed outlet. Since gas properties and areas change for these definitions, the choice of Reynolds numbers is also important.

For all of the analyses, the screen wire diameter is defined as the diameter for the Reynolds number calculations. The wire diameter is ~ 0.0381 cm with the alumina coating. The real PBR particle diameter is expected to be 0.035 to 0.05 cm, and since the measured screen bed porosity is ~0.37 compared to ~0.35 to ~0.40 for the real PBR, the wire diameter is a good variable for Reynolds number calculations for stability criterion.

Prior to the experiments, Reynolds number calculations were performed to set the flow rates for the experiments for a specific Reynolds number in order to try to determine stability/instability regions. After the fact, there were some problems with these calculations. It was decided that the cold frit inlet would be the region used to determine the Reynolds number variables. Equation 5-4 was used to determine the Reynolds number. In order to calculate the average velocity, \bar{u} , the flowmeter reading was used. A sample calculation using this method is as follows:

Flowmeter reading = 2288 lpm of He
Pressure of Vessel (cold frit inlet) = 119 psi = 8.1 atm = 809.5 kPa
 ρ at this pressure = 1.348 kg/m³

Flowmeter to STP = 2288/8.1 = 282 lpm

In order to get gas velocity =

$$\bar{u} = 282 \text{ lpm} \cdot 1000 \text{ cm}^3/\text{l} \cdot 1/317 \text{ cm}^2$$

where 317 is the superficial flow area

$$\bar{u} = 891 \text{ cm/min} \cdot 1/60 \text{ s} \cdot 1/100 \text{ cm} = 0.1485 \text{ m/s}$$

Therefore,

$$\text{Re} = (1.348 \cdot 0.1485 \cdot 0.000381) / 1.07 \cdot 10^{-5}$$

$$= \sim 7 \text{ (estimate prior to the experiment)}$$

The problem with this method is twofold. First, the stability curves generated in the last section assume that the Reynolds number used is at the bed inlet (just as the gas has passed through the cold frit). Second, the wrong superficial flow area is used to calculate the average velocity. The above calculation assumes that $A_S = \pi r^2 l$ instead of $2\pi r l$ (The volume was calculated instead of the area). This error gave Reynolds numbers ~ 1.575 lower than the value calculated with the proper A_S for the cold frit flow region. Due to this error, the flow rates for the experiment were established to be higher than they needed to be. The proper calculations used $A_S = 2\pi r l$, \dot{m} = to the flowmeter \dot{m} , D_p = coated wire diameter, and μ the viscosity for the inlet temperature to the region studied.

Since flow area, and gas properties (density, pressure, and viscosity) are important parameters for the Reynolds number, a wide variety of Reynolds numbers could be calculated and compared to the stability curves. Figures 5.3.2.1- 5.3.2.5 show the $\phi = (T_{\text{final}} - T_{\text{inlet}}) / T_{\text{inlet}} = (\text{Thermocouple \#8} - \text{Thermocouple \#7}) / \text{Thermocouple \#7}$ vs Reynolds number for Reynolds numbers calculated at the bed inlet, middle of the bed, and bed outlet. Reynolds numbers and ϕ 's were calculated for each data point. (e.g. flowmeter \dot{m} , thermocouple #7 & #8 readings, and viscosities (different inlet temperatures for each region) for every 10 sec interval) .

Figure 5.3.2.1 Phi vs Reynolds Number for Test #1

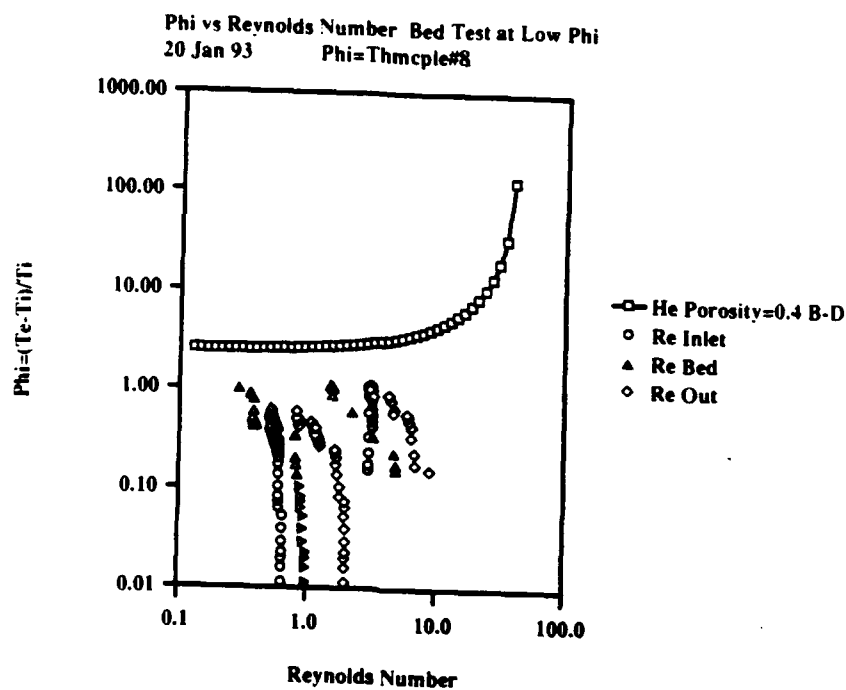


Figure 5.3.2.2 Phi vs Reynolds Number for Test #4

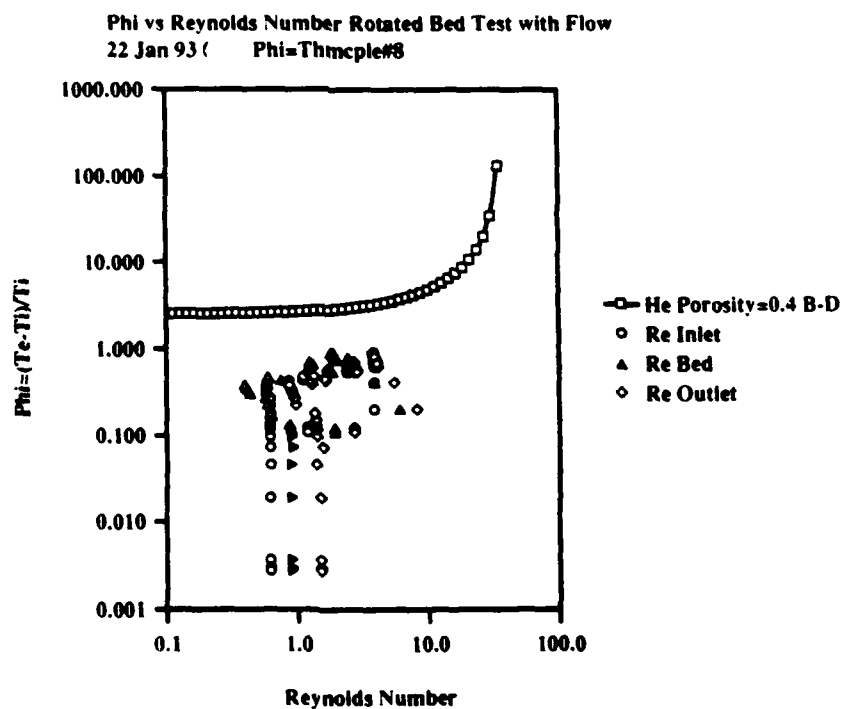


Figure 5.3.2.3 Phi vs Reynolds Number for test #5

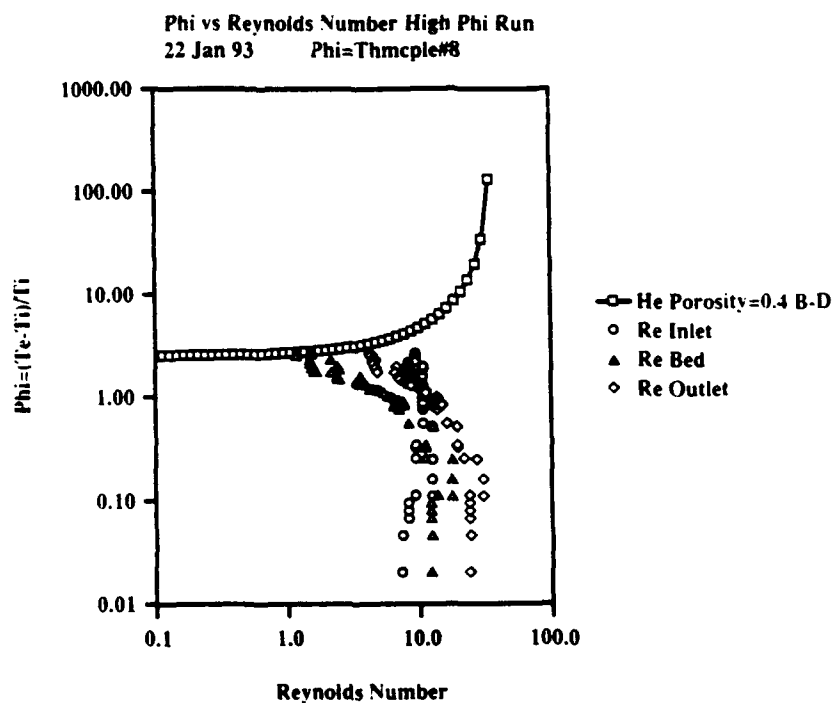


Figure 5.3.2.4 Phi vs Reynolds Number for Test #6

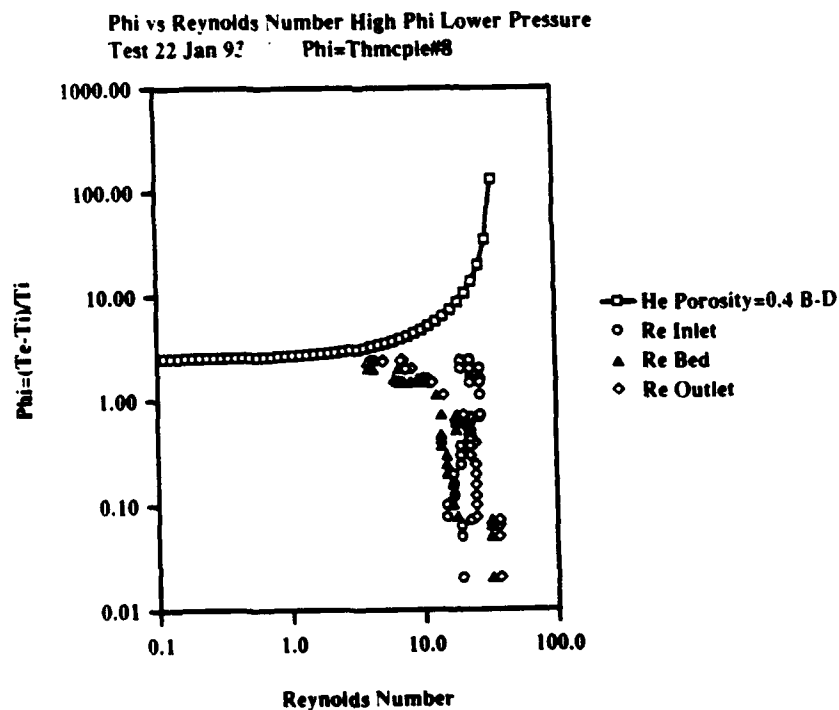
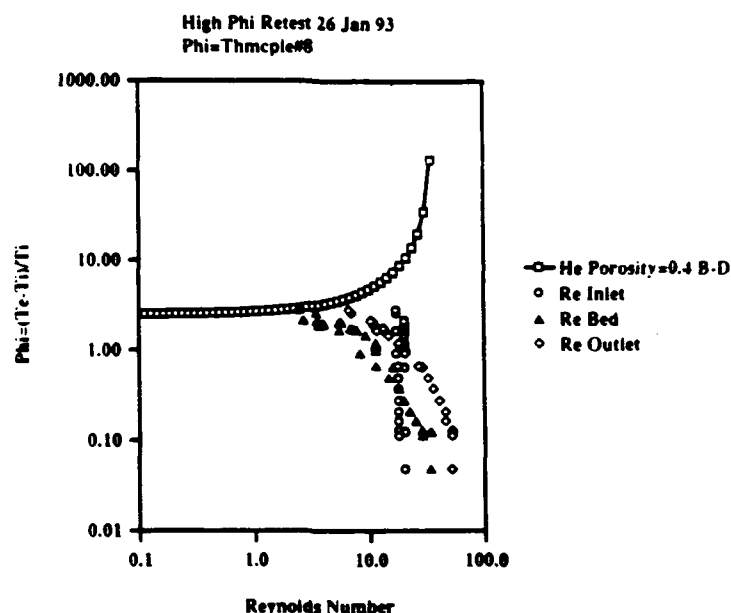


Figure 5.3.2.5 Phi vs Reynolds Number for Test #8



In order to have a proper comparison with the calculated stability criteria, the Reynolds numbers need to be at the bed inlet. The Reynolds number calculations in order to generate these Reynolds numbers used equation 5-5 where,

$$\begin{aligned} \dot{m} &= \text{flowmeter reading readings in lpm in order to get to} \\ &\text{kg/s: } \dot{m} = \text{lpm} \times 4\text{g/L} / 22.4\text{ l/m} \times 1/60\text{s} \times 1/1000\text{kg} \\ A_S &= 2\pi r l = 0.01885\text{ m}^2 \text{ (superficial area at bed inlet)} \\ D_p &= \text{coated wire diameter} = 0.000381\text{ m} \\ \mu &= \text{gas viscosity in kg/ms taken from W-2, changes with} \\ &\text{thermocouple \#7 temperature.} \end{aligned}$$

Since the flow meter was pressure and temperature compensating, the flowmeter reading was directly used for the Reynolds number calculations. Since thermocouple #8 was the best representative of the exit gas temperature, it was used in the phi calculations.

Figures 5.3.2.6 - 5.3.2.11 show the results of the phi and Reynolds numbers calculated at every 10 s interval for the entire length of each test. These numbers show that for the low phi runs, all of the phi clearly were in the

stable region. For the high phi runs, the points came close to the stability curves, and touched one of the curves in Test #5.

Figure 5.3.2.6 Phi vs Reynolds Number Test #1

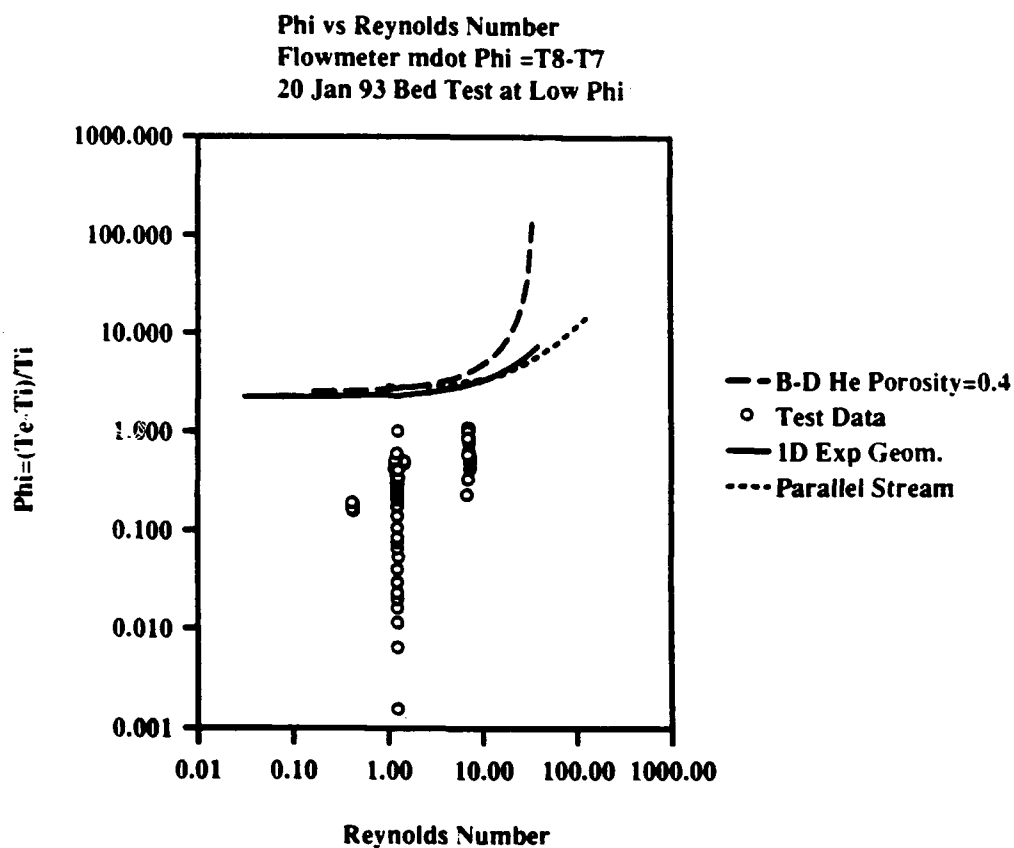


Figure 5.3.2.7 Phi vs Reynolds Number Test #4

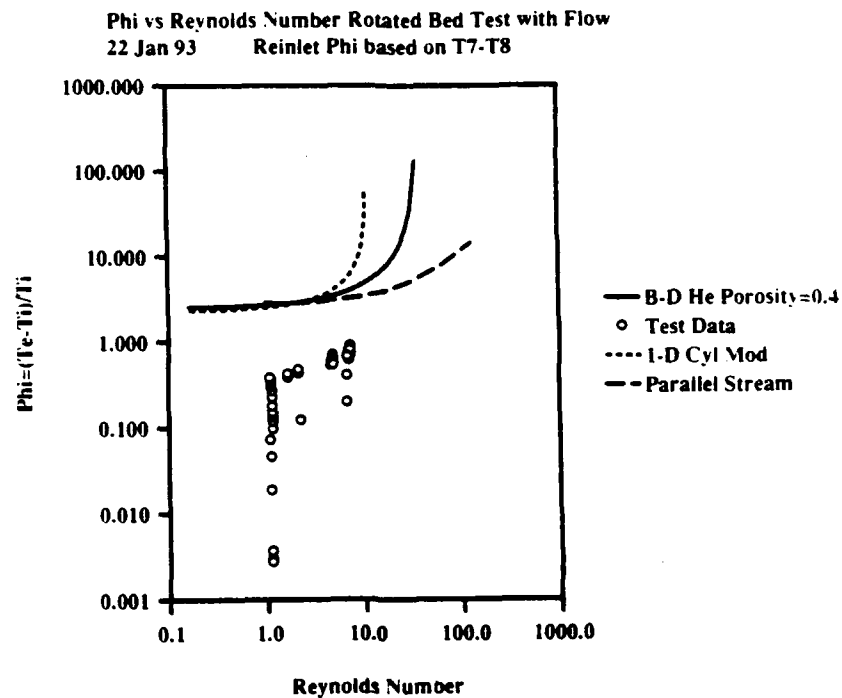


Figure 5.3.2.8 Phi vs Reynolds Number Test #5

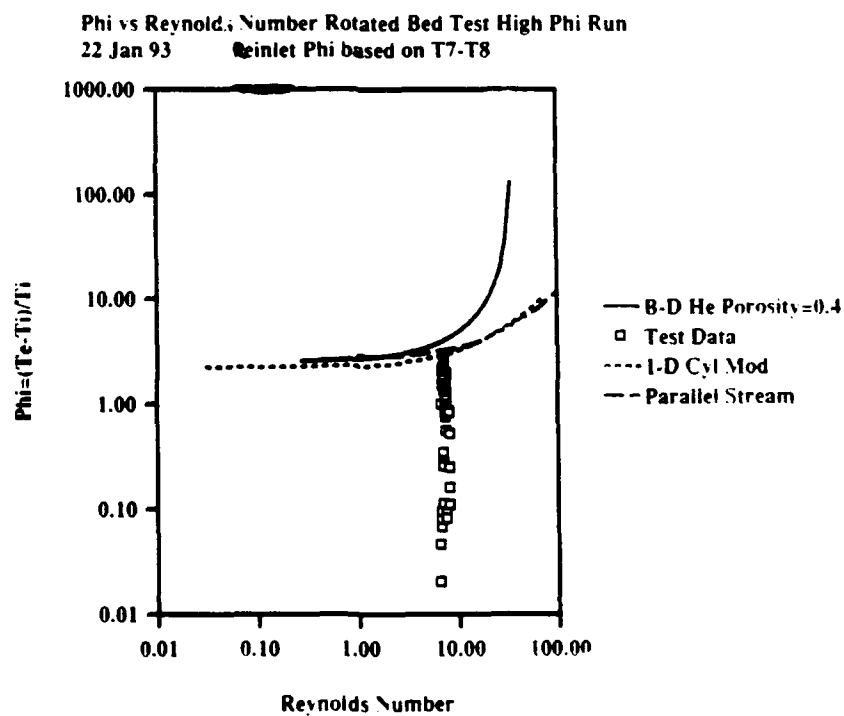


Figure 5.3.2.9 Phi vs Reynolds Number Test #6

Phi vs Reynolds Number Rotated Bed High Phi Lower Pressure
22 Jan 93 Reinlet Phi based on T7-T8

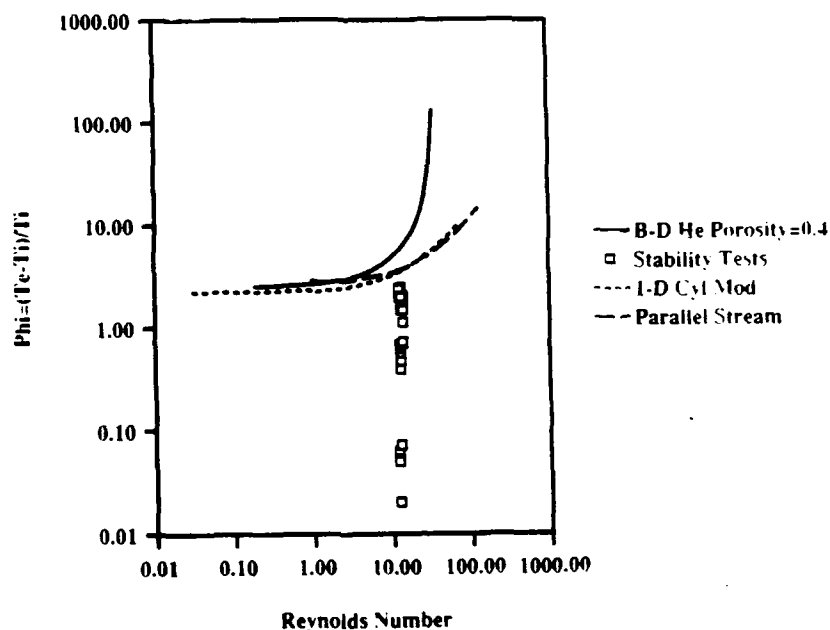


Figure 5.3.2.10 Phi vs Reynolds Number Test #7

Phi vs Reynolds Number Repeat Low Phi Test Rotated Bed
25 Jan 93 Reinlet Phi based on T7-T8

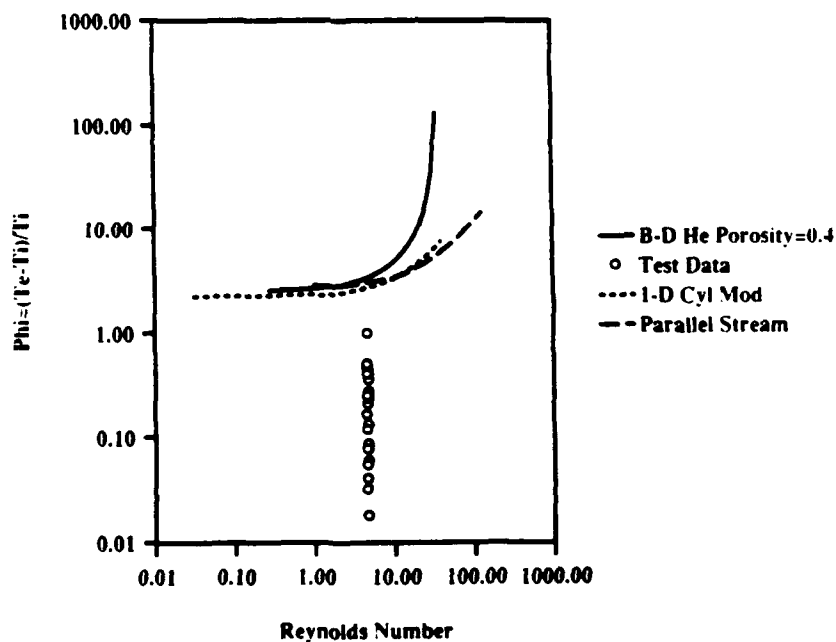
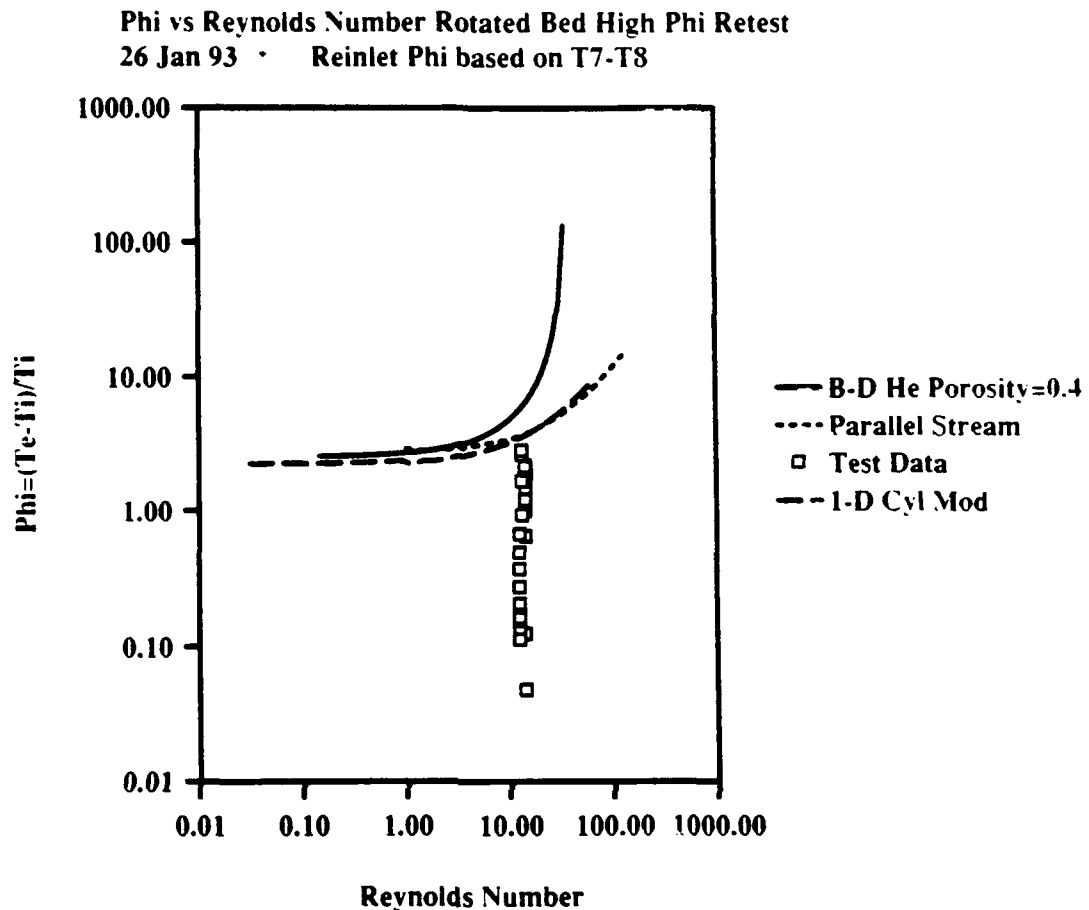


Figure 5.3.2.11 Phi vs Reynolds Number Test #8



Figures 5.3.2.12 - 5.3.2.14 show the results of phi vs Reynolds number for the three high phi runs. Instead of plotting at every interval, these figures show the points for the time interval where the temperature divergences were observed. The temperature divergences for the three high phi tests is as follows: for test #5 , time = 3:40 - 5:50, for test #6, time =3:00 - 5:10, and for test #8 time = 4:00 - 6:30. In test #5, one of the points intersects the 1-D cylindrical model line, otherwise, the points show that the temperature divergences occurred in regions defined as stable according to the stability criteria for the curves for the Reynolds numbers and phi's generated in the experiments.

Figure 5.3.2.12 Phi vs Reynolds Number (Temperature Divergences) Test #5

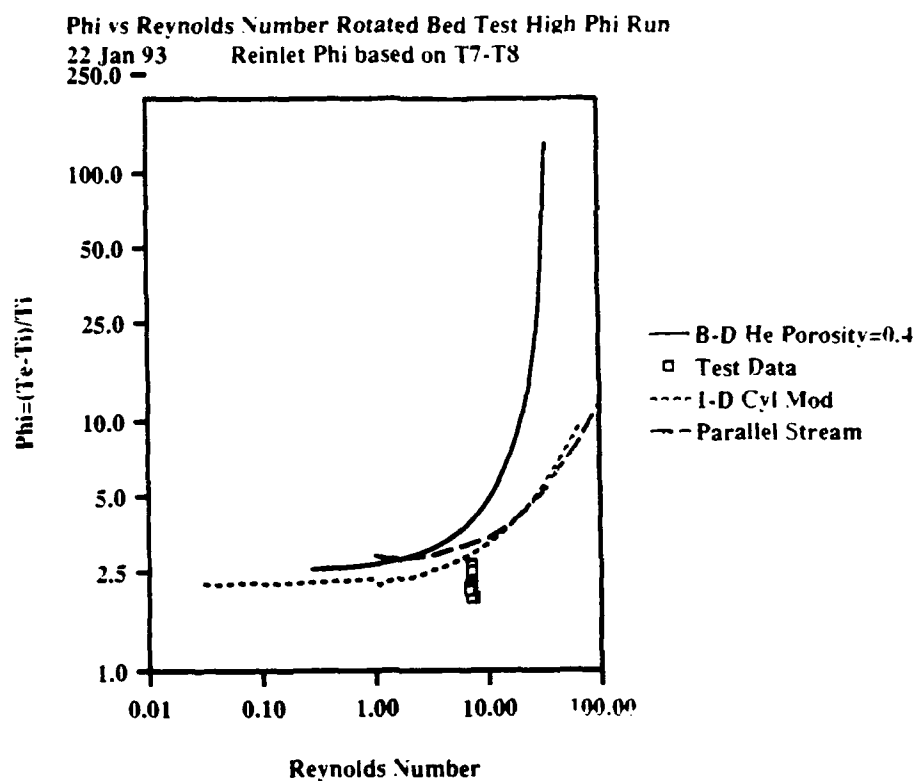


Figure 5.3.2.13 Phi vs Reynolds Number (Temperature Divergences) Test #6

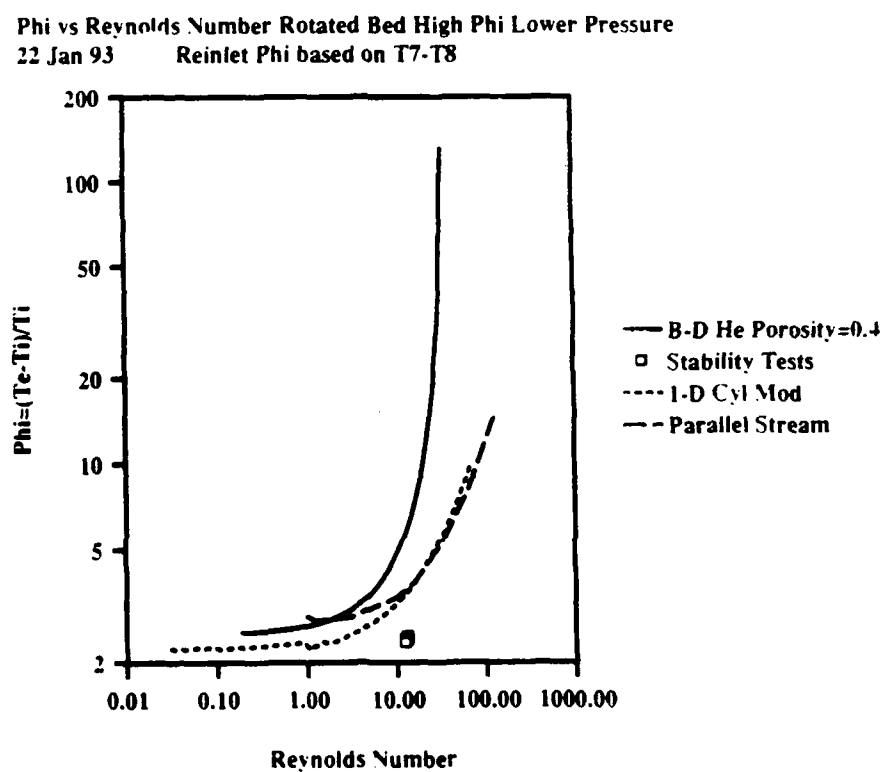
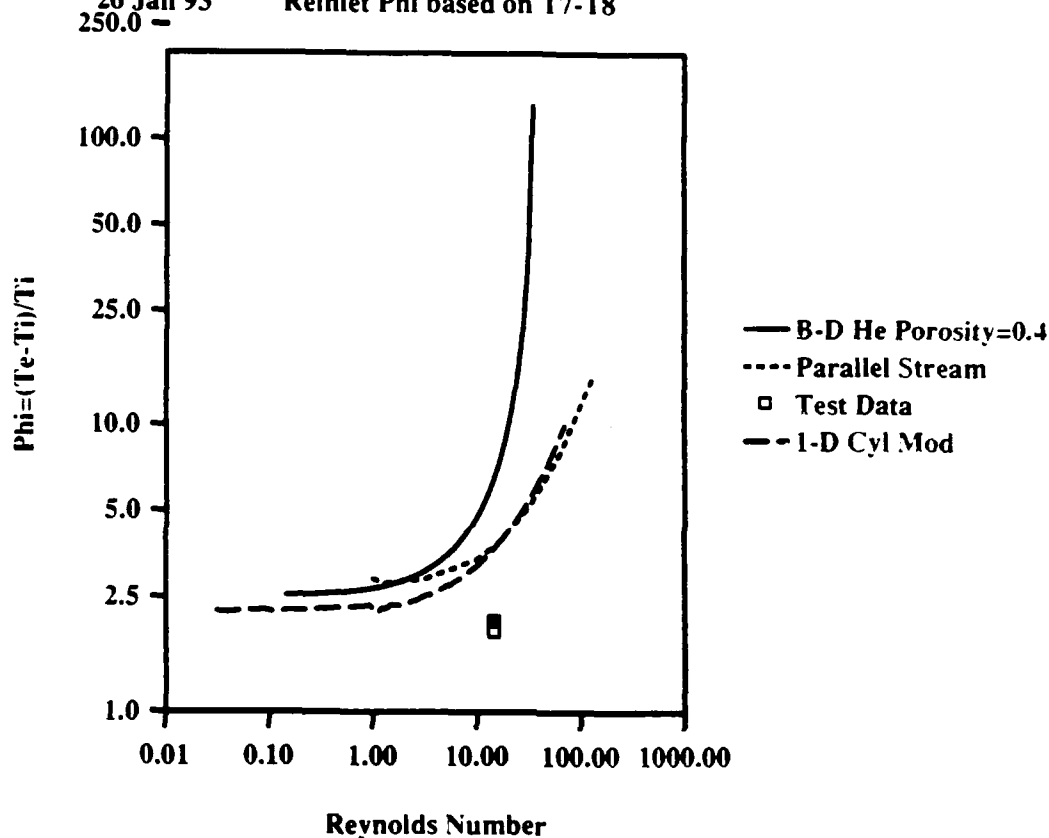


Figure 5.3.2.14 Phi vs Reynolds Number (Temperature Divergences) Test #8

Re did not change much over time interval so points overlap

Phi vs Reynolds Number Rotated Bed High Phi Retest

26 Jan 93 Reinlet Phi based on T7-T8



5.4 Uncertainty in Data Analysis

5.4.1 Seams in Frits

Since there were asymmetries in the temperature distribution of the experiments, it was decided to use the SIMBED 2D steady state code for a more detailed analysis.

The first case studied was to place a blockage in the hot frit and cold frit nodes. Since the seam in the cold fit was approximately 0.3 cm in width, it was decided to block one node in SIMBED for the cold frit and hot frit. A subroutine was written to let the user decide which node and how much of a

blockage was needed. The cold fit node (20,24) was blocked with a porosity of 0.0025. The hot frit node (21,15), since there was a slight offset between the seams, was blocked with a porosity of 0.005. The porosities of the nodes could not be set to zero for convergence issues. The hot frit porosity was set a little higher since it was not as wide as the cold frit node. The case was set to run for the same time as the the run shown in Figure 5.2.2.1-5.2.2.3 for ease of comparison.

Figure 5.4.1.1 High Phi Run T=5 minutes Temperature Distribution

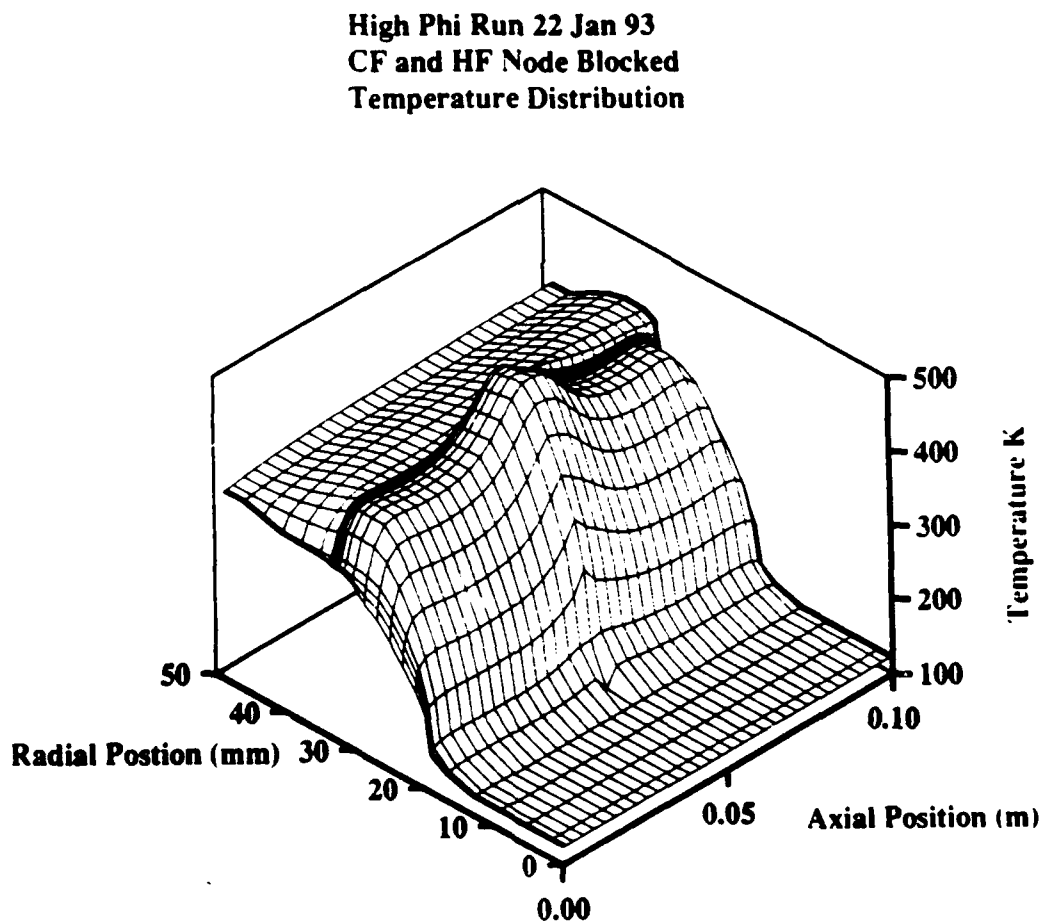


Figure 5.4.1.2 High Phi Run T=5 minutes Pressure Drop

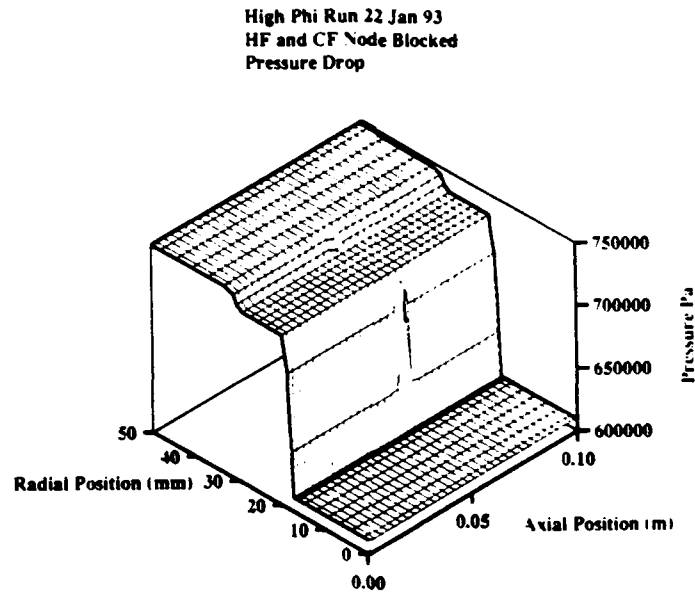


Figure 5.4.1.3 High Phi Run T=5 minutes Velocity Profile

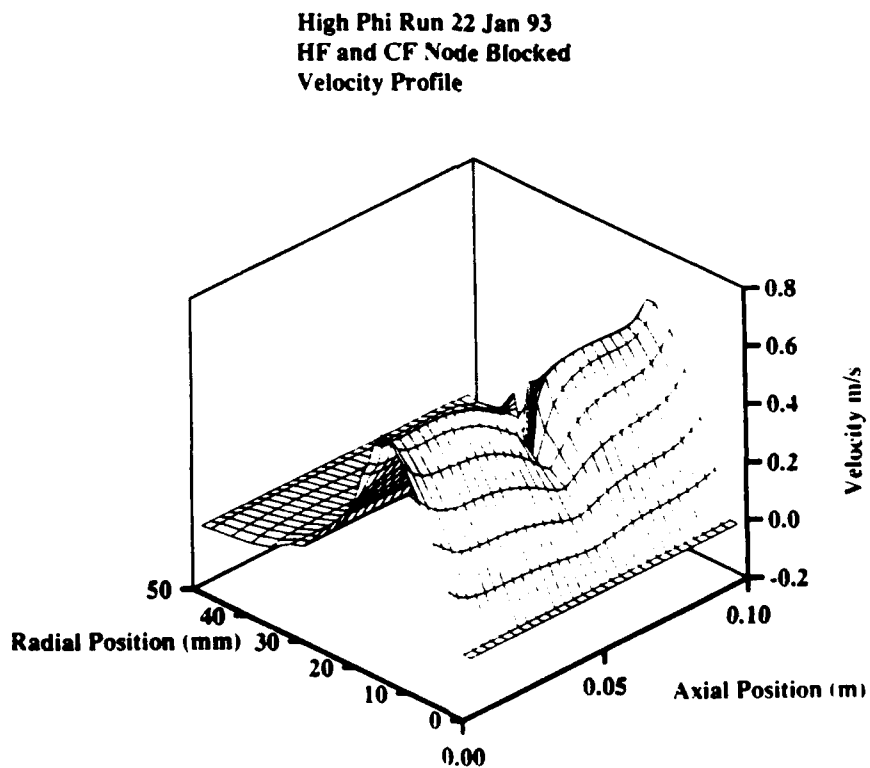
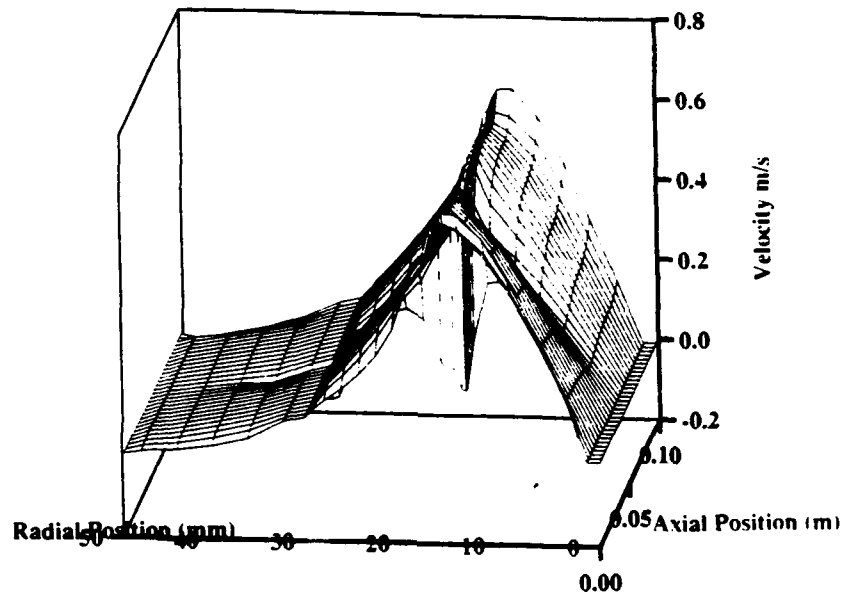


Figure 5.4.1.4 High Phi Run T=5 minutes Velocity Profile (Rotated)

High Phi Run 22 Jan 93
HF and CF Node Blocked
Velocity Profile



These results show that the seams have an impact on the temperature, pressure drop, and velocity profile in the bed. The seams show a slight temperature increase which makes a good argument that they were a cause for some of the asymmetries in the bed. The spike was not that severe to have caused a melt down in the bed (~ 26 K difference in temperatures).

5.4.2 Variable Porosity

After winding the bed, it was noticed that a random porosity could occur in the bed due to the orientation of the wires. As the wires are wrapped, the wires could align and form an open area, or they could overlap and form a covered area (not a full blockage). It was deduced that a random number generator could be placed into the SIMBED code to create a random porosity.

A numerical recipe was found in *Numerical Recipes in FORTRAN, Second Edition* [P-2], to generate the random porosity. A subroutine was written into SIMBED that would allow the user to input the porosity and then the random generator would give that porosity for 95 % of the run with a standard deviation of 10%. Therefore, the porosities would range from 0.27 to 0.47 if the input porosity was 0.37. The same high phi run studied before was used for comparison. The heat generation within the bed is shown in Figure 5.4.2.1

The temperature distribution and velocity profile for the random porosity bed for the High Phi Test at $t=5$ min is shown in Figures 5.4.2.2 - 5.4.2.3.

Figure 5.4.2.1 Heat Generation Within The Bed For A Random Porosity

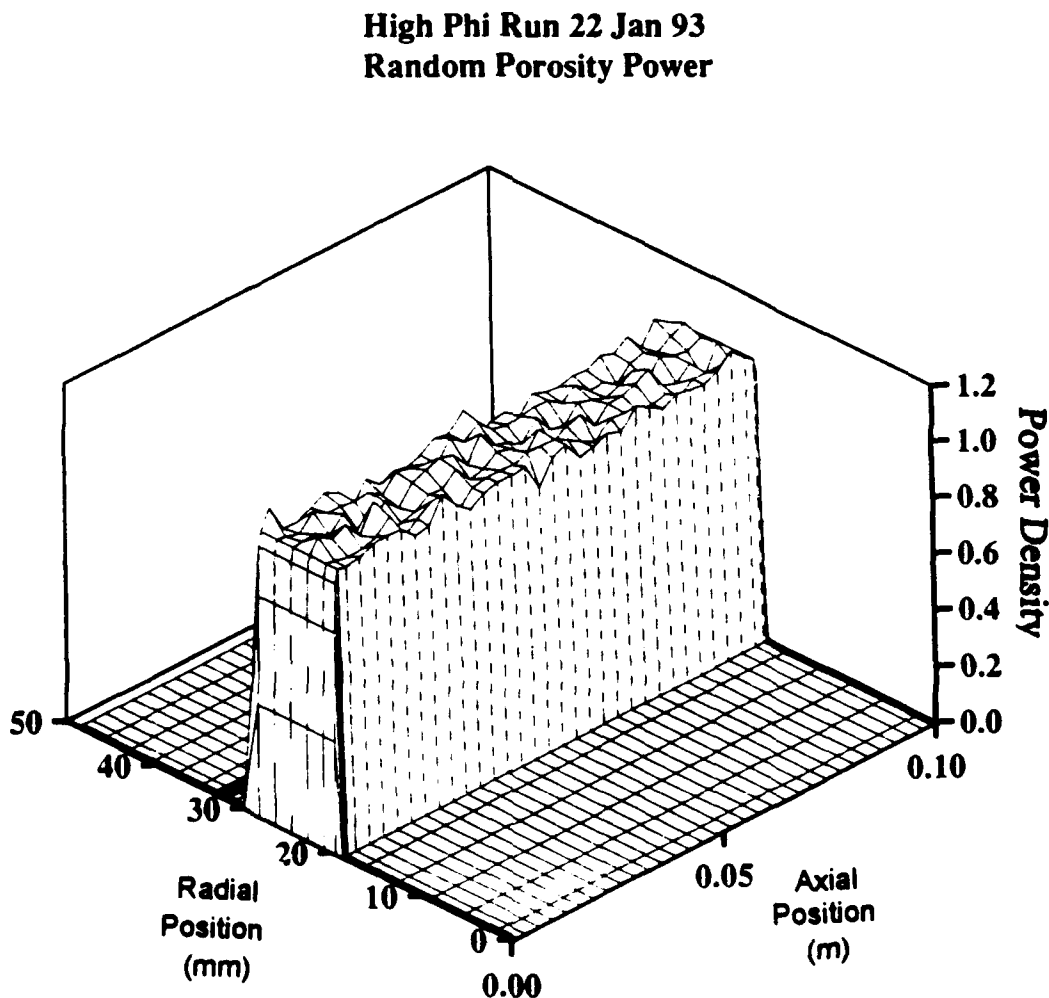


Figure 5.4.2.2 Random Porosity Temperature Distribution

High Phi Run 22 Jan 93
Random Porosity
Temperature Distribution

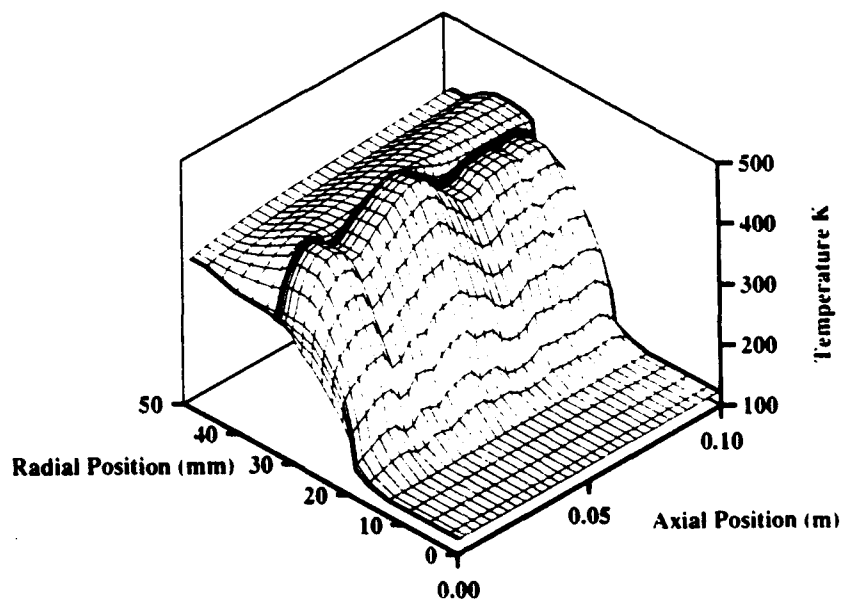
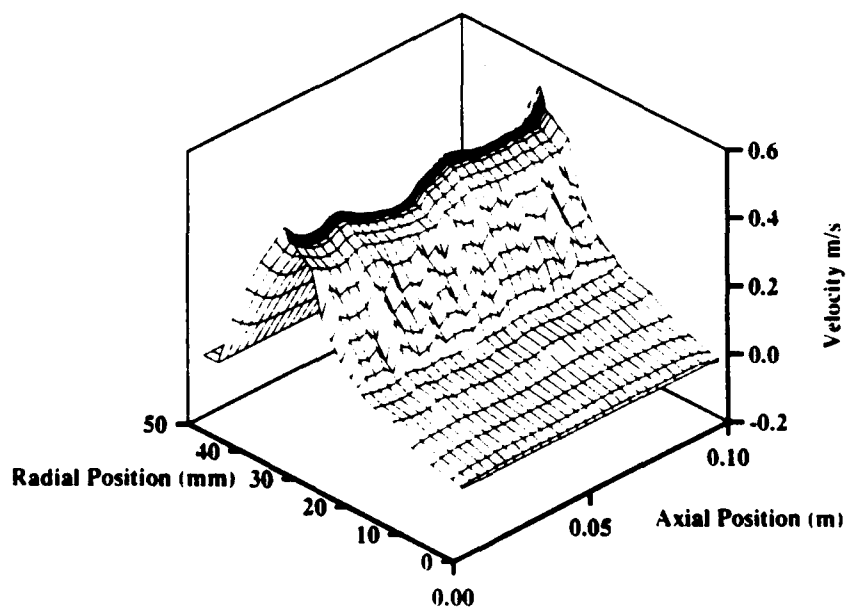


Figure 5.4.2.3 Random Porosity Velocity Profile

High Phi Run 22 Jan 93
Random Porosity
Velocity Profile



The results from the analysis show that the variable porosity definitely makes the temperature distribution more asymmetric since the flow through the element is more random (velocity profile). The pressure drop is not plotted since it remained the same as Figure 5.2.2.2.

5.4.3 Variable Porosity and Seams

The final approach was to apply the random porosity and block the cold frit and hot frit seams. The same High Phi Run at $t = 5$ minutes was used and the same hot frit and cold frit blockages as before were applied. The results of the temperature and velocity profiles are shown in Figures 5.4.3.1 - 5.4.3.3 (pressure drop profile same as Figure 5.4.1.2).

Figure 5.4.3.1 High Phi Run Variable Porosity and Seams Temperature Distribution

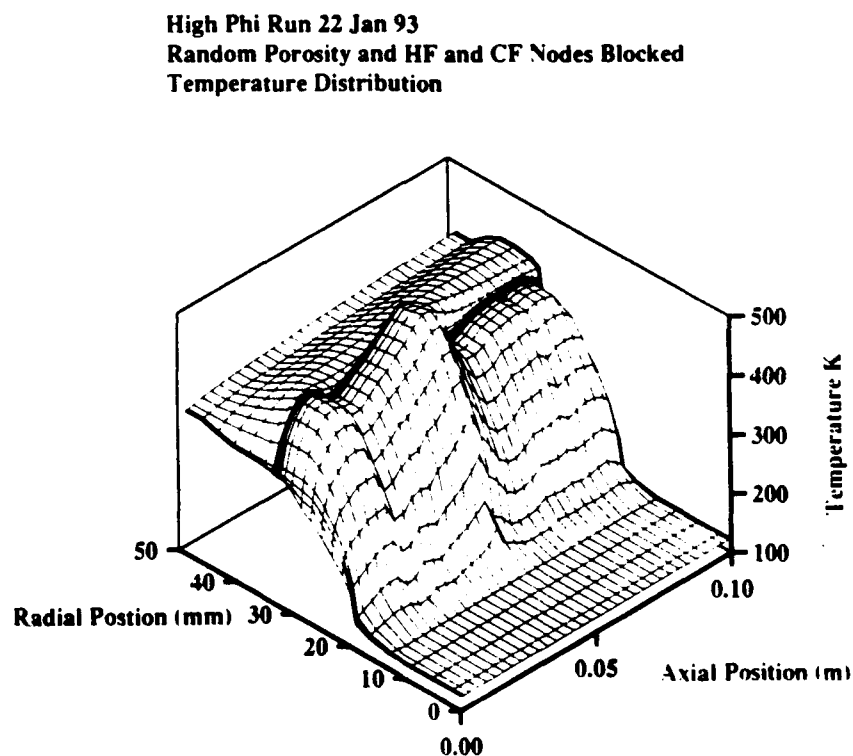


Figure 5.4.3.2 Variable Porosity and Seams Velocity Profile
 High Phi Run 22 Jan 93
 Random Porosity and HF and CF Nodes Blocked
 Velocity Profile

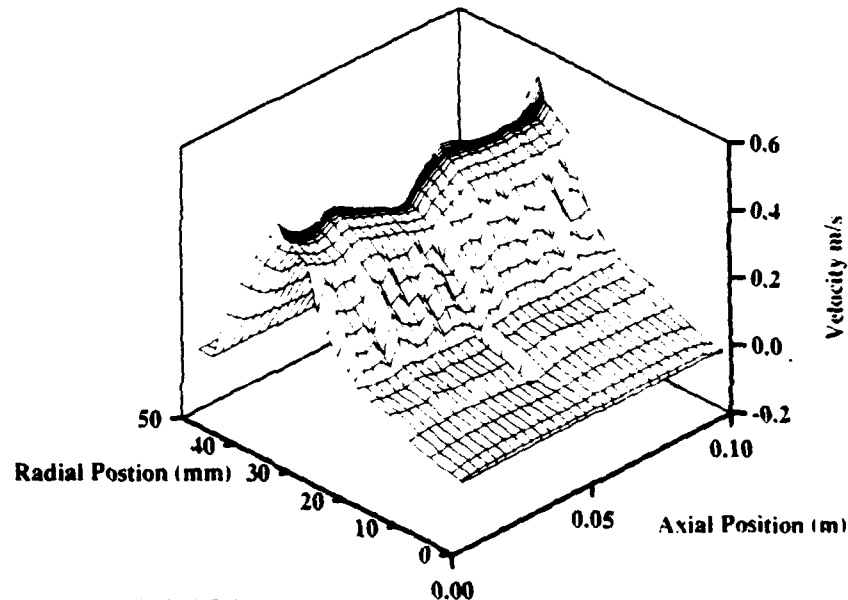
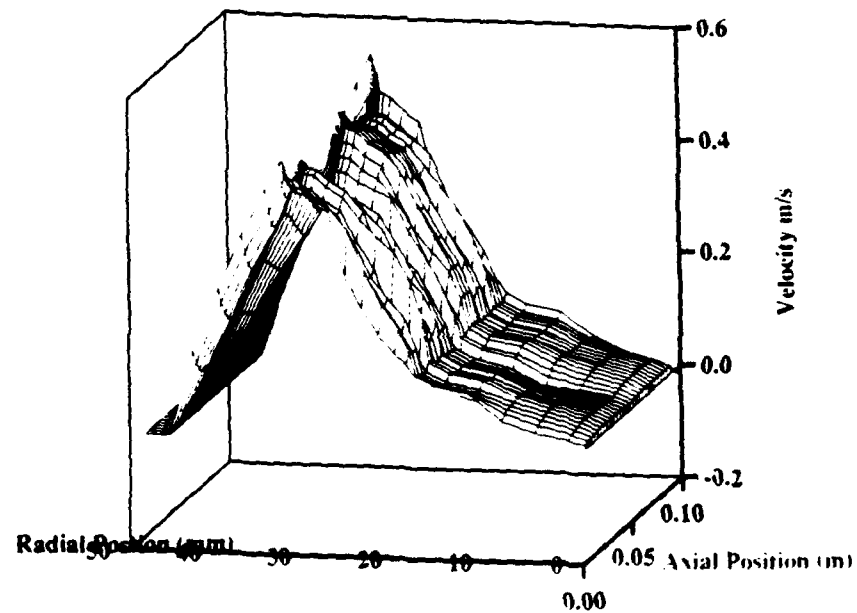


Figure 5.4.3.3 High Phi Run Variable Porosity and Seams Velocity Profile
 (Rotated)

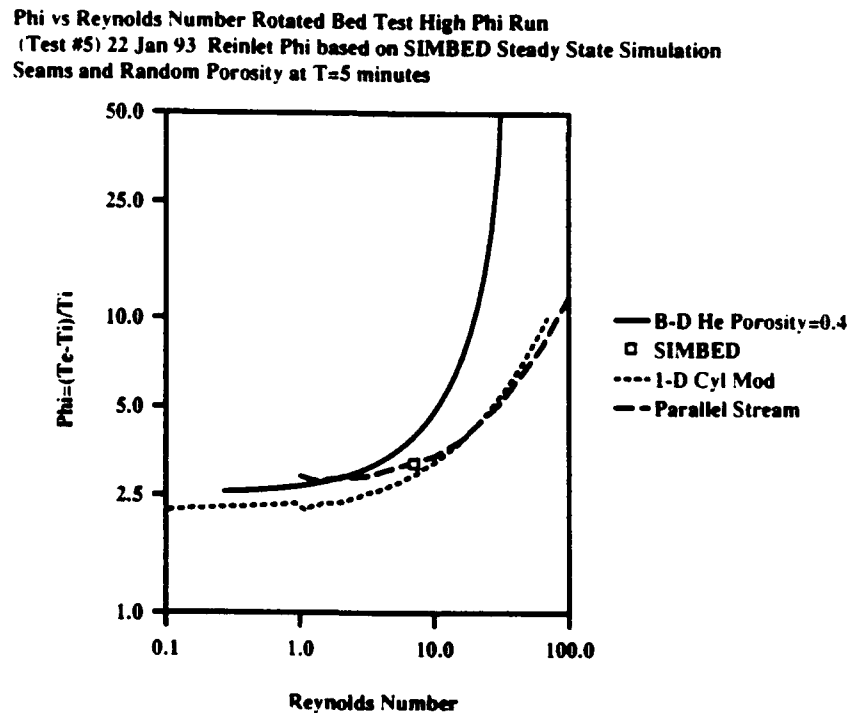
High Phi Run 22 Jan 93
 Random Porosity and HF and CF Nodes Blocked
 Velocity Profile



The results of this analysis show that the variable porosity combined with the seams makes the bed temperature distribution even more asymmetric. The temperature distribution is spiked in the middle of the bed (axially and radially). The temperature is lower before the middle of the bed, increases in the middle to the spike, decreases, and then increases a little bit to the outlet. Since all of the thermocouples are located at the hot frit, it is hard to relate these temperatures to the thermocouple readings, but it would seem to indicate that asymmetries in the bed of this analysis would relate to asymmetries in the thermocouple readings at the hot frit.

The gas temperature from the SIMBED analysis was plotted on the phi vs Reynolds number curve. As seen from the previous plots, the SIMBED random porosity and seams gas temperature is higher than the measured experiment temperature at t=5 minutes. This point is higher up on the stability curve, inside the 1D numerical methods cylindrical model curve.

Figure 5.4.3.4 Phi versus Reynolds Number Showing SIMBED Point



No more simulations were run. Since SIMBED is a steady state code, other simulations would only allow a snapshot (1 time interval for each run) of the total experimental temperatures. Another issue was that the computer run times were long for each steady state run (~15 hours depending on the number of users on the Vax system).

This Chapter showed the analyses conducted to investigate the experiments. The first analyses revealed that there was a mismatch in powers in some of the experiments. The plots of ϕ versus Reynolds number showed that the points where the temperature divergences were observed were close, but not in the unstable region of the curves (one point touched one curve). The SIMBED analyses showed that the asymmetries in the bed were caused by a random porosity in the wires and the seams on the frits. Analysis of one point of one run, revealed that the gas temperature was higher than the experiment, pushing the point higher up on the stability curve into the unstable region (Important since temperature divergences were occurring at this point of the experiment). Further analyses should use a transient version of SIMBED or a similar code to try to understand the time dependence for a better comparison to the experimental results.

CHAPTER 6

CONCLUSIONS AND RECOMMENDATIONS

6.1 CONCLUSIONS

The flow in bodies that have many parallel channels may be susceptible to laminar flow instabilities due to high power heating of the gas at low flow rates. At low flow rates, the impact of gas viscosity and density with temperature can be such that the pressure drop decreases with increasing flow rate. If a perturbation in a channel causes the temperature to rise, the gas viscosity will increase and the density will decrease. Since the pressure drop is maintained by the plenums, the mass flow rate in the channel will decrease, causing a further increase in temperature. As this channel heats up, one or more of the parallel channels will gain the extra heat and the perturbed channel could continue to heat up until it fails, even though the power and flow remain steady.

This phenomena is important to the PBR since it is a multi-channeled reactor proposed for space propulsion missions. A 500 MW concept (OTV type missions) consists of 19 fuel elements arrayed in a cylindrical moderator block (either beryllium or lithium-7). A fuel element consists of spherical fuel particles (350 - 500 μm) packed in between two porous tubes (called frits). The hydrogen gas (chosen due to its high performance) flows in radially across the cold frit, the bed, the hot frit, and then expands out axially through the element, producing thrust. Since the flow passages are highly irregular with many branches and interconnections, and since these branchings can occur after passage through the inlet plenum (cold frit), flow instability is an issue for the PBR.

Several studies have analyzed the flow stability in PBR's. Different approaches have determined stable/unstable flow regions based on the Reynolds number and ϕ defined as $(T_{\text{final}} - T_{\text{initial}})/T_{\text{initial}}$ of the gas. Although these stability criteria curves have different shapes based on different assumptions (bed geometry, dimensions of flow, bed porosity, cold frit resistance, type of gas used, etc), they all show that regions of low Reynolds number (low flow rate) and high ϕ are the most probable areas for flow instabilities to develop. Due to the high power density of the PBR, the nominal operating point is at high Reynolds numbers and hence full power operation is not a concern for stability, according to the analyses. However, at start up and shut down, the engine is at low flow rates and could enter these unstable regions. It is important to try to determine and characterize these instabilities (if they exist) for the given reactor fuel element geometry, so an operation strategy can be developed to avoid instabilities of the element. (Control strategies can be designed to avoid these analytical regions, see S-4). Therefore, experiments need to be performed to confirm/disaffirm these analytical predictions.

The experimental apparatus chosen under this investigation was an electrically heated, insulated, stainless steel screen bed. The experiments were conducted at Brookhaven National Laboratory. The insulated, stainless steel screen bed was chosen due to its flexibility and relatively low cost. The electrical power could be supplied into the stainless steel mesh to produce the internal heat generation similar to nuclear heating of the fuel in the PBR. A screen mesh was found with the wire diameter and spacing to give the element a porosity of 0.37 once the insulated coating was placed on the mesh. The hot and cold frit were made of stainless steel and were sintered to the desired porosity (0.30). Other support structure needed besides the screen and

frits were as follows: containment vessel, power supply, gas flow system, chill down tank, instrumentation, and a data acquisition system. Thermocouples were placed at the bed inlet, middle of the bed (touching the inside of the hot frit), and outlet to determine the temperature profile of the bed. Analyzing the temperature profile, mass flow, and pressure determined the ϕ and Reynolds numbers generated during the experiments for comparisons to the analyses.

The design went through many evolutions mainly due to coating problems with the screen. The final design that produced the best results was as follows: stainless steel screen edges were etched for ~8 min , 30 s to remove 0.005 cm of s.s; a 0.005 copper coating was electroplated onto the edges and tabs of the screen to carry current into the screen and prevent hot spots on the edges; a Cotronics 989 Al_2O_3 ceramic adhesive was mixed with 989 thinner and sprayed onto the screen using a paint gun; the entire screen was cured for 12 hours; and the screen was rolled into the frits and assembled and the resistance readings showed there was an adequate coating for the experiments.

Nine experiments were conducted using the painted alumina screen. Six of these experiments produced results with data that could be analyzed to address flow stability. In all of the experiments, there were asymmetries in the temperatures in the bed according to the thermocouple temperatures. Analytical results revealed that there was a high probability that these asymmetries occurred due to seams in the hot and cold frit, and a random porosity in the screen bed due to overlap of the wires.

Energy balance calculations based on the power input and inlet and outlet gas temperatures revealed that there was a slight mismatch between power input and gas temperatures. System calibration tests showed that the power

supply console reading was slightly off and more power was being supplied to the bed than the display indicated. After review of the manufacturers information and calibration, and consultation with other flowmeter users, there was uncertainty regarding the accuracy of the flowmeter. However, it was felt that the manufacturers experience was the best data source, so the flowmeter readings were interpreted as accurate. The results of the system calibrations showed that the power to flow match was very close in some cases (specifically at high powers), but at lower powers there may be a slight energy balance mismatch.

Of the six useful tests, three were tested using ambient inlet temperatures to insure low ϕ 's by having a high T_{inlet} thus giving stable flow based on prior analyses and for the other three tests low inlet temperatures were used (~ 100 K) to create higher ϕ 's and thus enable the apparatus to reach the unstable regions at low Reynolds numbers. Analysis of the low ϕ experiments revealed that even though these experiments produced asymmetries in bed temperatures, the temperatures remained constant with constant power input. Analysis of the high ϕ (~ 3) experiments, revealed that as power was increased, a condition was reached where all six of the bed thermocouples diverged while the mixed mean outlet remained constant (three of the bed temperatures increased, while three of the bed temperatures decreased). This phenomena can not be explained due to asymmetries in the bed alone, since the temperatures did not diverge at lower ϕ 's with the same bed asymmetries. It is important to note that, the divergences were relatively slow in propagation and the bed could be controlled by reducing the power before temperatures reached the coating limits. However, if action is taken in the wrong direction, as in the last run, the bed can be melted down. In the last run, a 10% increase in power was made at a ϕ around 4 which was already

in or close to the unstable region. On the other hand, it was not known if this was due to flow instability or repeated use of the same screen bed caused a hot spot to develop in one region, causing the bed to short out.

The high runs were compared to the analytical predictions, using the inlet and outlet temperature for the ϕ 's, and the flowmeter reading to calculate the Reynolds number at the bed inlet. Over the temperature diverging ranges, the ϕ vs Reynolds number calculations reveal that the points are close to the predicted instability regions based on the inlet and outlet gas temperatures, and in one test one of the points intersects one of the curves.

However, the SIMBED 2D steady state results showed that one of the experiment points ($T = 5$ minutes for Test #5, High ϕ Run 22 Jan 93) was inside one of the predicted instability curves. This analysis took into account the seams on the frits and a random porosity in the bed. The asymmetries from this analysis seemed to follow the asymmetries from the experiment. Even though the experimental bed was not completely prototypic to the real PBR (e.g. hot frit dominates the pressure drop, seams in frits, etc.), the experimental results were able to be modeled using the steady state code. Another important point is that the temperature divergences *were observed* in an apparatus that had a higher lateral thermal conductivity than the real PBR which should have mitigated the chances of creating instabilities. The energy balance calculations revealed that the power to flow match was the best when the temperature divergences were occurring. The tests were duplicated (three times) and asymmetries in the apparatus can not be blamed as the cause since divergences did not occur at lower ϕ 's.

6.2 RECOMMENDATIONS FOR FURTHER STUDY

The tests conducted under this investigation revealed that flow stabilities may exist in PBR's. Analysis of the data revealed that asymmetries in the apparatus were caused by the seams in the frits and a good chance of a random porosity in the bed. However, this analysis was conducted on single testing points using a modified 2D steady state code called SIMBED on a Vax computer. In order to have a better understanding of the phenomena, it is recommended that a transient version of this code or a similar code be used to have a better feel for the transient behavior of the bed, especially with the seams and random porosity factors for the high ϕ runs. A more powerful computer is also recommended (higher than a Vax) in order to ease computational times (SIMBED runs usually took 15 hours to converge on a Vax 3100).

The analysis conducted by Jim Kalamas in Chapter 2 would also support this recommendation. His analysis took into account the time dependence and effective bed thermal conductivity to generate a stability curve that is very stable (ϕ 's of ~ 15 for instabilities due to the high thermal conductivity of the bed).

It is also recommended that another series of flow instability tests be conducted to study this phenomena in more detail. The existing apparatus could be used for more tests, but other non-nuclear methods may be able to produce useful results. It would be good to duplicate the results using the same approach, but the author believes the number of tests have already demonstrated the usefulness of the current apparatus and if the results can be produced using another apparatus, it would help to better define the flow instability tests. The proposed bigger, high conducting ball experiments with

internal electrical heaters or the microwave experiments using zirconia balls could be excellent follow-on experiments. Whatever experiments are pursued, precautions should be taken to insure all instruments are calibrated prior to testing and a flow system and bed materials are designed to offer full testing of the analytical stability curves.

It is the author's opinion that in any reactor development program, many "out of pile" thermal hydraulics experiments should be performed first to help characterize flow stabilities, flow characteristics (e.g. pressure drop, power extraction, acoustic vibrations, etc) , materials development, etc. before the more costly "in-pile" reactor tests are pursued in existing test reactors or the new reactor itself. This lesson was learned in the NERVA program when fuel elements were spread over the Nevada desert. In this day of age, under tight fiscal climates, the push is to develop the technology as fast as possible in order to demonstrate the technology as quickly as possible. In order to accomplish this task at a lower cost, corners are cut, especially in early testing, which usually leads to failures of all most fully developed systems which ends up hurting everybody in the long run.

It is the opinion of the author that flow instability is not a "show stopper" for the PBR. The results of this investigation have shown that flow instabilities may exist in the PBR and further tests should be designed and conducted to help characterize this region further. The temperature divergences observed were slow in propagating, and could be controlled at the experimental powers and flows. However, there were two meltdowns in the campaign, which shows that once unstable flow is observed, in order to be safe the experimenter should leave the region as quickly as possible (lower temperature and increase flow). This theory is applied in practice today for BWR (Boiling Water Reactor) nuclear power plants. Flow instabilities have

been observed at low flow rates and powers. In this region there is a chance for boiling to occur in one fuel region and prevent feedwater flow from entering the extra boiling region. The experience with these system tests indicate that once the operator gets into a flow instability region, if he/she gets out of the region as soon as possible, no problems occur. The operator can observe the temperature increase in the one region and have means to increase flow or power to get out of the region. The same strategy can be applied to PBR's, once the region has been defined.

REFERENCES

- B-1 R.W. Bussard and R.D. DeLauer, Fundamental of Nuclear Flight, McGraw - Hill, New York, 1965.
- B-2 J. R. Powell et al, "Particle Bed Reactor Orbit Transfer Vehicle Concept," AFAL-TR-88-014, Air Force Astronautics Laboratory, July 1988.
- B-3 S. K. Borowski, "The Rational Benefits of Nuclear Thermal Propulsion for NASA's Lunar Space Transportation System," AIAA/SAE/ASME/ASEE 27th Joint Propulsion Conference, June 24 - 26, 1991, Sacramento, CA.
- C-1 R. J. Cerbone and T. J. Lawrence, "Nuclear Heating in the Upperstage of a Particle Bed Driven Nuclear Propulsion System," AIAA/SAE/ASME/ASEE 27th Joint Propulsion Conference, June 24-26, 1991, Sacramento, CA.
- C-2 Cotronics Corporation, Adhesives Ceramics and High Temperature Materials Handbook, Cotronics Corporation, 1992.
- C-3 CRC Handbook of Chemistry an Physics, The Chemical Rubber Company, 1969.
- C-4 W.E. Casey, "Thermal-Hydraulic Transient Analysis of a Packed Particle Bed Reactor Fuel Element," SM and Naval Engineer Thesis, Department of Nuclear Engineering, Massachusetts Institute of Technology, May 1990.
- C-5 M. Charmchi, "Heat Transfer and Fluid Flow Characteristics of the Hydrogen-Cooled Small Particle Bed Reactor (PBR)," UL-MEE-89[05-5012]-F, Brookhaven National Laboratory, October 1989.
- E-1 Enerpac Basic Pressure Gauge, Model DGB Technical Manual, Enerpac, 1988.
- H-1 P.G. Hill and C. R. Peterson, Mechanics and Thermodynamics of Propulsion, Addison-Wesley, New York 1992.
- H-2 D.E. Hastings, Course 16.53 Rocket Propulsion Class Notes, Massachusetts Institute of Technology, September 1992.

- H-3 H. Herman, "Plasma-Sprayed Coatings," Scientific American, September 1988.
- K-1 J. L. Kerrebrock, "Flow Instability in Particle-Bed Nuclear Reactors," Massachusetts Institute of Technology Informal Report, November 1992.
- K-2 J. Kalamas, "Particle Bed Reactor Stability Analysis," SM Thesis, Department of Aeronautics and Astronautics, Massachusetts Institute of Technology, May 1993.
- M-1 G. Maise, "Flow Stability in the Particle Bed Reactor," Informal Report BNL/RSD-91-002, Brookhaven National Laboratory, January 1991.
- M-2 Matheson, "Mass Flowmeters - Linear Mass Flowmeter - Series 8100 Technical Data Sheet," Matheson, 1988.
- M-3 Metals Handbook, 9th Edition, Volume 5, Surface Cleaning, Finishing, and Coating, American Society for Metals, Metals Park, OH, 1982.
- O-1 Omega Engineering Inc., "The Temperature Handbook," Omega Engineering Inc., Stamford, Ct, 1992.
- O-2 Omega Engineering Inc., "PX100 Low - Level Pressure Transducer Data Sheet," Omega Engineering Inc., Stamford, Ct, 1988.
- O-3 Omega Engineering Inc., "Omega WB-ASC Card Technical Manual," Omega Engineering Inc., Stamford, Ct, 1988.
- P-1 Private Communication, D. R. Perkins, Astronautics Laboratory, Edwards AFB, CA, 1990.
- P-2 W H. Press, et al, Numerical Recipes in FORTRAN, The Art of Scientific Computing, 2nd Edition, Cambridge University Press, Port Chester, NY, 1992.
- R-1 Rapid Power Technologies Inc., "Thyristor (SCR) Power Supplies - for High Quality dc Power Supply Applications", Rapid Power Technologies Inc., 1990.
- S-1 V. V. Sychev, et al, Thermodynamic Properties of Helium, Hemisphere Publishing, New York, 1987.
- S-2 A. E. Sheidegger, Physics of Flow Through Porous Media, Toronto University, Toronto, 1963.

- S-3 Stafford (Chairman), "America's Space Exploration Initiative: America at the Threshold," The Report of the Stafford Committee to the President of the United States, May 1991.
- S-4 D.E. Suzuki, "Development and Analysis of Startup Strategies for a Particle Bed Nuclear Rocket Engine," SM Thesis, Department of Aeronautics and Astronautics and Nuclear Engineering, Massachusetts Institute of Technology, May 1993.
- U-1 H. H. Uhlig, Corrosion and Corrosion Control: An Introduction to Corrosion Science and Engineering, Wiley, New York, 1971.
- V-1 M. E. Vernon, "PIPE Series Experiment Plan," Sandia National Laboratory, Albuquerque, NM 1988.
- V-2 Vahalla Scientific, " Model 4100 ATC Digital Ohmmeter Technical Data Sheet", Vahalla Scientific, 1992.
- W-1 J. K. Witter, D. D. Lanning, J.E. Meyer, "Flow Stability Analysis of A Particle Bed Reactor Fuel Element," in Proceedings of Tenth Symposium on Space Nuclear Power and Propulsion, CONF-930103, M.S. El-Genk and M.D. Hoover, eds, American Institute of Physics, New York, 1993 1541.
- W-2 J. T. Watson, Viscosity of Gases in Metric Units, Her Majesty's Stationary Office, Edinburgh, England, 1972.
- W-3 J. K. Witter, "Modeling for the Simulation and Control of Nuclear Reactor Rocket Systems," Ph.D. Thesis, Department of Nuclear Engineering, Massachusetts Institute of Technology, June, 1993.

APPENDIX A

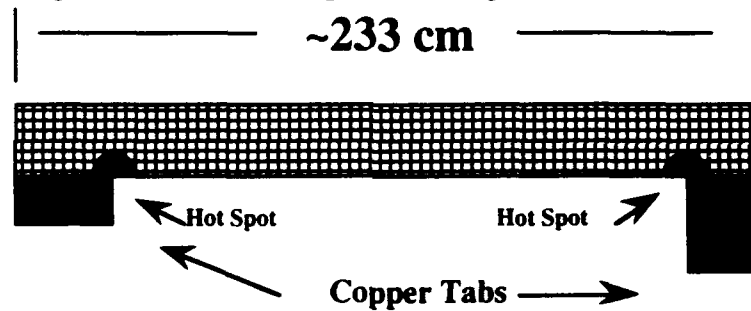
DESIGN EVOLUTION

A.1 COPPER COATINGS

A.1.1 Need for Copper Coatings at Ends and Tabs

Initial tests revealed problems with the original design. The first issue was hot spot development on the screen. The hot spots appeared around the tabs (see Figure A.1.1.1).

Figure A.1.1.1 Hot Spot Development On Screen



*** Not to Scale**

These hot spots developed due to uneven current flow. The uneven current flow was caused by the current taking the shortest path from tab to tab since the s.s. screen had the same resistance. The hot spots developed at voltages of 4 to 7 V (currents 30 -70 amps). A red glow was seen in the lab in the regions shown in Figure A.1.1.1. At 15 - 20 V the hot spot melted the screen from the copper tabs. This condition was unacceptable for an experiment to be conducted.

A proposed solution to this problem was to coat the ends of the screen with a material of smaller resistance than s.s. Copper seemed to be the best choice due to its resistivity of $1.67 \mu\Omega\text{cm}$ compared to $70 \mu\Omega\text{cm}$ for s.s. [C-3]. The smaller resistance at the end of the tab would allow the current to flow straight up from the tab and then disperse across the screen instead of concentrating in the corners. This theory was tested in the lab.

Figure A.1.1.2 Copper Piece on Screen

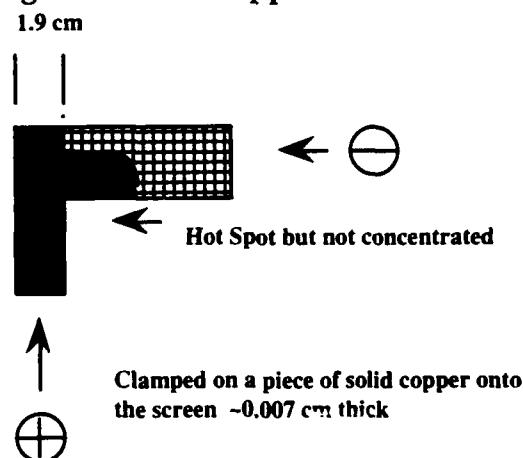


Figure A.1.1.3 Wider Copper Piece on Screen

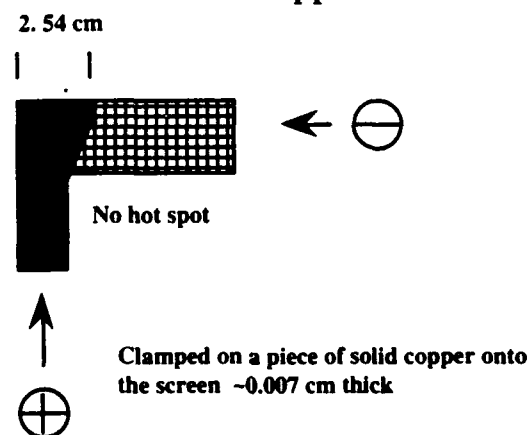


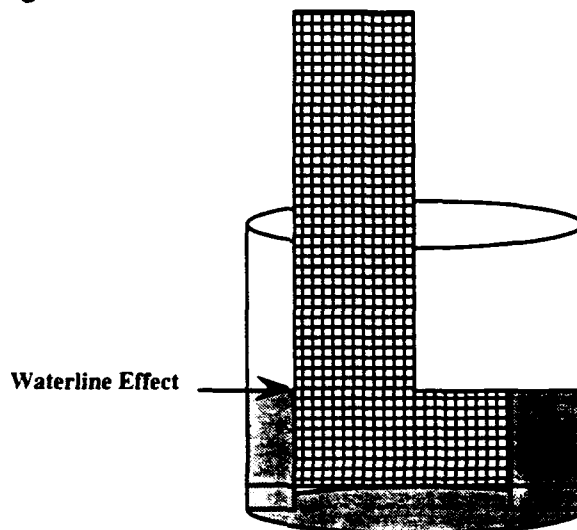
Figure A.1.1.2 and A.1.1.3 show the results of the tests. The Lambda power supply provides 15 V and 100 amps of power for both tests. Figure A.1.1.2 shows that a copper piece helped "spread out" the current, but a hot spot still

appeared and is not as concentrated. Figure A.1.1.3 presents that if more copper is added at the top, the current flow becomes more even and no hot spot appears (similar to irrigation methods used by farmers). This test proves that if copper could be coated onto the screen (a coating had to be used to maintain hole porosity), the hot spot problem is solved.

Since the ends of the screen would be coated with copper and alumina (the rest of the screen just with alumina), a method was needed to decrease the diameter of the wires in this area in order to maintain an uniform porosity across the screen. The book, *Metals Handbook, 9th Edition, Volume 5 Surface Cleaning, Finishing, and Coating*, was used to determine that Aquaregia would be a good agent to etch the stainless steel [M-3]. Aquaregia was made with 4 parts HCl (hydrochloric acid) and 1 part HNO₃ (nitric acid) for any volume. The solution was stirred and sat for 30 minutes at room temperature, no heat needed. As time evolved, the color of the mixture changed from clear to yellow to orange to rust. When the stainless steel was added to the solution, it immediately reacted, off-gassed, and turned the solution black. The solution turned the stainless steel shiny and according to micrometer measurements, it took off 0.00254 cm of stainless steel every 3 minutes. However, this is not a concrete number. It seemed that if a solution was used more than once, it became more reactive with use. Several screens were lost this way (e.g. the first time a solution was used it was determined 12 minutes would take off 4 mills (0.01 cm), the second time this solution was used, the screen was soup after 12 minutes). This problem was solved by placing the screen into the bath for shorter time intervals and measuring the screen with the micrometer after each time interval. The total time needed to etch the stainless steel 0.005 cm on the ends varied from 5 - 12 minutes.

Another problem encountered in etching was a waterline effect.

Figure A.1.1.4 Waterline Effect in Etching

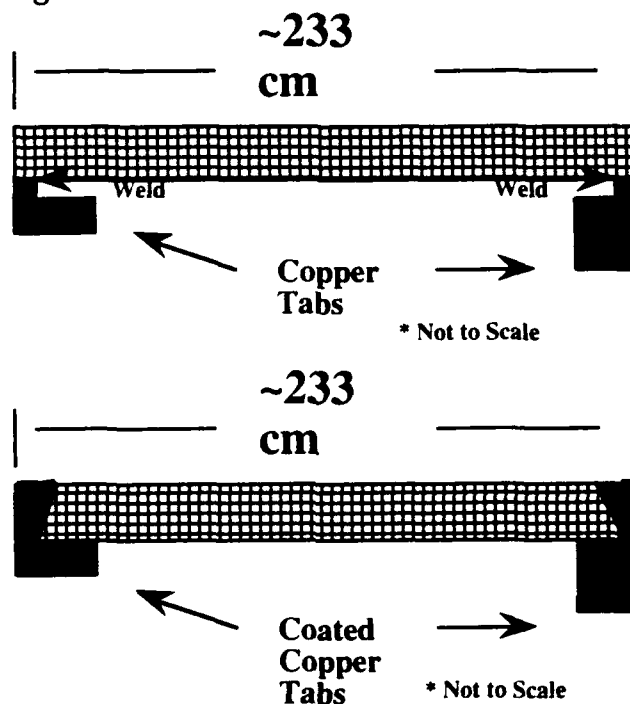


Since the screen was very long, in order to etch the ends, the screen was clamped into place. If the screen remained in the same place for the entire etching period, a "waterline" was seen on the screen where it touched the solution at the top. This area was very thin causing the wires to tear. A possible solution to this problem was to find masking material and mask this area from the solution. Three masking solutions were tried, and were not found to be effective. The waterline just formed above or below the masked area. The masked coating was very difficult to remove, so this option was not pursued. The second proposal was to constantly move the screen as it was being etched in order to reduce the time that a certain region was exposed to the waterline. Every one to two minutes, the screen was moved ~ 2 mm upwards. This allowed some of the areas that were not going to be copper coated to become etched, but the thinning in this area was small due to the small movements. Using this procedure, the waterline effect was not seen on the screen.

Since it was determined that a copper coating was needed on the ends of the screen, it was determined that the screen could be cut to include the tabs, and

the tabs could also be copper coated. There was a problem using the solid copper tabs, since they had to be welded onto the screen. This weld was not a strong attachment and was easy to tear. The coated copper tabs was a better option (see Figure A.1.1.5).

Figure A.1.1.5 Coated Tabs vs Welded Tabs



A.1.2 Plasma Sprayed Copper Coating

Since the alumina coating was plasma sprayed onto the screen for insulation (see Appendix A.2), it was decided that a plasma sprayed copper coating would be the best option for applying the coating.

Plasma spraying involves use of a plasma gun to apply the coating. The plasma gun has two electrodes, a cone-shaped cathode inside a cylindrical anode, which extends beyond the cathode to form a nozzle. An inert gas flows through the space between the electrodes, where it is ionized to form a

plasma. A tube then directs powdered coating material into the jet of plasma that develops in the nozzle. Water circulates through passages in the anode and cathode for cooling [H-3].

The gun starts operating when a pulse of current creates an arc across the gap between the electrodes. A steady DC of ~ 100's of amps at ~ 50 V then sustains the arc. As the arc forms, electrons are torn from the atoms of gas. The electrons and positive ions these atoms leave behind are accelerated toward the anode and the cathode respectively. These rapidly moving particles collide with each other, neutral atoms or molecules in the gas, dissociating any molecules into their constituent atoms and ionizing the atoms. In this way the gas within the arc is transformed into a collection of ions and energetic electrons (a plasma). The stream of gas that flows between the electrodes stretches the arc, so that in its course from one electrode to the other the arc loops out of the nozzle of the gun as a plasma flame. The gun consumes 20 to 80 MW of electrical power [H-3].

The powdered coating material, carried in a stream of gas such as argon, is injected into the flame either within the nozzle or as it emerges from the outer face of the anode. The flame accelerates the particles, and they are melted by its high temperature. The molten droplets are propelled onto the target surface, where they solidify and accumulate to form a thick bonded coating [H-3].

There are many variables in this process which has lead to many companies setting up proprietary processes. These variables are as follows: heat content and velocity of the plasma flame; geometry and power level together with the composition and flow rate of the plasma gas; size and shape of the particles - for a given coating material and gun there is an optimum particle size (particles much smaller than the ideal will overheat and vaporize, much

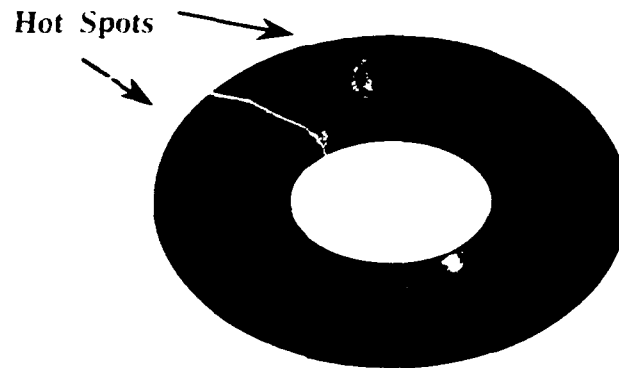
larger particles will not melt and may fall from the flame or rebound from the target); feed rate of particles into the flame - pressure of the carrier gas must be adjusted to blow the particles into the flame but not through it; angle of injection - downwind injection minimizes the disruption of the flame by the influx of particles and increases their velocity, whereas injection in the upwind direction gives the powder more time to take heat from the flame; spraying in air - the particles begin to cool and slow down as they collide with air molecules after leaving the plasma flame; and distance from the gun to the coated surface [H-3].

A local vendor was chosen and was told to plasma spray the copper coating as shown in Figure A.1.1.5. The first screen was etched and then coated by the vendor (0.005 cm thick copper coating, 2.54 cm wide on the ends) and assembled into the cold and hot frits. Once the bed was assembled, voltage was applied to check the resistance/current flow. The results were as follows:

I	33 A	34 A	87A	90 A	160 A	175 A	210 A
V	1 VDC	2.5 V	2.5 V	2.5 V	4.5 V	4.5 V	7 V
R	0.030 Ω	0.0294 Ω	0.0287 Ω	0.0277 Ω	0.0281 Ω	0.0257 Ω	0.033 Ω

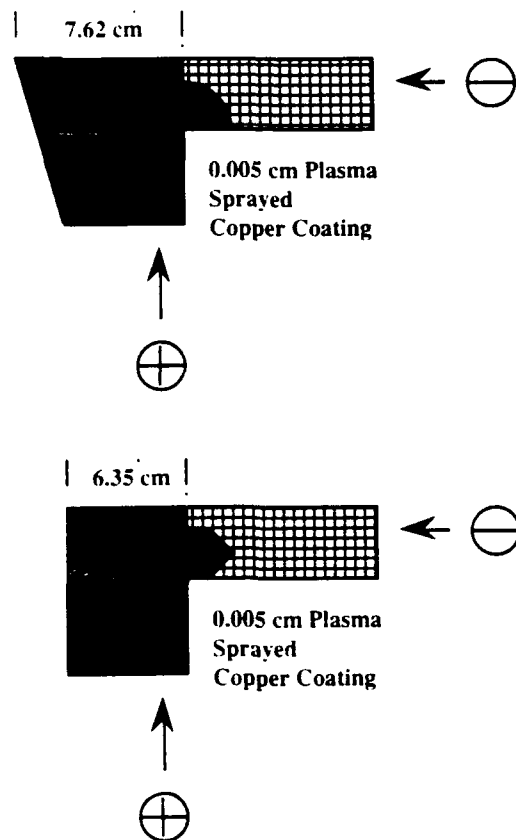
The resistance numbers were low compared to what was expected. The test was repeated and two hot spots appeared on the edge of the screen (see Figure A.1.2.1).

Figure A.1.2.1 Hot Spots on Screen Bed



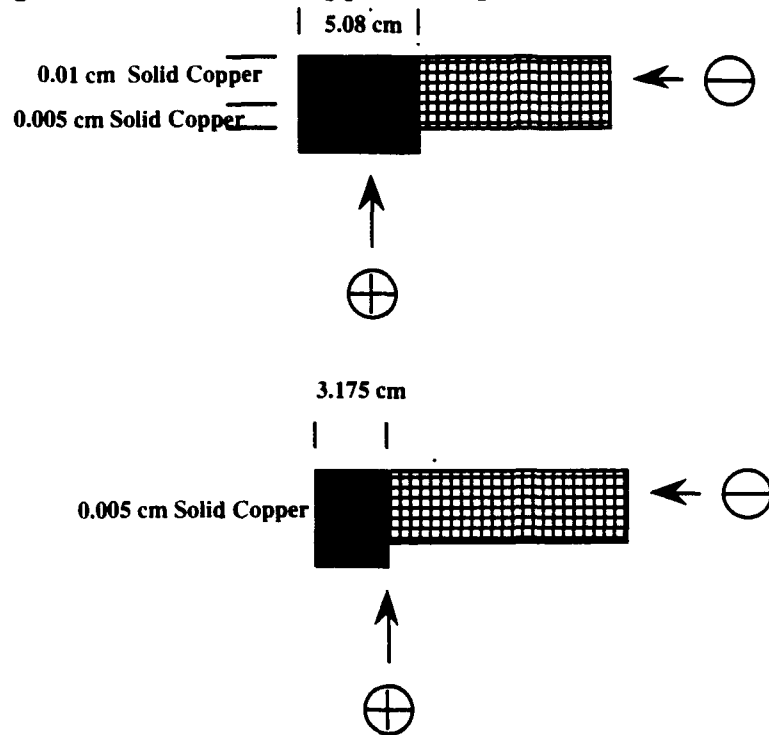
The element was disassembled and the screen was rolled out flat. Hot spots similar to Figure A.1.1.1 appeared at the ends. This may have been due to not enough copper coating applied to the screen. Several other pieces of screen coated by the vendor were cut out in the following configurations (see Figure A.1.2.2). The power supplied to the screen was 2.5 VDC at 250 amps (Inert gas was supplied as cooling in order to prevent oxidation of the copper). Hot spots developed on these pieces also as per Figure A.1.2.2. Even though the copper coating was a little bit thinner than the solid piece tried earlier, it was thought this was enough coating to thoroughly cover the area. The 0.005 cm thickness was the limit since more coating would require more etching which would make the wires too thin. If the wires were not etched, the coating would be too thick and clog the holes. The copper coating was inspected under a microscope (1x) and open areas of stainless steel was observed. The coating also looked very granular. A piece was taken from one of the samples below and was sent to be looked at under an electron microscope to determine how much copper was on the screen (Never got the results due to scheduling conflicts, but this did not matter due to other developments). It was also decided to repeat the earlier experiments with solid copper tabs to ensure that copper application would prevent the development of hot spots.

Figure A.1.2.2 Plasma Sprayed Copper Coated Pieces



The experiments were set up as per Figure A.1.2.3.

Figure A.1.2.3 Solid Copper Clamped On Pieces Retest



The tabs were configured in different ways than before. The first test put more coating of copper at the top (0.01 cm), and 0.005 cm at the bottom. It was thought it would be better to have more copper at the top try to divert more current to the upper region to prevent the hot spots at the corners. Up to 350 amps were applied to the first sample and no hot spots appeared. The second sample had a 0.005 cm thickness of solid copper spread evenly for 3.175 cm by 10.16 cm. This smaller piece showed no hot spots with power applied up to 300 amps. These tests showed that a 0.05 cm thick (flat for 3.175 cm, no change in width of coating) copper piece could spread the current even enough to not have hot spots.

The plasma sprayed copper coating does have limitations. The above discussion showed all the variables that could effect performance. The plasma sprayed coating provided by the vendor did not look like an even coat. Some areas looked like oxidation occurred in the spraying process.

Newark Wire Inc. was contacted to determine if copper wire could be woven onto the stainless steel at the end and tabs. They said this procedure could be done, but it would be considered a "special job" and a unique weave would have to be set-up which would be costly. Thus, electroplating the copper coating onto the screen was considered.

A.1.3 Electroplated Copper Coating

The *Metals Handbook, 9th Edition, Volume 5 Surface Cleaning, Finishing, and Coating* [M-3] is a reference for copper plating. Copper can be electrodeposited from numerous electrolytes. Pyrophosphate alkaline baths are used primarily to produce thick deposits, because they exhibit good plating rates. However, they must be carefully controlled. The cyanide alkaline baths can be easily controlled to produce thin deposits of relatively uniform thickness on all surfaces. They have the best throwing power and are the most widely used baths. Since a thin coating is needed for the screen and sophisticated control is not required, the cyanide alkaline baths are used for the experiment [M-3].

The coating is applied in two stages. The first bath used is a dilute cyanide to deposit a strike coating of 1.0 to 3.0 μm of copper before copper plating. This bath characterized by low copper metal and high free-cyanide content cleans the screen and must be used before a high-efficiency concentrated bath is applied [M-3].

The second stage is a high-concentration bath to produce deposits ranging from 8 to 50 μm . This high-efficiency baths are characterized by relatively high operating temperature, high copper content, and rapid operation. Deposition rates are three to five times faster than the rates for the dilute

cyanide bath. Potassium or sodium cyanide is used in the high efficiency baths. The potassium complexes formed by the combination of potassium cyanide and copper cyanide are more soluble than those formed when sodium cyanide is used. Therefore, a higher metal content and higher rates of deposition are possible than with the sodium cyanide high-concentration bath. The potassium bath also has more operating flexibility than the sodium bath and is favored because it raises the resistance to deposit burning and accordingly permits the use of higher current densities (faster plating rates). Therefore, potassium baths are the first choice in electroplating of the screen.

The operation of these baths can be improved by the use of proprietary additives, which improve anodic and cathodic bath efficiency and anode corrosion. These additives produce matte to full-bright, fine-grained deposits. They are also used to control the effects of organic and inorganic contaminants. The use of agitation (e.g. solution movement, cathode-rod movement, or use of air), filtration, removal of carbonate buildup, current interruption cycles, current reversal, and removal of impurities in the electrodes and bath also help the plating process.

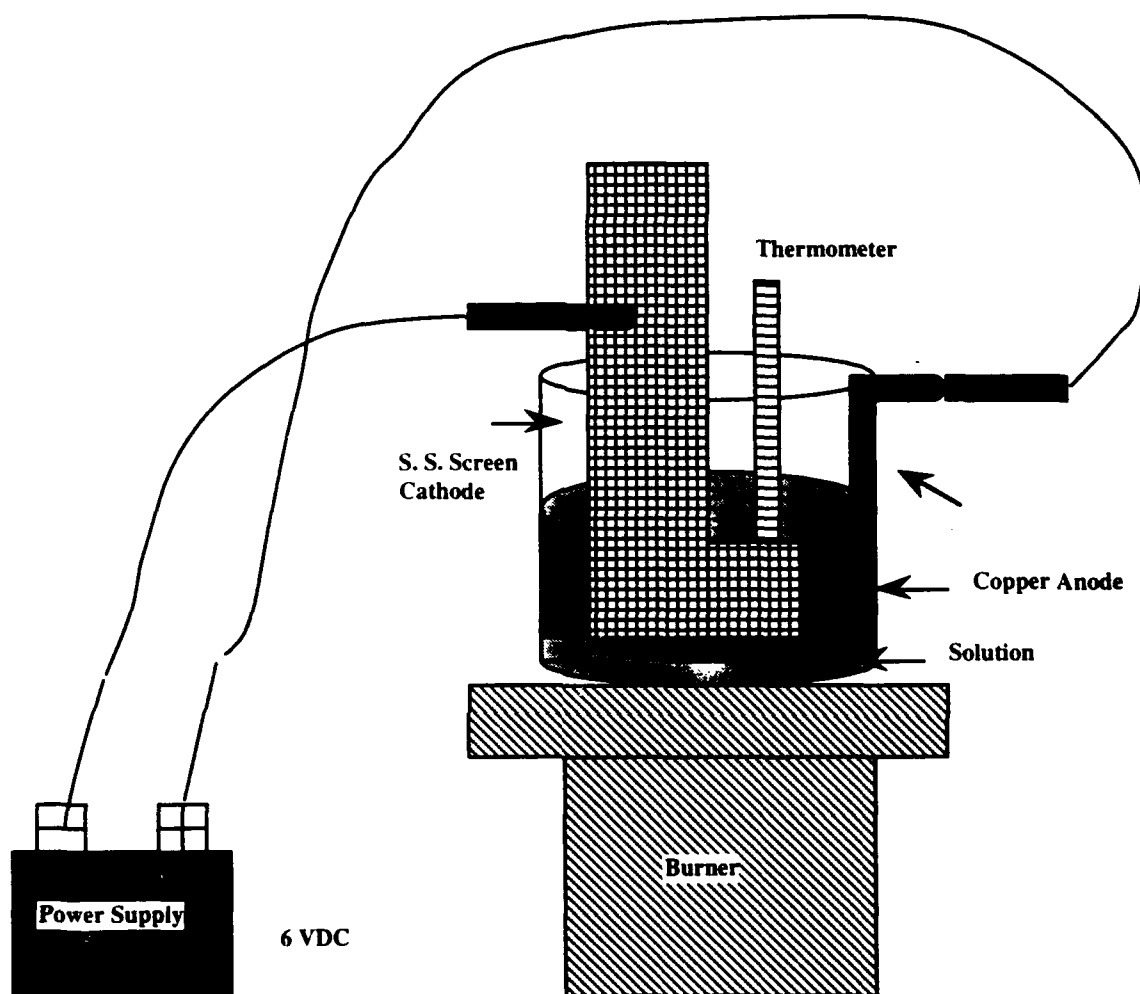
Table A.1.3.1 Chemicals Used for Electroplating

Bath Composition g/L	Dilute Cyanide	High Efficiency	
		Sodium Cyanide	Potassium Cyanide
Copper cyanide	22	80	80
Sodium cyanide	33	105	105
Sodium carbonate	15
Sodium hydroxide	to pH	30	...
Potassium hydroxide	35
Operating Conditions			
Temperature °C	30 - 50	60 - 75	60 - 75
Current Density A/dm ²	1.0 - 1.5	2.0 - 6.0	2.0 - 6.0
Cathode efficiency %	0 - 50	70 - 100	70 - 100
Voltage, V	6	6	6
pH	12.0 - 12.6	> 13	>13
Anodes	Copper	Copper	Copper

From Ref [M-3]

The first bath prepared used the dilute solution and the high efficiency potassium cyanide with the ingredients stated above. Distilled water was added to make two 1 L solutions. Eight pellets (~1 mm in diameter) of sodium hydroxide were added to reach a pH of 12.6. The dilute solution was heated to 40 °C and 6 V was applied for 3 minutes to put on the strike coating. The high efficiency solution was heated to 65 °C and 6 volts was applied for 20 minutes. The temperature varied from 65 - 76 °C as the voltage was added (see Figure A.1.3.1 for a drawing of the electroplating system).

Figure A.1.3.1 Electroplating System



The first attempt was not successful. Even though every wire was fully covered, the coating was very coarse and uneven. Ten of the holes were fully clogged. It was decided to repeat the procedure, but add glycerine and urea (It was rumored that these were proprietary materials that helped to smooth out the coating. The use of urea is an interesting story. An individual use to work in an electroplating outfit that had large volume baths for electroplating. The rest room was quite a distance from his work area. He

decided that it would be more convenient to relieve his bodily fluids into the baths instead of walking to the bathroom. One day, his boss came in and caught him in the act. He was immediately fired. Several days later the baths were changed and coating continued. The coating produced by the baths was not as colorful and of the same quality as before. After analysis, it was determined that the urea helped the electroplating process and was used in future baths. It was not known if the man was allowed to come back to work).

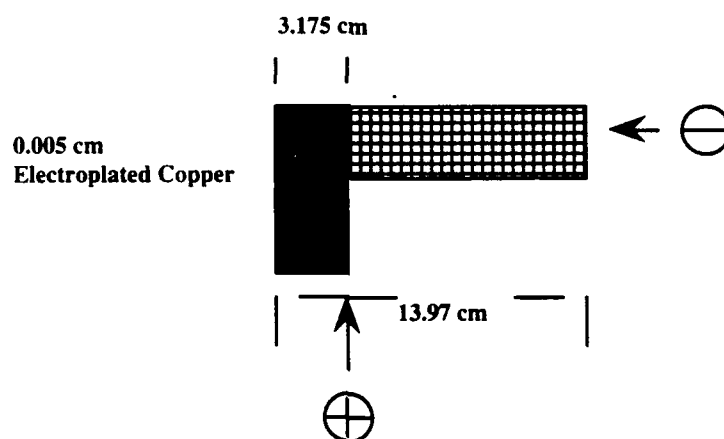
The next batch of baths were made. The dilute solution remained the same. The potassium cyanide solution contained the following ingredients: 80 grams copper cyanide, 105 grams sodium cyanide, 35 grams potassium hydroxide, 35 grams glycerine, and 10 grams of thio-urea crystals. The same temperatures as before were used for both solutions, but the times changed. The sample was coated for 7 minutes in the dilute solution. It had a nice, even copper coating around it. The sample was coated in the heavy solution for 10 minutes. The solution started to form black chunks, specifically around the copper anode. The solution was stirred (previous instructions said this could help) several times during the coating process. The sample coating was very good. It had a nice uniform coat (every wire covered) and was not as coarse as the previous test. It was decided next to coat a half screen (similar to Figure A.1.2.2) and apply power to it to determine if this coating would alleviate the hot spot problem.

The same procedure as above was applied except that the times changed to apply more coating. The above tests were proof of concept, now the exact amount of coating had to be applied. The screen was etched and 0.005 cm of stainless steel was removed (micrometer used for measurement). The screen was then placed in the dilute solution for 105 minutes at 6 VDC and 1 amp at $\sim 40^{\circ}\text{C}$. The concentrated potassium solution was used for 24 minutes at the

same power and $\sim 60^{\circ}\text{C}$. The solution was continuously stirred for the 24 minutes. The coating looked good, it was a little coarse (like cauliflower), but was uniform. The micrometer revealed that 0.005 cm of coating was applied.

The screen (Figure A.1.3.2) was wired up and current was applied (inert gas was applied for cooling and to minimize oxidation).

Figure A.1.3.2 Copper Electroplated Test Screen



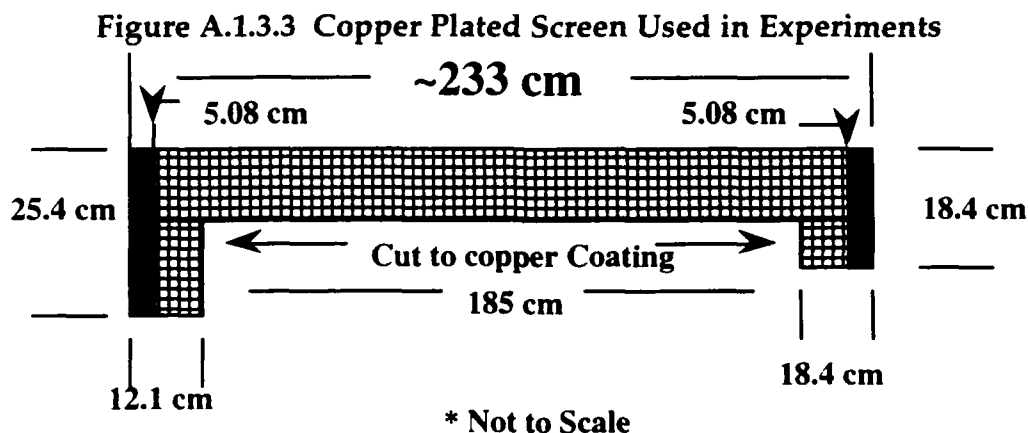
The current was applied for 5 seconds at 200 amps and no hot spots were found. The current was then applied for 5 seconds at 250, 400, and 430 amps. No hot spots were found in these intervals. The current was then applied at 430 amps for as long as possible. The entire screen showed a nice orange glow for about 10 seconds, then the copper began to burn away and by ~ 20 seconds the copper was gone and the stainless steel screen melted. Since no hot spots were found and the coating took a high load for a period of time with very little cooling, it was decided that the electroplating of copper was a solution to the hot spot problem.

An electroplating vendor was contacted in the local New York area for the electroplating job. The proprietary processes might give an even better coating. The vendor refused to do the job because of the large size of the screen.

Other options were looked at for electroplating since it had to be done internally in order to get the best possible coating. Some of the enhancement options mentioned previously were tried. Filtration was not applied due to the small volume of the bath (see Figure A.1.3.1, more equipment would cause problems with the cathode touching the anode). However, each solution was filtered after the plating. Current interruption was used. For every one minute of coating the current would be turned off for 10 seconds. This process seemed to enhance the coating. Current reversal was applied and was not found to be effective. The only agitation applied in the process was the constant stirring of the bath. Several methods were attempted to maintain a clean bath to reduce contaminants. Deionized water was used for each bath. Alcohol was applied to the screen prior to coating for cleaning. The black chunks that formed on the copper anode were cleaned off after every plating process. The cylinder used for containing the baths was cleaned after each time the baths were used.

Taking all of the previous discussions into account (a lot of trial and error), the following process was found to be the best way to electroplate 0.005 cm of copper onto the screen (see Figure A.1.3.3 for a picture of the copper plated screens used in the experiments). Chemical content used was the same as Table A.1.3.1 for the dilute solution (8 NaOH pellets to get the proper pH) and the potassium cyanide except that 35 grams of glycerine and 10 grams of thio-urea were added to the latter solution. Both baths used 1 L of deionized water for these chemical concentrations (Usually 2 batches were mixed together to give a high enough water level for the tray used so the complete screen area for coating could be covered). The temperature for the dilute solution was held around 40 °C at voltages ~ 6 V for 8 minutes. The coating was thin and evenly covered the screen after this stage. The temperature for the high

efficiency bath was ~ upper 60's °C at voltages ~ 6 V for 10 minutes, 10 s with 10 s interruptions at every minute. The coating was 0.05 cm thick, was even with every wire covered, and was very granular (no thick blotches).



Due to logistics issues with plating (volume of baths, problems with masking materials, and issues with acids) as much copper was applied to give a coating at the end, than the tabs were cut to the copper coating line to use as a thinner tab (The original tabs were cut to wrap around the entire electrode, this was still done except the screen only carried current at the cut end with copper. The slimmer region had no problems at the electrode connection). The above coating process solved the hot spot problem, no hot spots were found on any screen after a test was conducted.

As stated previously, many trial and error experiments were conducted to find the best process and even then problems occurred. A few brief comments are shared to show where the problem areas occurred.

Several times the process did not work out, mainly due to leaving the sample in the bath for too long. In order to remove the copper and not have to use a new screen, the screen was placed in nitric acid. The acid immediately removed all of the copper. The screen was then thoroughly washed with water and alcohol and placed back into the electroplating baths and no copper could be plated onto the screen. New baths were used and still

no copper would plate on to the screen. It was then deduced that the nitric acid may have changed the properties of the screen even though it was thoroughly washed. The screen was placed into aquaregia for a few seconds and then washed and put into the electroplating baths. The plating process continued to work well after dipping it in aquaregia.

There were problems with the high efficiency baths. This problem occurred on the last screen used in the series of experiments. The dilute coating was fine as described above. The screen was then placed into the high efficiency coating. The current in this bath jumped way up to 30 - ~40 amps (usually the current was between 1 -7 amps for both solutions at 6 VDC) at 6 VDC. The screen was removed and the coating was much blacker and had many blotches of thick chunks of copper deposited on it. The test was tried over again at lower voltage (4.5 VDC) and the same phenomena occurred. The time was then lowered until even at 30 seconds the coating was on too thick with big chunks of copper. The bath was thoroughly cleaned and a new solution was made which delivered the same results. Another solution was made per Table A.1.3.1 (no glycerin or thio-urea). The same results were obtained. The copper cathode was placed farther way from the anode to avoid the chunks. The same results were achieved. It was deduced, there may have been some contaminant or more agitation and filtration was needed. This was very frustrating since the same procedures were followed *exactly* and different results were occurring. The solution to this problem was to use the dilute solution for a longer period of time. The dilute solution was used for 17 minutes and a nice, even, 0.005 cm coating was applied to the screen. This may be a better alternative for electroplating since only one bath was required.

A.2 ALUMINA COATINGS

A.2.1 Plasma Sprayed Alumina

Due to the resistivity of stainless steel, the wraps in the screen had to be coated to prevent electrical contact between the layers and allow enough heating in the bed. The following criteria was needed in this insulating material: adherence to s.s.without clogging the holes, high resistivity, and high temperature. The first criterion was very important. Most of the candidate materials were oxides, which are ceramics and can be applied to the screen, but due to the high brittleness of these materials, they have problems when they are put under loads (cracks are formed). If an electron microscope were used, it would reveal cracks on the screen before it was rolled because of the material properties of ceramics. As long as these cracks do not cause the coating to flake off (give an open area of s.s), these ceramics can be used. It was noticed by placing the ceramic under loads, that the ceramic can handle tension loads (the ceramic elongates, cracks spread out), but can not handle compression loads (the coating flakes off).

Alumina oxide (Al_2O_3) looked like a candidate ceramic material. Its thermal properties are as follows:

melting point	2050 C
density	3.96 g/m ³
specific heat	1050 J/kg C
thermal expansion	$8 \cdot 10^{-6} / \text{C}$
thermal conductivity	4 W /m C
resistivity	1000000 Ω /cm

[C-2]

Tests were performed to determine the thermal properties of the alumina on the stainless steel (coefficient of thermal expansion, heating loads for

swelling, etc). The first action item was to determine a coating that could bond to the screen and handle the bending loads before heating was applied. Plasma sprayed alumina looked like the best first approach to try.

The same vendor that plasma sprayed the copper onto the screen was contacted for alumina plating. The first screen was copper and alumina sprayed, but as seen from the previous discussion, the copper plating was focused on first. The vendor said that there were problems in the plasma spraying process. The alumina did not stick to the screen when sprayed. The vendor then tried to create a rougher surface by sandblasting the screen before trying the coating. This sandblasting process worked, and the vendor said alumina adhered to the screen with a nice even coating. After inspection under a 1x microscope, the coating was nice and even and most of the wires were fully covered. There were some problems on the edges. The screens were cut out with shears from a large sheet of woven screen to the desired dimensions. In the cutting process, a path was chosen to cut along the line of wires, but it was very difficult to stay on line with such a thin wire diameter, and occasionally the shears would slip and frayed wires would be formed. It was difficult to remove these wires (pulling a piece of string out of a sweater). Smaller tin snips and files were used to cut off as much of the edge as possible. Boron nitride spray, or alumina paint was used to cover the edges as much as possible since the plasma spray process had trouble in covering these areas.

Assembly of the plasma sprayed screen changed the outlook on the coating. Many areas of the wires were exposed (see Figure A.2.1.1).

Figure A.2.1.1 Coating After Being Rolled

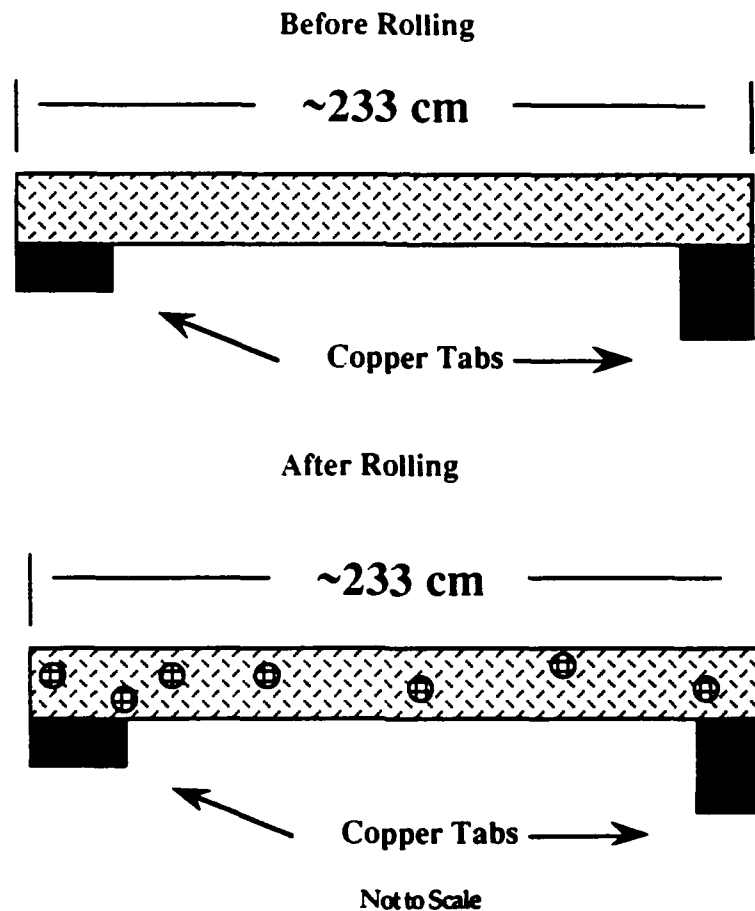


Figure A.2.1.1 is not exactly correct. The alumina coating did not clog up the holes, but ~ 1 mm chunks of coating flaked off in the assembly process (flake offs were random like the drawing). The measured bed resistance dropped by a factor of 2 throughout assembly ($\sim 0.2 \Omega - 0.09 \Omega$). This was unacceptable for the experiment.

A.2.2 Plasma Sprayed Spinel

Dr. Herb Herman of SUNY Stony Brook has had much experience with plasma sprayed ceramic coatings [H-3]. He was consulted about the coating

problems with alumina on the stainless steel and that the screen had to be rolled for assembly. He said that this is a tough problem and that he had been trying to put some science into the "black art" of plasma spraying. He mentioned that Spinel (alumina with magnesium) might be a better coating since he had experience with it and it seemed to have better properties under temperature.

Another vendor (in the local area) was contacted since the first vendor had scheduling problems. The vendor said they could plasma spray on the Spinel. Their operations were more complex than the other vendor's. The first vendor plasma sprayed the screen with a hand gun. The vendor had a lot of experience that allowed him to do an adequate job. The second vendor had a fully automated plasma spray system. A robot was programmed for the dimensions of the screen and thickness of coating needed. The Spinel coating was sprayed on and also had problems with adhering to the screen. The particles tended to blast past the screen and did not adhere. Grit was used to roughen up the surface, and the spinel adhered much better. Under a 1x microscope, the coating looked good. The screen was then rolled for assembly, and the coating flaked off worse than the alumina coating. It was found that the coating would stretch under tension and could handle a much better load than compression (small load would pop-off the coating). Scratching the surface by hand could remove the coating which was truly unacceptable. These concerns were mentioned to the vendor and they proposed some sample screens be sprayed in order to look at different options.

Four samples were prepared which are as follows: (1) coated on both sides with 95 % Ni 5 % Al bonding layer and 0.005 cm Spinel; (2) coated on both sides with a coarse layer, 95 % Ni 5 % Al bonding layer, and 0.005 cm Spinel; (3) coated on both sides with a coarser layer, 95 % Ni 5 % Al bonding layer

and 0.005 cm Spinel; (4) same as 3, except coated on one side. Out of these samples, (4) looked the best. The coarseness and bonding layer helped the adhesion process. The difference with (3) was that there were quite a few flake - offs when the sample was bent in half on the compression side. The tension side looked very good with no open wire. The possibility of only coating one side was explored.

An investigation was conducted to determine how much coating was lost under rolling of the bed (losses mainly due to compression). A full length screen was coated on both sides (similar to (4)) and rolled. The resistance was checked prior to wrapping and then at each wrap as the screen was wrapped around the hot frit with the ohmmeter. Two screens were checked, Table A.2.2.1 shows the results:

Table A.2.2.1 Impact of Wrapping on Resistance

Initial	0.0952 Ω	Initial	0.1142 Ω
1 Turn	0.0937 Ω	1 Turn	0.1125 Ω
2 Turns	0.0901 Ω	2 Turns	0.1108 Ω
3 Turns	0.0815 Ω	3 Turns	0.1094 Ω
4 Turns	0.0873 Ω	4 Turns	0.1067 Ω
5 Turns	0.0828 Ω	5 Turns	0.1030 Ω
6 Turns	0.0753 Ω	6 Turns	0.0977 Ω
		7 Turns	0.0924
		8 Turns	0.0896 Ω

These results showed coating was being removed in the rolling process which confirmed speculation. The single coated screen was then placed into the cold frit to check for losses in rubbing against the frit as it was pushed into position. The results of this test showed that there was coating loss in several places. The friction between the cold frit and screen caused the losses. Even though this coating looked good in tension, it was determined to not pursue this coating process since even if one side was coated, friction with the frits

and layer upon layer would probably cause too much of a coating loss and too low of a resistance.

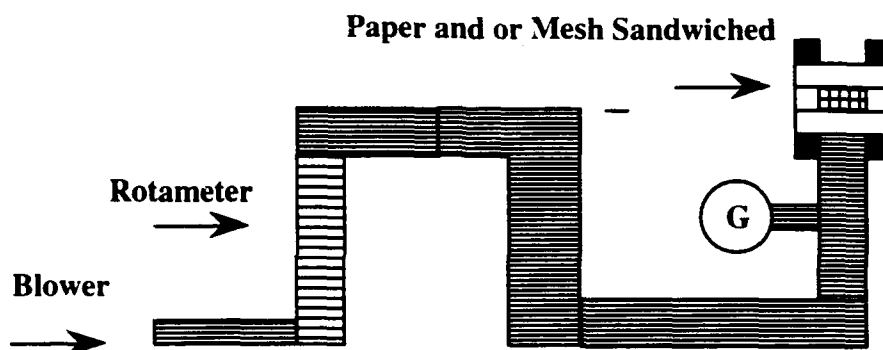
A.2.3 Ceramic Paper Insulator

The severity of the above coating problems made it impossible to test. Other approaches needed to be discovered. Methods were investigated to find materials that could be placed between the wraps to stop contact between the wires, but not be too thick to create voids and flow problems. A very thin ceramic paper looked like a possible solution.

A ceramic paper made with alumina refractory fibers by Cotronics was discovered [C-2]. The paper was flexible enough to be rolled. It was placed on top of the screen and was rolled and the resistance was fine (ohmmeter read overload, ∞ resistance, no contact between the layers). The melting point of the paper was 1777 °C. The smallest thickness available for order was ~0.08 cm. A press was used to cut down the thickness to 0.05 cm. This still was thicker than the alumina coating, therefore a smaller screen would have to be used. The total screen length was shortened to 200 cm (2 screens in parallel - 99 cm, 101 cm) in order to fit in the cold frit.

Since the paper had little perforation, pressure drop measurements were needed (see Figure A.2.3.1).

Figure A.2.3.1 Test for Pressure Drop Across Ceramic Paper



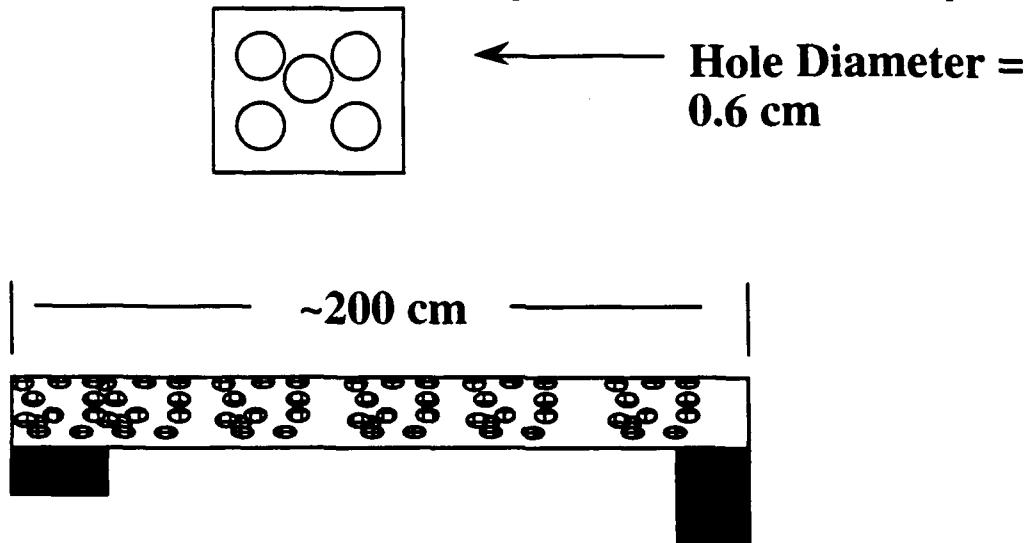
The readings recorded from the above apparatus were as follows: no paper no screens - 42 scfm at 0.5 psig, two screens no paper - 56 scfm at ~ 1 psig , two screens with paper sandwiched in between - 28 scfm at 1.75 psig. Holes per Figure A.2.3.2 were put into the paper to change the reading to 45 scfm at 1 psig. For each test the blower was pushed to its maximum flow.

The following equation

$$\Delta P = R_{\text{Total}} W^2 \quad [A-1]$$

shows the relationship between a change in pressure to the flowrate through a control volume, where R_{Total} = total equivalent resistance and ΔP = pressure drop [C-4]. There was a factor of 1.5 difference in the equivalent resistances between the screen and the screen with paper.

Figure A.2.3.2 Holes Put in Paper to Minimize Pressure Drop



As many holes of 0.6 cm in diameter were placed onto the paper without causing a tear. Many methods were tried to place the holes on the paper since it was 200 cm in length (e.g. sandblasting, drilling through a grid, pounding with blunt nails). The most effective method found was using a cork borer with a cardboard background.

Since the paper insulated the screen layers, it was used as an insulating material in some of the experiments.

A.2.4 Ceramic Tapes

Ceramic tapes were used in the same philosophy as the paper (sandwiching between the layers), but were thinner (~0.01 cm in thickness). It was hoped that the thinner paper would lower the porosity close enough to be prototypic. The issue with the tapes was the adhesive needed to be removed (for high temperature in experiment) and the tape needed to be as wide as the screen (in order to minimize shifting of the tape in assembly and exposing

open wires). Most of the tapes that were found were low temperature (277 °C operating temperature). The high temperature quartz tapes (~ 2200 °C) were only 3.175 cm wide (instead of the required 10.16 cm). A thicker tape could be special ordered, but the time required was too long (several months). It was discovered that the adhesive could be removed with heptane, but this option was not pursued due to the time required to get the wider tape.

A.2.5 Zirconia Balls

Another option considered was to use tiny zirconia balls (1000 μm in diameter) to insulate the layers from making contact (see Figure A.2.5.1).

Figure A.2.5.1 Zirconia Balls as an Insulator



The balls were high temperature (melting point of 2800 °C). An adhesive was needed to allow the zirconia balls to bond to the screen. A high temperature paint was found and spread out onto the screen to act as an adhesive. The balls were scattered onto the screen in a random manner. The paint dried and the balls adhered to the screen while it was flat. The screen was rolled and the balls seemed to stay bonded to the screen. The ohmmeter read over load, ∞ resistance, so it looked like the balls were preventing contact between the layers. The sample was put into a Lindberg 3100 W (200 - 1200 °C) tube furnace at 900 °C for a hour. The screen was removed from the oven and most of the balls fell out. According to the ohmmeter, the resistance reading was still in the over load condition. If more force was put onto the screen, the reading would change to 0.04 Ω . This was an interesting

phenomenon, since the balls had fallen out of the screen , what was causing the insulation ? A 1 x microscope revealed that the s.s. screen had oxidized (a black coating had formed). The coating was powdery, and rubbed off by hand (not in big chunks, but in sand-size particles), but it was worth pursuing.

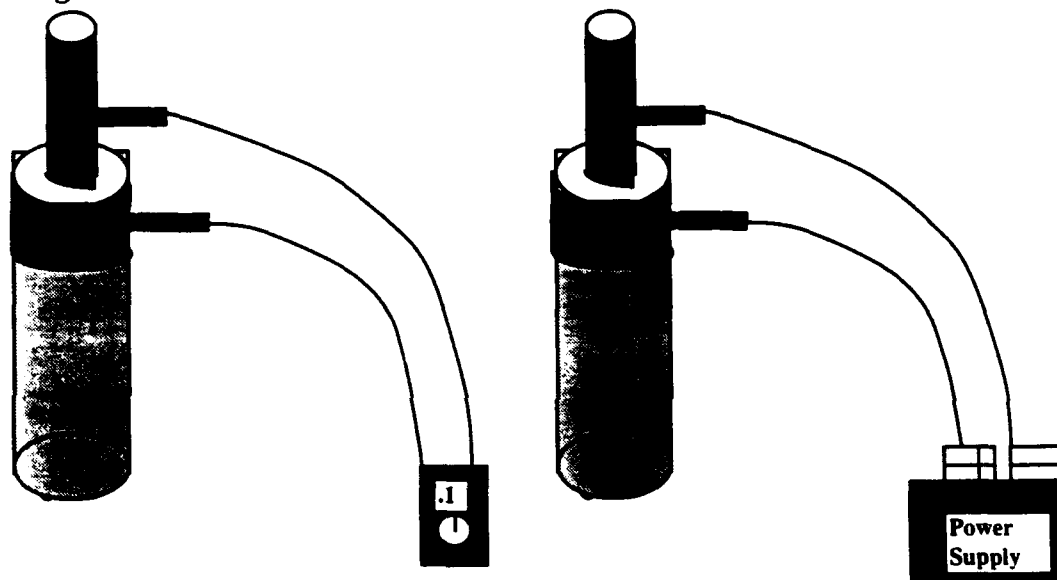
A.2.6 Oxidized Screen

The oxidized screen was worth pursuing. It was not a good stand alone coating, but it could be used as a base coating with another alumina coating. Two sample screens were put into the Lindberg oven at 950 °C for 7 hours. They then were sent to the first vendor (plasma sprayed by hand) for coating. One screen had the oxidized s.s., a Ni bonding layer, and a 0.005 cm alumina coating. The other screen had the oxidized s.s. layer, and 0.005 cm of alumina. The screens were analyzed and it was determined that the oxidized s.s.with alumina was the better coating.

There was an issue with oxidizing the screen and the electroplating. The screen would first be oxidized, than the oxidized coating was removed from the tabs and ends, the copper coating was electroplated, and then the screen was sent out to the vendor for plasma sprayed alumina coating. Methods were tried to remove the oxide coating for electroplating. Aquaregia did not do the job at room temperature. The aquaregia was heated and the oxidation was removed but at a slow rate. There was some concern about using aquaregia for a period of time since it was already originally used to remove s.s. at the ends and too much use could cause the wires to become too thin. Sandblasting with fine sand was found to be an effective way to remove the oxide.

Two screens were etched, oxidized, ends sandblasted, electroplated, and coated with alumina. The bed resistance before assembly was measured with the ohmmeter to be $0.17\ \Omega$. After the screen was assembled into the frits, the measured resistance was $0.11\ \Omega$. This resistance reading was a little low. It was not as bad as the original plasma sprayed readings, but the resistance needed to be around $\sim 0.2\ \Omega$. It was concluded that in-situ oxidation should be applied to increase the resistance (see Figure A.2.6.1).

Figure A.2.6.1 Resistance Test and In-Situ Oxidation of the Screen Bed



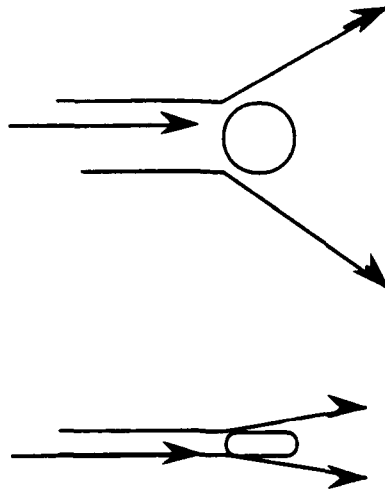
There was some concern that the in-situ oxidation would oxidize the copper. At $450\ ^\circ\text{C}$ in air copper oxidizes at the rate of "less than about 20 to 40 $\text{mg}/\text{dm}^2\text{-hr}$ " according to Uhlig [U-1]. Taking into account the density of copper, this corresponds to $< 2.286 \times 10^{-5}\ \text{cm}$ to $4.572 \times 10^{-5}\ \text{cm}$ per hour. The temperature for the oxidation was held below $450\ ^\circ\text{C}$ and the copper also had the alumina coating over it for added protection. These rates were so low that in-situ oxidation should not be a problem.

Power was added at 17 V at 50 amps for 4 hours. After the bed was cooled down, the ohmmeter read $0.13\ \Omega$. (this result was encouraging). It was

decided to let it oxidize for another 5 1/2 hours. As the screen was oxidizing, hot spots were seen in the bed (mainly on the edges, but some could be seen inside the bed). This was not due to hot spots on the edges, but exposed wires where coating had flaked off. However, as the screen oxidized the hot spots would disappear/reappear in different areas or the same areas. It was suggested that the hot spot would oxidize itself and the short would then go away. The newer hot spots showed up in different places. This effect was due to as the bed was oxidizing itself current flow was changing and may have become more concentrated in new areas, creating new hot spots. As these hot spots oxidized, the effect continued. The new resistance after the second heating was 0.16 Ω . This was a good improvement and this bed was assembled into the full assembly.

Another screen was made under the same process. This screen was rolled into the cold frit backwards so the the tabs would not fit. This screen was put through a roller first to flatten the wire. It was thought that the flat wire would make it harder for the coating to pop off and would not create as much friction between the wires. The resistance was measured on this screen and no big improvements were seen (~0.13 Ω). Since the flat wires did not create the same flow effect as round wires, this approach was terminated (see Figure A.2.6.2).

Figure A.2.6.2 Flow Effect of Round Wires vs Flat Wires



A.2.7 Glossy Coatings

An attempt was made to make a silicon monoxide coating. The hope was that this glossy coating would be similar to coatings on pottery, and would be able to handle the bending loads. Current was needed to form the coating. Problems with the current did not allow the coating to form. It was believed that more current was needed for the process, but other options seemed more appealing so this process was not pursued.

A.2.8 Painted Alumina

Another approach for coating the mesh was to apply a ceramic adhesive. These adhesives were developed to bond ceramic to ceramic, metals, glass, plastics, etc. The following adhesives were available from Cotronics for coating the screen :

Table A.2.8.1 Ceramic Adhesives

	#901	#989
Service Temp F	2600	3000
Base	Al ₂ O ₃	Al ₂ O ₃
Compressive Strength psi	1200	3000
Flexural Strength psi	600	3000
Thermal Expansion 10 -6	4	4.5
Thermal Conductivity BTU -in/Hr - F -Ft ²	2	9
Dielectric Strength volts/mil	200	200
Volume Resistivity ohm -cm	10 **12	10**8

The following criteria were used in selecting the materials for the screen (in priority): (1) choose maximum temperature; (2) match thermal expansion between materials to be bonded; (3) select required electrical properties; and (4) select bond strength requirements. Temperature was a key parameter since a high phi was required. The thermal expansion for s.s was 9.6×10^{-6} °F [C-3]. All of the resistivities were so high that it was really not needed as a discriminating parameter.

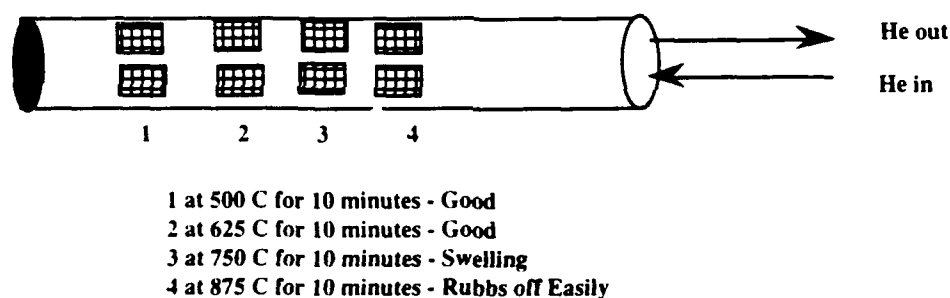
The 989 and 918 coatings were in paste form and had to be mixed with thinner (50% adhesive, 50% thinner for 989, 2 /1 adhesive to thinner for 918, both volume ratios) in order to put it on the screen. Since the wires were so thin, the best procedure found was to mix the adhesive and thinner into a paint gun and paint the 0.005 cm of coating onto the screen. Fortunately, Cotronics had thinner that matched the adhesive.

Two samples were prepared for comparison of the two coatings. The coatings were mixed with thinner and sprayed onto a 7.62 cm by 10.16 cm screen. Each screen was then cured at 75 °C for 4 hours. The 989 screen performed much better. Both screens were bent and many open areas

appeared on the 901 and only 2 small open areas were detected on the 989. This made sense, since the 989 had a higher CTE (coefficient of thermal expansion), and higher stress limits.

The next test was to determine the effects of the 989 at temperature, especially since there was a factor of 2.13 difference in the CTE's. A sample was cured at 120 °C for 18 hours and another sample was uncured. Both samples were placed into a Lindberg furnace with a flow of He gas. The cured sample performed better, but around 750 °C, the coating started to swell and rubbed off easily. Therefore, 700 °C was set as the upper bound for the coating to allow some margin since the temperatures inside the bed would be a little bit higher than the thermocouples touching the hot frit (see Figure A.2.8.1).

Figure A.2.8.1 Alumina Coating Test



The coating was then exposed to LN₂ for one hour and no changes were found. It then was placed into LN₂ for a couple minutes and then placed into the oven at 875 °C (thermal shock experiment). The coating did not initially swell, but rubbed off easily after being in the heater for 10 minutes (same result as A.2.8.1).

Another issue with the 989 coating was that it had to be sprayed on with a paint gun. The lab paint shop was used, but it was hard for the painter to add 0.005 cm of coating onto the screen. Sometimes he sprayed on too much and

the coating would not fit into the bed; sometimes he did not have enough on and the resistance was too low. It was difficult to remove the coating to have it re-sprayed. Aquaregia was tried and a reaction occurred that spilt acid all over the lab and destroyed the screen. Hydrofluoric acid was found to be effective in removing the coating or a new screen would be cut for re-coating.

The screen for this method was etched, electroplated, painted, and cured (no copper problem). The bed resistance measurements for this coating was 0.1889 Ω prior to assembly, 0.166 Ω after rolling the bed into the frits, and 0.15825 Ω after complete assembly for one test and remained 0.2 Ω for another experiment. This was the best resistance numbers of all the methods performed.

Another approach using the painted alumina screen was to cut the screen one wrap short, coat it similar to previous discussions, but then just have one wrap coated with 989 to wrap around the rest of the bed and have contact with the cold frit. The coating loss would be minimal (not enough to allow the cold frit to carry current), and the bed resistance would remain high. Unfortunately, this approach was never used due to issues discussed in Chapter 4.

A.3 SINGLE SCREEN

The first tests performed in July 1992 used two screens wrapped in parallel with alumina paper. It was thought that two screens in parallel would be needed to place enough power in the bed. After this first experiment, it was deduced that one screen would be adequate, but it was thought that the original design showing the methodology for two screens should be included in this Appendix.

The goals of the experiment were to achieve an inlet Re (that is the Reynolds number just as the gas has passed through the cold frit and is at the bed inlet) of 12 or less, where:

$$Re = \frac{m D_p}{A_s \mu} \quad [A-2]$$

where $m = 0.00638$ kg/s for He (can be varied), $D_p = 0.00381$ m (coated wire diameter), $A_s = 0.018849$ m² (superficial area of the bed), $\mu = 1.07 \times 10^{-5}$ kg/ms (viscosity at bed inlet from W-2). The max ϕ with stainless steel = 11, ($\phi = (T_{Final} - T_{Initial})/T_{Initial}$), where $T_{Final} = 1200$ K and $T_{Initial} = 100$ K). The 1200 K max outlet temperature was chosen due to the 1700 K melting point temperature of stainless steel; swelling or material degradation would cause porosity problems, shorts, and adhesion problems with the coatings. The insulating coating were oxide based with melting temperatures ~ 2200 K (before swelling tests were performed). The 100 K inlet temperature was the max anticipated inlet temperature that the chill down system could support. This ϕ and max Re would allow a broad range of testing in the unstable/stable regions.

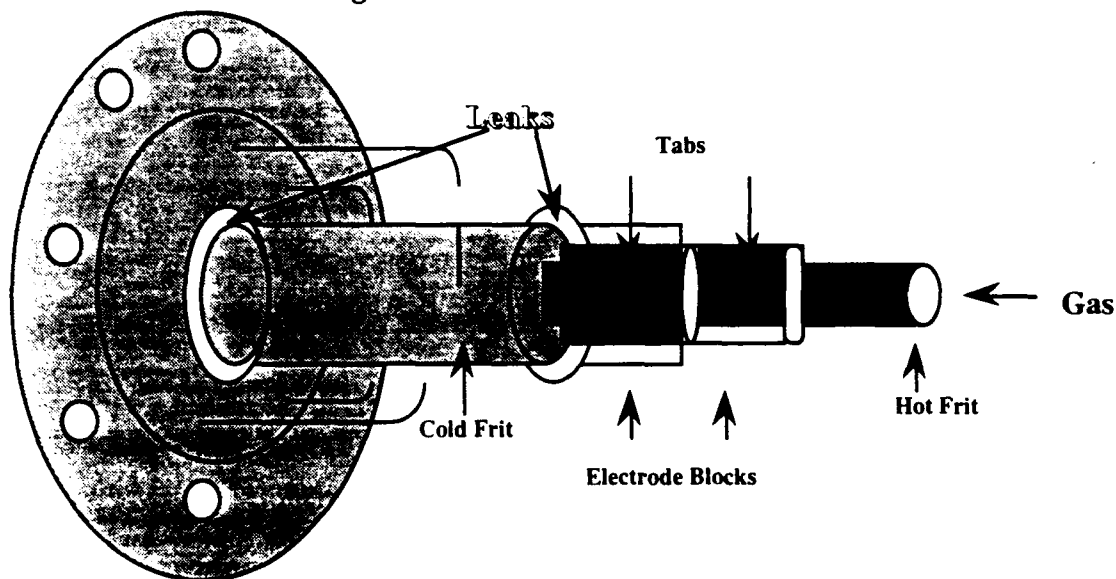
An energy balance was performed to estimate the energy required to the screen. Since

$$Q = \dot{m} c_p \Delta T \quad [A-3]$$

and $m = 6.38$ g/s, $c_p = 5.193$ kJ/kg K, $\Delta T = 1100$ K.[S-1]. The power required for He from this relation = 36 kW. The total power available from the power supply was 90 kW (DC supply 60 V and 1500 A max). Preliminary

preventing leakage of gas. However, some small leaks occurred around the bed and some check - out experiments were conducted to insure that the leaks were sealed as best as possible. The first leaks detected came out at the ends of the bed (see Figure A.4.1).

Figure A.4.1 Leaks at Ends of Bed



A He 1A cylinder was used to flow gas from the inside of the hot frit. This procedure was used to make it easier to detect leaks. A soapy solution was used to detect leaks by squirting the solution onto different areas and looking for bubbles. Two leaks were found at the ends of the bed. These areas had solid boron nitride plugs for the cold frit to slide over with ceramic paper on the inside covering the bed. They also acted as insulation. In order to seal these leaks, ceramic rope was wrapped around the edges of the boron nitride plugs, more ceramic paper was added around the inside of the bed, and a sealing paste of RTV (silicone paste) and Zircar alumina powder was spread around the outer crevices at both ends. The same test was performed again and the leaks were sealed. When the apparatus was fully assembled, no

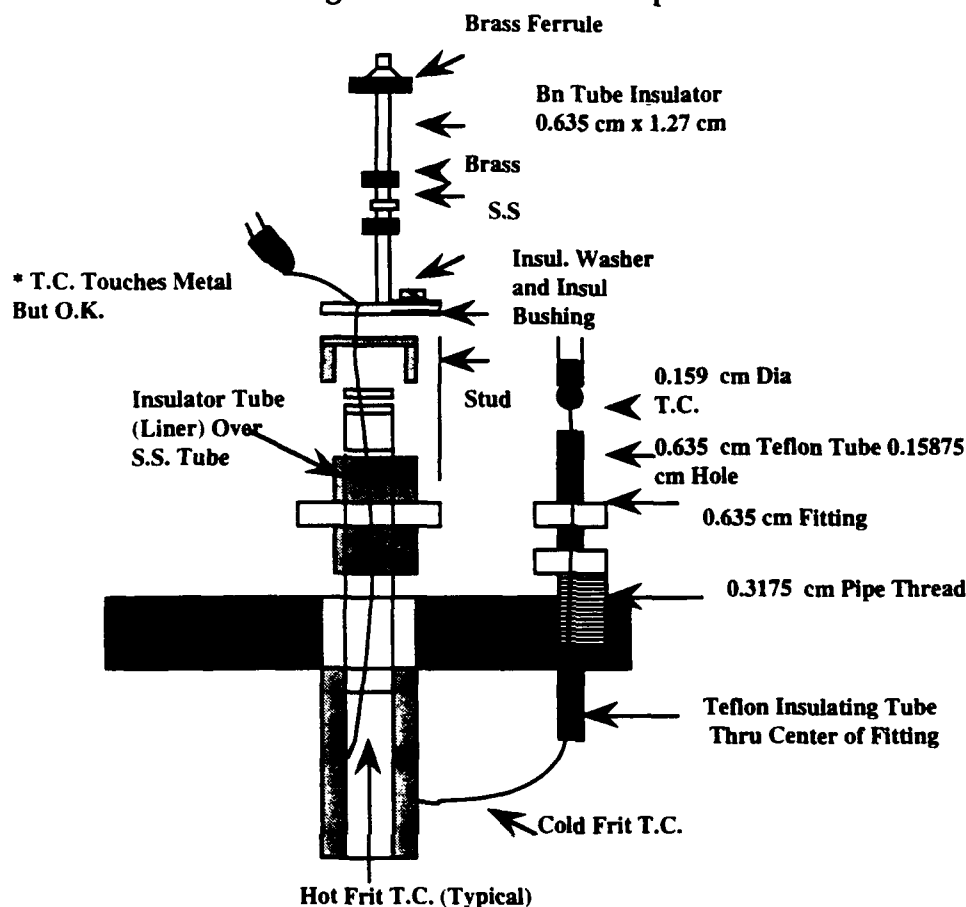
leaks were detected in any of the inlet pipes, outlet pipes, or in the outer pressure vessel.

A.5 THERMOCOUPLES

Section 3.5.1 discussed the thermocouples used in the experiment. The orientation of these thermocouples did change as experiments evolved. Minor changes were discussed in Chapter 4 and Appendix B for each experiment. One of the major changes was to add thermocouple #8 at the outlet in the middle of the gas stream. This was added to give a reading for the exit gas temperature which was an important parameter for energy balance calculations. All of the other thermocouples continued to touch the bed. They needed to touch the bed to determine bed temperature so the bed maximum temperature was not exceeded (coating issues). Thermocouple #7 always touched the cold frit to determine that the cold frit did not heat up in the tests (insured that it was insulated).

All of the thermocouples were checked out before assembly. In the early experiments, there were problems with thermocouple temperature based on power input. This problem was attributed to thermocouples carrying currents. The entire rig was re-insulated to insure this phenomena would not happen (see Figure A.5.1).

Figure A.5.1 Thermocouple Insulation



This drawing showed how the thermocouple's were kept from being "grounded" since they were "ungrounded" thermocouples. It mainly showed that *all* of the connecting pieces were insulated. The ohmmeter readings for the thermocouples read from 0.9 to 2.5 M Ω which seemed to support that the added insulation worked.

Continued tests showed that the thermocouple temperatures did not make sense for the power input. Troubleshooting revealed that the power supply had an influence on temperature readings. If the power supply was turned on the readings (based on ambient temperature) would read all over the place e.g. -16 °C to 33 °C. Then if the power supply on/off switch was turned off, but the cooling fan was allowed to run, the temperatures would change. A few

thermocouples would be at ambient temperature, but others (specifically #1) would be $\sim 10^{\circ}\text{C}$ off. This was a hard problem to diagnose, since all of the ohmmeter reading around the vessel showed that everything was isolated. It was decided to place all of the thermocouples away from touching the bed as a possible solution. A test was run with none of the thermocouples touching, but there still were problems with the results (see Appendix B.3). Another solution was to completely turn the power supply off and take a temperature reading than turn it back on again. A test was conducted using this approach (Section 4.2), but it limited the amount of temperature readings taken which was a limitation, and a logistics nightmare (The power supply was located ~ 10 m from the computer data acquisition system). An amplifier was added to one of the thermocouples to see if the signal could be tuned to match the proper ambient thermocouple readings. The amplifier just tuned the temperature farther away from the proper reading. The final approach was to check the thermocouple connections into the data acquisition system. It was discovered that the negative connection was ungrounded (not screwed into the board). The thermocouple manual said this was the proper procedure for these type of thermocouples. The negative wire was screwed into the board and the readings immediately adjusted to the proper readings with the power supply turned on (compared the results with an outside thermometer). The tests in Section 4.3 all used this set-up.

The reason this problem was not discovered and fixed in earlier tests is that the temperature display looked good in the beginning part of the run (-170°C). The power supply was not turned on until all of the temperature readings were close to -170°C and then it would be turned on and power would be immediately added. The temperatures than would immediately rise and made sense according to the power console. Post - test analysis revealed a

tremendous mismatch between temperatures and powers. At the time of the analysis, there still were questions about the screen coatings which lead to focusing in on that problem. Once a good coating was found, (painted alumina) the thermocouple problem could be pinned down.

A.6 ASSEMBLY ISSUES

Dr. John Bernard at MIT says that "the joys of doing an experiment is that 90% of the work is spent in hours of agony for 10% of the real results that occur in minutes". This is true of the design evolution in this experiment. A coating had to be found that could handle the bending loads from a ~233 cm rectangle to a 10 cm cylinder with a 1.1 cm radius. This same coating had to handle the scraping friction as it was pushed into the cold frit. As seen from this Appendix, once the coating problem was solved, the other issues were relatively minor .

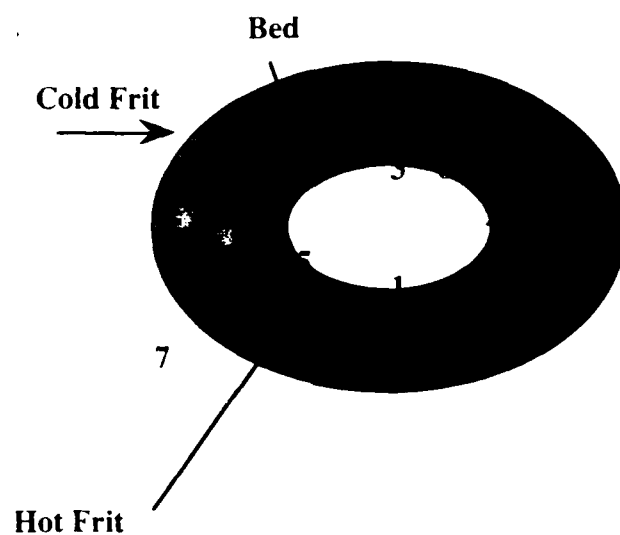
APPENDIX B

PRELIMINARY TESTS

B.1 INITIAL FAILURES

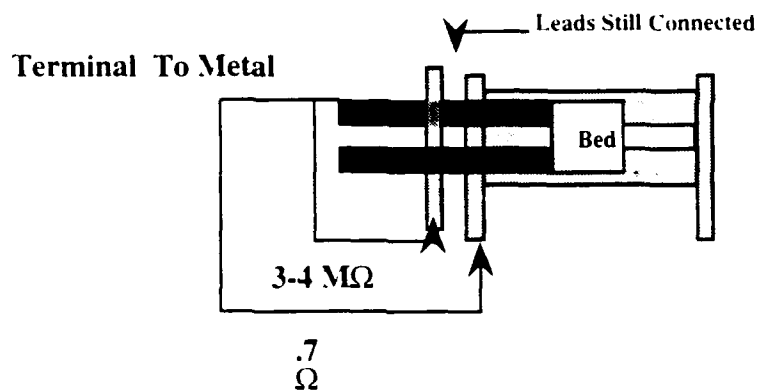
The first tests were conducted on 7 April 1992. The screen bed used was plasma sprayed alumina on the bed and copper coated tabs (no copper on the ends). Nitrogen gas was used as the working fluid. The flow rate was set at 250 lpm. Power put into the bed from the console reading was 419.4 W (1.8 V at 233 amps). The results from the experiment were as follows: (1) a thermocouple placed at the flowmeter inlet showed that the temperature varied between 33 and 42.9 °C which was within the 0 - 50 °C temperature window that the flowmeter required; (2) the bed inlet reached -15 °C which showed that the chill down system was not performing up to expectations; (3) the bed temperatures were sporadic - thermocouple #1 at 560 °C, #5 at 520 °C, #2, #3, #4, #6 all negative temperatures (see Figure B.1.1 for thermocouple positions. They were located in the same radial positions as Figure 3.5.1.1).

Figure B.1.1 Thermocouple Positions

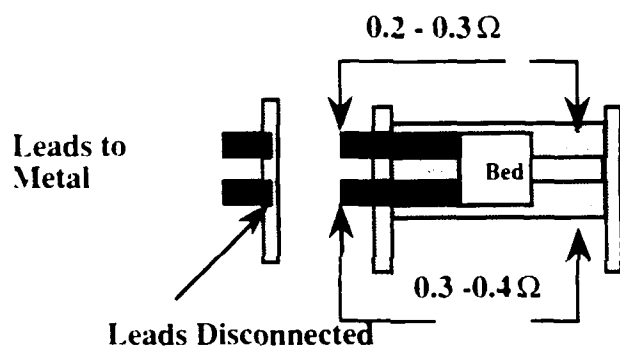


Several investigations were conducted to determine the problems with the experiment. The thermocouples were switched around and revealed that #1 and #5 still continued to read high and the others continued to read low. Therefore thermocouple problems were ruled out. An ohmmeter was used across the entire assembly to determine if there were any shorts anywhere in the apparatus (see Figure B.1.2).

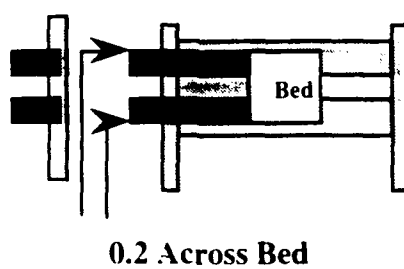
Figure B.1.2 Ohmmeter Tests on Apparatus



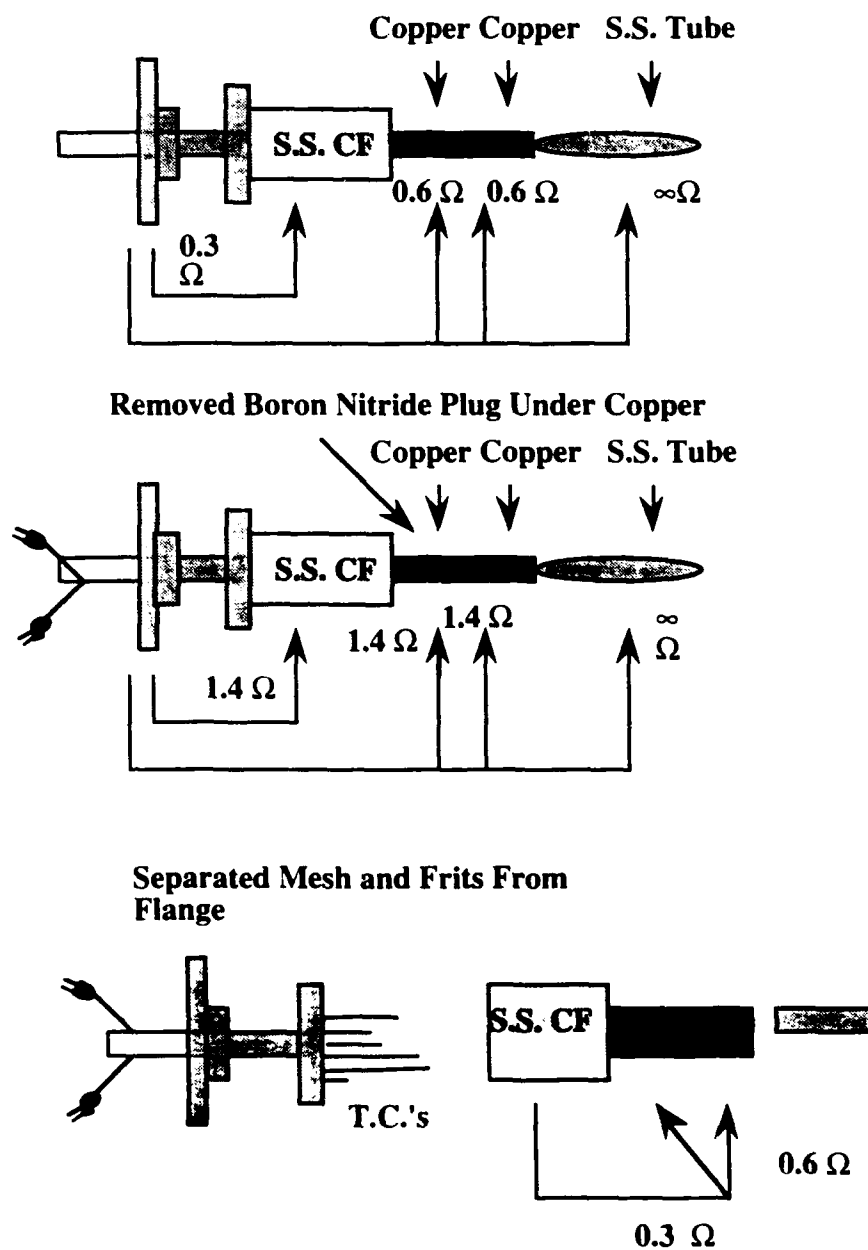
Separated Flanges and Tested for Resistance



Across Bed



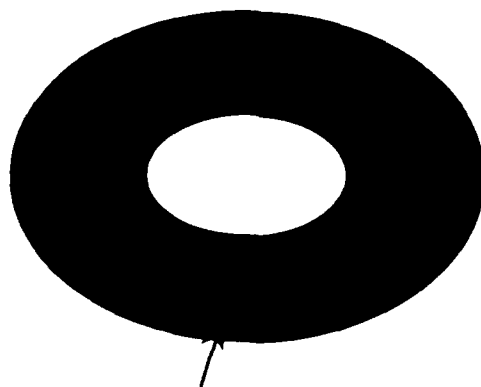
Then all the parts down to the cold frit and copper terminals were removed and the resistance was measured.



No visual inspections revealed obvious shorts outside of the bed. As a precaution, the leads were wrapped in alumina tape to insure no current was

carried to the vessel. The bed was then inspected and problems were found (see Figure B.1.3).

Figure B.1.3 Bed Inspection After Test



Several Windings Welded Together

Inspection showed that several of the wraps had welded together. When the screen was rolled out flat, the hot spot problem on the ends was first discovered. The edges also showed areas where melting had occurred. Better inspections of the edges and ways to remove tiny wires from the edges was needed.

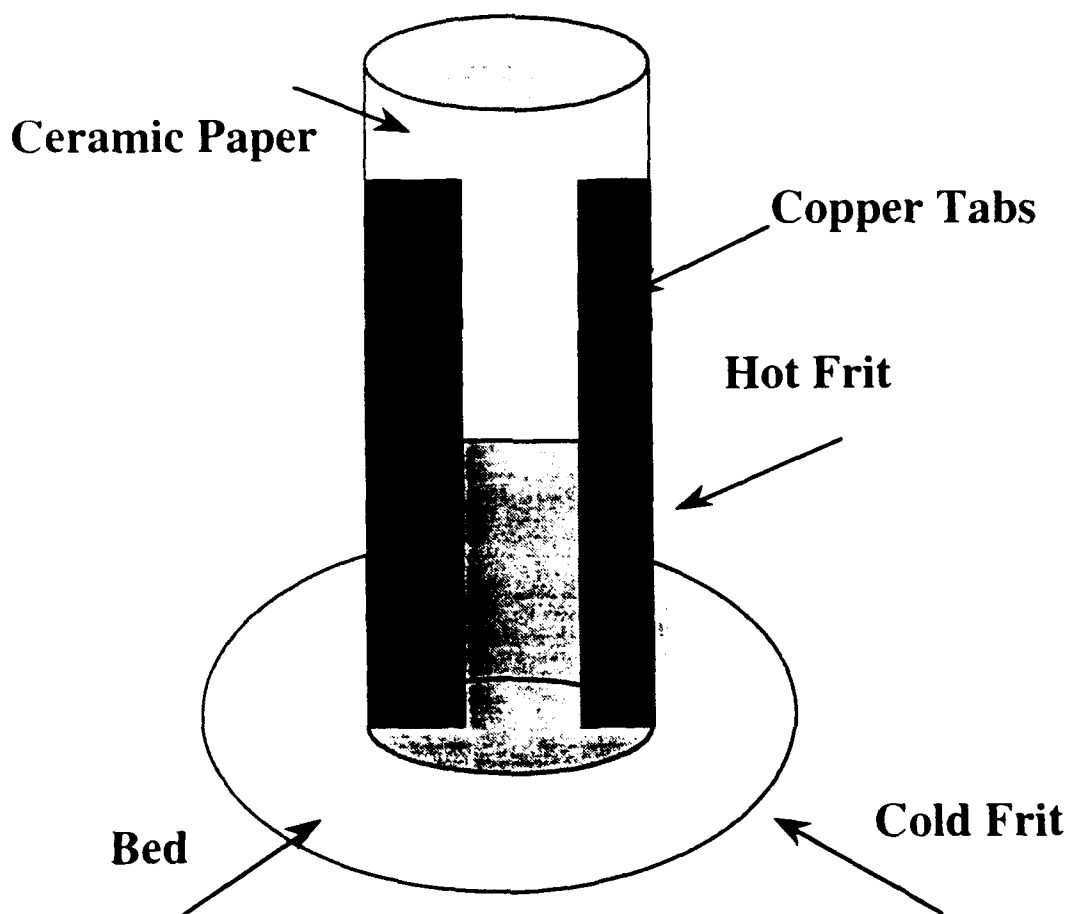
The overall conclusion for this experiment was that the current was getting into the bed properly, but the bed was not behaving properly. A coating would have to be found to take care of the hot spot problem. Also the chill down tank would have to perform better in order to reach the desired ϕ 's.

B.2 7 Screen with Paper Insulator Tests (July 92)

As mentioned in Appendix A, a possible solution to the hot spot problem was to copper electroplate the edges and use ceramic paper as an insulating material. Two screens of 101.16 cm and 99.06 cm in length were rolled and connected in parallel at the electrodes. An issue in assembly was the final covering of paper between the bed and cold frit. The cold frit slid over the bed when the plasma sprayed insulator coating was applied. The paper crinkled

as the cold frit was placed over the bed. This problem was solved by filing the cold frit edge to make it a little rounded, and off-setting the paper by 2.54 cm over the edge, so when the cold frit was placed over the bed the paper would slide a little bit to completely cover the bed and would not crinkle. There also was some difficulty in insulating the hot frit. A thin piece of ceramic paper was wrapped around the hot frit, to prevent shorting (did not want current to flow directly from the electrodes to the hot frit see Figure B.2.1).

Figure B.2.1 Hot Frit Insulation



The ohmmeter readings revealed that no shorts were occurring before the electrode blocks were clamped on to the screen. However, when the electrode blocks were clamped over the tabs, the ohmmeter revealed shorts. This problem was solved by putting thicker paper around the hot frit. It was

also decided to insulate the inner vessel lid and the four tie rods for the first time.

The flow pipes (Section 3.3.1) were added to the inlet manifold. These pipes provided better flow through the bed and were thoroughly tested.

The bed was then fully assembled and was ready for testing. Nitrogen was decided as the working fluid for the first test. The gas was turned on and a leak was detected at the outlet end (pressure relief valve). The system pressure was below 1020 kPa, so a better seal was added at this end and the leak stopped.

The thermocouples were arranged in the same configuration as Figure B.1.1 (The 8th data channel was used for the flowmeter reading). The thermocouple readings for the N₂ gas through the chill down tank revealed that the inlet gas was ~ -120 - -130 °C. In order to lower this gas temperature, it was decided to use a higher heat capacity gas such as He or chill down the apparatus with LN₂ directly (through the inlet to the bed). Since He gas was not readily available, it was decided to use the LN₂ idea.

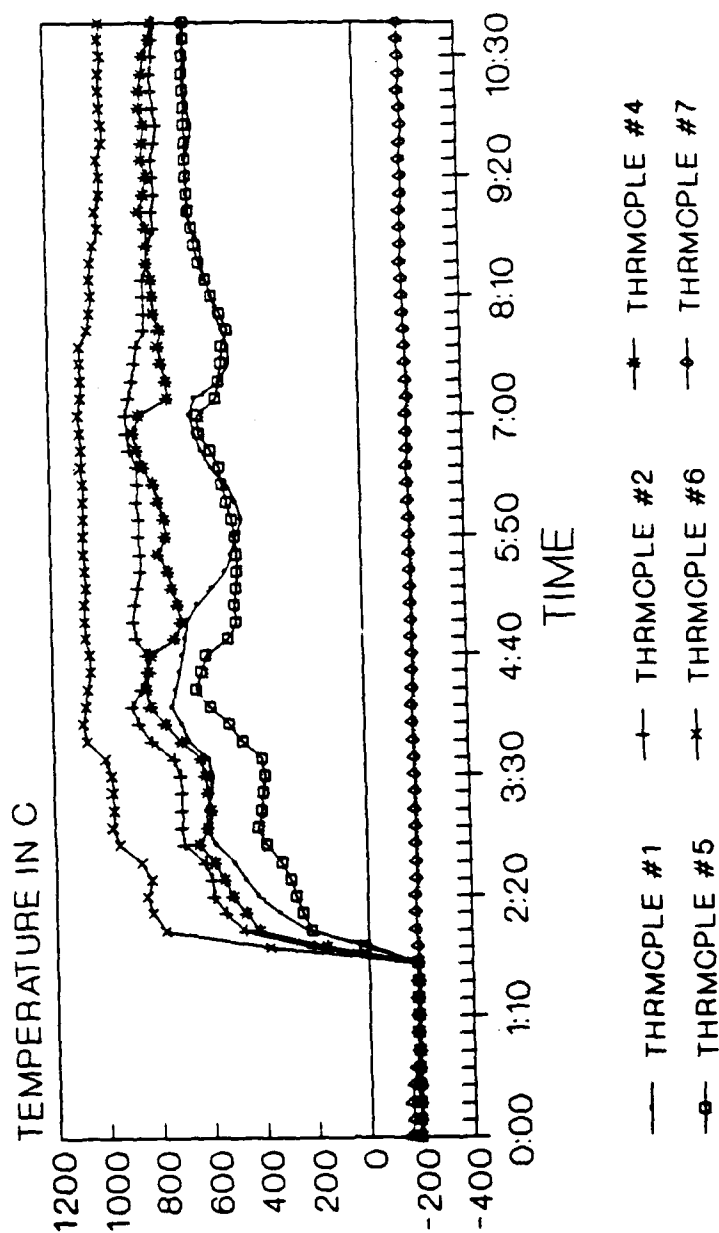
Figures B.2.2 - B.2.8 show the results of the tests conducted. A brief discussion of each test follows.

In Test #1, the thermocouples showed that the pre LN₂ chill down into the apparatus cooled the inlet temperature down to LN₂ temperatures. The gas through the refrigerator was able to hold at this temperature for the entire run (Thermocouple #7). The gas flow for the run was ~ 225 lpm at 408 kPa (bed inlet before the cold frit). Power was added up to 2.0 V at 128 amps. The results from Figure B.2.2 show that the thermocouples responded with the power increase and no strange anomalies were observed, except that thermocouple #3 stayed negative with #7 throughout the experiment (-180°C).

SCREENED TEST #1

SS SCREEN & PAPER INSULATOR

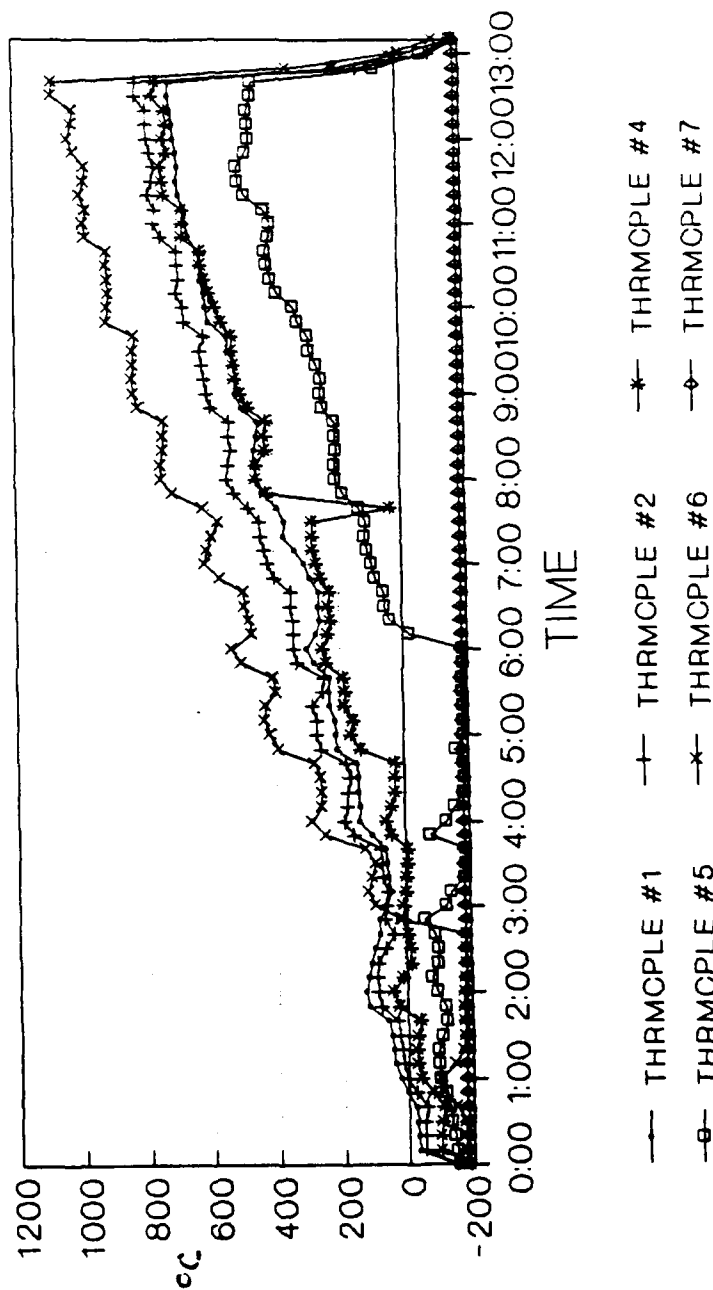
Figure B.2.2 Test #1 (Time in Minutes - Min:Sec)



GAS: N2 PRESSURE: 60 psi FLOW: 225 lpm

SCREEN BED TEST #2

SS SCREEN & PAPER INSULATOR

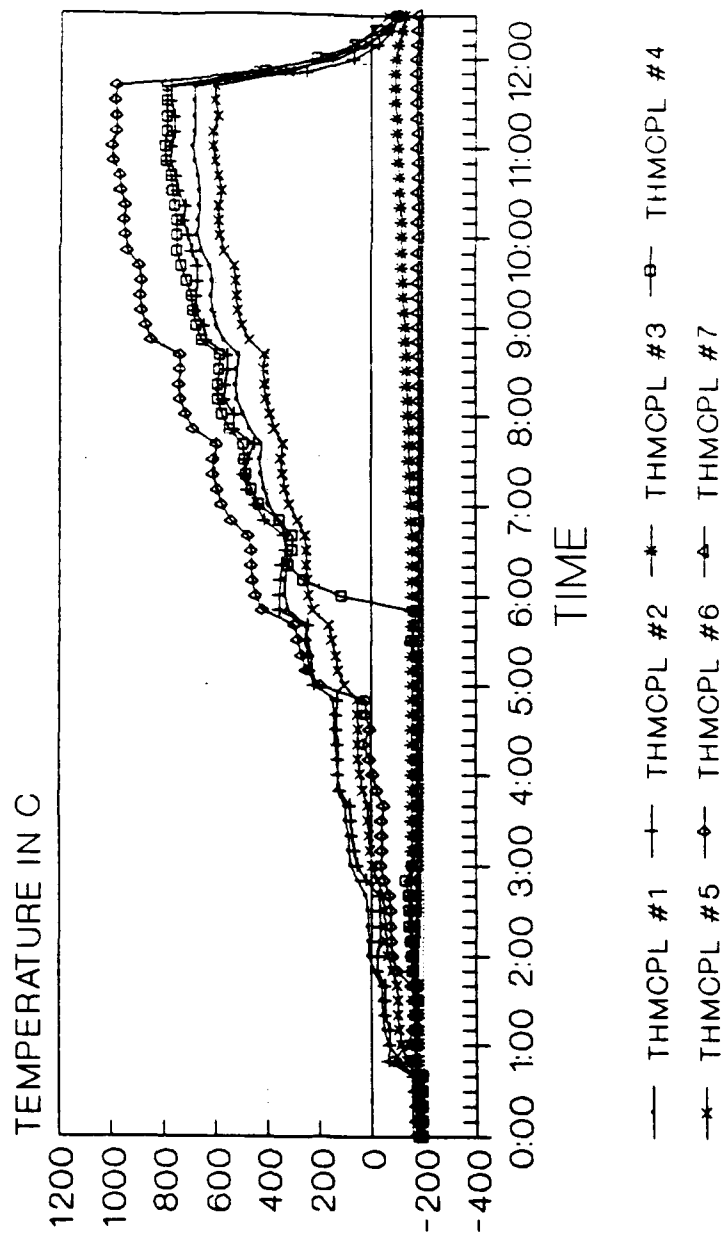


GAS: N PRESSURE: 50 psi FLOW: 225 lpm

Figure B.2.3 Test #2

SCREENBED TEST #3

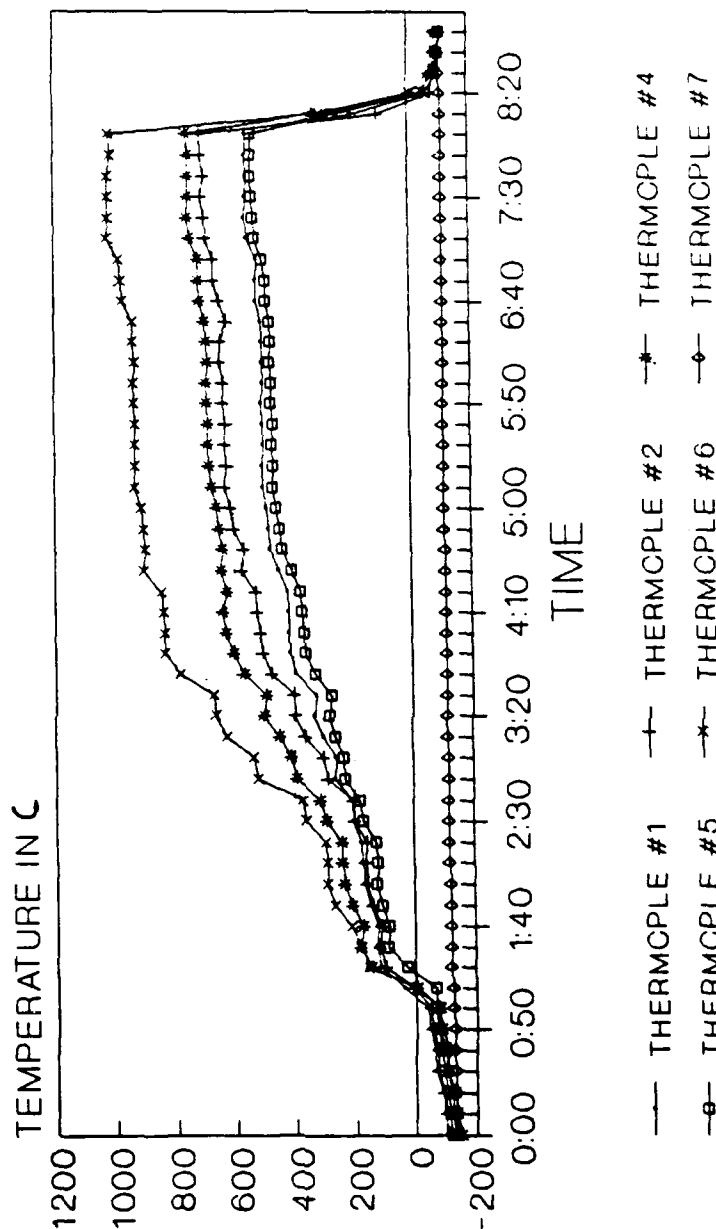
SS SCREEN & PAPER INSULATOR



GAS: N2 PRESSURE: 60 psi FLOW: 150 lpm

SCREENED TEST #4

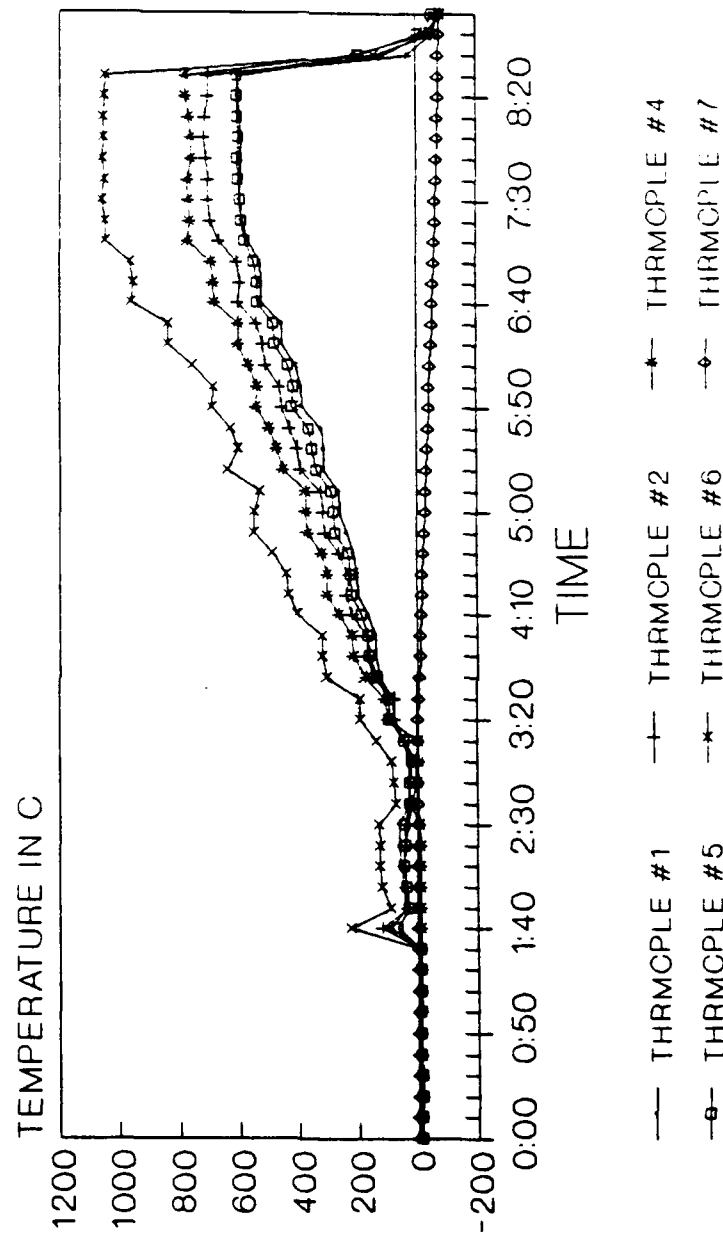
SS SCREEN & PAPER INSULATOR



GAS: He PRESSURE: 140 psi FLOW: 730 lpm

SCREENBED TEST #5

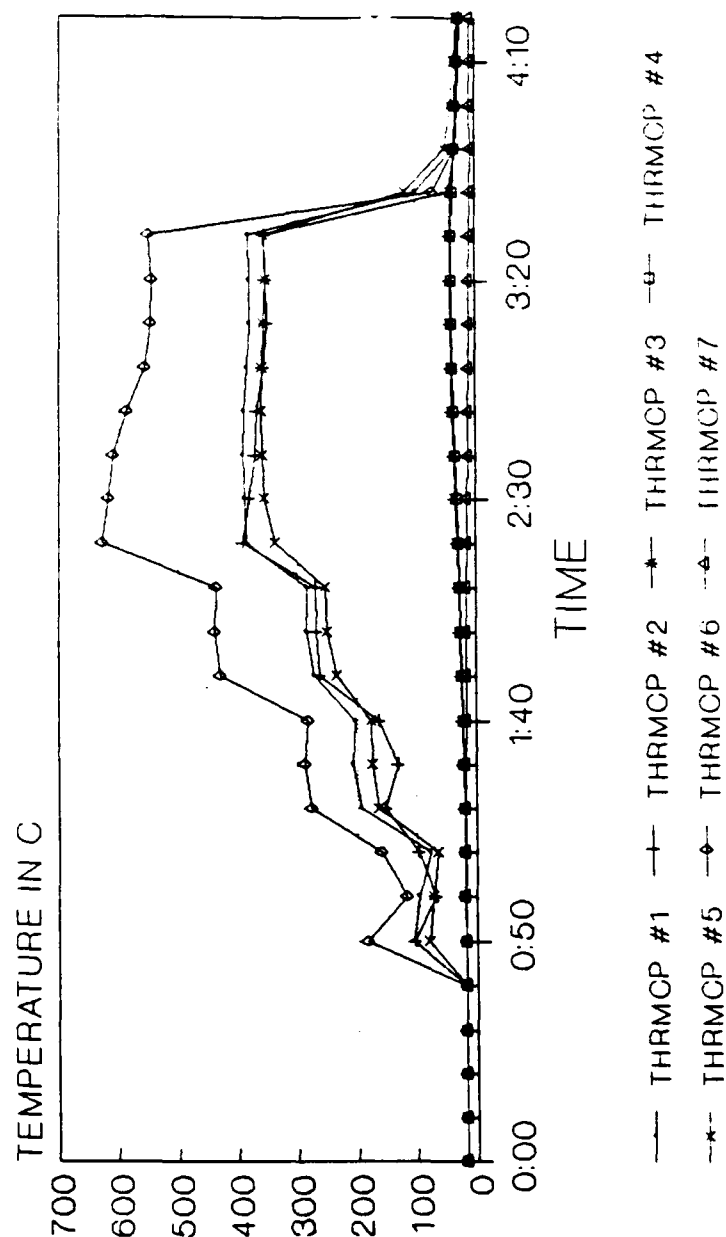
SS SCREEN & PAPER INSULATOR



GAS: He PRESSURE: 140 psi FLOW: 765 lpm

SCREENBED TEST #6

SS SCREEN & PAPER INSULATOR

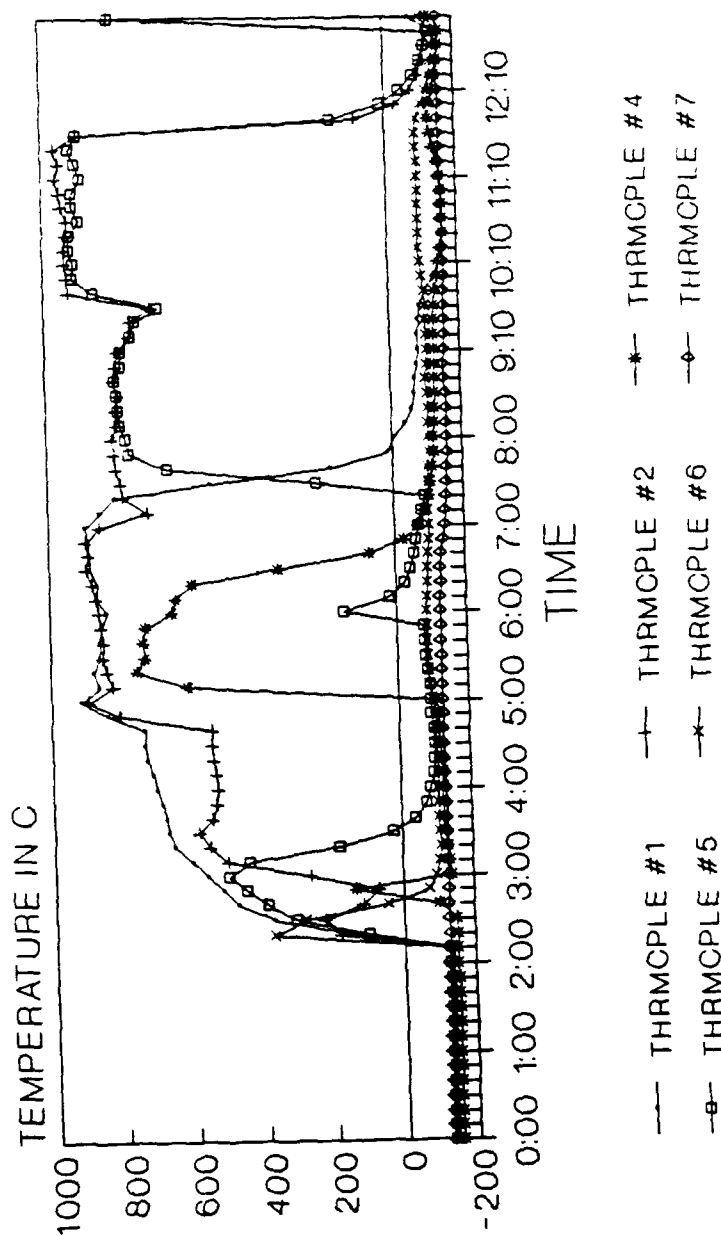


GAS: He PRESSURE: 40 psi FLOW: 400 lpm

Figure B.2.7 Test #6

SCREENED TEST #7

SS SCREEN & PAPER INSULATOR



GAS: AIR PRESSURE: 50 PSI FLOW: 250 lpm

Two conclusions were reached for the bad thermocouple #3 reading, the thermocouple was bad (even though it was pre inspected) or that a non-uniform flow distribution and bad heating in the bed was allowing the region to stay at the inlet temperature.

It was decided to conduct two more tests at approximately the same conditions. Pressure stayed the same while the flow rate was the same for the first test and a little lower for the second test. Power was increased from 0.2 V at 10 amps to 1.85 V at 115 amps in pretty much equal increments for both tests. In Test #2 (Figure B.2.3), thermocouple #3 remained near #7 through out the entire test. Thermocouple #4 remained low at the start and then started to increase half way through the test. In Test #3 (Figure B.2.4), the same results occurred (Even though most of the other charts do not show #3, Figure B.2.4 shows the temperature for thermocouple #3. The temperature profile looked the same for all of the tests performed in this paper insulator test campaign. It was not included on the charts since it was believed it was a bad thermocouple at the time). An interesting observation observed in these two tests was that #4 started out cool and then gradually warmed up half way through the run. It was deduced that the cause of this was that LN₂ was trapped inside of the bed and it took awhile for the bed to warm up the gas and release it through the system. The same reasoning was applied to thermocouple #3, but it never warmed up (Thermocouple #3 was mis-marked, and at the time it was believed that #3 was located at the bottom of the rig which made it easier to believe that LN₂ was trapped there).

The above conclusions lead to Test #4 and Test #5. In Test #4 , He was replaced as the working fluid in order to give a higher heat capacity. The flow rate was also increased in hopes of blowing out any LN₂ if that was the cause. Power was added in increments up to 3 V at 190 amps. The results,

shown in Figure B.2.5 , were that #4 responded as it should have, but that #3 remained near #7 through out the test. In Test #5, it was decided to start at a warmer inlet temperature to insure that LN₂ was not the cause for the low reading in #3. The flow rate was pretty much the same for Test #4. The inlet temperature stayed around -3 °C for the test. The reason that it was not higher was that the chill down tank still had LN₂ in it and the gas still had to pass through the chill down tank in order to enter the bed. Power was added in equal increments up to 1.9 V at 191 amps. The results from Figure B.2.6 were that all the thermocouples responded to power except that #3 stayed at inlet conditions again.

For Test #6, the chill down tank was left over night so that most of the LN₂ would evaporate over night (high ambient temperatures at the time of the test ~ 30 °C). The He gas then could enter into the bed at room temperature. He flow was set at 400 lpm at 272 kPa. Only 1 V and 70 amps of power were added. The test revealed (Figure B.2.7) that there was not a LN₂ problem, but a flow problem. The results showed that #3 and #4 remained at inlet conditions with #7 through out the entire run. It was deduced that these regions were getting more gas or that shorts in the bed had caused these regions to get no heating at all.

For Test #7, it was decided to use air as the working fluid. Air was chosen to try to see if oxidation in the bed could color different regions of the screen to determine the heat profile in the bed. The power was added up to 70 amps at ~ 1 V. The thermocouple readings (Fig B.2.8) were all over the place. The only conclusions reached from this test was that the bed either had major shorts in it (but current continued to flow) or the thermocouples were not reading correctly.

The bed was disassembled. The screen was inspected and no shorts were discovered. The paper had turned brownish in color, but the screen looked like it had even heating during the experiments. No hot spots were found on the edges which showed that the copper electroplating had performed well. All of the thermocouples were individually tested and revealed that they were O.K. Therefore, no obvious problems were shown in visual inspection after assembly.

An energy balance calculation was performed for one of the runs. An average bed temperature was used as the outlet temperature. Since

$$Q = \dot{m} c_p \Delta T \quad [B-1]$$

and for Test #4 at time = 4:10 $T_1 = 620$ K, $T_2 = 720$ K, $T_3 = 123$ K, $T_4 = 820$ K, $T_5 = 480$ K, $T_6 = 1020$ K, therefore $T_{ave} = T_{exit} = 630.5$ K and $T_7 = T_{inlet} = 120$ K
 $\dot{m} = 730 \text{ lpm} \cdot 4 \text{ g/mole} / (22.4 \text{ l/mole} \cdot 60 \text{ sec/min} \cdot 1000 \text{ kg/g}) = 0.00217$ kg/sec.

$c_p = 5.193$ kJ/kg K, therefore, $Q = 5.75$ kW. At this time the console read that the power supplied to the bed was 570 W. This showed that the energy balance was off by a factor of ~10. There should be a slight difference since the thermocouples touched the bed (not the gas temperature), but not an order of magnitude.

The following conclusions were reached with this series of experiments. A single screen should be wrapped in future experiments since it looked like high temperatures were being reached with two wraps and it will ease logistics and cause less problems. The paper insulator caused the bed to be too porous (~.60) causing the gas to not get heated to the desired temperatures and may have caused thermocouple #3 and #4 to read low in some parts of the tests. Another thermocouple was needed at the outlet to get a feeling for the mixed mean outlet temperature of the bed for energy balance calculations.

Thermocouple readings could be suspect due to the huge energy balance error, meaning that they could be picking up currents affecting the readings. Therefore, this bed was ineffective and other ways of insulating the bed had to be tried. None of the results could be used for analysis regarding flow stability.

B.3 4 Oxidized Screen Tests (Aug 92)

Another series of experiments were conducted using an oxidized stainless steel screen coated with plasma sprayed alumina (Appendix A.2.6). The thermocouples were rearranged into the configuration shown in Figure 3.5.1.1 with number eight representing the mixed mean outlet. More ceramic paper and ceramic cloth were added at the ends of the bed in order to try to get better sealing. The screen was spot welded completely around the edges of the entire screen in hopes that this might help the sharp edge problem. It really did not help and wires had to be cut off as in previous screens.

The bed was assembled after in-situ oxidation with a starting resistance of $0.16\ \Omega$. As more parts were added the resistance dropped to 0.11 and to $0.07\ \Omega$ (measuring at the leads). This was a frustrating phenomena since the bed was assembled, the loss of alumina coating should be minimal (occasionally the bed was moved as the element was assembled to the manifold and the electrodes). It was decided to continue with full assembly and try to perform an in-situ oxidation on the first test in the full assembly.

There were some problems in final assembly. One problem was connecting the inlet pipe for the gas flow to the vessel. Assembly over a period of time had stripped the threads for the pipes. A metal paste was applied that allowed the bolts to tighten to the pipe. It was also noticed that the chill down

refrigerator took a long time to fill up. It was thought this was due to the high ambient temperature (long distance from dewar to refrigerator) of 30 °C. It than was deduced that the dewar only was half filled with LN₂ from the vendor and was sent back for refilling.

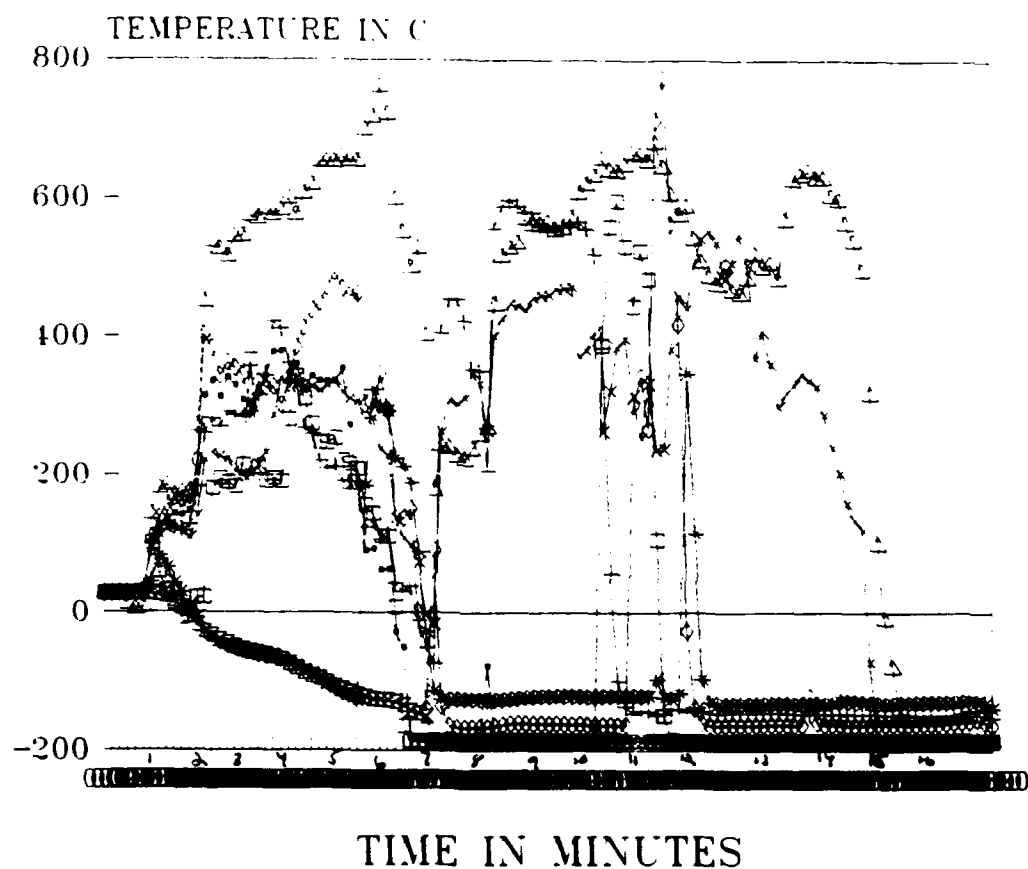
Once these problems were fixed, the in-situ oxidation test was started. Air was the working fluid set at 350 lpm. The power was set initially at 3 V and registered 19 amps. As seen from Figure B.3.1, the thermocouple readings were very sporadic. This test started to confirm that the thermocouples were not reading correctly, especially #7 which showed that the cold frit temperature was the highest for some periods. The power was decreased to 1.5 V at 15 amps after the first two minutes and then was increased to 2 V at 12 amps for 5 minutes. The thermocouple readings still were sporadic, only #5 and #7 showed that any heat was being produced in the bed. It was determined that this still may be a flow problem so it was decided to conduct a test with no flow, just bed heating.

The same bed was left in the assembly. When the flow meter showed no flow was left in the system the power was started at 2 V at 12 amps. The power was left at this setting for 15 minutes (see Figure B.3.2). The next power setting increased to 3 V at 19 amps for 4 minutes and then to 4 V at 27 amps for 3 minutes. At the 3 minute mark for this setting, a huge surge in all of the thermocouples occurred. The power was immediately turned off.

Figure B.3.1 Test #8 (Oxidized Test #1)

SCREENBED TEST = 8

OXIDIZED SS SCREEN & AL2O3 COATING



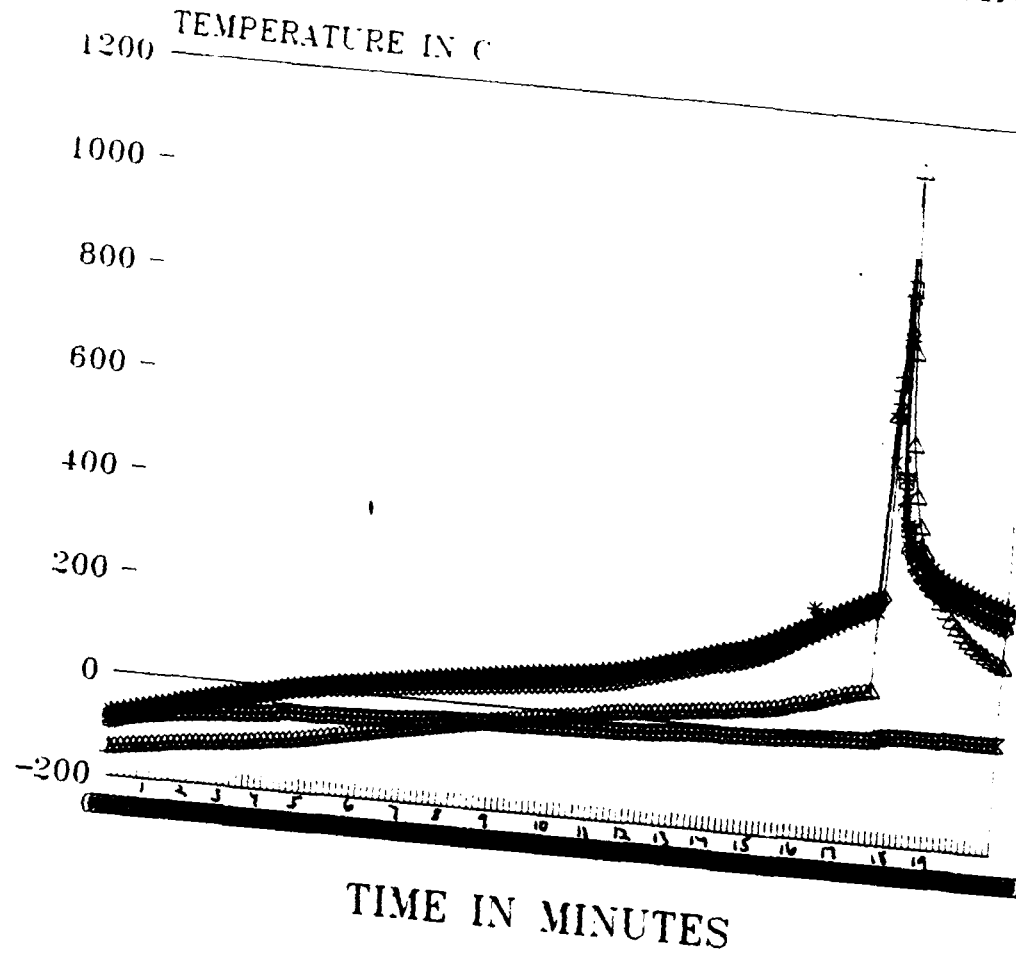
—●— TMCP #1 ——— TMCP #2 —+— TMCP #3 —□— TMCP #4
—■— TMCP #5 —+— TMCP #6 —△— TMCP #7 —○— TMCP #8

GAS: AIR FLOW: 350 LPM POWER:
3V, 1.5V, 2V
IN-SITU OXIDATION OF BED

Figure E.3.2 Test #9

SCREENBED TEST = 9

OXIDIZED SS SCREEN & AL2O3 COATING

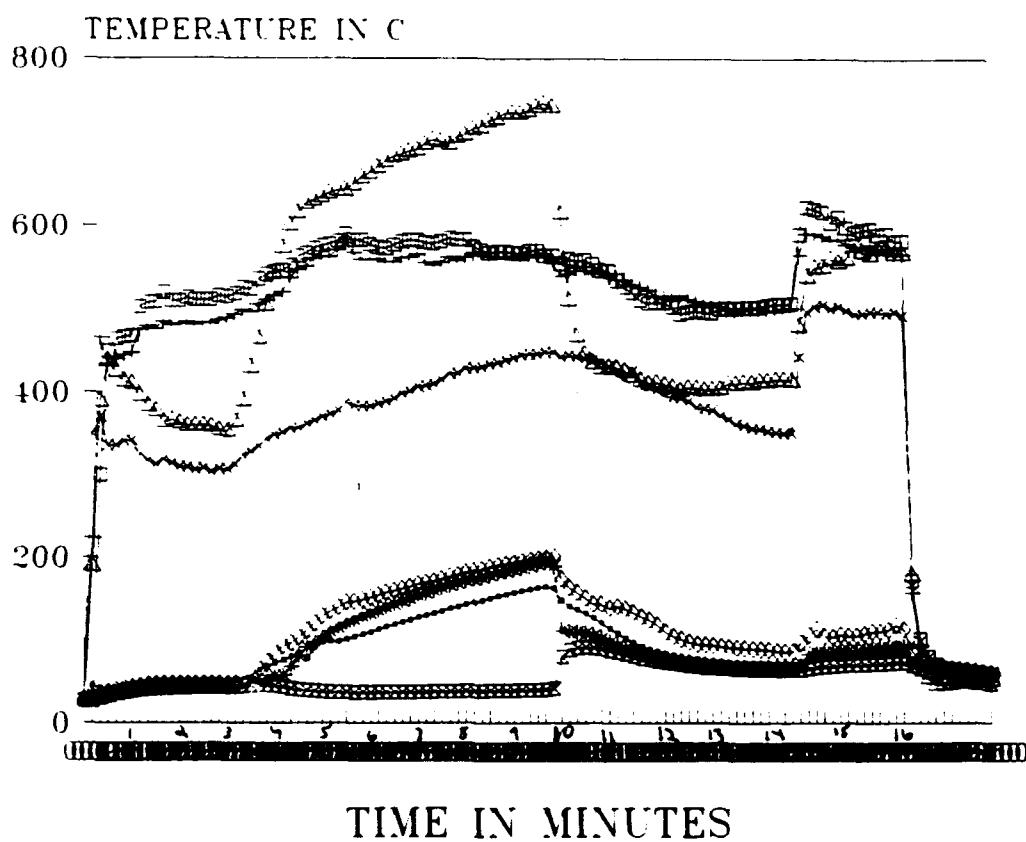


NO GAS ELECTRIC HEATING 2V,3V,4V
(12-27 AMPS)

Figure B.3.3 Test #10

SCREENBED TEST = 10

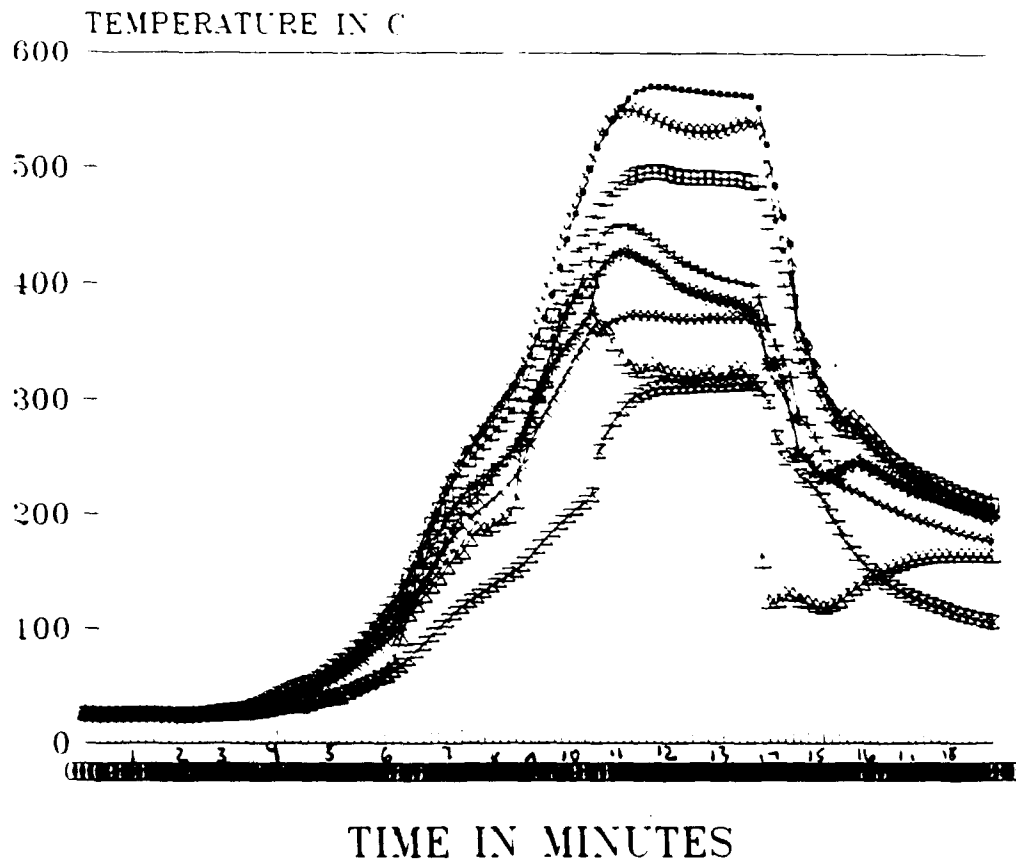
SAME SCREEN AS =8 & =9



WARM GAS TEST WITH HE AT 500 lpm
POWER AT 26 amps 1-15 min (2-2.5V)
38 amps 16-17 min; No Flow 5-8 min

Figure B.3.4 Test #11

SCREENBED TEST = 11 REOXIDIZED SS SCREEN & AL₂O₃ COATING



—●— TMC #1	— TMC #2	—+— TMC #3	—□— TMC #4
—*— TMC #5	—x— TMC #6	—△— TMC #7	—○— TMC #8

GAS:HE PRESSURE:60 psi FLOW:143-286 lpm
TIME-POWER 0-5, 1-15, 2-26, 3-41,
4--6-72, 7--12-133 AMPS(1-8V)FLW 2* 7MIN

The bed thermocouples read very evenly. Thermocouple #7 read low and then started to increase (read the highest at the spike). It was concluded that a short in the bed may have caused a spike. However, a run had not yet been done using He so a third test was planned for using He with a room temperature inlet to check the bed heating and gas flow.

Figure B.3.3 showed the results of the He test with a room temperature inlet. Since the refrigerator was already filled, it was decided to take two 1A bottles connected in series and connect them directly to the bed inlet. The flow rate from the bottles was 500 lpm. Power was applied for the first 15 min at 2.0 V (26 amps), and 2.5 V (38 amps) for 10 minutes. The gas flow was turned off for the last 8 minutes with the power at 2.5 V. It was decided to disassemble this bed since it had serious problems. The thermocouple #7 reading did not make sense, which lead to believe that the bed had shorts or thermocouple problems. Figure B.3.3 also showed that thermocouple #8 barely raised above room temperature which lead to the conclusion that most of the gas was bypassing the bed, was not being heated in the bed, or the thermocouple readings were wrong.

Disassembly of the bed revealed no obvious shorts. The serious flow problems discussed in section A.4 were discovered and solutions were found. The screen looked in good condition and it was decided to re-oxidize it again at 60 V at 230 amps for another 6 hours (using the big power supply) outside of the bed. The bed resistance was at 0.21 Ω after oxidation.

The screen was then rolled again and put into the assembly. The resistance dropped to 0.13 Ω . It was decided to try in-situ oxidation again at 8 V (50 amps) for 3 hours. The resistance measured at the electrodes increased to 0.16 Ω . As assembly continued, the resistance again dropped to 0.07 Ω to 0.05 Ω (measured at the electrodes). It was deduced that the thermocouples were

causing the reading and were not properly insulated. In order to insure that the thermocouples were isolated, they would each have to be individually isolated as they slid into the apparatus from the aft end. (as discussed and shown in Appendix A.5). Instead of disassembling the apparatus, it was decided to perform a run with none of the thermocouples touching the hot frit or cold frit. Figure B.3.4 showed the results of this experiment. He gas was entered into the bed at a flow rate between 143 - 286 lpm using the 1 A cylinders directly connected to the bed inlet again. The power was added in the following increments: Time = 0 -1 minute, 1 V at 5 amps, ; 1-2 minutes, 2 V at 15 amps; 3-4 minutes, 3 V at 41 amps; 4-6 minutes 4 V-6 V at 72 amps; 7-12 minutes, 8 V at 133 amps. At time equals seven minutes, the flow was doubled to 286 lpm. The results were confusing. The bed temperatures behaved relatively uniformly in the beginning, but half way through the test when power and flow were increased, there became a bigger spread. Thermocouple #7 continued to read higher than #8, which did not make sense. Disassembly of the bed revealed that Thermocouple #7 was still touching the bed and therefore was probably still carrying current. There were no shorts or hot spots found in the bed.

The conclusions from this campaign of experiments was that there still were two major issues: (1) insuring that the thermocouples were not carrying spurious currents ; (2) and finding a coating that could stand up to assembly. The results of these experiments shed no new light on the flow stability issue.

APPENDIX C

SUPPORT EXPERIMENTS

C.1 POROSITY

The porosity of the screen bed is a key parameter. As seen from previous analyses in Chapter 1, the more porous the bed, the stability curve shifts upwards and to the left, increasing the stable flow region. In order to have a screen bed prototypic of a real PBR, it is best to have the porosity between 0.35 to 0.40. Therefore, porosity tests and calculations for the screen bed are performed.

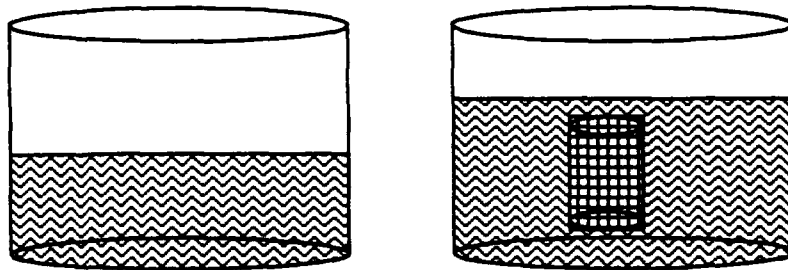
The wire mesh ordered from Newark Wire Inc. said that the mesh count per inch was 30 with a 0.330 mm diameter wire and a 0.52 mm opening for an open area of 37.1 %. However, since the screen was wrapped and the wires could overlap each other, porosity tests still had to be performed.

The Physics of Flow Through Porous Media [S-2] describes several methods for porosity experiments. Some of these methods include optical, volume displacement, microscopic examination, gas expansion, and measurement. Since sophisticated instruments are not available, measurement and volume displacement are the best ways to determine the screen bed porosity. It is also important to determine the porosity of the frits to help characterize the pressure drop and fluid flow through the entire bed.

The first method tried was volume displacement and measurement. A full length uncoated screen (~233 cm) was wrapped and then tied with a small s.s wire to make it easier for measurement. The mass of the screen was measured to be 456.10 grams using a Mettler PN 2210 Scale. The screen was then placed in a graduated beaker of water (see Figure C.1.1).

Figure C.1.1 Volume Displacement With Water

Volume Change = 60 cc's



According to *The Physics of Flow Through Porous Media* [S-2], the porosity of a media can be determined by :

$$P = 1 - \frac{\rho_B}{\rho_G} \quad [C-1]$$

where P is the porosity, ρ_B is the measured density, and ρ_G is the known density of the material.

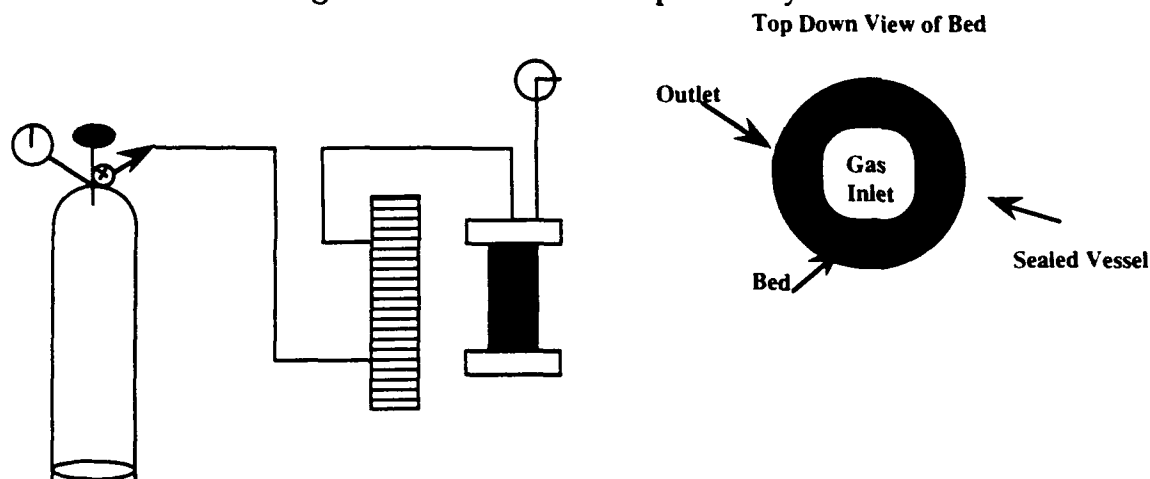
The density of 316 s.s is 8.0272 g/cm^3 . The measured density is $456.10 \text{ g}/60 \text{ cc} = 7.6 \text{ g/cc}$. These numbers gave a porosity of 0.05, which is not realistic since the screen is not coated and visual inspection (looking at the holes) determined that the porosity should be around 0.50. It is believed that the error came in the water displacement method, due to the water could not get through the completely wrapped screen, or the water measurement is inaccurate (should have had a higher volume). Therefore, another porosity measurement method is needed.

Since the screen when rolled represents a packed bed of particles, the Ergun pressure drop relation is a means to determine the porosity of the bed. The Ergun relation is :

$$\frac{\Delta P}{L} = 150 \frac{(1-\epsilon)^2}{\epsilon^3} \mu \frac{U_M}{D_p^2} + 1.75 \frac{(1-\epsilon) U_M G}{\epsilon^3 D_p} \quad [C-2]$$

where ϵ is the porosity, D_p the particle diameter, μ the viscosity, U_M the superficial velocity and G the mass flow rate per unit total area [M-1]. An apparatus is set up to determine these variables (see Figure C.1.2).

Figure C.1.2 Pressure Drop Porosity Test



Nitrogen gas flows from a 1A cylinder through a rotometer into a sealed vessel. The sealed vessel contains an inlet hose, a rolled screen bed, and an outlet hose connected to a gauge. The results of this test is as follows:

P_{inlet} (at 1A gauge) = 112.24 kPa Diameter of the particle = .000381 m

P_{outlet} (at bed gauge) = 102.04 kPa $L = .03$ m

$\dot{m} = 113$ lpm = 0.0011 kg/sec per unit area = 0.0624 kg/m² s

$\mu = 1.8 \text{ E-}5$ kg/ms $U_M = (\dot{m}/1.1224)/A = 0.089$ m/s

Using these numbers in C-2, gives a porosity (ϵ) of 0.15262. In order to get a porosity of 0.4 the ΔP has to equal 286 Pa.

There were also some issues with this test. The gauges were in 1 psig increments from 1 psig up to 20 psig. Therefore, it is not known if the gauge readings were really accurate. The rotometer was in SCFM from 1 to 10 in increments of 1, so it could also be inaccurate. Another factor is that the

Ergun correlation may not be the best correlation for the screen bed. With these uncertainties, it was decided to find another method to determine the porosity.

It was determined that the best way to determine the porosity, was to find an accurate volume. An uncoated screen was inspected. The number of wires counted determined that there were 40 wires per inch of screen. Since the wires overlap each other, one of the wires was pulled out and measured to determine the real length of the wire. The measured length determined that the real length of the wire differed by a factor of .25 from the length of the wire woven in the screen. Therefore, since the screen was 4 inches wide by 92 inches long, the following calculations reveal:

$$W = 4 \text{ in.} * 0.25 = 5 \text{ in.}$$

$$92 \text{ in} * 40 = 3680 \text{ wires, } 5 \text{ in. long}$$

$$L = 92 \text{ in.} * .25 = 115 \text{ in.}$$

$$4 \text{ in.} * 40 = 160 \text{ wires, } 115 \text{ in. long}$$

since,

$$V = \pi r^2 h$$

for W:

$$\text{since diameter of wire} = 0.13 \text{ in } r = 0.13/2 = .065 \text{ in} = 0.1651 \text{ cm}$$

$$V = 3.14 * .00027258 * 12.7 * 3680 = 40 \text{ cc's}$$

for L:

$$V = 3.14 * .00027258 * 292.1 * 160 = 40 \text{ cc's}$$

thus, the total volume occupied by the screen =

$$80 \text{ cc's}$$

Now, assume the screen is perfectly rolled into the open volume between the cold frit and hot frit (it is a very tight fit, with a little void on the first wrap with the hot frit). Therefore, the total bed volume is:

$$r^2 = \frac{(\text{Cold Frit Inner Diameter})^2 - (\text{Hot Frit Outer Diameter})^2}{4}$$

$$= (36 - 14.44)/4 = 5.39 \text{ cm}^2$$

$$V = 5.39 * \pi * 10 = 169.33 \text{ cm}^3$$

Taking the screen bed volume divided by the total bed volume :

$$P = 1 - \text{Screen Volume} / \text{Bed Volume} = 0.528$$

This number made much more sense (again by visual inspection of the screen) and the method was tried for the coated screen.

W= 3680 wires, 12.7 cm long

For three wire diameters (even though measurements of the screen revealed that a 0.005 cm coating was applied to the screen)

$$d = .0155 \text{ in} = 0.03937 \text{ cm} \quad r = .019685 \text{ cm}$$

$$d = .015 \text{ in} = 0.0381 \text{ cm} \quad r = .01905 \text{ cm}$$

$$d = .0145 \text{ in} = 0.03683 \text{ cm} \quad r = .018415 \text{ cm}$$

$$V = \pi (.019685)^2 * 12.7 * 3680 = 56.89 \text{ cm}^3$$

$$V = \pi (.01905)^2 * 12.7 * 3680 = 53.2833 \text{ cm}^3$$

$$V = \pi (.018415)^2 * 12.7 * 3680 = 49.79 \text{ cm}^3$$

L = 160 wires, 292.1 cm long

$$V = \pi (.019685)^2 * 292.1 * 160 = 56.89 \text{ cm}^3$$

$$V = \pi (.01905)^2 * 292.1 * 160 = 53.2833 \text{ cm}^3$$

$$V = \pi (.018415)^2 * 292.1 * 160 = 49.79 \text{ cm}^3$$

Thus, the $P = 1 - \text{Screen Volume} / \text{Bed Volume} =$

$$1 - 113.78 / 169.33 = 0.328$$

$$1 - 106.5667 / 169.33 = 0.371$$

$$1 - 99.58 / 169.33 = 0.412$$

These porosities made sense, and were a little conservative since it assumed the bed occupied all of the volume in between the frits. Since the coated wire

diameter was measured to be 0.0381 cm, a porosity between 0.37 and 0.40 was a very good assumption for the painted alumina experiments (takes into account the little voidage that occurs on the first wrap).

The porosity of the frits was determined by volume displacement and measurement. It was thought that volume displacement would be more effective since the frits were of much smaller thickness. The volume of the cold frit using water displacement equaled 30 c.c.'s. The measured volume using two methods equaled :

$$V1=2\pi rlh$$

where r is the annulus radius, l the length, and h the thickness.

$$V2= \pi R^2h - \pi r^2h$$

where R equals the cold frit outer diameter and r equals the inner diameter.

$$V1 = 29.688 \text{ cc's} \quad V2=28.981\text{cc's}$$

The mass of the cold frit was 167.85 g. Using equation C-1, the porosities for these three volumes equal:

$$P = 1 - \frac{\rho_B}{\rho_G}$$

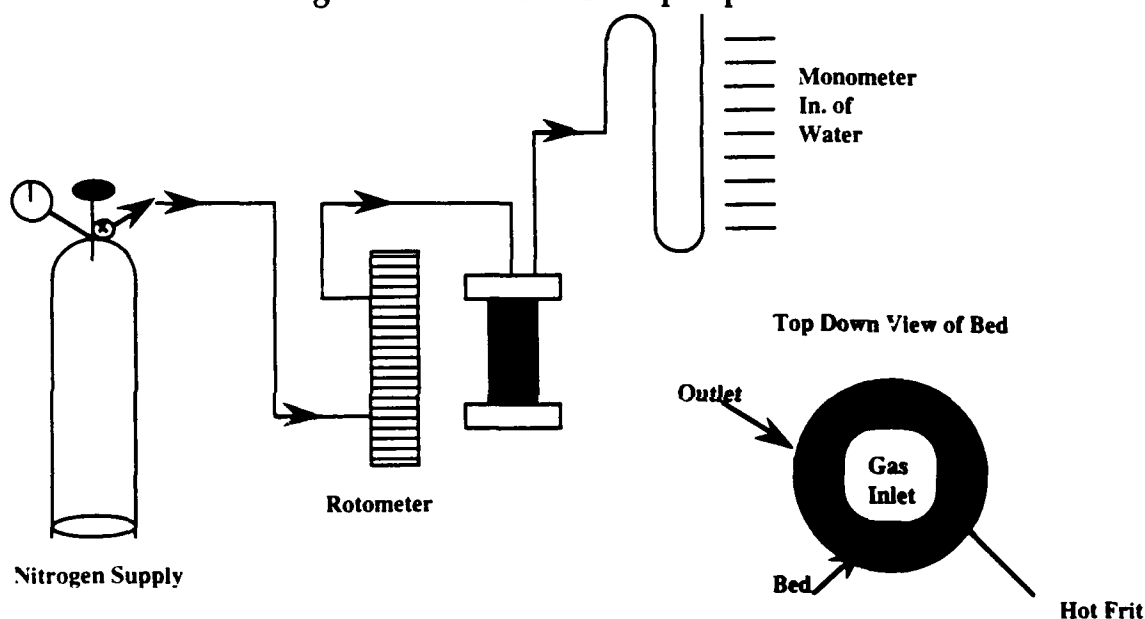
where the measured density = 5.595 g/cc , 5.654 g/cc, and 5.79 g/cc; the density of 314 s.s. = 8.00 g/cc; thus P = 0.30, 0.29, and 0.28.

The porosity of the hot frit should be the same since they were both made of 314 s.s with 20 μm sintered holes.

C.2 PRESSURE DROP

Since a pressure transducer could not be placed inside the bed, pressure drop experiments are performed to determine the pressure drop behavior of the bed. This test is important to determine if the bed behaves similar to the Ergun type pressure drop correlation, especially for modeling purposes. Figure C.2.1 shows the apparatus assembled for these pressure drop tests.

Figure C.2.1 Pressure Drop Experiments



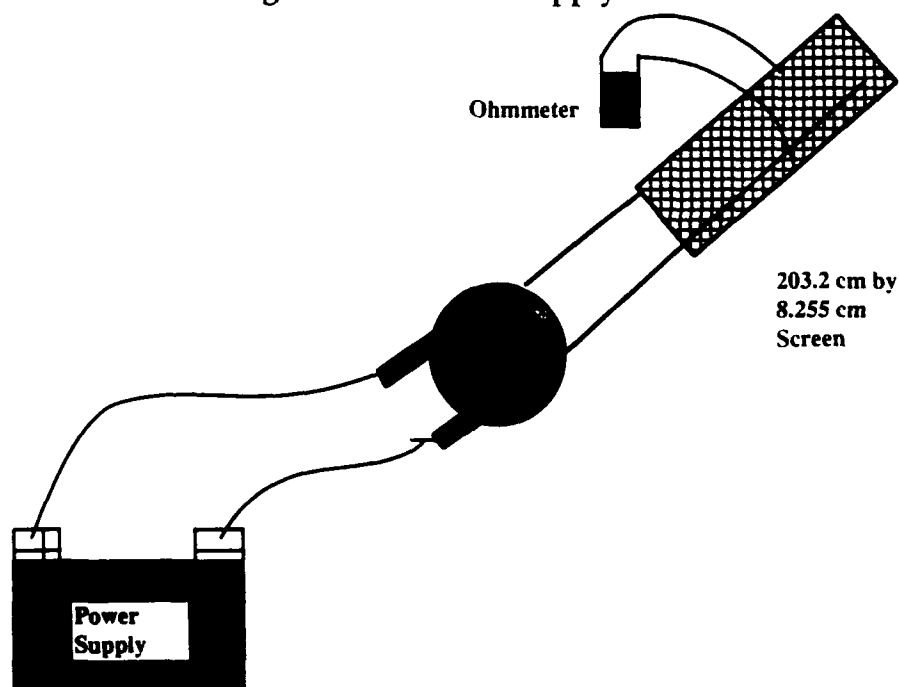
The readings for the apparatus were as follows: 4 psig at the gauge, 70.8 lpm at the rotometer, and 36 in. of water displacement which equals 1.3 psi. This apparatus represented flow through one frit (backwards) and most of the bed. There could have been uncertainties in these readings due to the accuracy of the equipment (similar arguments to Section C.1). A full scale pressure drop test (e.g. through both frits, and the bed,) was not accomplished due to lack of a vessel that was readily available to seal both frits.

C.3 POWER SUPPLY CORRECTION

Analysis of the experimental results revealed that there was a mismatch between power and temperatures in some parts of the experiments. It was decided to check the power supply readings on the console to insure that the power readings were accurate. Several tests were performed to check this calibration.

The first test performed was to place an ohmmeter (Fluke Digital Portable Voltmeter) on a sample of s.s. screen and compare the readings with the power supply console (see Figure C.3.1).

Figure C.3.1 Power Supply Test #1



The readings for this experiment are shown in Table C.3.1

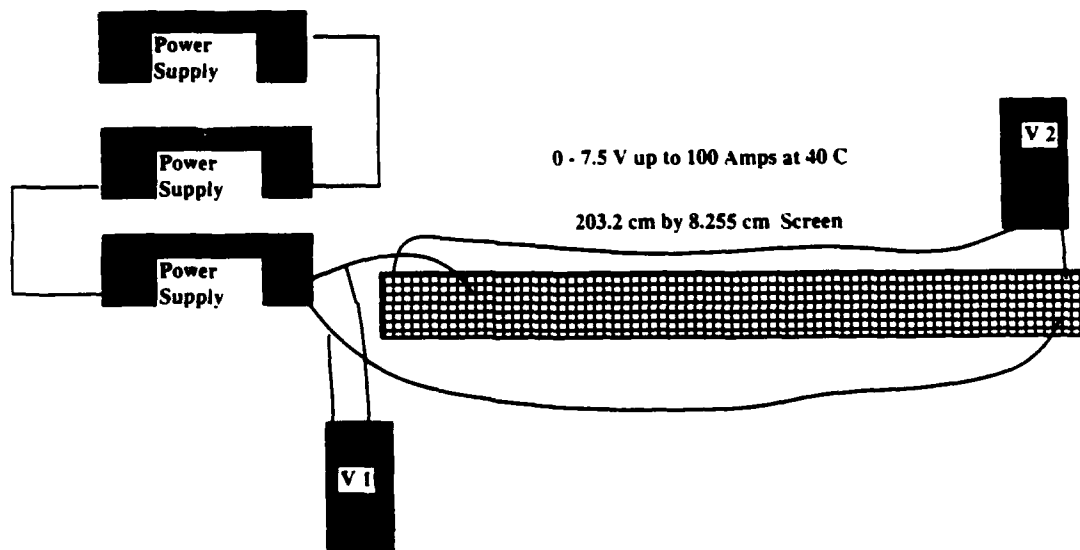
Table C.3.1 Power Readings

Console	Ohmmeter
10 V / 45 Amps	10.03 V
20 V / 80 Amps	20.07 V
30 V / 111 Amps	30.11 V
40 V / 143 Amps	40.1 V
50 V / 176 Amps	50.2 V
60 V / 207 Amps	60.3 V
70 V / 239 Amps	70.3 V

The readings indicated that more power was being supplied to the screen than the power supply was generating !

The next test performed was to check the validity of the ohmmeter readings. Two ohmmeters (both Fluke Digital Portable Voltmeters) were connected to the smaller Lambda power supply as shown in Figure C.3.2.

Figure C.3.2 Ohmmeter Test



The results of this test are shown in Table C.3.2.

Table C.3.2 Ohmmeter Test

V1	V2
2.00 V	1.97 V
4.00 V	3.93 V
6.00 V	5.90 V
* 6.00 V	5.90 V
8.00 V	7.88 V
10.00 V	9.85 V
12.00 V	11.82 V
4.00 V	13.80 V
16.00 V	15.78 V
18.00 V	17.75 V
22.00 V	21.71 V

*** Switched the meters and they read the same**

These results revealed that the ohmmeters were reading correctly and that the screen did have a slight loss in power from the reading just coming out of the power supply.

The two ohmmeters were then connected to the big power supply with one reading at the screen and the other one at the power supply. The power console display was also used for comparison (see Figure C.3.3 and Table C.3.3).

Figure C.3.3 Power Supply Test #2

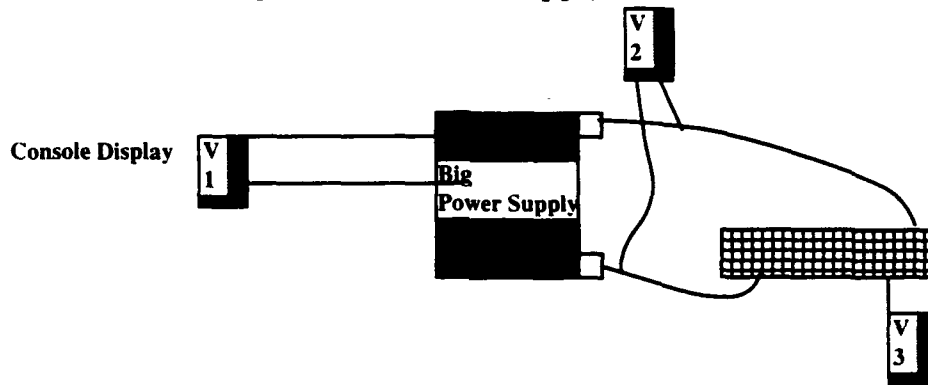


Table C.3.3 Power Supply Test #2 Results

V1	V2	V3
10 V	10.18 V	0.14 V
20 V	20.23 V	20.19 V
30 V	30.38 V	30.32 V
40 V	40.4 V	40.3 V
50 V	50.5 V	50.4 V
60 V	60.6 V	60.5 V
70 V	70.7 V	70.6 V

These results showed that the console reading was off by a little factor. Using the measured resistance of the stainless steel screen of 0.2Ω , and the amps reading from the first test (an ammeter was not available), a power correction factor of 1.14244 was calculated and used as the real power discussed in Chapter 5.

C.4 FLOWMETER

Analysis in Chapter 5 showed a slight imbalance between powers and temperatures based on mass flow rate for the tests conducted, especially at the lower powers. There was some concern that the flowmeter was not reading properly for the following reasons: (1) it was a nitrogen flow meter and the He heat capacity factor was not very reliable; (2) the flow meter was used past the 1500 lpm capacity in trying to go to higher Reynolds numbers (the screen display read to 2000 lpm); (3) the flowmeter was not calibrated; (4) and the inlet temperature conditions. Each of these issues were separately addressed.

Since the flowmeter was calibrated for nitrogen, there was a concern that it may be reading improperly for He. Some of the early tests in Appendix B used nitrogen, but the beds and thermocouples were so misbehaved that no strong conclusions could be drawn. A He flowmeter was borrowed to try to discover if this was a source of error. Table C.4.1 shows the first helium and nitrogen flowmeter test performed. All tests were done at room temperature.

It was hard to interpret the results from Table C.4.1. For the runs with a 200 psig regulator setting, there was a different result with the He and N₂ flowmeters with He as the working fluid. The N₂ flow meter started out with a reading of 250 lpm and slowly increased in increments of 1 every 2 seconds up to 390 lpm and held there for 10 seconds before the gas ran out of the 1A cylinder. The He flow meter started at 800 lpm and held at 805 lpm. This test showed that the heat capacity correction factor for the N₂ flowmeter was 2.06 instead of 1.43. For the N₂ gas tests, the heat capacity correction factor was 1.96 between the two flow meters. For the 225 psig settings, the He flowmeter went off scale so nothing could be interpreted. The correction factor for N₂

gas was 2.14 at 225 psig. Since these readings were not consistent, it was decided to do another test with the flowmeters in series.

Table C.4.1 Helium and Nitrogen Flowmeter Test #1

Type of Gas	Type of Flowmeter	Flow Setting / Meter Reading lpm	Pressure @ Regulator psig	Flow Setting / Meter Reading lpm	Pressure @ Regulator psig	Flow Setting / Meter Reading lpm
He	He	800 / 805	200		225	off-scale
N ₂	N ₂	240 / 244	200	225 psig 900 up to 965	225	720 788
N ₂	He	250 up to 390	200		225	1412
He	N ₂	690 down to 480	200	off scale	225	1685

The next test performed connected both flow meters in series (see Figure C.4.1). He and N₂ were used again for the working fluids. The results of the test is shown in Figure C.4.2. There were two set points for the tests, set the He flowmeter at 800 lpm and run both gases and then set the N₂ flowmeter and run both gases. The heat capacity correlation for these tests came out to be ~1.5 (1246/801 = 1.55, 803/526=1.53, 333/218=1.52).

Figure C.4.1 Flowmeter Calibration Test #2 (Meters in Series)

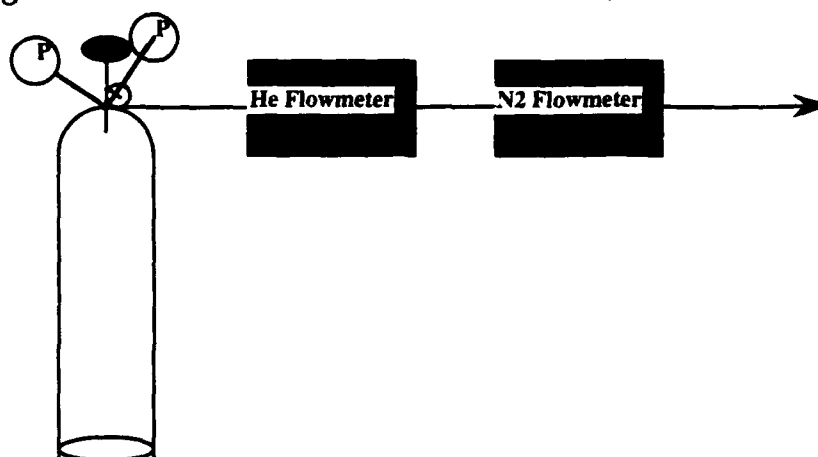


Table C.4.2 Results of Flowmeters in Series Tests

Regulator at 230 psi for all Tests		
Gas	He Flowmeter	N ₂ Flowmeter
N ₂ for 1 minute	1246 lpm	801 lpm *
	1242	800
	1236	799
	1231	797
	1228	796
	1225	795
	1218	794
	1214	792
He for 10 sec	off-scale	1566 lpm
He for 1 min	803 lpm *	526 lpm
	801	525
	800	524
	800	523
	799	523
	798	522
	798	522
	797	522
N ₂ for 3 min	259 lpm	165 lpm
	262	169
	268	170
	270	174
	279	175
	282	180

(cont.)	286	181
	287	183
	291	184
	293	187
	299	190
	300	192
	302	193
	308	196
	309	198
	311	199
	314	200
	315	202
	316	204
	319	205
	320	207
	323	208
	325	210
	327	212
	329	214
	331	216
	333	218

*Set Point

These tests showed that the 1.43 correction factor for the N₂ flowmeter for He gas could be inaccurate. However, there are some issues. It was not known if both flowmeters were calibrated. Matheson (the vendor) was contacted, and they said that the conversion factor could be a little off, but it was based on theoretical calculations. They suggested that the flowmeter be calibrated and the error could be determined.

Grumman Aircraft System's Quality Assurance Department, Measurement Standards Section, Bethpage, NY, was contacted to calibrate both flowmeters. They refused to calibrate the He flowmeter since they had problems with them in the past. They could never get the flowmeters to match the 1.43 correlation. They calibrated the N₂ flowmeter up to 2000 lpm. It was found

to be within tolerance up to 1500 lpm \pm 1% error, and up to 2000 lpm with a -2.96 % error (see Appendix E).

The temperatures to the flowmeter inlet were monitored through out the runs. The temperatures usually ranged from 38 - 42 °C, never falling out of the 0 - 50 °C. The pressures never were above the 10000 kPa max. This proved that the chill down system was working effectively and temperature and pressure deviations were not a cause of flowmeter error.

No conclusions could be drawn for the flowmeter. The tests showed that the nitrogen flowmeter with the 1.43 correction factor was reading a little low compared to the helium flowmeter. Calibration tests showed that the nitrogen flowmeter was in tolerance. Grumman refused to do the calibration tests for the helium flowmeter, and Matheson said that they could calibrate it, but time constraints were a limiting factor. Matheson did support their 1.43 calibration number. Therefore, since the He flowmeter tolerances were not known, it is not known if the flowmeter readings were accurate. If the He flowmeter was calibrated, the flowmeter readings for the tests conducted in Chapter 4 and Appendix B read low (\sim 1.05 - 1.06). (even a little more above 1500 lpm due to the -1 to -2.96 % error).

APPENDIX D

TESTING DATA SHEETS

This Appendix contains the data sheets that were used to record the data for power , pressure, and mass flow rate as a function of time for the tests described in Chapter 4. The mass flow rate shown did not include the 1.43 correction factor for He. Power was controlled by a rotary dial that adjusted the console display digitally. For each power change, the power ramp was started ~5 - ~15 s before the power change was recorded in order to have the setting at the desired power for the given time. The Oct 92 test is listed first, and then the eight tests conducted in January.

Figure D.1 Data Sheet From 14 Oct 92 Experiment

Test: PM 14 Oct 92

Low inlet temperature run, He ~ 2000 lpm through out test

Have to turn off power supply to take readings

*Note Time for this test was clock time (The test started at 2:34 pm)

Time	Volts	Amps	He Flow lpm	Remarks
2:34	0	0	2000	Temp not low enough and pressure too low need to adjust
2:36	0			
Pause to adjust			2145	p=140 psi
2:55	7	52		
2:56	12	84		
2:57	20	133		
2:59	30	166		
3:00	40	200		
3:01	50			Flow dropped Power off (temp reading)
3:02	40	196		
3:03.25	50	245		off-flow too low
3:04.75	50	250		Back on flow
Keep at 50	50			current varies Lost Bed

Figure D.2 Data Sheet From 20 Jan 93 Test #1

Test: Test at Low Phi 20 Jan 93 14:10

* Note: Time for this test and all of the further tests is in Min:sec

Time	Volts	Amps	He Flow lpm	Remarks
0:00	0	0		Trying to go up to 1600 lpm and 500 °C
0:00	1.5	9	270	Not doing much
1:00	3	19	278	Ts going up
2:00	6	49	278	
3:00	6	47	280	
4:00	6	48	280	
5:00	6	53	281	
6:00	8	66	281	
7:00	8	69	283	
8:00	8	69	282	
9:00	8	69	353	
10:00	8	69	288	
11:00	8	69	288	
12:00	8	69	289	
13:00	8	69	289	
14:00	15	139	1640	
15:00	20	159	1600	
16:00	35	228	1602	
17:00	37	237	1600	p=40 psi
18:00	37	236	1600	
19:00	37	236	1610	
20:00				shut off by gradually bring power down
22:00				Flow down to 100 lpm Power off and then flow off

Figure D.3 Data Sheet From 20 Jan 93 Test #2

Test: Check Bed Temperatures No Flow 20 Jan 93 1530

Time	Volts	Amps	Remarks
0:00	2	15	T's pretty even
1:00	2	14	T's pretty even
2:00	2	14	T's pretty even
3:00	2	14	T's pretty even
4:00	2	13	T's pretty even
5:00			stopped, went up to 107.89 °C

Figure D.4 Data Sheet From 22 Jan 93 Test #3

Test: Check Bed Heating after Rotation (No Flow) 22 Jan 93 0900

Time	Volts	Amps	Remarks
0:00	2	15	#6 is a couple of degrees ahead, else look pretty even
1:00	2	15	
2:00	2	15	#1,2,3,4 within 2°C
3:00	2	14	
4:00	2	14	#3 lowest, 4° with #2
5:00	2	14	
6:00			cut power off
7:00			#1,2,3,4 - 101 - 104 °C
8:00			added gas - He at 200 lpm #1 and #2 not as cool
9:00			He at 215 lpm #1 2 - 82, 81 °C #3,4 at 67, 57 °C
10:00			He at 204 lpm
11:00			He at 191 lpm
11:30			gas off

Figure D.5 Data Sheet From 22 Jan 93 Test #4

Test: Rotated Bed Test with Flow Room Temperature Inlet 22 Jan 93 0945

Time	Volts	Amps	He Flow lpm	Remarks
0:00	5	38	243	
1:00	10	76	259	
2:00	10	71	257	
3:00	15	99	392	
3:30	15	98	504	
4:00	15	98	1087	
5:00	25.2	161	1092	
5:30	25.2	165	1092	
6:00	35	224	1607	p=50 psi
7:00	30	195	1607	
8:00	30	196	1600	
9:00			1600	power off
9:30			1500	
10:00			500	
11:00			87	

Figure D.6 Data Sheet From 22 Jan 93 Test #5

Test: High Phi Run 22 Jan 93 1405

Time	Volts	Amps	He Flow lpm	Remarks
0:00	5.1	45	982	p = 110 psi
0:30	10.1	87	981	
1:00	10.1	87	980	
1:30	20	157	983	
2:00	20	153	986	
3:00	30	208	905	2 taking off, cutting back to 25 volts
4:00	25.1	177	990	2,4,taking off,1,3,5 diverging
5:00	20	145	999	
6:00	15.8	119	1008	
7:00	13.5	107	1003	
8:00	12	100	1002	Dropping , warm thermocouples coming down faster than lower ones increasing in temperature
9:00	10	103	1002	
9:15	10	87	1004	thermocouples converged
10:00	10	90	1005	
11:00				cut off power

Figure D.7 Data Sheet From 22 Jan 93 Test #6

Test: High Phi Lower Pressure Test 22 Jan 93 1445

Time	Volts	Amps	He Flow lpm	Remarks
0:00	10	100	1600	p=60 psi
1:00	20	175	1613	
2:00	30.1	238	1627	Seeing same effects 1 down 2 up 3 down 4 up in temperature
3:00	30.1	218	1630	
4:00	30.1	219	1637	
4:30	25	180	1631	
5:00	25	181	1629	
6:00	16.9	129	1624	
7:00	16.9	139	1620	
8:00				cut off power
10:00				cut off flow

Figure D.8 Data Sheet From 25 Jan 93 Test #7

Test: Room Temperature Inlet Retest (Repeat Low Phi) 25 Jan 93 1525

Time	Volts	Amps	He Flow lpm	Remarks
0:00	5.1	44	1023	p=70 psi
1:00	10.1	84	1028	
2:00	10.1	82	1035	
3:00	15	120	1030	
4:00	15	118	1018	
5:00	15	117	1006	
6:00	15	119	1011	
7:00	15	119	1016	
8:00				
9:15				

Figure D.9 Data Sheet From 26 Jan 93 Test #8

Test: High Phi Retest, Shooting for Higher Reynolds Number 26 Jan 93 0943

Time	Volts	Amps	He Flow lpm	Remarks
0:00	15	149	1766	p = 90 psi
1:00	15	145	1769	
2:00	20.2	175	1770	
3:00	25	204	1783	
4:00	25	206	1797	
5:00	25	199	1800	
6:00	25.1	196	1795	
7:00	25.1	195	1795	
8:00	30.0	227	1764	
8:58				Got high reading on #5 (1000 °C) shut off power immediately, maintained gas flow ,Thermocouples responded went back down to -150 °C

Figure D.10 Data Sheet That Showed Bed Was Damaged 26 Jan 93

Test: Low Power No Flow, Bed Test 26 Jan 93 1055

Time	Volts	Amps	He Flow lpm	Remarks
0:00	2	0		Lost Bed

APPENDIX E

EQUIPMENT CALIBRATION SHEETS

This Appendix contains the calibration sheets for the Vahalla ohmmeter and nitrogen flowmeter used in the experiments. The other equipment was calibrated when it was purchased, but calibration sheets were not available.

Figure E. 1 Calibration Sheet for Ohmmeter

VALHALLA SCIENTIFIC		Certification of Calibration	
Model No.	4100A/C	Serial No.	8-3568
		Report No.	14529
Applicable NBS Report No.			
DC Voltage	USN22783C.45662-3.5.2		
AC Voltage	G-45911		
Resistance	51131C		
<p>Valhalla Scientific does hereby certify that the above referenced instrument was tested and calibrated using standards whose accuracies are traceable to the National Institute of Standards and Technology within the limitations of the Institute's calibration service, or have been derived from accepted values of natural physical constants, or have been derived by the ratio type of transfer self-calibration techniques.</p>			
Temperature	23	°C	Calibration Due
Humidity	45	%	Return Status
Certified by <i>A. Bland</i>		Date	OCTOBER 16, 1992
		Quality Assurance	

Figure E.2 Calibration Sheet for Flowmeter

APP 14 1993 13:54 ONE

Grumman Aircraft Systems
Bethpage, New York 11704-3582

QUALITY ASSURANCE DEPARTMENT MEASUREMENT STANDARDS SECTION

REPORT OF CALIBRATION

SUBMITTED BY : BROOKHAVEN NATIONAL LAB
ASSOCIATED UNIVERSITIES
UPTON NY 11973

PURCHASE ORDER:	596820	CAL DATE :	4-8-93
NOMENCLATURE :	MTR FL NITRO W/READOUT	MODEL :	8104-1416-FM
MANUFACTURER :	MATHESON CO INC	SERIAL NO:	L91741749/89132
PROCEDURE NO. :	C3340371	REV: --	CUST IDEN: 62614

THE ABOVE ITEM WAS CALIBRATED IN ACCORDANCE WITH GRUMMAN AIRCRAFT CALIBRATION PROCEDURES AND MIL-STD-45662A, UTILIZING STANDARDS TRACEABLE TO THE NATIONAL INSTITUTE OF STANDARDS AND TECHNOLOGY.

ACTUAL VALUES AND STANDARDS USED ARE LISTED ON THE ATTACHED DATA SHEETS.

NOTE: AS FOUND - IN TOLERANCE, AS LEFT - IN TOLERANCE.

NOTE: RANGE 200 TO 2000 LPM N2 - ACCURACY $\pm 1\%$ FS


JOHN E. BOWER
ENGINEERING SUPERVISOR

Grumman Aircraft Systems

Bethpage, New York 11714-3582

SERVICE REPORT

CUSTOMER: Brookhaven National Lab
 P.O. NUMBER: 59682D CUSTOMER I.D.: G2614
 MANUFACTURER: Mettler G Inc MODEL: 8104-1416-FM S/N: 19071749/89132
 NOMENCLATURE OR ITEM DESCRIPTION: Meter Flow with Digital Display

DISCREPANCY FOUND: Unit is within manufacturers $\pm 1\%$
Full scale tolerance for normal calibration of 1500 SLPM.
Above 1500 SLPM Unit exceeds $\pm 1\%$ Full scale of
2000 SLPM. Customer requested meter to be calibrated
past 1500 SLPM

CORRECTIVE ACTION: Use With Correction Data

FINAL STATUS OF INSTRUMENT

- () Adjusted and Recalibrated.
- () Performed Complete Internal Alignment and Recalibrated.
- () Accepted to Limited Use Status as Described Above.
- () Returned, Not Calibrated for Reason Stated Above.
- () Beyond Economical Repair.
- () Repaired and Calibrated.
- () Resized.

TECHNICIAN STAMP:  VERIFIED BY: JS DATE: 4-9-93

APP 14 199 13:55 ONE

5.1.7

GRUMMAN AIRCRAFT SYSTEMS - MEASUREMENT STANDARDS

PAGE 1 OF 3

SELF-READING FLOWMETER CALIBRATION

METHOD: SELF-READING FLOWMTR. (LAM./VENTURI/TURB.) VS. LAM.FLOWMTR. STD

CALIBRATION PROCEDURE: 3340371

BASECUB FLOWLAB. PROGRAM DISC NO.1, PROG.H7

NOTE: 1. DATA IS ADJUSTED TO STANDARD CONDITION OF
70 DEG.F & 14.7 PSIA

2. WHEN THE INSTRUMENT BEING CALIBRATED REQUIRES A
CALIBRATION GAS OTHER THAN AIR, A CONVERSION FACTOR
STIPULATED BY THE MANUFACTURER WILL BE USED TO
ADJUST THE DATA AND WILL APPEAR IN THE DATA HEADING

CUSTOMER: BROOKHAVEN NATIONAL LABS
CALIBRATION DATE: 4-8-93
MANUFACTURER: MATHERSON CO. INC.
MODEL NUMBER: 8104-1416-FM
SERIAL NUMBER: L91741749/99132
I.D. NUMBER: 62514
ACCURACY: 1 %FS
MAX. FLOWRATE: 2000 SLPM
CALIBRATION GAS: AIR
INSTRUMENT GAS: NITROGEN
GAS CONVERSION FACTOR: 1



BAROMETRIC PRESSURE: 30.08 in.HgA
ROOM AMBIENT TEMP.: 70 DEG.F
ROOM AMBIENT HUMIDITY: 36 % RH

THE FOLLOWING DATA IS FIRST RUN (AS FOUND) DATA.

APP 14 199 13:55

PH-5E1-004

APR 14 '93 13:11 CNE

FILE

LAMINAR FLOWMETER STANDARD:

PAGE 2 OF 3

I.D. NUMBER197255
 SERIAL NUMBER10276
 MAX.DELTA P 10 IN.H2O
 MAX.FLOWRATE 70 SCFM
 A COEFFICIENT-3.335891E-08
 B COEFFICIENT 2.940094E-05

SELF-RDG. FLOWMETER AIR	INLET PRESS. IN.H2O	TRUE FLOW SLPM	% ERROR FULL SCALE	VOLTS OUTPUT
200.00	3.60	204.33	-0.22	0.66
400.00	7.20	406.09	-0.30	1.33
600.00	10.80	607.68	-0.38	1.99
800.00	14.40	809.48	-0.47	2.65
1000.00	18.00	1011.33	-0.57	3.32
1200.00	21.60	1213.11	-0.61	3.98
1400.00	25.20	1413.06	-0.65	4.64
1600.00	28.80	1622.26	-1.14	5.31
1800.00	32.40	1835.09	-1.75	5.97
1996.00	36.00	2047.19	-2.56	5.62



APR 14 '93 13:59

P-38.005

RAW DATA:

PAGE 3 TO 3

LAMINAR FLOWMETER STANDARD				SELF-READING FLOWMETER	
P _g IN. H ₂ O	P _g -c IN. H ₂ O	T _g DEG. C	T _g DEG. C	INLET PRESS. IN. H ₂ O	IND. RDG. AIP
410.10	1.0990	22.60	22.60	3.80	200.00
411.20	2.1750	22.60	22.60	11.80	400.00
412.41	3.2140	22.60	22.40	23.60	600.00
413.70	4.3040	22.30	22.30	39.00	800.00
414.90	5.3570	22.20	22.20	57.80	1000.00
416.30	6.1970	22.20	22.20	80.20	1200.00
417.60	7.4320	22.20	22.20	105.30	1400.00
419.10	8.5040	22.20	22.20	135.60	1600.00
420.50	9.5840	22.10	22.30	169.30	1800.00
422.10	10.6470	22.30	22.30	206.00	1996.00

GRUMMAN AIRCRAFT SYSTEMS - MEASUREMENT STANDARDS FLOW METROLOGY LABORATORY CALIBRATION STANDARDS				NUMBER 3349371 CUSTOMER
SYMBOL/CLAY/RE		MODEL	SN: 191741249/29132	
MANUFACTURER		CODE	IDENT. NUMBER	DATE
Meter Flow w/Reagent		M34	62614	4-8-93
Matheson Co. Inc.				
	CALIBRATION STANDARD	MODEL	IDENTIFICATION	DUE DATE
[✓]	LAMINAR		009725S	02-05-94
[]	LAMINAR		009726S	04-02-94
[]	LAMINAR		009727S	03-08-94
[]	LAMINAR		009728S	08-31-93
[]	LAMINAR		009730S	09-09-94
[]	LAMINAR		148196G	09-20-93
[]	LAMINAR		300017M	08-28-93
[]	LAMINAR		348745M	
[]	LAMINAR		010666S	12-03-93
[✓]	PRESSURE GAGE		153271G	11-23-93
[]	PRESSURE GAGE		199409G	
[]	PRESSURE GAGE		199410G	05-12-93
[✓]	PRESSURE GAGE		199411G	04-09-93
[]	PRESSURE GAGE		336132M	04-28-93
[]	INCLINE MANOMETER		348772M	02-21-93
[]	INCLINE MANOMETER		348773M	02-21-93
[]	MANOMETER		124099G	07-10-93
[✓]	MANOMETER		142270G	04-22-93
[✓]	ALTIMETER		003536B	04-30-93
[]	DIGITAL TEMP. INDICATOR		335392M	03-29-93
[✓]	DIGITAL TEMP. INDICATOR		307689M	07-29-93
[]	BALLISTIC CALIBRATOR		177100G	12-17-93
[]	WIND TUNNEL		209350G	05-29-93
[]				
[]				
[]				

TEMPERATURE: 70 DEG. F HUMIDITY: 36 %

APPENDIX F

TEMPERATURE DATA FROM JAN 93 EXPERIMENTS

This Appendix contains the temperature readings for the eight experiments conducted in January 1993. The temperatures are shown in table format with time in minutes:seconds, and temperature in degrees Celsius for the eight thermocouples. The temperature readouts were sent to computer disk and the printer every 10 seconds, but the computer display showed temperature data every 1 seconds for quick control if needed. The tables for the experiments conducted are in chronological order. The temperatures for the October 1992 experiment are not included since they were taken every minute and the temperature chart should be self explanatory. For descriptions of thermocouple placement, see Chapter 4.

Figure F.1 Bed Test At Low Phi 20 Jan 93

X Data	Thmcple#1	Thmcple#2	Thmcple#3	Thmcple#4
0:00	1.43	1.67	1.43	1.8
0:10	2.19	2.73	2.26	2.54
0:20	4.17	4.65	4.29	4.19
0:30	6.44	6.51	6.54	5.67
0:40	8.69	8.09	8.77	6.98
0:50	10.55	9.26	10.62	7.89
1:00	12.21	10.28	12.19	8.65
1:10	14.98	12.83	14.79	10.56
1:20	19.26	16.65	19.06	13.74
1:30	24.79	20.85	24.57	17.49
1:40	29.95	24.21	29.58	20.49
1:50	34.4	26.88	33.88	22.59
2:00	38.59	29.35	37.73	24.42
2:10	47.75	38.2	46.43	31.58
2:20	62.88	50.93	61.35	43.6
2:30	80.59	61.78	78.22	55.35
2:40	95.84	70.01	92.1	63.96
2:50	109.01	76.56	103.6	70.3
3:00	119.26	81.55	112.41	74.68
3:10	128.01	85.53	119.63	78.11
3:20	134.56	88.54	125.13	80.58
3:30	140.77	91.15	130.49	82.81
3:40	145.93	93.41	134.71	84.61
3:50	150.2	95.05	138.28	86.03
4:00	153.85	96.63	141.15	87.02
4:10	156.8	97.7	143.37	87.69
4:20	160.04	99.01	145.73	88.85
4:30	163.56	100.64	148.64	90.38
4:40	166.43	101.62	150.59	90.63
4:50	169.36	102.74	152.76	91.7
5:00	172.94	104.16	155.35	92.92
5:10	176.23	104.95	157.47	93.67
5:20	178.68	105.19	158.87	94
5:30	180.3	105.23	159.49	93.31
5:40	182.06	105.02	160.03	93.78
5:50	183.66	105.13	160.56	93.84
6:00	185.59	105.46	161.24	94.49
6:10	191.31	110.24	166.14	99.84
6:20	201.4	118.08	175.77	107.91
6:30	211.54	124.7	185.55	114.11
6:40	221.5	131.33	194.89	120.03
6:50	231.78	137.5	203.89	124.92
7:00	241.05	142.11	211.74	128.37
7:10	250.45	145.9	219.42	131.02
7:20	258.57	146.65	224.51	134.72
7:30	268.69	145.46	228.04	137.33
7:40	275.67	145.55	231.79	139.57
7:50	281.31	146.53	235.35	141.34
8:00	286.31	147.61	238.86	143.2
8:10	290.98	148.96	241.95	144.65
8:20	294.73	149.77	244.68	146.24
8:30	295.54	154.34	246.32	144.3
8:40	297.31	163.11	247.72	147.3
8:50	296.42	165.06	251.51	151.62
9:00	307.87	182.51	256.84	148.99
9:10	309.98	174.52	257.76	145.09

9:20	307.9	150.88	254.88	144.95
9:30	309.45	150.85	256.85	147.52
9:40	307.76	164.81	258.88	148.22
9:50	313.58	160.18	261.07	151.37
10:00	316.96	160.76	263.12	151.75
10:10	319.15	161.89	265.14	152.34
10:20	320.74	162.92	266.87	152.85
10:30	322.16	163.99	268.56	153.39
10:40	323.36	164.67	270.06	153.78
10:50	324.16	165.03	271.22	154.27
11:00	325.03	165.82	272.47	154.71
11:10	325.8	166.54	273.59	155.21
11:20	326.3	166.93	274.43	155.53
11:30	326.46	166.56	275.02	155.57
11:40	326.77	167.16	275.86	156.43
11:50	329.03	169.39	278.27	158.38
12:00	330.89	170.65	280.23	159.16
12:10	332.6	171.51	281.97	159.94
12:20	333.93	172.58	283.37	160.71
12:30	334.85	173.17	284.5	161.18
12:40	335.37	173.11	285.5	159.41
12:50	328.08	172.79	285.47	155.98
13:00	326.87	173.31	286.11	156
13:10	327.15	173.76	286.72	156.5
13:20	327.39	174.11	287.21	156.95
13:30	327.66	174.45	287.86	157.23
13:40	286.07	183.44	272.21	128.37
13:50	171.24	75.24	134.52	67.59
14:00	110.99	58.43	75.18	58.58
14:10	94.57	67.19	78.32	65.18
14:20	114.57	85.86	103.02	81.28
14:30	120.65	88.99	113.3	82.8
14:40	120.38	88.28	114.41	82.23
14:50	139.74	105.87	132.7	91.13
15:00	166.1	124.67	154.55	97.94
15:10	182.62	134	168.92	101.24
15:20	185.14	134.19	170.06	101.55
15:30	205.57	153.77	190	116.01
15:40	274.33	204.33	251.16	145.3
15:50	337.94	218.85	291.72	153.06
16:00	364.94	212.36	292.83	150.11
16:10	378.65	213.86	285.66	154.01
16:20	432.98	244.75	317.81	173.76
16:30	457.78	253.56	339.86	179.6
16:40	470.79	251.7	340.86	180.65
16:50	484.19	258.37	344.3	185.2
17:00	510.74	267.86	353.38	190.57
17:10	525.75	273.61	358.86	193.26
17:20	536.76	274.2	358.2	194.31
17:30	544.44	275.04	356.42	194.72
17:40	550.8	276.02	354.27	195.61
17:50	552.82	277.31	353.48	196.42
18:00	557.46	278.23	352.74	197.12
18:10	559.51	278.53	351.94	197.41
18:20	563.66	279.81	352.68	198.12
18:30	566.2	279.9	353.16	198.27
18:40	565.27	281.08	353.86	198.75
18:50	563.95	282.46	354.46	199.78
19:00	562.42	284	355.53	200.23
19:10	562.27	285.66	356.83	200.88

19:20	562.24	287.27	359.03	201.89
19:30	563.47	286.71	361.6	203.05
19:40	560.64	286.96	363.38	203.53
19:50	561.59	288.54	365.64	204.41
20:00	559.89	288.95	366.95	204.73
20:10	556.95	279.61	359.35	199.11
20:20	554.91	256.06	336.33	183.01
20:30	511.61	199.52	272.54	148.58
20:40	373.89	118.1	162.52	100.38
20:50	229.46	50.42	64.37	53.07
21:00	119.41	32.94	38.25	39.73
21:10	53.43	28.64	30.48	33.88
21:20	40.32	29.07	30	33.51
21:30	36.11	28.74	29.94	34.16
21:40	34.25	28.87	30.04	34.51
21:50	33.28	28.93	30.12	34.28
22:00	32.96	29.14	30.47	32.86

X Data	Thmcple#7	Thmcple#8	Thmcple#5	Thmcple#6
0:00	1.77	1.65	1.59	1.78
0:10	1.84	2.27	2.59	2.73
0:20	1.91	3.69	4.75	4.38
0:30	2	5.13	7.21	5.91
0:40	2.08	6.48	9.35	7.19
0:50	2.1	7.57	10.99	8.18
1:00	2.18	8.45	12.21	8.98
1:10	2.32	10.35	14.72	11.26
1:20	2.48	13.35	19.02	14.54
1:30	2.67	17.17	24.69	18.16
1:40	2.84	20.64	29.77	21.09
1:50	2.99	23.55	33.73	23.27
2:00	3.21	26.21	37.18	25.53
2:10	3.73	32.78	46.46	33.33
2:20	4.47	42.91	62.66	44.51
2:30	5.37	53.89	81.82	54.23
2:40	6.2	63.06	98.5	61.31
2:50	7.01	70.71	112.36	66.63
3:00	7.86	76.62	122.67	70.71
3:10	8.62	82.15	130.61	73.81
3:20	9.33	86.2	136.06	76.33
3:30	10.12	90.61	141	78.37
3:40	10.88	94.02	144.75	80.08
3:50	11.65	97.25	147.66	81.35
4:00	12.39	99.81	149.82	82.41
4:10	13.05	102.38	151.6	83.27
4:20	13.85	104.81	153.46	84.54
4:30	14.64	107.85	155.87	85.83
4:40	15.42	109.87	156.87	86.51
4:50	16.15	112.1	158.16	87.82
5:00	16.86	115.22	159.76	88.9
5:10	17.63	117.12	160.93	89.71
5:20	18.47	119.29	161.4	90.06
5:30	19.21	121.32	161.28	90.12
5:40	20.03	122.8	160.99	90.21
5:50	20.79	124.59	160.72	90.27
6:00	21.47	126.21	161.09	90.88
6:10	22.62	129.67	166.84	95.59
6:20	23.78	134.72	178.51	102.37
6:30	25.13	140.52	189.54	107.67
6:40	26.19	145.87	199.84	112.96
6:50	27.37	151.03	209.11	117.79
7:00	28.44	155.54	216.21	121.33
7:10	29.6	160.06	222.76	124.82
7:20	30.84	163.92	226.94	127.81
7:30	31.81	167.55	229.04	129.64
7:40	33.04	170.08	231.24	130.74
7:50	34.13	173.12	233.56	132.05
8:00	35.27	175.82	235.78	133.12
8:10	36.33	178.28	237.87	134.58
8:20	37.32	181.03	239.68	135.5
8:30	37.76	184.57	241.78	140.09
8:40	41.85	180.24	241.16	133.62
8:50	46.93	181.05	241.84	134.25
9:00	41	196.81	256.55	167.84
9:10	40.25	197.66	257.28	160.21

9:20	41.65	194.51	251.3	136.32
9:30	44.45	193.86	246.84	136.98
9:40	44.02	200.67	249.07	149.99
9:50	44.77	200.63	249.28	147.08
10:00	45.44	201.88	249.84	147.74
10:10	46.17	203.51	250.46	148.81
10:20	46.69	204.84	251.09	150.01
10:30	47.28	206.24	251.75	150.89
10:40	47.87	207.42	252.29	151.48
10:50	48.35	208.29	252.6	152.13
11:00	49	209.38	252.96	152.92
11:10	49.47	210.58	253.3	153.25
11:20	49.95	211.03	253.5	153.92
11:30	50.58	211.77	253.4	153.83
11:40	51.1	213.21	253.65	154.27
11:50	51.47	214	255.47	156.26
12:00	51.86	215.01	256.92	157.2
12:10	52.24	215.71	258.2	158.05
12:20	52.61	216.3	259.07	159.16
12:30	52.91	216.5	259.64	159.85
12:40	53.23	217.91	260.31	159.01
12:50	53.64	220.13	261.76	157.97
13:00	53.96	220.37	262.24	158.6
13:10	54.34	220.63	262.52	158.86
13:20	54.66	220.9	262.62	159.47
13:30	54.99	221.43	262.76	159.53
13:40	37.81	222.89	239.26	166.1
13:50	27.38	151.22	119.52	80.5
14:00	23.8	123.67	79.71	60.8
14:10	21.09	121.54	87.79	67.25
14:20	19.19	137.13	116.72	84.52
14:30	17.76	140.11	128.45	88
14:40	16.72	140.82	129.45	88.09
14:50	15.81	155.05	144.71	103.06
15:00	15.04	169.74	167.62	117.68
15:10	14.53	177.67	180.85	125.63
15:20	14.15	179.48	181.12	126.54
15:30	13.98	197.15	202.17	144.32
15:40	14.1	239.31	264.83	188.67
15:50	14.39	262.88	305.65	205.12
16:00	14.86	268.29	314.48	204.28
16:10	15.19	273.79	323.86	207.7
16:20	15.66	300.16	384.83	237.86
16:30	16.22	313.31	435.81	250.64
16:40	16.71	317.07	456.06	252.69
16:50	17.46	324.34	477.04	260.85
17:00	18.2	333.35	503.79	270.87
17:10	18.89	338.51	521.69	278.36
17:20	19.69	341.55	531.06	280.56
17:30	20.51	342.19	535.64	281.66
17:40	21.23	343.55	536.47	282.6
17:50	21.93	344.23	538.23	283.18
18:00	22.63	345.21	538.75	283.58
18:10	23.37	345.37	539.41	283.61
18:20	24.07	346.69	541.93	285.12
18:30	24.64	347.02	542.68	285.14
18:40	25.22	347.98	544.82	285.7
18:50	25.87	348.72	546.79	286.45
19:00	26.46	349	547.87	286.75
19:10	26.98	350.1	547.97	287.12

19:20	27.53	350.38	548.28	288.12
19:30	28.09	351.19	550.46	289.4
19:40	28.54	352.01	551.95	289.29
19:50	29.04	352.78	552.77	290.45
20:00	29.49	352.84	552.17	290.52
20:10	29.78	348.98	550.35	284.73
20:20	29.97	334.06	532.53	263.03
20:30	29.89	291.21	447.15	210.97
20:40	29.38	207.71	303.44	124.33
20:50	28.9	129.37	133.39	54.4
21:00	30.19	100.57	54.46	36.18
21:10	29.15	76.59	31.28	31.1
21:20	30.58	84.35	28.93	32.34
21:30	32.41	89.06	28.68	32.21
21:40	33.62	90.32	28.72	31.46
21:50	34.67	85.17	28.78	31.32
22:00	33.72	92.37	29.06	33.17

Figure F.2 Bed Test With No Flow 20 Jan 93

X Data	Thmcp1e#1	Thmcp1e#2	Thmcp1e#3	Thmcp1e#4
0:00	22.67	22.73	22.77	22.58
0:10	22.64	22.71	22.77	22.57
0:20	22.63	22.68	22.71	22.54
0:30	23.06	23.11	23.08	22.68
0:40	24.45	24.43	24.33	23.32
0:50	26.82	26.66	26.59	24.8
1:00	29.62	29.36	29.18	26.83
1:10	32.52	32.24	32.06	29.29
1:20	35.62	35.27	35.06	31.98
1:30	38.82	38.32	38.14	34.84
1:40	41.94	41.4	41.22	37.82
1:50	44.72	44.09	43.96	40.48
2:00	47.96	47.23	47.16	43.6
2:10	51.09	50.24	50.19	46.62
2:20	54.15	53.18	53.15	49.61
2:30	57.24	56.11	56.19	52.57
2:40	60.27	59	59.08	55.48
2:50	62.87	61.55	61.72	58.06
3:00	65.84	64.39	64.59	60.86
3:10	68.71	67.15	67.44	63.67
3:20	71.65	69.98	70.3	66.52
3:30	74.47	72.71	73.08	69.25
3:40	76.88	75.08	75.47	71.61
3:50	79.57	77.64	78.13	74.23
4:00	82.19	80.22	80.72	76.74
4:10	84.77	82.71	83.33	79.27
4:20	87.34	85.18	85.85	81.72
4:30	89.73	87.61	88.29	84.14
4:40	91.83	89.65	90.41	86.22
4:50	94.21	92.01	92.79	88.57
5:00	96.52	94.31	95.15	90.79
5:10	98.77	96.54	97.44	93.06
5:20	101	98.71	99.65	95.23
5:30	103.09	100.81	101.82	97.31
5:40	104.89	102.67	103.7	99.11
5:50	106.97	104.72	105.8	101.18
6:00	107.89	105.7	106.9	102.7
6:10	107.74	105.67	106.96	103.43
6:20	107.09	105.17	106.48	103.47
6:30	106.21	104.36	105.78	103.09
6:40	105.26	103.5	104.95	102.49
6:50	104.15	102.47	103.92	101.59
7:00	91.49	83.82	91.21	48.39
7:10	90.4	82.73	90.33	47.82
7:20	87.45	80.71	87.74	46.34
7:30	84.23	78.08	84.66	44.89
7:40	81	75.31	81.49	43.51
7:50	78.01	72.72	78.47	42.27
8:00	75.18	70.23	75.58	41.08
8:10	72.83	68.19	73.21	40.12
8:20	70.32	65.96	70.62	39.09
8:30	68	63.9	68.26	38.16
8:40	65.83	61.93	66.02	37.27

X Data	Thmcp1e#5	Thmcp1e#6
0:00	21.3	22.71
0:10	21.29	22.69
0:20	21.29	22.66
0:30	21.77	22.81
0:40	23.34	23.59
0:50	25.89	25.23
1:00	28.84	27.53
1:10	31.9	30.27
1:20	34.94	33.25
1:30	37.8	36.34
1:40	40.72	39.52
1:50	43.12	42.23
2:00	45.82	45.41
2:10	48.34	48.38
2:20	50.83	51.23
2:30	53.13	54.03
2:40	55.41	56.72
2:50	57.32	59.03
3:00	59.44	61.58
3:10	61.52	64.08
3:20	63.57	66.54
3:30	65.57	68.91
3:40	67.27	70.96
3:50	69.12	73.21
4:00	70.87	75.34
4:10	72.75	77.47
4:20	74.43	79.55
4:30	76.07	81.53
4:40	77.49	83.26
4:50	79.19	85.23
5:00	80.69	87.09
5:10	82.26	88.91
5:20	83.72	90.7
5:30	85.14	92.43
5:40	86.41	93.95
5:50	87.8	95.59
6:00	87.95	96.71
6:10	86.95	96.86
6:20	85.49	96.33
6:30	83.94	95.32
6:40	82.5	94.19
6:50	80.97	92.77
7:00	69.44	75.47
7:10	68.12	75.72
7:20	64.81	74.8
7:30	61.68	72.78
7:40	58.94	70.48
7:50	56.62	68.23
8:00	54.51	66.04
8:10	52.84	64.2
8:20	51.07	62.2
8:30	49.51	60.36
8:40	48.04	58.63

Figure F.3 Rotated Bed Test With No Flow 22 Jan 93

X Data	Thmcp1e #1	Thmcp1e #2	Thmcp1e #3	Thmcp1e #4
0:00	7.64	7.64	7.6	7.6
0:10	7.64	7.63	7.6	7.62
0:20	7.66	7.64	7.62	7.62
0:30	7.68	7.66	7.63	7.63
0:40	7.66	7.69	7.65	7.62
0:50	7.87	7.89	7.79	7.92
1:00	9.11	9.09	8.71	9.32
1:10	11.21	11.23	10.58	11.61
1:20	13.87	13.88	12.82	14.3
1:30	16.41	16.44	15.12	16.86
1:40	19.41	19.49	17.89	19.92
1:50	22.55	22.65	20.89	23.03
2:00	25.86	25.91	23.92	26.23
2:10	29.01	29.12	27.01	29.4
2:20	31.85	31.99	29.78	32.22
2:30	35.1	35.25	32.9	35.41
2:40	38.38	38.47	36	38.55
2:50	41.53	41.69	39.1	41.68
3:00	44.64	44.83	42.18	44.72
3:10	47.73	47.94	45.15	47.76
3:20	50.54	50.75	47.88	50.45
3:30	53.52	53.74	50.87	53.34
3:40	56.47	56.7	53.65	56.19
3:50	59.34	59.58	56.43	59.04
4:00	62.14	62.44	59.19	61.8
4:10	64.95	65.25	61.92	64.56
4:20	67.67	68	64.58	67.23
4:30	70.01	70.39	66.89	69.57
4:40	72.67	73.07	69.46	72.13
4:50	75.28	75.78	72.06	74.75
5:00	77.86	78.32	74.55	77.24
5:10	80.25	80.81	76.96	79.91
5:20	82.68	83.28	79.36	82.12
5:30	84.75	85.44	81.4	84.23
5:40	87.03	87.8	83.7	86.54
5:50	89.4	90.12	85.99	88.83
6:00	91.61	92.43	88.21	91.09
6:10	93.88	94.74	90.5	93.38
6:20	96	96.93	92.62	95.53
6:30	97.91	98.84	94.49	97.42
6:40	99.95	100.95	96.55	99.51
6:50	102.01	103.05	98.61	101.58
7:00	104.03	105.15	100.58	103.67
7:10	105.07	106.5	102.27	105.15
7:20	106.17	107.5	103.41	105.89
7:30	106.29	107.61	103.72	105.87
7:40	105.85	107.18	103.57	105.41
7:50	105.03	106.48	103.05	104.7
8:00	104.09	105.54	102.32	103.84
8:10	102.98	104.53	101.45	102.85
8:20	101.82	103.39	100.49	101.81
8:30	100.77	102.37	99.58	100.86
8:40	99.55	101.21	98.54	99.77
8:50	98.33	100.02	97.46	98.63
9:00	97.01	98.57	96.05	96.72
9:10	95.17	96.64	88.35	91.13

9:20	93.68	94.03	79.43	81.94
9:30	91.89	92.09	76.16	74.07
9:40	89.15	88.36	78.35	71.06
9:50	87.06	86.97	75.28	66.71
10:00	83.98	83.87	72.15	62.95
10:10	80.24	79.96	68.63	59.07
10:20	76.42	76	65.12	55.44
10:30	71.89	71.32	61.1	51.46
10:40	67.2	66.52	57.08	47.58
10:50	62.47	61.79	53.11	43.97
11:00	57.81	57.21	49.31	40.65
11:10	53.4	52.89	45.71	37.65
11:20	49.28	48.89	42.43	35.37
11:30	45.37	45.01	39.39	35.38
11:40	41.9	41.79	36.41	30.74
11:50	38.6	38.68	33.85	28.69
12:00	35.67	35.79	31.49	27.33
12:10	32.95	33.2	29.34	25.73
12:20	30.59	30.9	27.44	24.25
12:30	29.14	29.78	26.53	26.04
12:40	28.12	28.75	26.61	26.7

X Data	Thmcp1e #5	Thmcp1e #6
0:00	7.59	7.65
0:10	7.62	7.64
0:20	7.64	7.68
0:30	7.66	7.72
0:40	7.64	7.7
0:50	7.84	8
1:00	8.95	9.66
1:10	10.93	12.36
1:20	13.38	15.6
1:30	15.76	18.67
1:40	18.5	22.19
1:50	21.36	25.78
2:00	24.23	29.38
2:10	27.01	32.87
2:20	29.4	35.91
2:30	32.1	39.28
2:40	34.67	42.52
2:50	37.22	45.66
3:00	39.61	48.73
3:10	42.04	51.7
3:20	44.07	54.27
3:30	46.33	57.03
3:40	48.42	59.7
3:50	50.51	62.34
4:00	52.49	64.86
4:10	54.46	67.34
4:20	56.35	69.78
4:30	57.96	71.84
4:40	59.77	74.07
4:50	61.58	76.39
5:00	63.33	78.56
5:10	65.01	80.66
5:20	66.67	82.69
5:30	68.1	84.49
5:40	69.66	86.45
5:50	71.2	88.33
6:00	72.68	90.24
6:10	74.26	92.14
6:20	75.64	93.91
6:30	76.98	95.53
6:40	78.37	97.25
6:50	79.75	98.93
7:00	81.12	100.64
7:10	81.61	102.65
7:20	82.15	102.66
7:30	81.81	101.75
7:40	80.91	100.25
7:50	79.73	98.5
8:00	78.44	96.67
8:10	77.14	94.83
8:20	75.77	93.02
8:30	74.64	91.48
8:40	73.41	89.8
8:50	72.15	88.17
9:00	70.82	86.45
9:10	67.71	82.82

9:20	62.33	71.41
9:30	57.49	71.35
9:40	56.1	72.88
9:50	51.15	62.14
10:00	47.04	59.07
10:10	43.36	56.1
10:20	40.22	53.36
10:30	36.95	50.27
10:40	33.97	47.19
10:50	31.31	44.23
11:00	28.86	41.4
11:10	26.78	38.77
11:20	24.97	36.47
11:30	23.18	33.47
11:40	21.77	31.83
11:50	20.7	30.35
12:00	19.64	28.98
12:10	18.68	27.43
12:20	17.92	26
12:30	18.2	27.14
12:40	18.59	27.32

Figure F.4 Rotated Bed Test With Flow 22 Jan 93

X Data	Temp#1	Temp#2	Temp#3	Temp#4
0:00	12.73	12.68	12.48	12.31
0:10	12.49	12.48	12.12	12.1
0:20	12.9	12.84	12.49	12.74
0:30	20.81	20.27	19.99	21.19
0:40	35.31	33.39	32.32	32.66
0:50	50.66	48.84	44.42	42.79
1:00	65.52	63.2	54.48	51.29
1:10	78.63	76.24	62.37	58.29
1:20	88.88	86.48	67.83	63.36
1:30	99.24	97.08	72.97	69.16
1:40	120.12	117.31	88.03	88.98
1:50	154.33	150.24	109.25	119.06
2:00	188.49	183.89	127.16	145.83
2:10	217.01	212.43	141.03	166.09
2:20	246.25	241.88	154.48	184.15
2:30	271.66	267.9	165.88	197.38
2:40	294.37	290.66	175.1	207.67
2:50	311.93	307.82	182.01	215.24
3:00	330	324.52	188.95	223.21
3:10	346.56	339.12	194.91	230.65
3:20	362.01	295.54	206.3	249.71
3:30	368.39	292.9	208.44	257.89
3:40	384.86	307.3	217.78	270.62
3:50	410.86	331.81	232.19	288.73
4:00	425.99	387.24	247.93	342.55
4:10	435.45	410.96	253.66	364.68
4:20	448.22	396.81	253.66	364.88
4:30	445.46	345.21	242.82	350.24
4:40	396.64	306.34	197.44	286.12
4:50	332.55	267.37	161.04	225.52
5:00	277.7	234.14	145.71	195.71
5:10	241.09	217.23	140.58	184.25
5:20	223.46	208.6	141.57	182.36
5:30	262.09	247.67	186.99	232.01
5:40	339.7	300.43	234.16	299.66
5:50	369.03	341.64	247.16	304.42
6:00	311.52	321.76	200.46	260.56
6:10	264.26	303.85	183.01	238.11
6:20	244.29	296.78	179.33	233.99
6:30	230.68	289.43	174.92	227.53
6:40	266.67	318.18	210.38	265.75
6:50	345.58	401.25	255.5	317.04
7:00	371.16	432.52	260.68	348.13
7:10	373.86	451.51	256.61	353.43
7:20	372.25	452.57	255.18	391.45
7:30	367.11	462.74	251.94	408.28
7:40	330.91	434.58	226.87	305.84
7:50	293.26	442.32	206.72	327.45
8:00	276.34	426.71	204.56	316.64
8:10	272.98	422.45	205.78	313.15
8:20	272.66	415.19	206.52	310.11
8:30	273.08	412.01	207.23	307.14
8:40	273.82	410.08	207.37	307.15
8:50	274.06	405.71	207.74	305.29
9:00	274.47	404.44	208.19	303.47
9:10	275.14	401.48	208.49	301.64

9:20	275.13	397.87	208.59	299.84
9:30	210.37	324.22	151.21	236.98
9:40	71.38	156.32	48.62	113.82
9:50	17.42	65.57	18.99	28.88
10:00	14.39	28.19	17.27	16.91
10:10	14.28	20.89	17.43	16.47
10:20	14.22	17.09	17.31	16.65
10:30	14.42	15.87	17.44	16.86
10:40	14.72	15.79	17.13	16.76
10:50	15.01	15.88	17.18	17.24
11:00	15.32	16.07	17.05	17.14
11:10	15.52	16.26	17.16	17.27
11:20	15.75	16.4	17.32	17.43

X Data	Temp#7	Temp#8	Temp#5	Temp#6
0:00	11.47	12.32	11.35	12.14
0:10	11.33	12.12	11.25	11.92
0:20	11.28	12.33	11.7	12.63
0:30	11.64	17.02	19.67	21.84
0:40	12.28	25.32	32.96	35.59
0:50	12.93	33.68	45.62	49.13
1:00	13.51	41.31	56.4	62.04
1:10	14.06	48.14	64.97	74.46
1:20	14.54	53.23	71.03	84.83
1:30	15.15	58.53	76.77	95.77
1:40	16.54	68.18	92.68	117.8
1:50	19	84.67	118.72	152.49
2:00	21.51	100.49	140.48	185.87
2:10	23.74	112.96	156.1	212.26
2:20	26.24	125.27	170.17	238.15
2:30	28.66	134.63	181.58	260.61
2:40	31.12	143.44	191.51	279.29
2:50	33.27	150.25	198.92	293.41
3:00	35.73	155.03	206.11	308.24
3:10	38.14	159.13	212.56	321.09
3:20	36.45	167.66	237.1	341.3
3:30	35.64	169.69	241.44	353.93
3:40	36.49	176.4	263.14	374.96
3:50	38.33	186.48	289.04	405.63
4:00	37.85	205.02	252.92	451.69
4:10	37.35	213.86	260.38	478.99
4:20	36.84	225.24	248.94	492.58
4:30	27.11	238.76	212.85	468.74
4:40	24.97	219.38	181.07	418.06
4:50	23.35	201.93	157.64	359.77
5:00	22.36	190.64	145.87	325.39
5:10	21.62	184.03	141.73	304.19
5:20	21.12	181.39	142.74	294.75
5:30	21.15	204.54	186.95	345.05
5:40	21.43	238.95	232.87	429.53
5:50	19.17	256.04	232.85	460.33
6:00	17.89	238.35	200.64	441.26
6:10	17.03	230.31	188.31	417.67
6:20	16.47	224.57	186.2	412.16
6:30	15.9	219.62	181.64	403.42
6:40	15.7	243.44	216.57	441.03
6:50	15.67	276.75	266.7	500.14
7:00	15.73	276.82	277.56	557.87
7:10	15.85	277.12	280.14	585.25
7:20	16.04	276.33	280.33	646.93
7:30	16.29	277.12	282.28	677.06
7:40	16.36	267.65	257.13	651.74
7:50	16.38	258.57	233.57	592.03
8:00	16.35	256.77	228.73	574.69
8:10	16.36	254.51	227.44	563.22
8:20	16.35	253.87	226.83	559.32
8:30	16.28	253.43	226.72	549.76
8:40	16.23	252.72	225.72	549.76
8:50	16.26	251.69	224.91	544.13
9:00	16.24	251.53	225.3	541.95
9:10	16.24	251.26	225.44	535.33

9:20	16.32	250.66	224.68	529.24
9:30	16.07	212.69	163.64	458.42
9:40	15.69	133.94	55.33	318.7
9:50	15.34	73.269	20.81	230.28
10:00	15.23	50.694	20.5	114.18
10:10	16.86	48.46	18.88	56.17
10:20	17.44	44.15	18.74	34.49
10:30	17.51	40.8	18.7	25.52
10:40	17.84	48.68	18.21	23.65
10:50	18.84	49.02	18.22	22.41
11:00	19.62	49.48	18.41	21.93
11:10	20.24	48.06	18.58	21.7
11:20	20.65	46.21	18.85	21.59

Figure F.5 High Phi Run 22 Jan 93

X Data	Thmcple #1	Thmcple #2	Thmcple #3	Thmcple #4
0:00	-159.41	-139.89	-151.71	-142.01
0:10	-145.72	-135.23	-139.65	-136.7
0:20	-139	-129.65	-134.03	-132.04
0:30	-136.51	-127.34	-131.85	-129.91
0:40	-136.83	-126.25	-132.75	-130.21
0:50	-138.94	-127.94	-135.13	-132.13
1:00	-142.18	-129.96	-138.3	-133.83
1:10	-144.54	-132.16	-139.98	-136.08
1:20	-129.24	-118.67	-123.91	-120
1:30	-122.88	-107.63	-119.27	-115.61
1:40	-125.2	-106.5	-121.48	-117.78
1:50	-127.46	-108.04	-123.77	-120.23
2:00	-103.52	-89.74	-97.38	-95.72
2:10	-75.45	-55.6	-73.06	-72.24
2:20	-72.81	-42.03	-72.33	-71.35
2:30	-73.8	-34.44	-74.06	-72.25
2:40	-75.75	-30.06	-75.59	-73.49
2:50	-55.9	-19.76	-51.07	-49.7
3:00	39.08	61.94	32.75	43.96
3:10	88.58	129.14	55.71	83.49
3:20	99.02	170.52	53.86	89.06
3:30	98.82	199	45.65	92.07
3:40	93.95	212.66	36.81	99.72
3:50	85.68	199.45	29.18	114.54
4:00	75.09	191.75	23.78	134.51
4:10	134.07	283.69	88.82	194.4
4:20	215.52	415.88	132.33	270.18
4:30	254.52	501.03	133.83	329.6
4:40	267.95	569.9	122.75	370
4:50	260.44	564.78	87.84	378.03
5:00	212.48	484.95	40.06	369.26
5:10	174.06	461.94	31.99	378.58
5:20	147.38	471.05	33.1	402.82
5:30	127.24	481.48	36.96	415.84
5:40	111.34	488.26	35.93	435.46
5:50	101	499.95	41.41	451.32
6:00	93.94	512.56	45.66	457.87
6:10	60.76	519.28	19.36	407.62
6:20	18.43	499.54	-1.35	348.74
6:30	10.21	446.59	0.78	296.06
6:40	5.63	406.93	5.06	267.13
6:50	1.66	391.72	8.29	254.2
7:00	-2.04	382.93	11.75	242.08
7:10	-5.6	379.47	14.94	241.86
7:20	-9.25	365.51	16.72	238.62
7:30	-44.71	313.57	-17.24	183.5
7:40	-53.65	296.85	-25.9	160.61
7:50	-57.65	290.5	-27.69	154.46
8:00	-60.98	277.06	-28.23	153.61
8:10	-62.58	272.71	-28.58	145.5
8:20	-72.81	276.52	-38.05	131.4
8:30	-86.07	215.09	-53.51	111.3
8:40	-87.23	204.78	-56.65	95.48
8:50	-87.19	183.55	-57.9	83.88
9:00	-86.62	161.47	-58.84	72.03
9:10	-85.52	166.95	-60.42	59.19

9:20	-95.89	156.28	-75.04	34.74
9:30	-96.73	147.01	-77.57	19.99
9:40	-95.88	125.81	-77.91	14.16
9:50	-94.18	112.58	-77.39	5.77
10:00	-92.75	102.06	-77.31	-0.02
10:10	-91.22	90.31	-77.05	5.26
10:20	-90.13	78.9	-76.19	-9.32
10:30	-94.43	62.11	-81.86	-20.26
10:40	-107.92	33.33	-96.78	-41.11
10:50	-108.45	0.89	-98.09	-53.26
11:00	-107.05	-22.12	-97.51	-61.43
11:10	-105.53	-37.46	-96.43	-67.6
11:20	-104.06	-47.23	-95.57	-72.78
11:30	-102.84	-52.75	-94.61	-76.69
11:40	-102.12	-56.23	-94.13	-79.61
11:50	-101.44	-58.14	-93.61	-81.94
12:00	-101.26	-59.37	-93.53	-83.75
12:10	-101.02	-60.36	-93.71	-85.29
12:20	-100.8	-60.97	-93.53	-86.13
12:30	-141.11	-86.55	-140.39	-130.79
12:40	-170.29	-151.81	-167.06	-164.76
12:50	-171.23	-162.58	-168.23	-163.03
13:00	-172.01	-158.46	-164.87	-161.07
13:10	-171.94	-158.26	-169.72	-165.12
13:20	-170.55	-149.99	-169.12	-164.25

X Data	Thmcp1e #7	Thmcp1e #8	Thmcp1e #5	Thmcp1e #6
0:00	-142.67	-148.07	-114.02	-149.04
0:10	-138.31	-139.39	-99.62	-140.98
0:20	-136.92	-134.16	-95.23	-136.15
0:30	-137.95	-131.72	-94.86	-133.24
0:40	-140.32	-131.37	-96.42	-133.61
0:50	-143.25	-132.89	-98.76	-135.37
1:00	-146.5	-134.49	-102.33	-137.68
1:10	-149.4	-135.45	-103.33	-138.84
1:20	-151.71	-120.5	-89.05	-118.66
1:30	-154	-115.07	-78.71	-111.23
1:40	-155.73	-115.87	-79.77	-112.21
1:50	-157.22	-117.13	-81.38	-114.16
2:00	-158.41	-94.58	-59.3	-83.07
2:10	-159.27	-73.33	-35.06	-46.51
2:20	-159.7	-67.97	-29.57	-36.47
2:30	-160.31	-65.8	-28.47	-30.69
2:40	-160.81	-64.72	-28.52	-25.96
2:50	-161.02	-46.21	-13.45	-0.61
3:00	-160.99	17.22	50.04	102.9
3:10	-160.76	47.97	72.66	165.38
3:20	-160.28	58.23	78.28	193.43
3:30	-159.77	62.91	77.68	217.3
3:40	-159.16	65.64	77.15	239.41
3:50	-158.6	67.65	75.92	255.95
4:00	-157.96	69.4	74.46	279.2
4:10	-157.11	110.9	128.91	345.77
4:20	-155.98	147.59	177.59	469.62
4:30	-154.39	163.54	191.66	584.91
4:40	-152.57	167.27	193.34	652.86
4:50	-150.77	157.02	169.99	674.47
5:00	-148.92	137.05	124.98	634.07
5:10	-147.5	131.14	99.71	640.64
5:20	-146.29	129.23	88.68	655.7
5:30	-145.12	130.52	83.91	678.86
5:40	-144.11	129.55	78.2	683.79
5:50	-143.15	131.31	79.26	702.71
6:00	-142.38	131.66	78.54	713.8
6:10	-141.96	109.07	49.37	670.63
6:20	-142.07	86.96	8.92	618.32
6:30	-142.48	85.27	6.62	548.37
6:40	-143.04	83.5	8.54	507.44
6:50	-143.49	81.35	10.52	482.05
7:00	-144.25	79.14	12.16	466.82
7:10	-145.02	77	13.25	457.83
7:20	-145.67	75.1	12.9	447.12
7:30	-146.63	51.61	-25.72	384.47
7:40	-147.54	41.76	-36.92	357.45
7:50	-148.99	36.89	-35.73	338.7
8:00	-150.26	32.28	-33.93	312.12
8:10	-151.52	21.76	-32.35	366.67
8:20	-152.73	12.19	-39.91	320.12
8:30	-153.89	6.1	-55.29	286.79
8:40	-155.22	2.85	-53.02	258.87
8:50	-156.46	0.3	-49.28	241.23
9:00	-157.65	-3.88	-48.51	223.69
9:10	-158.74	-10.19	-49.83	230.37

9:20	-159.75	-24.63	-61.91	199.54
9:30	-160.71	-27.37	-61.78	157.09
9:40	-161.42	-29.62	-57.2	173.96
9:50	-162.28	-32.44	-53.48	158.87
10:00	-163.07	-35.02	-49.51	141.7
10:10	-163.83	-37.33	-46.73	131.56
10:20	-164.4	-39.45	-45.15	127.65
10:30	-164.82	-45.83	-49.38	117.35
10:40	-165.34	-57.72	-63.66	88.11
10:50	-165.86	-62.26	-63.06	76.79
11:00	-166.24	-66.17	-59.96	67.08
11:10	-166.77	-69.4	-58.61	57.22
11:20	-167.13	-72.29	-57.34	51.39
11:30	-167.43	-74.71	-56.4	41.15
11:40	-167.81	-76.51	-56.45	41.73
11:50	-168.09	-78.03	-56.05	31.27
12:00	-168.28	-79.31	-55.86	26.7
12:10	-168.53	-80.38	-55.7	22.5
12:20	-168.71	-81.51	-55.94	19.98
12:30	-169.13	-115.13	-85.81	-28.5
12:40	-169.78	-143.95	-124.06	-81.36
12:50	-170.44	-153.95	-130.65	-127.75
13:00	-168.45	-156.9	-134.42	-159.06
13:10	-164.01	-153.96	-127.58	-159
13:20	-161.66	-152.58	-127.02	-164.95

Figure F.6 High Phi Lower Pressure Test 22 Jan 93

X Data	Thmcp1e #1	Thmcp1e #2	Thmcp1e #3	Thmcp1e #4
0:00	-161.36	-149.31	-161.25	-160.51
0:10	-162.1	-152	-162.32	-159.77
0:20	-165.64	-155.18	-165.58	-162.84
0:30	-168.94	-160.78	-168.76	-165.37
0:40	-138.94	-130.45	-137.78	-133.97
0:50	-118.6	-105.4	-119.21	-115.21
1:00	-120.7	-101.03	-121.45	-117.64
1:10	-123.17	-101.51	-123.29	-119.3
1:20	-124.79	-102.26	-124.96	-120.71
1:30	-126.27	-103.33	-125.92	-121.85
1:40	-126.32	-103.67	-125.93	-121.77
1:50	-75.91	-58.45	-71.87	-66.1
2:00	-31.72	0.89	-33.95	-18.78
2:10	-39.17	20.29	-40.92	-18.28
2:20	-50.34	39.68	-47.71	-16.66
2:30	-59.41	55.53	-53.37	-12.27
2:40	-66.11	62.99	-56.75	-6.88
2:50	-15.91	109.94	-1.41	53.26
3:00	27.84	179.37	42.25	121.55
3:10	9.38	251.18	36.05	143.86
3:20	-12.75	292.19	27.87	153.87
3:30	-30.07	324.1	22.79	174.07
3:40	-39.54	349.32	17.7	193.1
3:50	-46.32	365.42	11.22	202.5
4:00	-49	354.46	5.55	199.56
4:10	-51.26	351.79	1.4	205.08
4:20	-52.83	358.28	-1.54	208.85
4:30	-53.27	375.13	-2.56	216.64
4:40	-53.61	394.11	-3.45	223.18
4:50	-54.15	421.68	-3.67	234.85
5:00	-53.77	439.72	-0.48	258.06
5:10	-54.64	454.74	-2.76	301.76
5:20	-78.14	471.59	-35	294.35
5:30	-81.58	424.01	-45.54	219.74
5:40	-82.54	440.32	-50.77	235.36
5:50	-82.82	395.17	-55.37	249.16
6:00	-83.34	388.18	-58.64	245.11
6:10	-83.52	379.58	-60.84	241.73
6:20	-82.76	375.99	-61.8	243.8
6:30	-83.08	375.1	-63.48	243.69
6:40	-83.28	366.45	-65.64	244.69
6:50	-116.19	331.23	-109.04	197.96
7:00	-119.44	300.71	-114.28	167.04
7:10	-119.99	240.73	-113.24	144.25
7:20	-119.75	221	-111.96	135.7
7:30	-118.91	215.52	-111.29	127.7
7:40	-117.47	209.48	-109.6	122.53
7:50	-115.13	197.53	-108.82	114.06
8:00	-113.26	176.17	-107.71	109.66
8:10	-111.28	151.17	-106.81	102.56
8:20	-109.2	133.52	-105.42	93.93
8:30	-106.7	120.55	-103.82	88.96
8:40	-109.72	107.03	-107.38	82.44
8:50	-109.14	101.86	-106.66	72.42
9:00	-178.95	12.42	-178.43	3.42
9:10	-180.26	14.56	-179.04	-93.96

9:20	-176.06	56.48	-154.1	-62.11
9:30	-170.06	38.76	-139.24	-51.39
9:40	-165.95	16.84	-133.94	-51.75
9:50	-162.36	-5.54	-131.33	-56.17
10:00	-159.39	-23.34	-130.3	-61.54
10:10	-157.2	-37.83	-130.07	-67.27
10:20	-155.31	-49.67	-130.17	-67.27
10:30	-153.71	-59.41	-130.52	-77.69
10:40	-152.48	-66.76	-130.9	-81.85
10:50	-151.26	-73.79	-131.3	-86.1

X Data	Thmcp1e #7	Thmcp1e #8	Thmcp1e #5	Thmcp1e #6
0:00	-162.02	-159.77	-129.11	-161.2
0:10	-165.03	-159.61	-132.43	-160.99
0:20	-168.05	-161.39	-134.35	-163.43
0:30	-171.02	-163.68	-136.15	-165.9
0:40	-173.5	-134.87	-108.48	-123.4
0:50	-175.25	-116.21	-89.9	-90.4
1:00	-176.7	-113.02	-90.14	-81.51
1:10	-177.52	-112.24	-91.12	-76.87
1:20	-178.17	-112.65	-92.13	-73.48
1:30	-178.67	-112.51	-92.85	-70.8
1:40	-178.97	-111.68	-92.82	-67.83
1:50	-178.99	-72.98	-49.83	-5.19
2:00	-178.96	-38.87	-18.57	76.28
2:10	-178.92	-32.48	-19.97	110.04
2:20	-178.66	-28.51	-23.44	129.58
2:30	-178.64	-26.81	-26.22	145.86
2:40	-178.28	-25.1	-28.92	158.76
2:50	-178.01	14.59	14.53	223.7
3:00	-177.56	55.66	47.28	292.46
3:10	-176.74	61.25	36.74	333.66
3:20	-175.92	64.34	21.11	349.13
3:30	-174.68	65.53	8.29	368.86
3:40	-173.59	67.44	-3.57	398.06
3:50	-172.52	69.9	-12.18	408.22
4:00	-171.58	74.37	-17.49	401.93
4:10	-170.57	77.99	-21.13	408.16
4:20	-169.72	80.19	-23.79	413.89
4:30	-168.95	82.71	-24.47	419.71
4:40	-168.24	86.59	-24.47	421.9
4:50	-167.68	88.69	-24.68	429.14
5:00	-166.91	89.43	-22.16	456.83
5:10	-166.33	85.49	-23.02	470.42
5:20	-166.04	50.92	-51.01	447.64
5:30	-166.59	46.05	-61.86	410.85
5:40	-167.23	44.35	-58.47	417.65
5:50	-168.01	42.92	-54.61	405.7
6:00	-168.83	40.23	-52.15	399.21
6:10	-169.5	37.09	-50.16	393.58
6:20	-170.09	36.69	-46.68	391.49
6:30	-170.47	34.64	-45.07	387.2
6:40	-171.02	33.38	-43.52	383.99
6:50	-171.7	-9.32	-82.49	316.48
7:00	-172.79	-20.84	-86.02	272.9
7:10	-174.01	-22.85	-92.68	233.76
7:20	-175.08	-25.92	-91.08	221.67
7:30	-175.89	-29.58	-88.17	215.77
7:40	-176.71	-34.64	-84.66	208.07
7:50	-177.28	-35.28	-82.18	193.27
8:00	-177.72	-35.86	-80.04	173.59
8:10	-178.07	-36.02	-77.15	162
8:20	-178.29	-35.99	-74.6	148.67
8:30	-178.54	-36.25	-72.38	142.83
8:40	-178.57	-37.86	-74.7	137.8
8:50	-178.69	-38.02	-68.7	131.52
9:00	-178.95	-111.06	-155.96	69.72
9:10	-176.88	-127.63	-159.71	-9.56

9:20	-172.72	-125.96	-155.79	10.51
9:30	-168.2	-124.45	-152.79	2.21
9:40	-164.8	-125.66	-150.25	-9.56
9:50	-160.98	-127.91	-147.8	-22.72
10:00	-157.64	-129.74	-145.78	-34.15
10:10	-154.45	-131.35	-144.22	-44.28
10:20	-151.32	-132.45	-142.85	-53.17
10:30	-148.48	-133.23	-141.64	-60.93
10:40	-146.32	-133.6	-140.71	-67.12
10:50	-143.94	-134	-139.75	-73.28

F.7 Repeat Low Phi Test 25 Jan 93

X Data	Thmcp1e #1	Thmcp1e #2	Thmcp1e #3	Thmcp1e #4
0:00	5.92	5.19	5.39	5.39
0:10	6.46	5.63	5.89	5.83
0:20	6.57	5.77	5.99	5.92
0:30	7.91	6.95	7.15	7.31
0:40	7.94	6.97	7.17	7.33
0:50	8.03	7.11	7.28	7.43
1:00	14.55	13.94	14.23	15.14
1:10	30.97	31.5	28.98	32.93
1:20	37.84	39.83	33.88	38.93
1:30	39.35	41.97	34.83	40.15
1:40	39.78	43.19	35.16	40.55
1:50	54.04	57.52	50.05	57.11
2:00	83.73	89.11	74.05	87.81
2:10	94.98	104.28	80.57	97.87
2:20	97.14	109.25	81.45	100.32
2:30	97.29	111.35	81.55	100.52
2:40	96.92	113.28	81.09	100.84
2:50	96.65	113.36	80.86	101.22
3:00	96.75	114.03	81.08	100.82
3:10	96.96	115.4	81.17	101.03
3:20	97.33	114.83	81.48	101.89
3:30	97.72	114.96	81.65	102.14
3:40	98.24	116.15	82.64	103.35
3:50	133.43	150.46	113.9	141.58
4:00	162.16	186.83	130.95	167.55
4:10	171.12	205.61	134.49	176.79
4:20	172.86	211.57	134.51	179.42
4:30	173.46	217.38	134.66	182.1
4:40	173.3	221.83	134.72	183.04
4:50	172.73	223.58	134.39	184.37
5:00	172.18	225.64	134.1	184.93
5:10	171.61	225.79	134.39	186.24
5:20	171.48	226.65	133.89	187.82
5:30	171.86	228.1	134.03	187.2
5:40	172.88	229.64	134.94	188.92
5:50	173.75	229.39	135.44	190.82
6:00	174.06	230.7	135.66	192.08
6:10	175.57	231.88	137.28	192.93
6:20	176.58	234.39	135.98	192.27
6:30	176.08	235.74	134.48	189.94
6:40	176.57	235.36	134.21	189.93
6:50	175.96	235.44	132.89	188.75
7:00	174.98	228.4	132.57	188.09
7:10	177.51	220.09	133.97	188.17
7:20	179.71	219.31	134.9	188.11
7:30	180.84	217.84	135.36	187.95
7:40	181.46	216.63	135.79	187.54
7:50	181.82	215.44	136.16	187.54
8:00	181.99	216.38	136.16	187.05
8:10	182.05	216.26	136.3	187.19
8:20	182.1	216.08	136.29	187.16
8:30	182.17	215.94	136.73	187.96
8:40	182.27	214.54	136.45	187.2
8:50	182.54	215.31	136.49	187.92
9:00	143	172.09	97.46	146.34
9:10	59.36	92.31	40.66	64.67

9:20	26.03	45.27	23.11	30.59
9:30	19.69	27.03	19.61	21.33
9:40	18.32	20.09	18.58	18.79
9:50	17.81	18.11	18.09	18.03
10:00	17.35	17.19	17.6	17.49
10:10	16.9	16.67	17.11	16.98

X Data	Thmcpie #7	Thmcpie #8	Thmcpie #5	Thmcpie #6
0:00	6.74	5.43	3.62	5.83
0:10	6.89	5.66	3.97	6.14
0:20	7.06	5.71	4.08	6.13
0:30	8.38	6.97	4.97	7.5
0:40	8.39	7.01	4.98	7.54
0:50	8.48	7.13	5.09	7.63
1:00	8.6	13.67	11.56	16.67
1:10	8.69	25.68	23.15	38.47
1:20	8.81	30.61	26.94	47.23
1:30	8.93	32.25	27.59	49.82
1:40	9.07	33.53	28.18	50.77
1:50	9.26	47.09	41.2	69.58
2:00	9.47	68.92	60.67	108.81
2:10	9.72	77.66	66.54	127.03
2:20	9.97	81.44	68.09	134.25
2:30	10.19	83.08	68.66	137.67
2:40	10.43	84.83	68.59	140.75
2:50	10.72	86.02	69.04	141.36
3:00	10.99	86.47	69.22	142.33
3:10	11.21	87.37	69.6	143.62
3:20	11.44	88.29	69.92	143.72
3:30	11.65	89.09	70.06	144.9
3:40	11.81	90.98	71.21	146
3:50	12.21	114.93	100.91	187.11
4:00	12.57	130.5	116.6	223.48
4:10	12.93	137.45	120.78	241.74
4:20	13.32	141.2	121.98	251.92
4:30	13.76	145.06	123.58	259.09
4:40	14.16	147.46	124.17	264.69
4:50	14.59	149.14	124.47	269.89
5:00	14.9	150.46	124.98	270.81
5:10	15.27	151.46	125.27	273.43
5:20	15.58	152.52	125.53	277.05
5:30	15.95	153.41	126.25	278.38
5:40	16.22	154.54	127.33	282.31
5:50	16.52	156.06	128.15	281.96
6:00	16.81	156.39	128.48	286.27
6:10	17.03	157.94	130.04	290.06
6:20	17.32	158.42	128.89	292.77
6:30	17.63	160.18	128.18	294.89
6:40	17.86	161.92	128.2	303.36
6:50	18.1	162.77	127.69	306.58
7:00	18.35	164.03	126.69	310.13
7:10	18.62	165.18	124.74	313.84
7:20	18.88	166.24	123.9	315.83
7:30	19.06	166.75	123.35	315.8
7:40	19.23	166.76	123.25	315.8
7:50	19.49	167.45	123.25	317.92
8:00	19.61	168.22	123.09	317.23
8:10	19.76	168.68	123.25	316.4
8:20	19.9	169.23	123.5	316.85
8:30	20	169.52	123.65	318.82
8:40	20.19	169.62	123.63	318.54
8:50	20.34	168.92	124.06	317.47
9:00	20	139.8	81.54	278.17
9:10	19.45	93.16	29.57	197.1

9:20	19.05	67.55	19.45	131.48
9:30	18.72	53.57	17.57	76.02
9:40	18.16	40.81	16.76	41.05
9:50	17.75	33.69	16.28	28.03
10:00	17.24	29	15.79	22.81
10:10	16.74	26.02	15.39	20.44

Figure F.8 High Phi Retest 26 Jan 93

X Data	Thmcp1e #1	Thmcp1e #2	Thmcp1e #3	Thmcp1e #4
0:00	-174.58	-163.38	-174.18	-171.41
0:10	-169.97	-159.42	-169.44	-166.3
0:20	-121.96	-105.62	-121.33	-109.9
0:30	-87.99	-40.54	-92.44	-70.54
0:40	-91.51	-13.82	-96.47	-71.57
0:50	-95.38	-2.22	-99.44	-72.05
1:00	-97.7	3.4	-101.21	-72.27
1:10	-98.95	6.54	-102.33	-72.34
1:20	-100.08	7.88	-103.77	-72.18
1:30	-101	9.89	-104.52	-71.95
1:40	-101.66	11.07	-105.03	-71.89
1:50	-102.14	9.75	-105.64	-71.8
2:00	-102.86	10.56	-106.32	-71.98
2:10	-103.17	10.56	-106.32	-71.98
2:20	-81.27	25.89	-82.65	-46.51
2:30	-57.85	70.49	-64.26	-15.87
2:40	-61.67	91.66	-67.48	-13.09
2:50	-59.95	100	-62.76	-5.96
3:00	-60.28	104.1	-62.21	1.2
3:10	-61.42	112.5	-62.45	5.88
3:20	-56.66	118.84	-55.43	17.28
3:30	-16.25	196.11	-21.16	59.95
3:40	-16.64	237.43	-24.7	71.98
3:50	-23.11	243.69	-28.45	83.24
4:00	-31.08	260.44	-32.75	93.32
4:10	-37.72	276.86	-36.28	104.22
4:20	-48.11	262.93	-41.83	130.23
4:30	-59.36	285.29	-53.33	162.57
4:40	-63.03	313.61	-61.02	197.93
4:50	-67.05	347.1	-67.15	224.52
5:00	-70.33	354.73	-70.72	264.81
5:10	-73.44	365.59	-74.24	274.46
5:20	-74.81	375.22	-76.37	289.92
5:30	-75.31	386.32	-78.09	302.78
5:40	-75.14	398.54	-79.59	312.69
5:50	-74.61	403.68	-80.63	319.52
6:00	-73.24	397.32	-80.99	313.27
6:10	-71.47	392.03	-81.69	321.33
6:20	-69.6	403.44	-82.07	322.53
6:30	-67.72	402.28	-82.62	324.95
6:40	-65.46	402.97	-82.84	322.97
6:50	-63.07	409.15	-82.95	327.95
7:00	-60.81	407.43	-82.75	325.69
7:10	-58.43	402.72	-83.13	331.68
7:20	-56.38	406.29	-83.28	328.43
7:30	-53.84	409.47	-83.18	329.03
7:40	-51.86	398.36	-83.29	332.69
7:50	-50.04	398.97	-82.88	336.27
8:00	-47.73	399.01	-82.94	333.01
8:10	-45.21	398.68	-82.9	335.66
8:20	-24.01	428.72	-61.33	343.52
8:30	-5.88	470.43	-56.65	368.83
8:40	-0.19	503.28	-61.41	378.37
8:50	8.218	469.37	-62.91	360.35
9:00	11.58	407.37	-56.48	342.74
9:10	210.99	462.53	70.019	355.37

9:20	11.213	200.26	-24.89	133.48
9:30	-75.63	96.42	-148	28.42
9:40	-120.46	13.43	-160.62	-25.15
9:50	-148.76	-35.55	-163.32	-60.48
10:00	-159.16	-70.77	-165.41	-91.31
10:10	-161.24	-95.441	-165.71	-113.71
10:20	-162.41	-115.31	-165.31	-132.06
10:30	-163.18	-133.75	-165.82	-151.14
10:40	-163.62	-155.56	-167.17	-166.35
10:50	-165	-166.91	-168.35	-168.06

X Data	Thmcp1e #7	Thmcp1e #8	Thmcp1e #5	Thmcp1e #6
0:00	-173.91	-169.14	-140.81	-171.33
0:10	-174.53	-162.25	-138.15	-164.48
0:20	-174.8	-111.21	-84.06	-98.39
0:30	-174.67	-76.51	-51.1	-36.75
0:40	-174.41	-66.4	-54.33	-9.48
0:50	-174.08	-62.12	-57.02	15.59
1:00	-173.83	-59.84	-59.1	32.74
1:10	-173.56	-57.54	-60.48	49.48
1:20	-173.42	-55.97	-61.99	59.61
1:30	-173.25	-54.61	-63.51	68.82
1:40	-173.2	-53.78	-64.62	72.46
1:50	-173.17	-52.98	-65.44	77.24
2:00	-173.17	-52.72	-66.46	83.28
2:10	-173.16	-52.54	-67.27	84.13
2:20	-173.14	-26.8	-46.05	108.58
2:30	-173.2	-5.89	-29.84	142.61
2:40	-173.01	-4.13	-34.49	145.05
2:50	-173.09	-3.71	-34.8	147.88
3:00	-173.24	-2.05	-37.84	148.46
3:10	-173.22	-2.25	-38.85	147.24
3:20	-173.32	3.09	-33.52	155.73
3:30	-173.34	31.69	-3.48	193.36
3:40	-173.24	34.41	-5.58	198.33
3:50	-173.12	34.58	-10.08	208.2
4:00	-173.15	33.44	-14.77	218.9
4:10	-172.85	35.02	-19.18	228.63
4:20	-172.84	30.86	-33.49	240.03
4:30	-172.68	25.02	-45.94	268.5
4:40	-172.4	25.57	-41.96	302.15
4:50	-172.25	24.77	-35.27	332.27
5:00	-172.04	26.22	-27.34	354.68
5:10	-171.83	26.13	-18.73	355.69
5:20	-171.74	24.73	-9.43	361.02
5:30	-171.52	23.83	-1.97	372.57
5:40	-171.34	23.81	4.05	367.37
5:50	-171.3	25.37	10.62	374.04
6:00	-171.13	24.74	15.49	378.64
6:10	-170.96	25.15	19.27	379.74
6:20	-170.82	24.04	22.14	378.6
6:30	-170.82	23.6	25.64	379.24
6:40	-170.64	24.33	27.91	377.6
6:50	-170.52	24.42	29.9	380.51
7:00	-170.52	24.62	32.86	385.01
7:10	-170.34	24.78	35.24	388.89
7:20	-170.31	24.65	37.14	379.84
7:30	-170.18	24.17	39.19	389
7:40	-170.32	24.05	40.31	380.99
7:50	-170.15	24.26	42.31	383.88
8:00	-170.09	25.6	44.46	388.28
8:10	-170.05	26.1	46.09	388.06
8:20	-169.89	46.44	64.43	405.72
8:30	-169.3	56.26	84.83	429.96
8:40	-168.61	53.74	94.03	443.45
8:50	-167.86	56.83	103.91	475.73
9:00	-166.59	110.61	88.64	442.43
9:10	-165.69	138.43	891.8	386.24

9:20	-166.03	12.62	202.13	215.56
9:30	-167.18	-68.92	2.84	118.89
9:40	-168.69	-98.94	-90.91	68.84
9:50	-169.98	-119.2	-142.29	21.85
10:00	-171.15	-133.04	-153.63	-14.89
10:10	-172.03	-144.23	-154.56	-46.56
10:20	-172.84	-152.12	-154.95	-73.23
10:30	-173.35	-157.11	-155.16	-103.75
10:40	-174.47	-161.74	-155.29	-156.9
10:50	-175.69	-164.71	-156.98	-171.14

APPENDIX G

EXTRA MODELING RESULTS

This Appendix contains modeling results of stability analysis, (ϕ vs Re) and other cases using 1D codes and SIMBED.

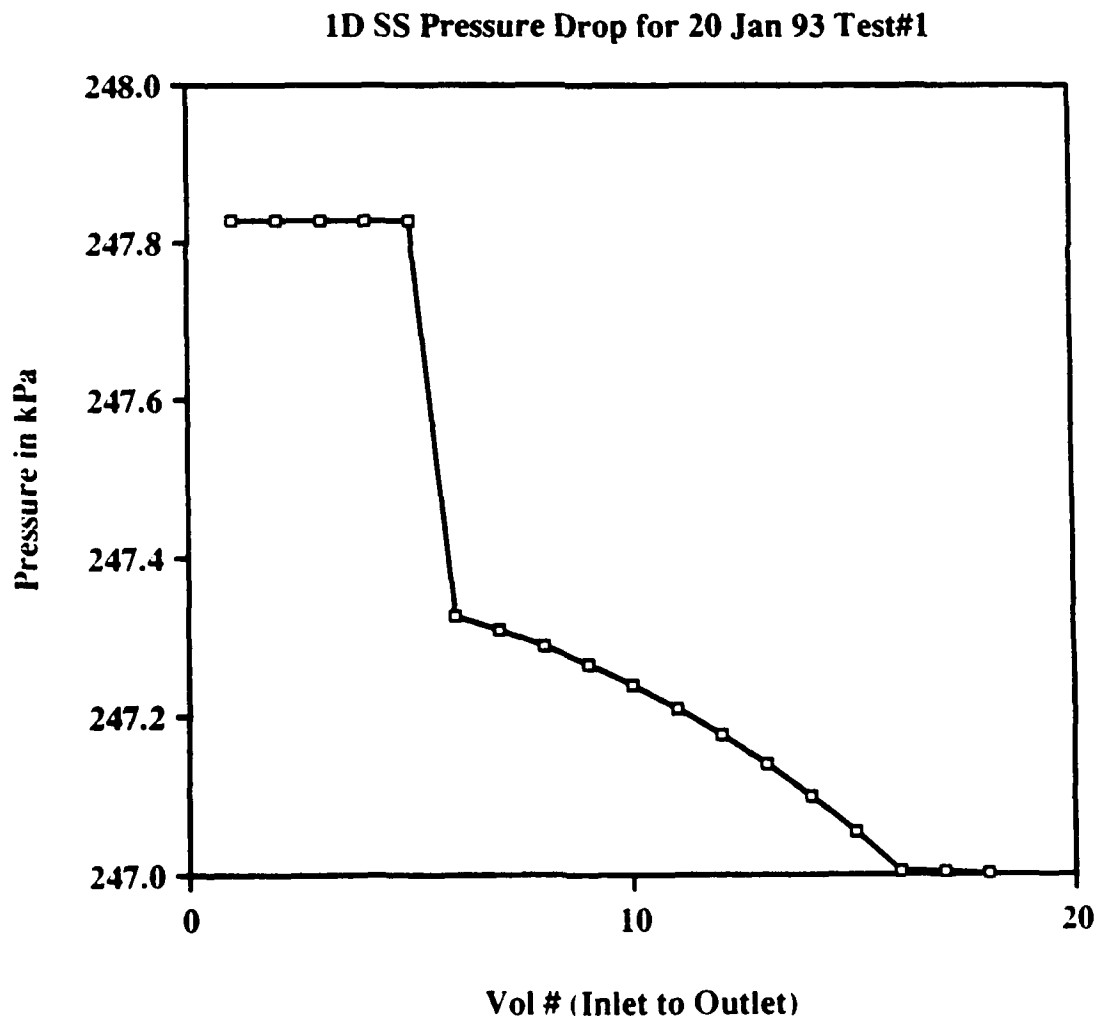
G.1 1D PRESSURE DROP

A steady-state code called STEADY was written by William Casey [C-4]. This code modelled the PBR element in three control volumes and solved for the element conditions given the inlet temperature, inlet and outlet pressures, and the power density. The primary outputs from the program were the outlet temperature and mass flow rate. Jonathan Witter modified this code to accommodate more for rocket engine performance, where chamber pressure and temperature are key parameters [W-3]. The new code called Particle Bed Reactor - Find Mass and Pressure (PBRFMP) requires the inlet and outlet temperatures, the outlet pressure, and the fuel region power density. It then iterates to solve for the inlet pressure and flow rate. The results of the pressure drop analysis are shown in Figure G.1.1. The pressure drop was low and was not a good comparison to the SIMBED run and the test conducted in Appendix C (The total resistances were very close, 3.3769×10^7 Pa/kg²s² for the pressure test and 2.969×10^7 Pa/kg²s² for the 1D run. These resistances seemed to match too closely since the experiment in Appendix C did not have gas pass through the cold frit). SIMBED showed that the hot frit had the biggest pressure drop since the porosities of the frits were equal. The PBRFMP result was typical to the more prototypic element (Figure G.1.1). It was

speculated that the low flow rates may of had an impact on the different result in the 1D case.

The gas properties are based on ideal gas assumptions and curve fits for the thermal conductivity and heat capacity as a function of only the gas temperature. Some of the steady state run results are shown in this Appendix. Since there were other transient codes available and the outlet pressure was not a known parameter in the experiments, the 1D SS code was not used for a lot of the analysis.

Figure G.1.1 1D SS Pressure Drop



G.2 1D TRANSIENT

The Triple Transient (TRITRAN) code was written by Jonathan Witter to study the 1D transient behavior of a PBR fuel element [W-3]. This code changed the heat transfer correlation from the Nusselt number correlation to the Auchenbach correlation from the 1D SS code. This code required the inlet temperature, the inlet pressure, the power density at the ramp endpoints, the duration of the ramps, and the mass flow rate as the variable boundary conditions. This code was better to use than the steady state version. Since the power, inlet temperature, inlet pressure, and mass flow rate were all known parameters for each test, they could be used to calculate the outlet temperature (thermocouple #8) for comparison and help in determining the experimental uncertainties. A sample input deck for a run is shown in Table G.2.1 and a picture of the element layouts.

Table G.2.1 Input for TRITRAN Runs and Pictures of Element Layouts

STANDARD FLOW DIMENSION DATA		FUEL PARTICLE BASELINE DATA	
1. ORIFICE RADIUS (m)	07000	1. FUEL KERNEL RADIUS (m)	.00017
2. ORIFICE LENGTH (m)	00500	2. LAYER 1 RADIUS (m)	.00017
3. INLET CHANNEL RADIUS (m)	06000	3. LAYER 2 RADIUS (m)	.00018
4. INLET SLOT WIDTH (m)	07000	4. LAYER 3 RADIUS (m)	.00019
5. INLET SLOT LENGTH (m)	00400	5. FUEL DENSITY (Kg/m3)	8000.00
6. INLET REGION RADIUS (m)	.05000	6. LAYER 1 DENSITY (Kg/m3)	3960.00
7. COLD FRIT OUTER RADIUS (m)	.03150	7. LAYER 2 DENSITY (Kg/m3)	3960.00
8. FUEL BED OUTER RADIUS (m)	.03000	8. LAYER 3 DENSITY (Kg/m3)	3960.00
9. HOT FRIT OUTER RADIUS (m)	.01900	9. FUEL Cp (J/Kg)	460.000
10. HOT FRIT INNER RADIUS (m)	.01750	10. LAYER 1 Cp (J/Kg)	1050.000
11. FUEL LENGTH (m)	.10000	11. LAYER 2 Cp (J/Kg)	1050.000
12. OUTLET EXTENSION LENGTH (m)	1.00000	12. LAYER 3 Cp (J/Kg)	1050.000
13. COLD FRIT POROSITY	.30000	13. FUEL k (W/m2/K)	19.000
14. FUEL BED POROSITY	.37000	14. LAYER 1 k (W/m2/K)	4.000
15. HOT FRIT POROSITY	.30000	15. LAYER 2 k (W/m2/K)	4.000
16. COLD FRIT PARTICLE DIAM. (m)	.0000200	16. LAYER 3 k (W/m2/K)	4.000
17. FUEL PARTICLE DIAM (m)	.00038		
18. HOT FRIT FLOW DIAM. (m)	.00002		
19. INLET MANIFOLD FACTOR	.95000		
20. OUTLET MANIFOLD FACTOR	1.10000		
ENTER [NUMBER] [VALUE] TO CHANGE (eg 2 .002)		ENTER [NUMBER] [VALUE] TO CHANGE (eg 2 .002)	
ENTER 0 0. TO MOVE ON		ENTER 0 0. TO MOVE ON	

TRANSIENT BOUNDARY CONDITION DATA

1. INITIAL INLET TEMPERATURE (K)	99.0000
2. INLET TEMP AT END OF FIRST RAMP (K)	99.9100
3. INLET TEMP AT END OF SECOND RAMP (K)	99.9200
4. INLET TEMP AT END OF THIRD RAMP (K)	99.9200
5. INITIAL INLET PRESSURE (kPa)	612.24
6. INLET PRESSURE AT END OF FIRST RAMP (kPa)	612.24
7. INLET PRESSURE AT END OF SECOND RAMP (kPa)	612.24
8. INLET PRESSURE AT END OF THIRD RAMP (kPa)	612.24
9. INITIAL FLOW RATE (kg/s)	.00350
10. FLOW RATE AT THE END OF FIRST RAMP (kg/s)	.00350
11. FLOW RATE AT THE END OF SECOND RAMP (kg/s)	.00350
12. FLOW RATE AT THE END OF THIRD RAMP (kg/s)	.00350
13. INITIAL POWER DENSITY (GW/m ³)	.0180
14. POWER DENSITY AT END OF FIRST RAMP (GW/m ³)	.0180
15. POWER DENSITY AT END OF SECOND RAMP (GW/m ³)	.0180
16. POWER DENSITY AT END OF THIRD RAMP (GW/m ³)	.0180

ENTER [NUMBER] [VALUE] TO CHANGE (eg 2 .5)
 ENTER 0 0. TO MOVE ON

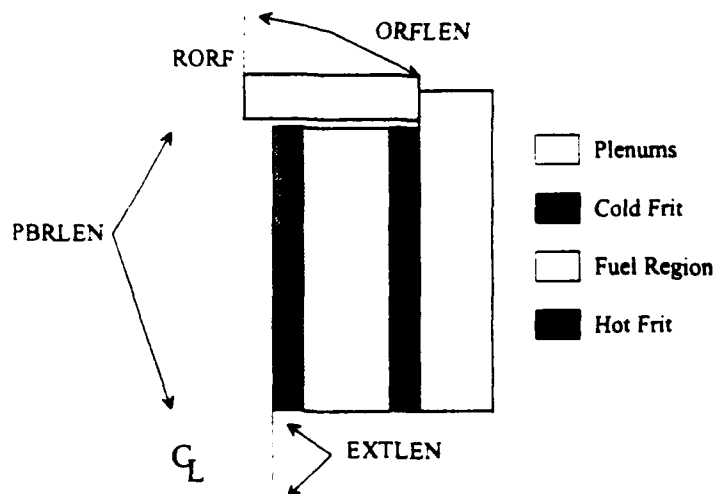
TRANSIENT DURATION TIMING DATA

1. TIME DELAY BEFORE TRANSIENT (sec)	.0120
2. DURATION OF RAMP 1 (sec)	.0100
3. DURATION OF RAMP 2 (sec)	.0100
4. DURATION OF RAMP 3 (sec)	.0100
5. RUN TIME AFTER TRANSIENT OVER (sec)	.0100
6. TIME STEP (sec)	.0001
7. INFO SAVED EVERY X TIME STEPS (#)	1000

ENTER [NUMBER] [VALUE] TO CHANGE (eg 2 .5)

ENTER 0 0. TO MOVE ON

Taken from W-3



Taken from W-3

The first analysis focused on the first test conducted on 20 Jan 93 (Bed Test at Low Phi). This test was looked at since it seemed the temperatures were high for the amount of power used. The outlet temperature from the runs compared to the measured temperatures showed that there was a mismatch (see Figure G.2.1). The mismatch followed the same energy balance trend where the calculated outlet temperature is lower than the temperature measured at thermocouple #8. However, Figures G.2.2- G.2.4 show that the analysis depended on what time of the experiment the transient was analyzed. In some cases there was much better agreement on the calculated to measured temperature.

Figure G.2.1 Bed Test At Low Phi Transient Analysis

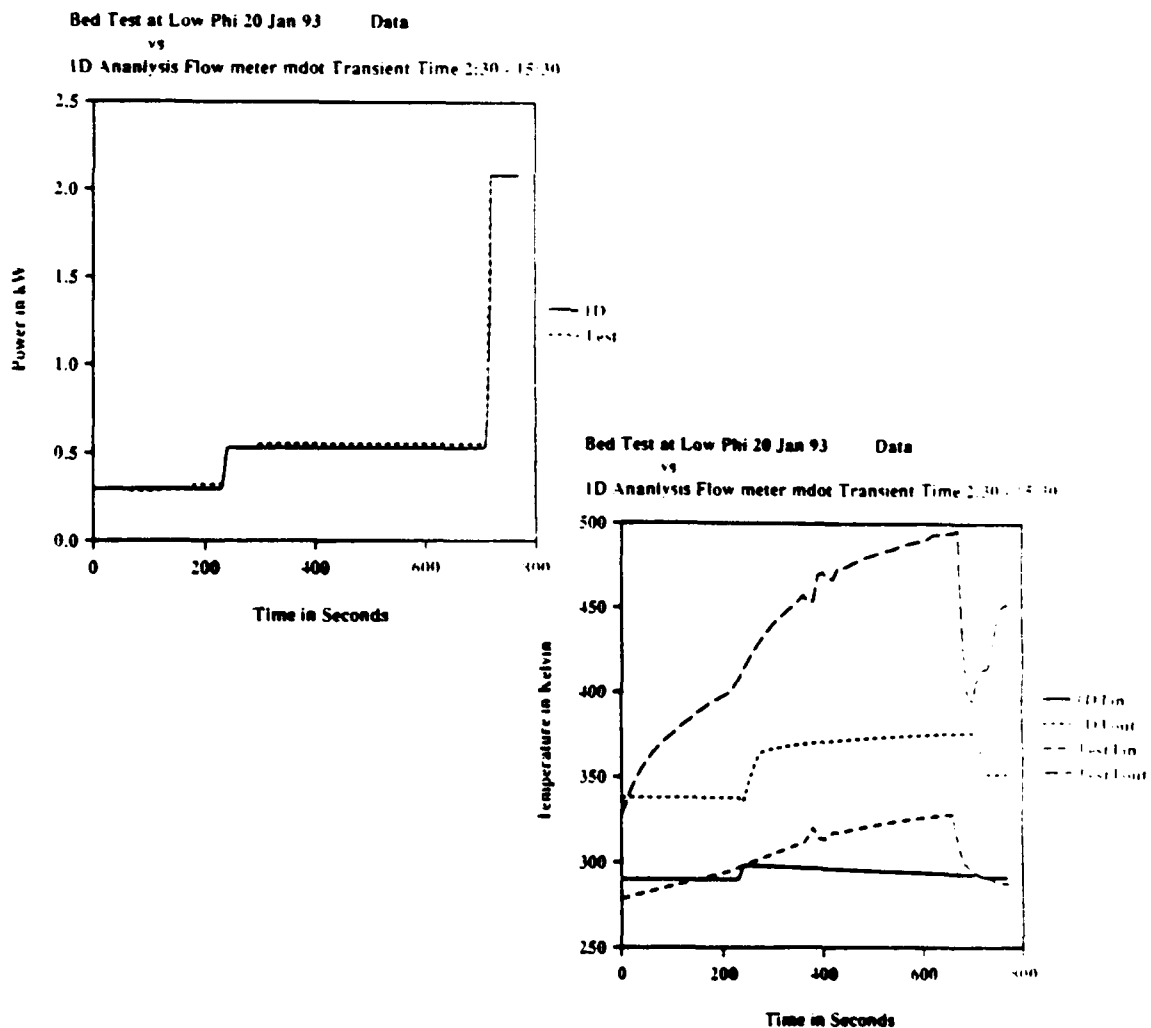


Figure G.2.2 Repeat Test at Low Phi Transient Analysis

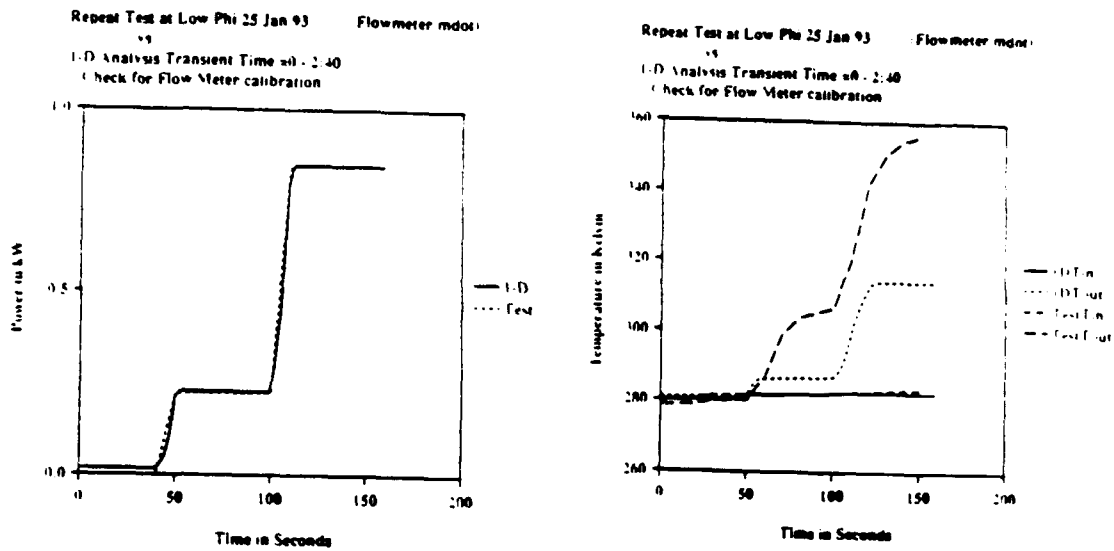


Figure G.2.3 High Phi Lower Pressure (Test #6) Transient Analysis

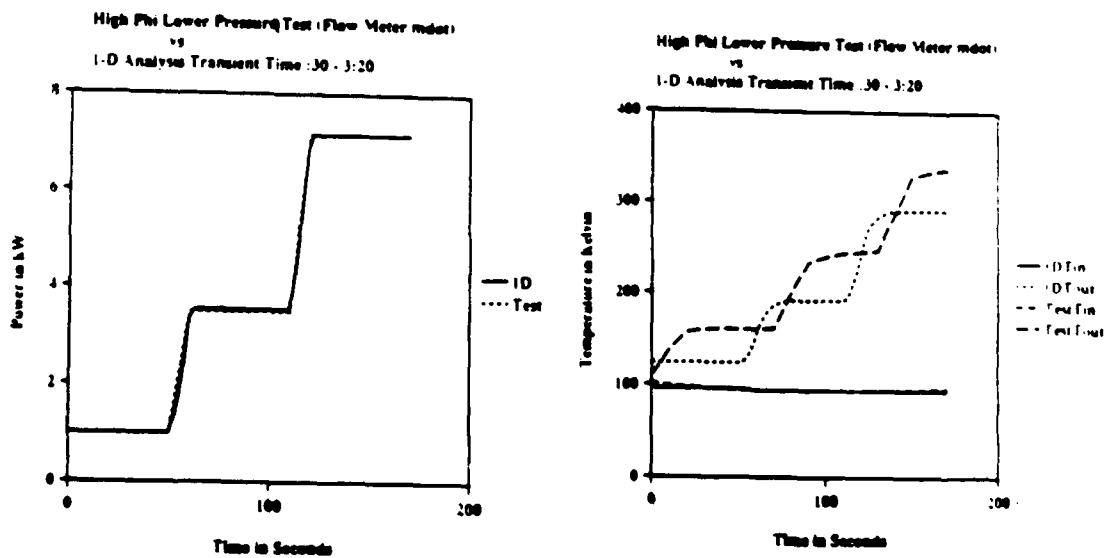
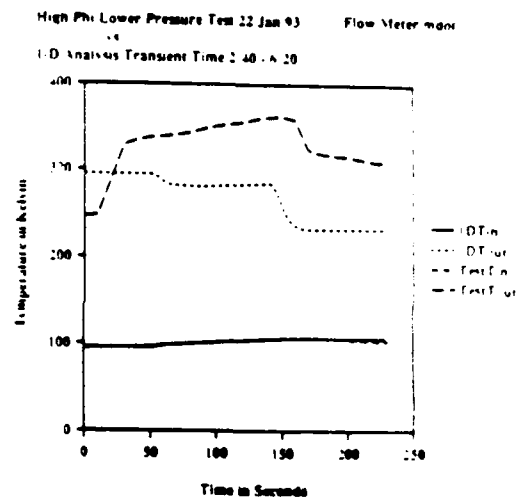
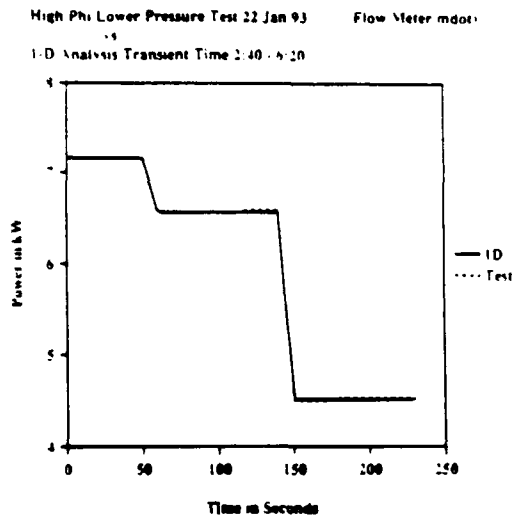


Figure G.2.4 High Phi Lower Pressure Test Different Transient



More plots for other transients analyzed are included further in the Appendix. These plots also include the power ramps for the transient (The plots shown above had equal powers for the experiment and code result). All of the power ramps analyzed used the console power display, which was shown to be a little bit lower than the actual power supplied to the bed. However, since these analyses were the first runs done after the experiment, the results lead to the power supply investigation discussed in Appendix C. Since the SIMBED code had better accuracy because of a finer mesh size, it was used to continue the analyses.

G.3 OTHER RESULTS

The pressure drop calculations for the SIMBED runs is not as sharp as the runs in Chapter 5 due to that the wrong cold frit and hot frit resistances were used. This error occurred due to the wrong porosity was used to calculate the resistance terms (0.64 instead of 0.30). This error was caused due that the runs were started before the frit porosity experiments were performed and the porosity in the literature [B-2] showed that the porosity for the frits was expected to be 0.64. Since the relative effects can still be shown, and many hours of computer time were used to generate the results, they are included in this Appendix.

The Phi versus Reynolds number calculations shown using the energy balance mass flow rate are included for an error bar analysis. Since the flowmeter calibration was not 100% (Appendix C), if the flow meter was a little off to match closer to the power input, these plots show the impact on Reynolds number for some of the experiments conducted.

Figure G.3.1 Phi vs Reynolds Number Showing 1DSS Result Test #8

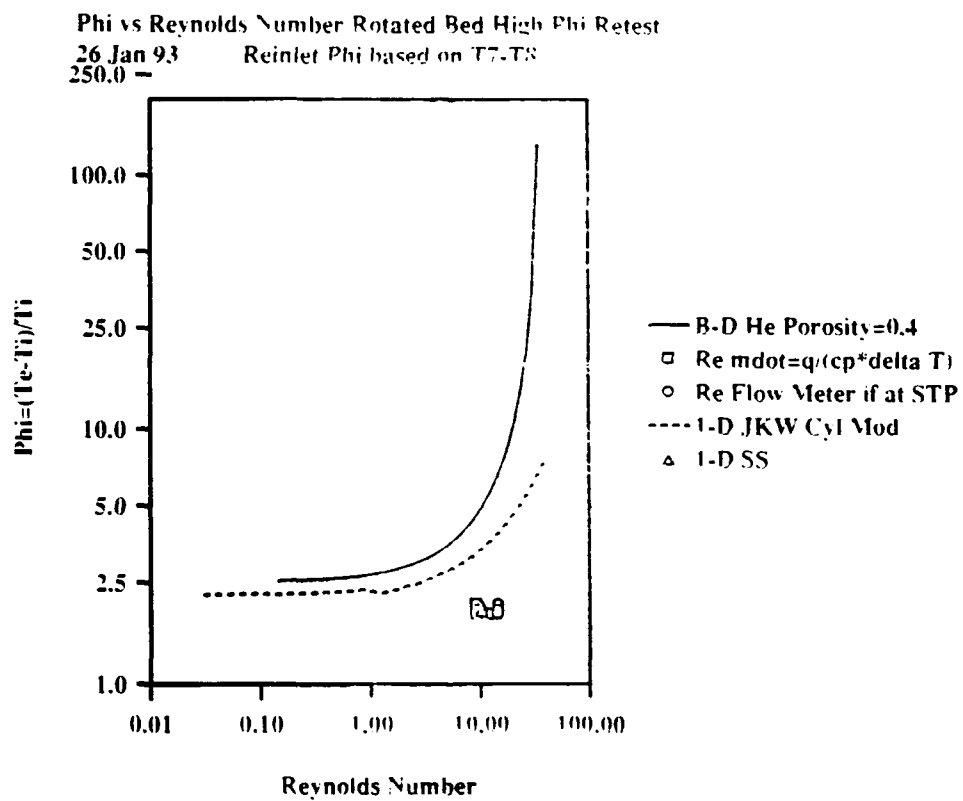


Figure G.3.2 Phi vs Reynolds Number Showing 1DSS Result Test #5

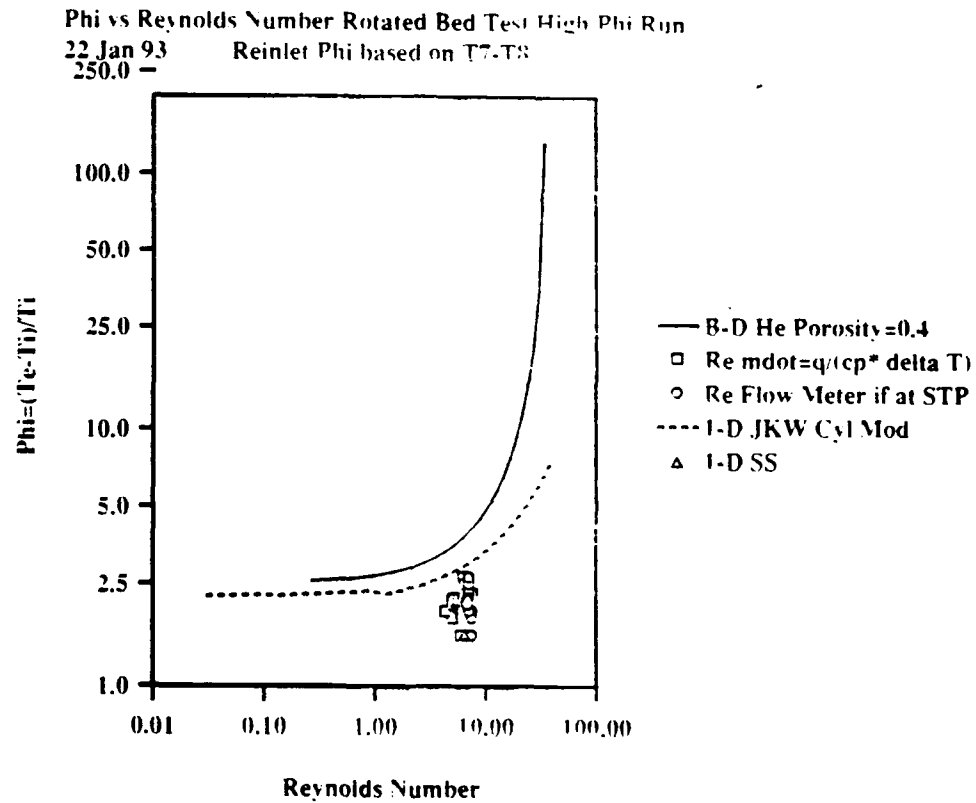


Figure G.3.3 Phi vs Reynolds Number Showing 1DSS Result Test #6

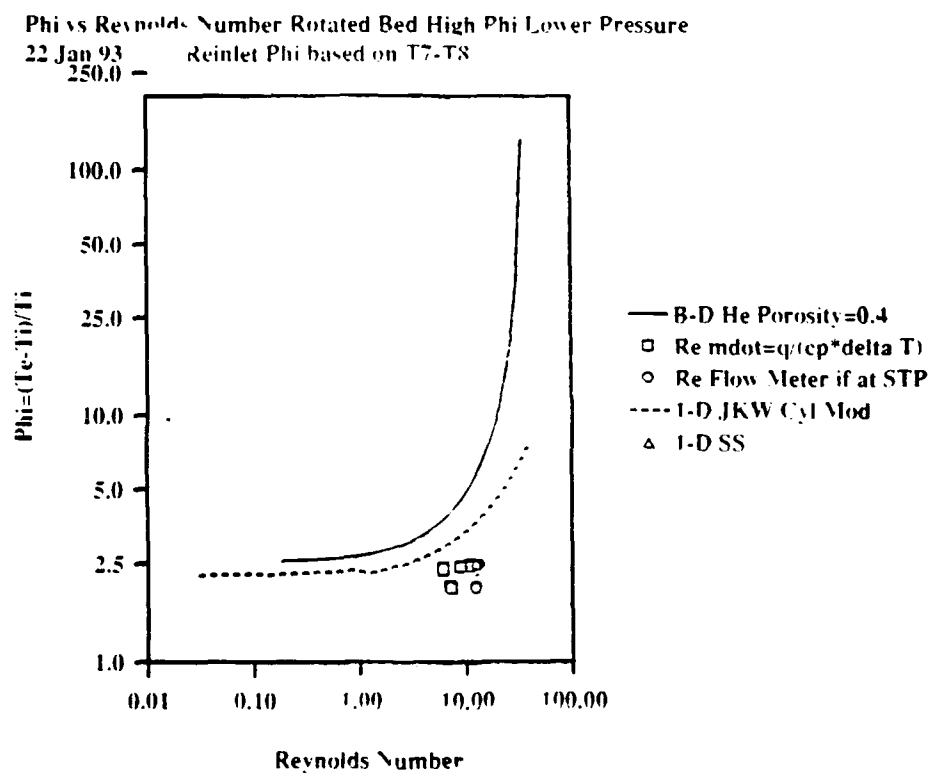


Figure G.3.4 Phi vs Reynolds Number for Energy Balance Mdot and
Flowmeter Mdot Test #5

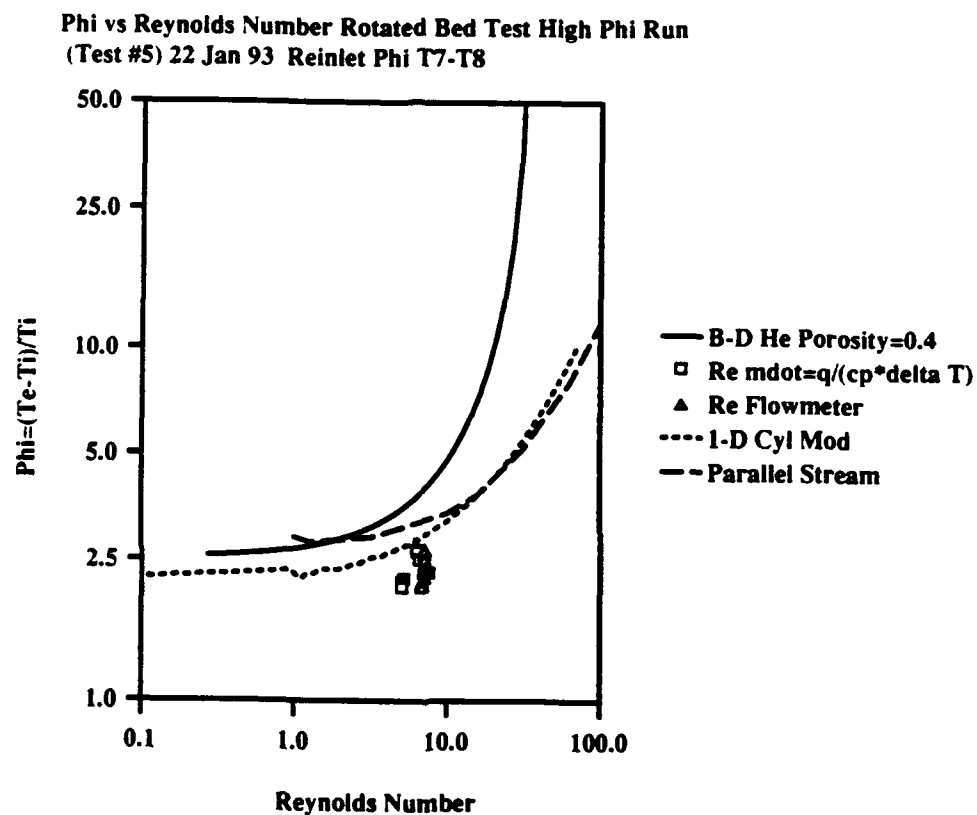


Figure G.3.5 Phi vs Reynolds Number for Energy Balance Mdot and
Flowmeter Mdot Test #8

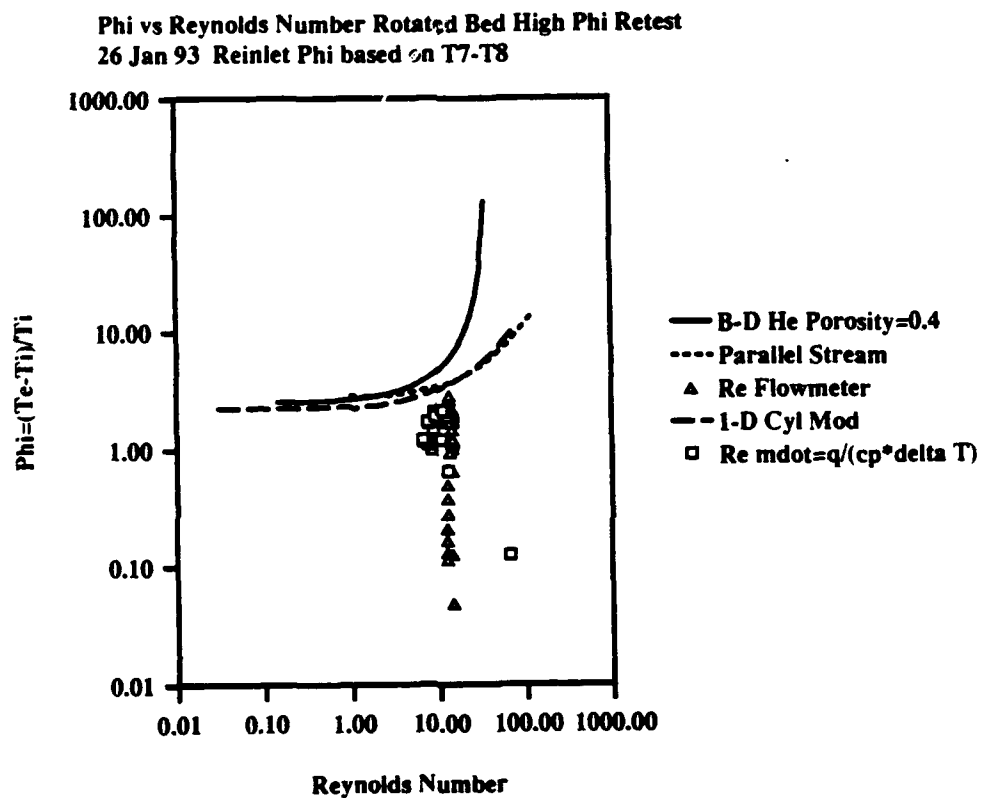


Figure G.3.6 Phi vs Reynolds Number for Energy Balance Mdot and
Flowmeter Mdot Test #6

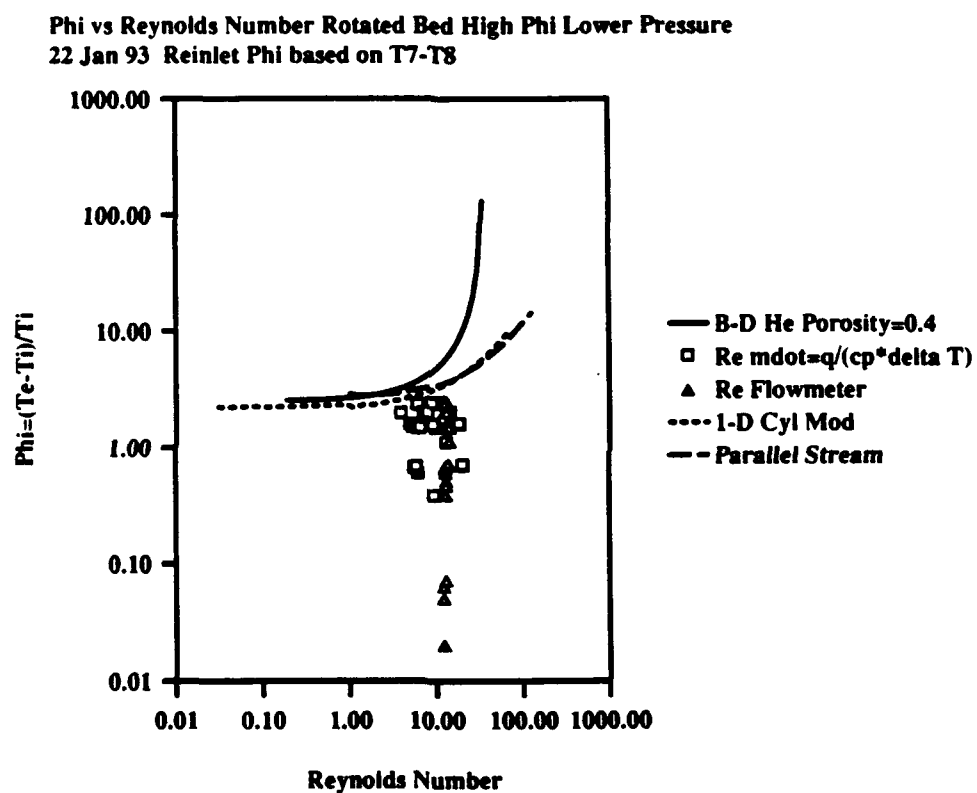


Figure G.3.7 TRITRAN Run for Test #4 (Power Ramps)

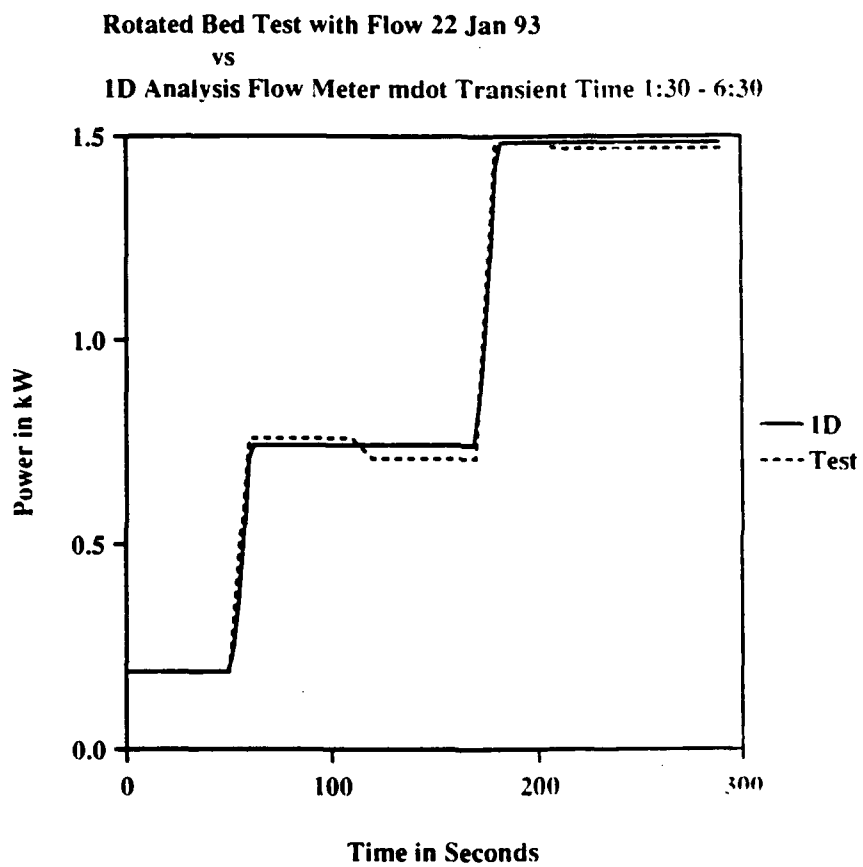


Figure G.3.8 TRITRAN Run for Test #4 (Temperatures)

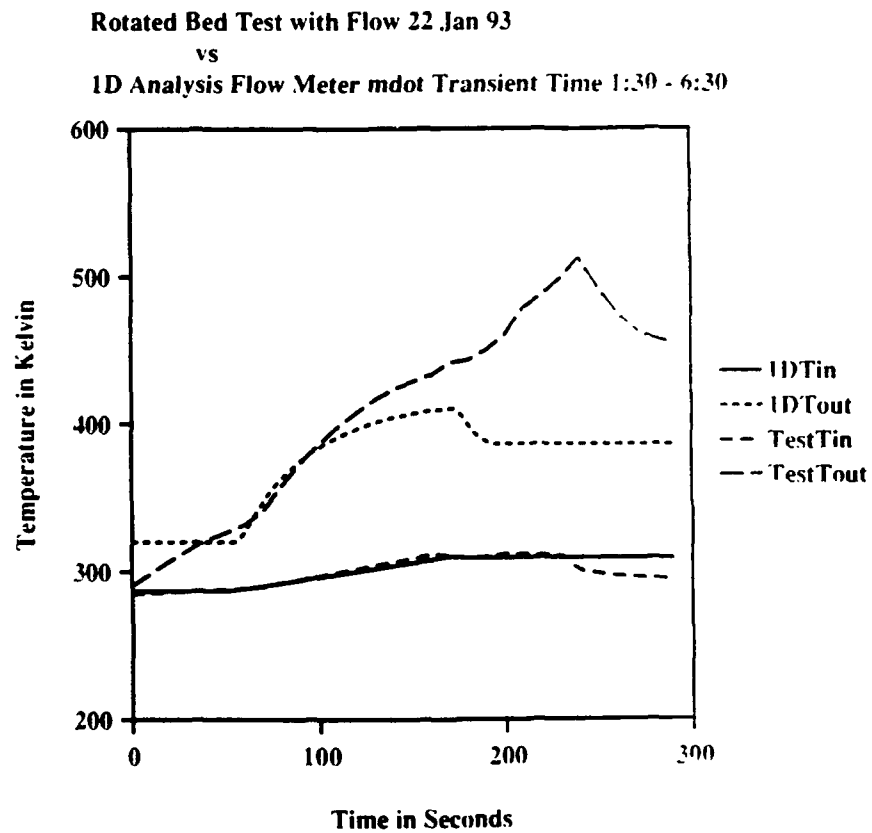


Figure G.3.9 TRITRAN Run for Test #1 (Power Ramps)

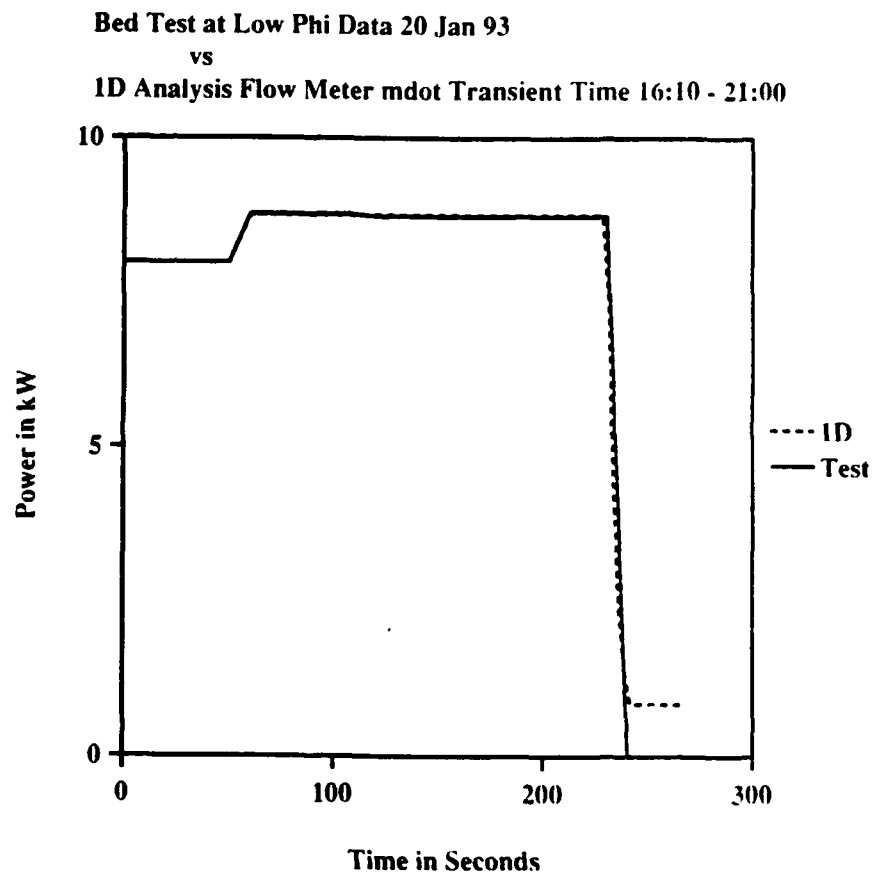


Figure G.3.10 TRITRAN Run for Test #1 (Temperatures)

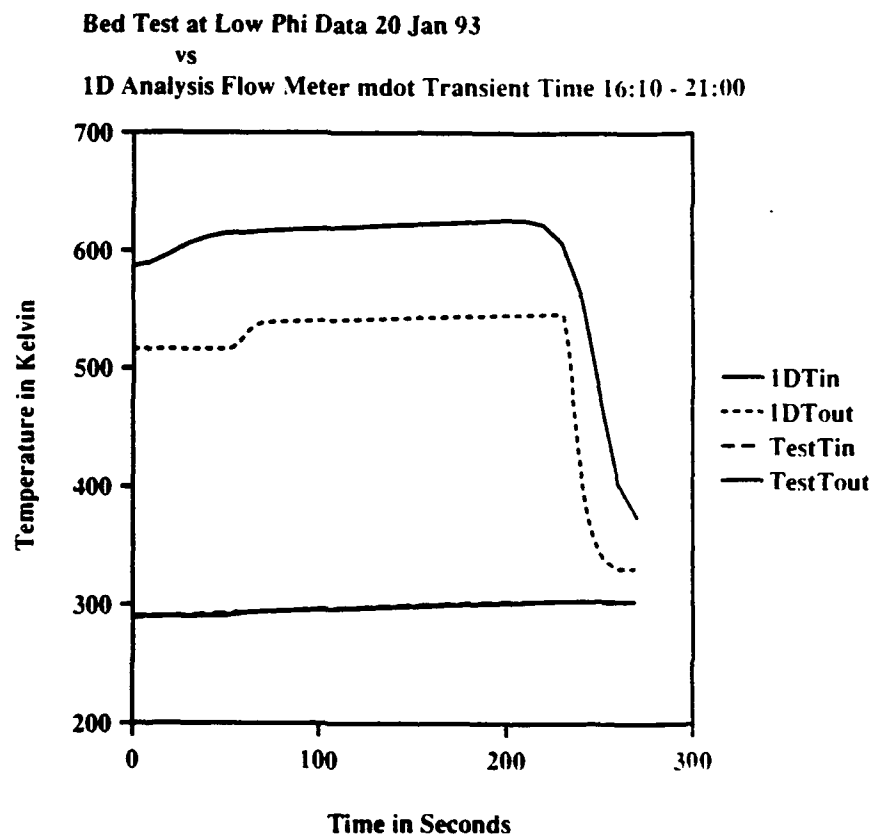


Figure G.3.11 TRITRAN Run for Test #4 - Different Time(Power Ramps)

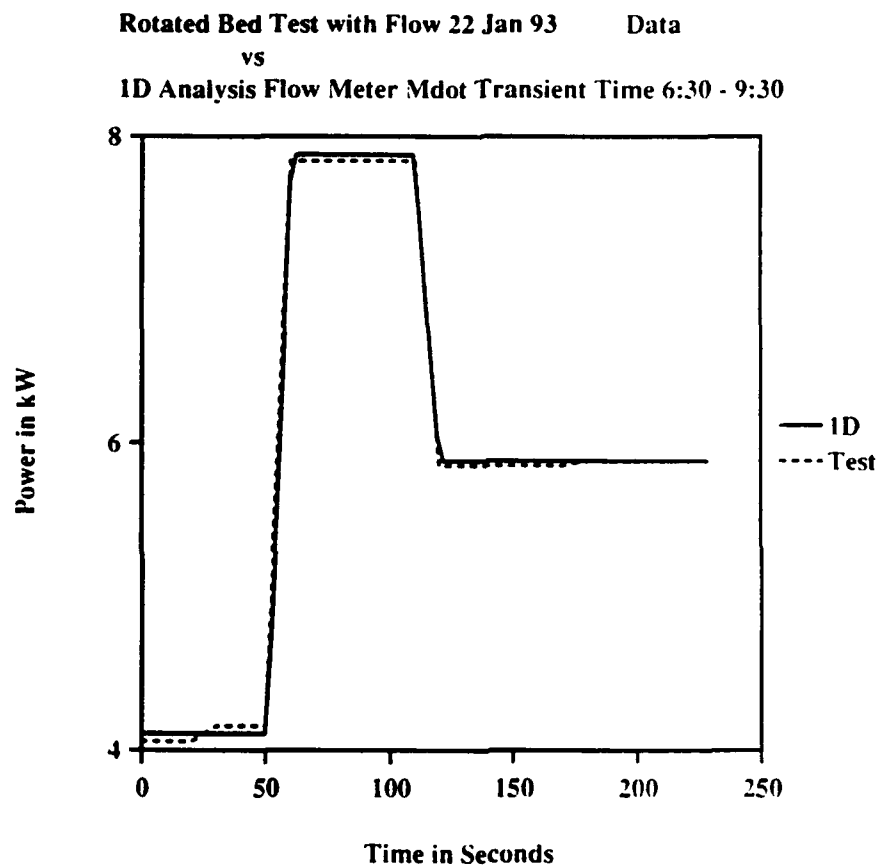


Figure G.3.12 TRITRAN Run for Test #4 - Different Time(Temperatures)

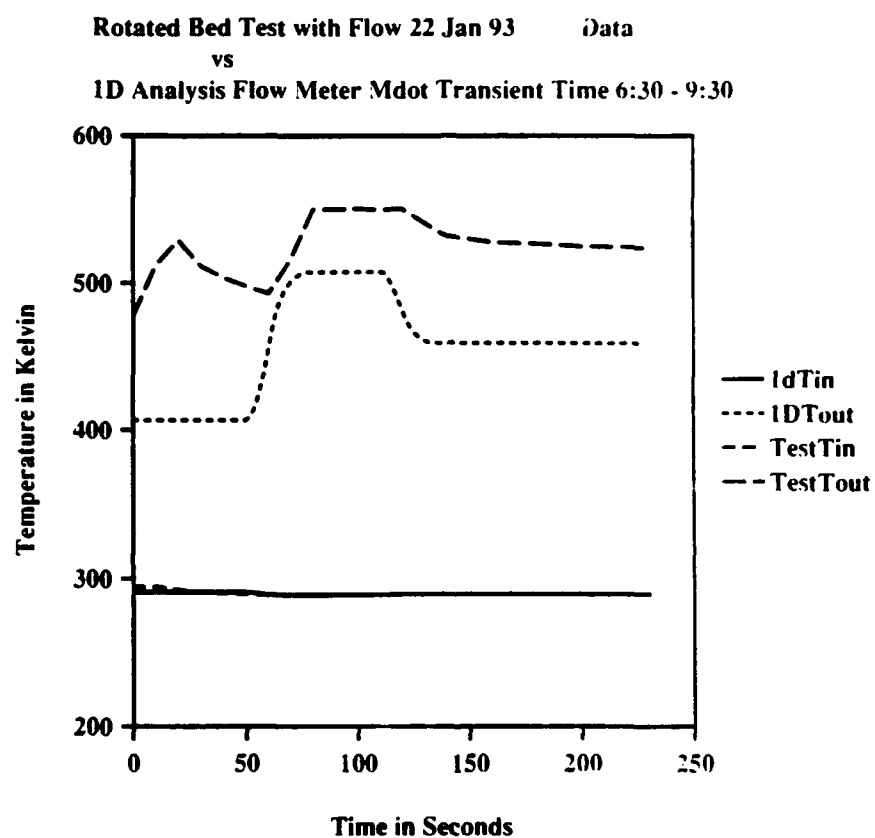


Figure G.3.13 TRITRAN Run For Test #5 (Power Ramps)

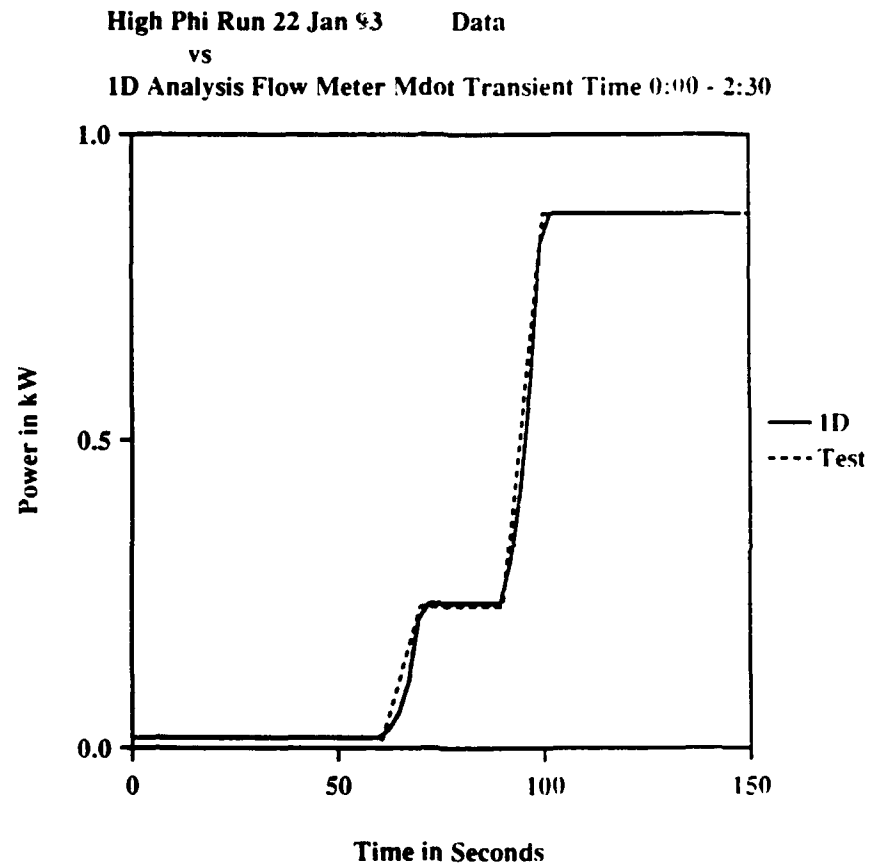


Figure G.3.14 TRITRAN Run For Test #5 (Temperatures)

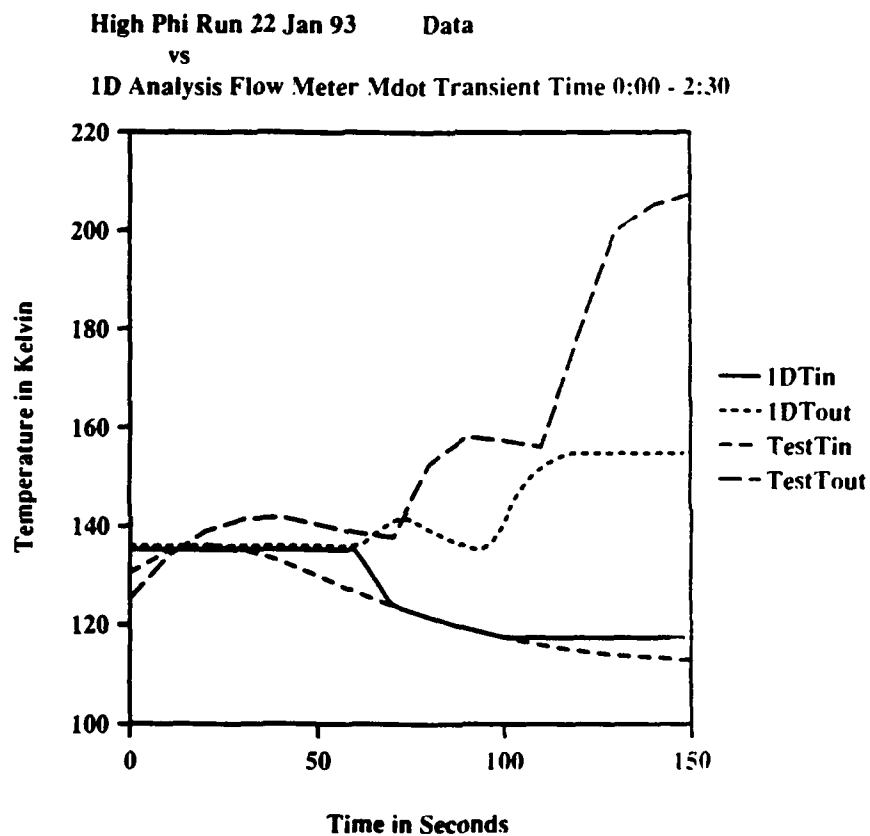


Figure G.3.15 TRITRAN Run For Test #5 -Different Time (Power Ramps)

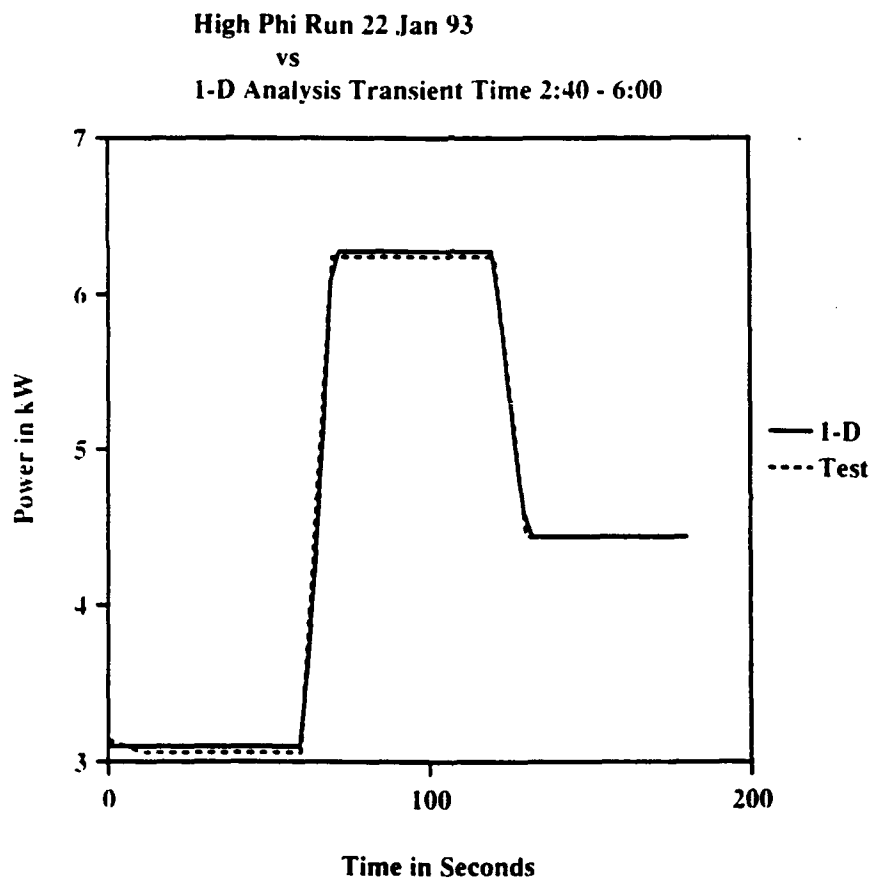


Figure G.3.16 TRITRAN Run For Test #5 -Different Time (Temperatures)

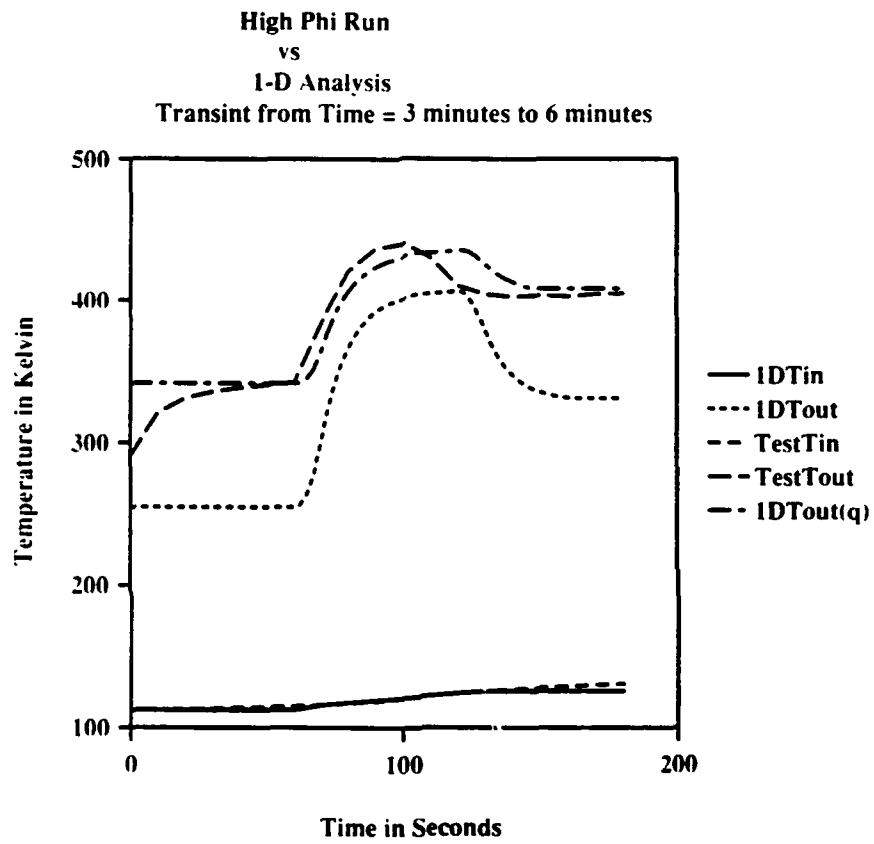


Figure G.3.17 TRITRAN Run Bigger Particle Size (Power Ramps)

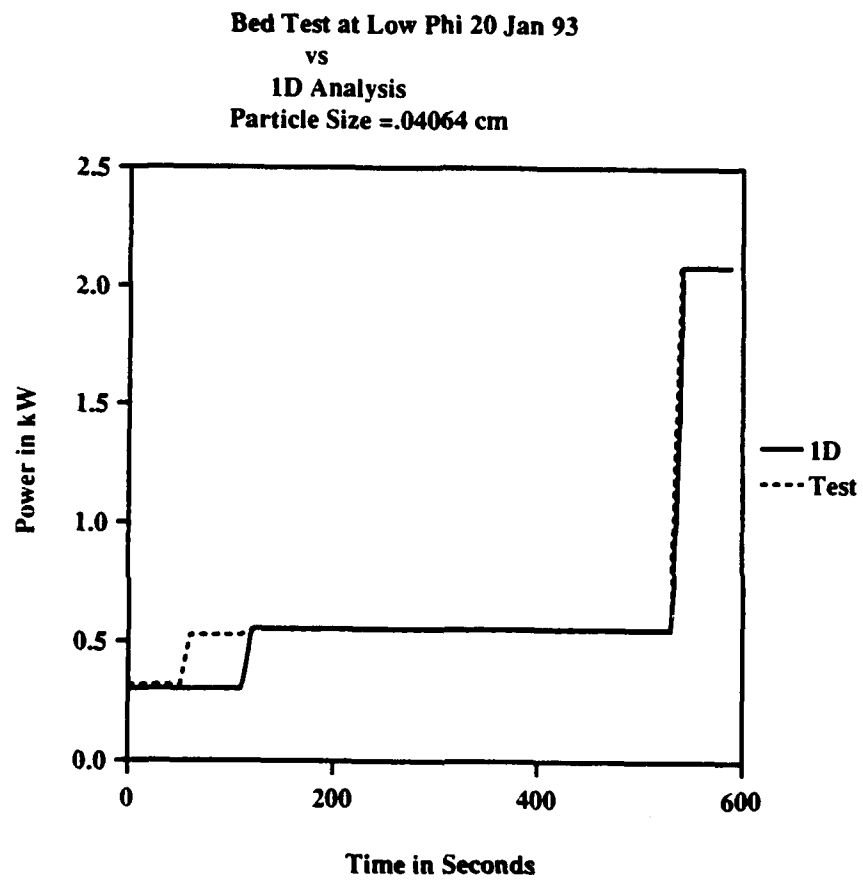


Figure G.3.18 TRITRAN Run Bigger Particle Size(Temperatures)

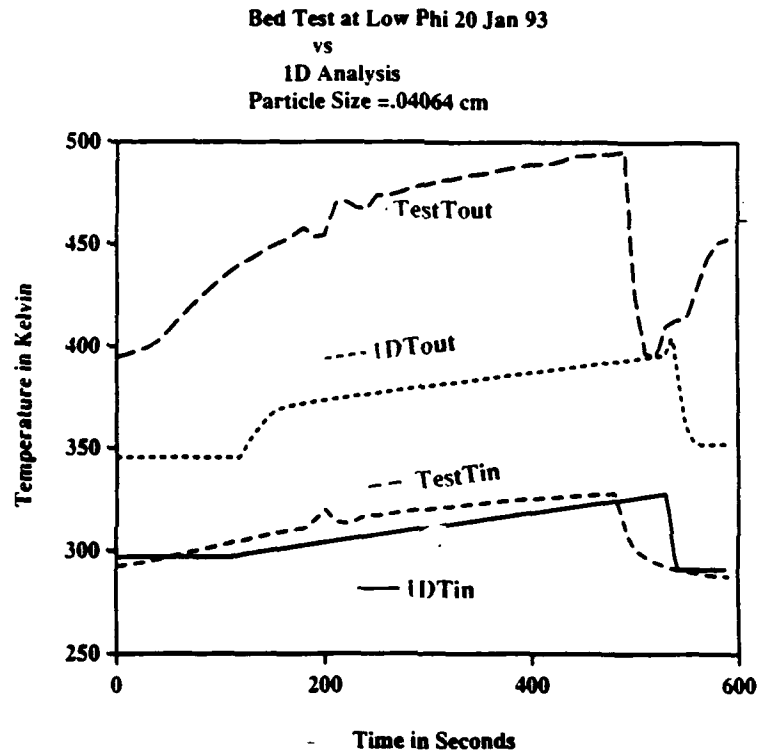


Figure G.3.19 SIMBED Run with One Node In Bed Blocked

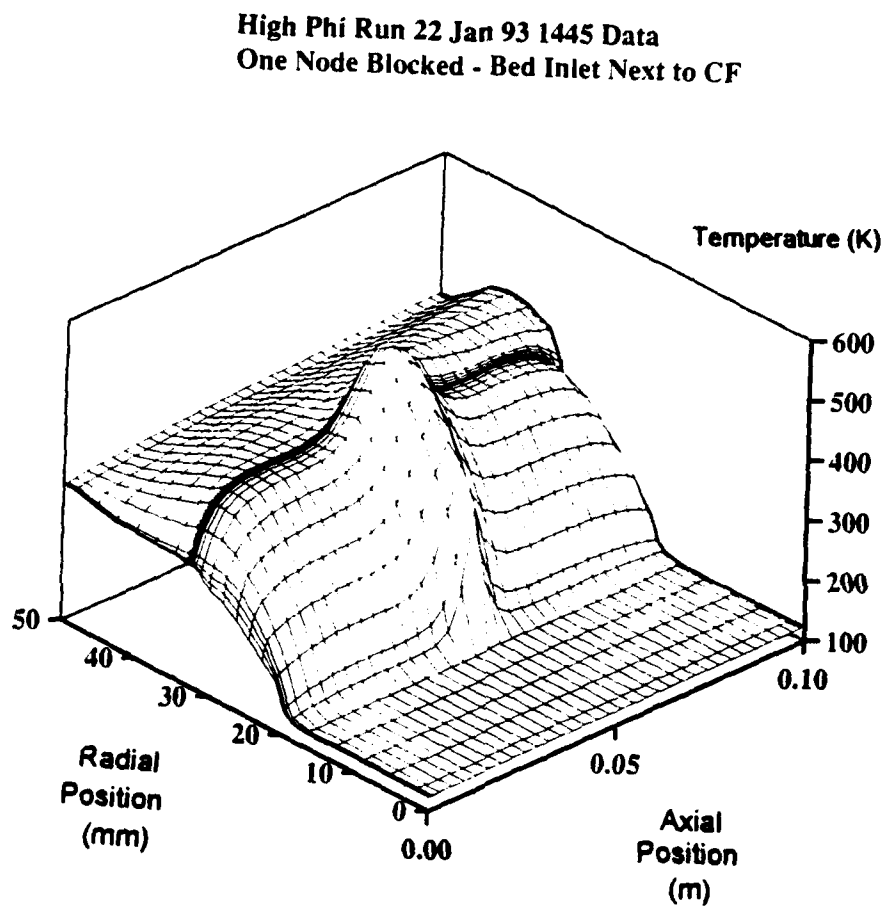


Figure G.3.20 SIMBED Run with One Node In Bed Blocked-More Iterations

**High Phi Run 22 Jan 93 1445
One Node Blocked -Bed Inlet Next to CF
More Iterations - Energy Balance Went Up**

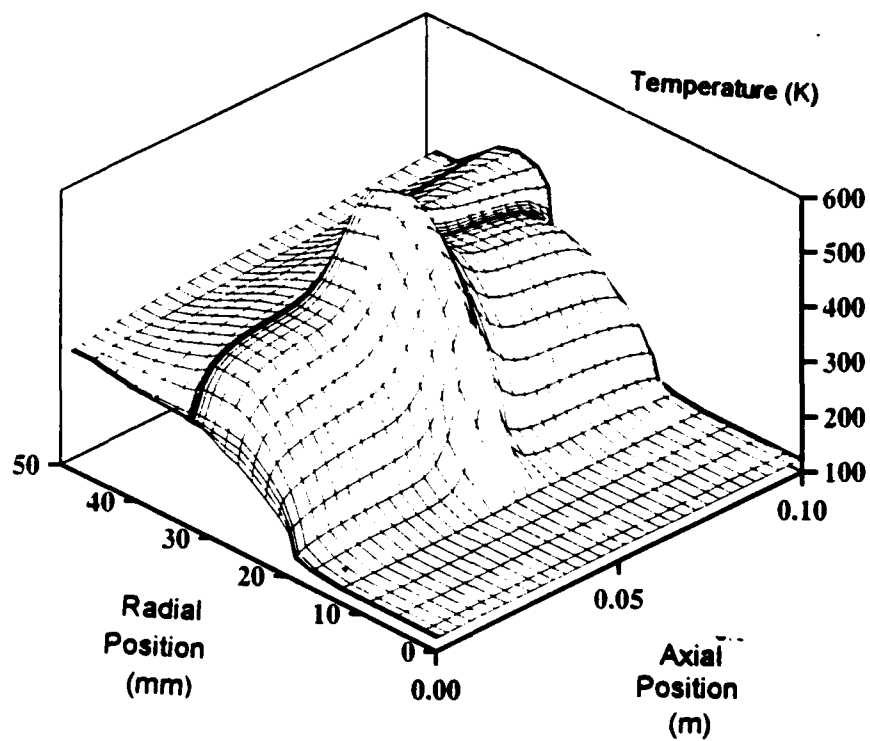


Figure G.3.21 SIMBED Run with Bed Porosity =0.3 (Temperatures)

High Phi Run 22 Jan 93 1445
Temperature Distribution Porosity =0.3

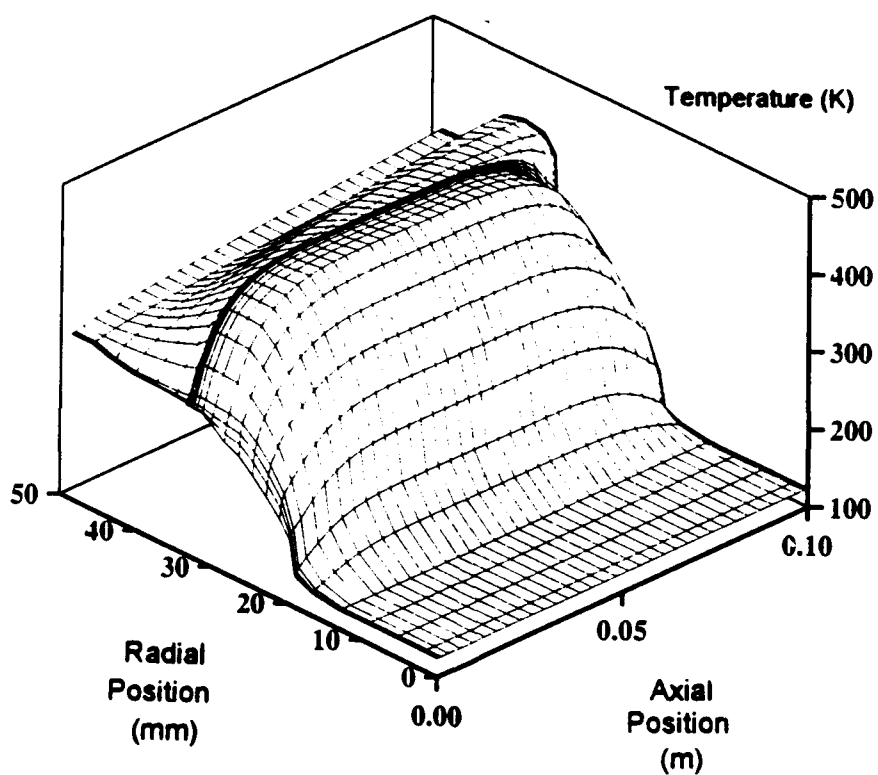


Figure G.3.22 SIMBED Run with Bed Porosity =0.3 (Pressure Drop)

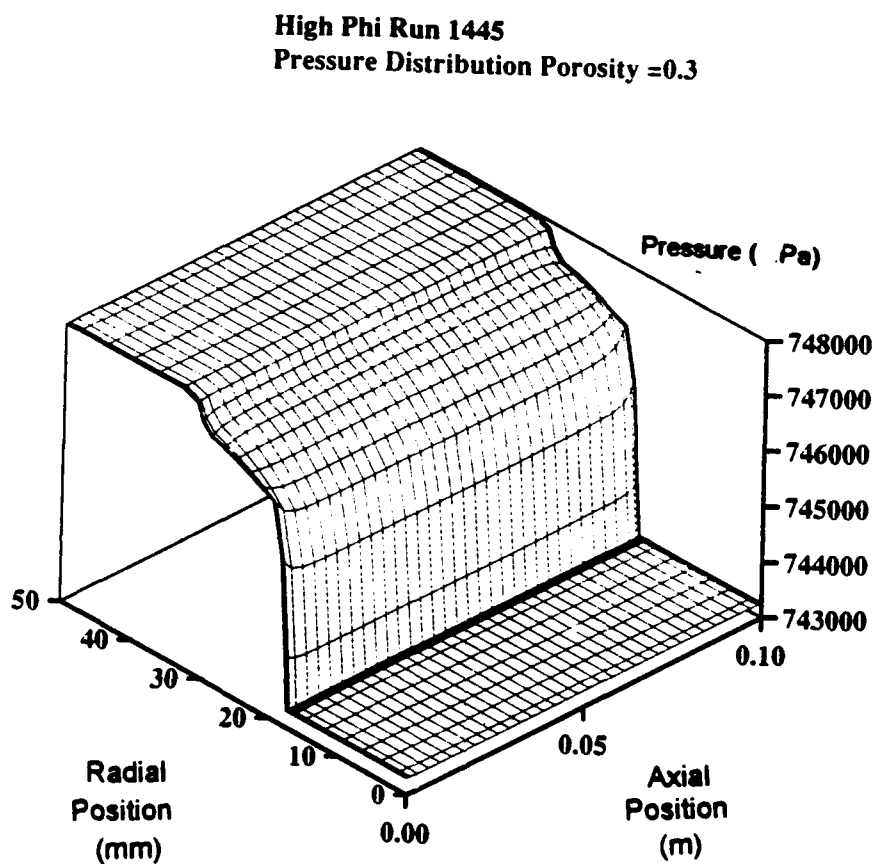


Figure G.3.23 SIMBED Run with Bed Porosity =0.4 (Temperatures)

High Phi Run 22 Jan 93 1445
Temperature Distribution porosity=0.4

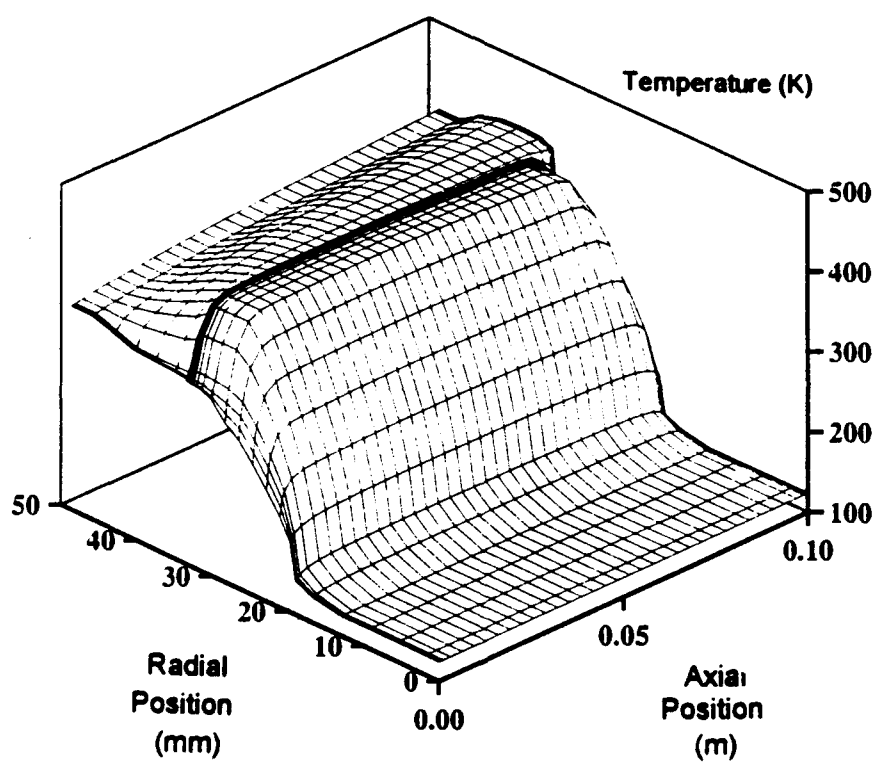


Figure G.3.24 SIMBED Run with Bed Porosity =0.4 (Pressure Drop)

High Phi Run 22 Jan 93 1445
Pressure Distribution porosity =0.4

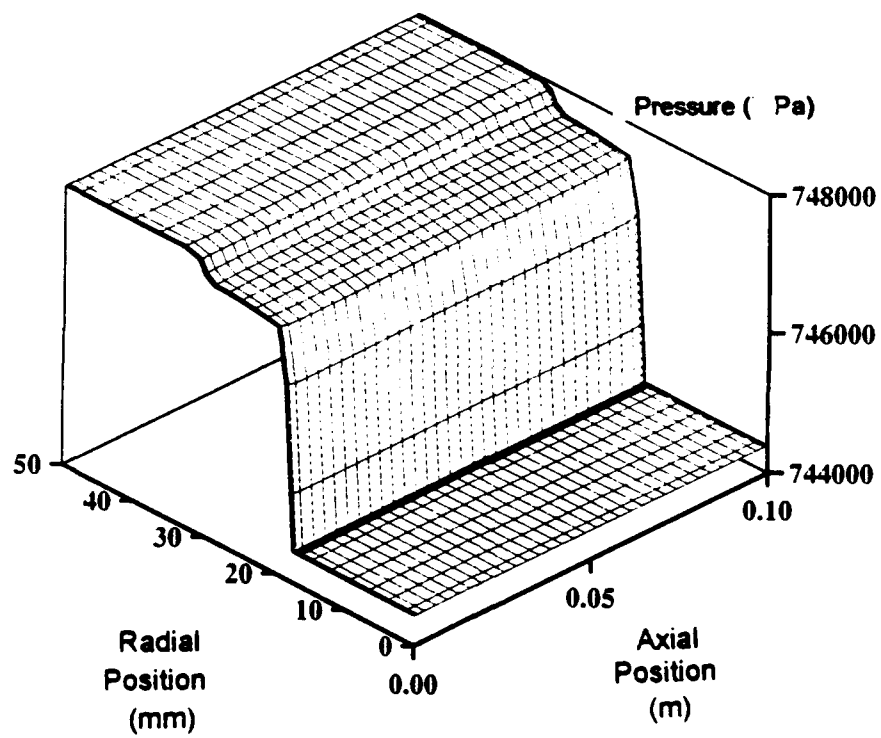


Figure G.3.25 SIMBED Run with Bed Porosity =0.5 (Temperatures)

High Phi Run 22 Jan 93 1445
Temperature Distribution $p=0.50$

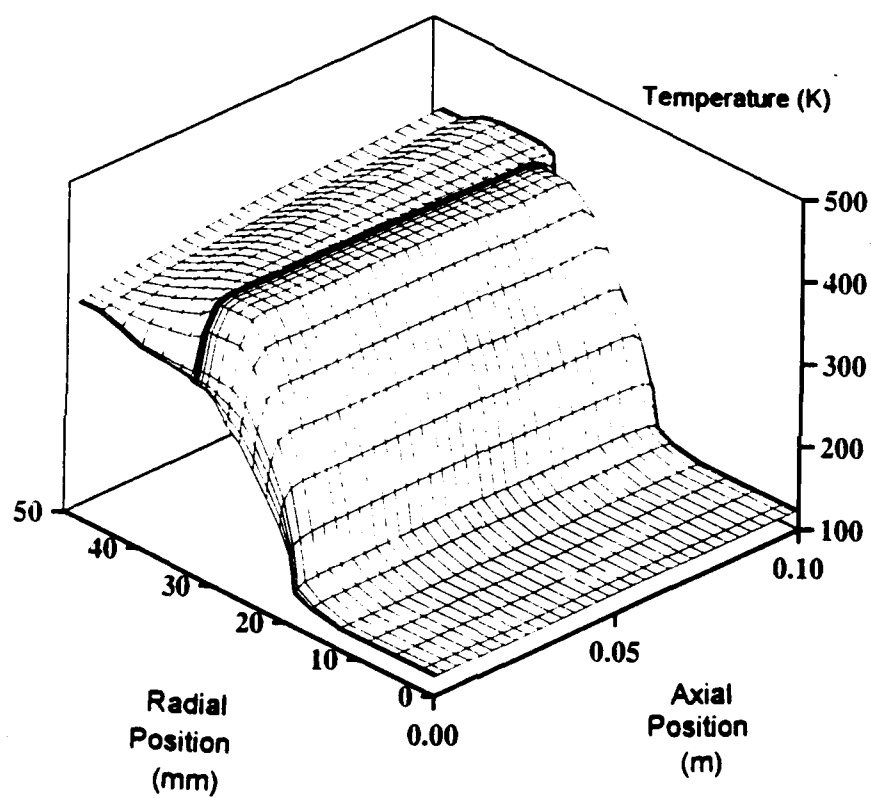


Figure G.3.26 SIMBED Run with Bed Porosity =0.5 (Pressure Drop)

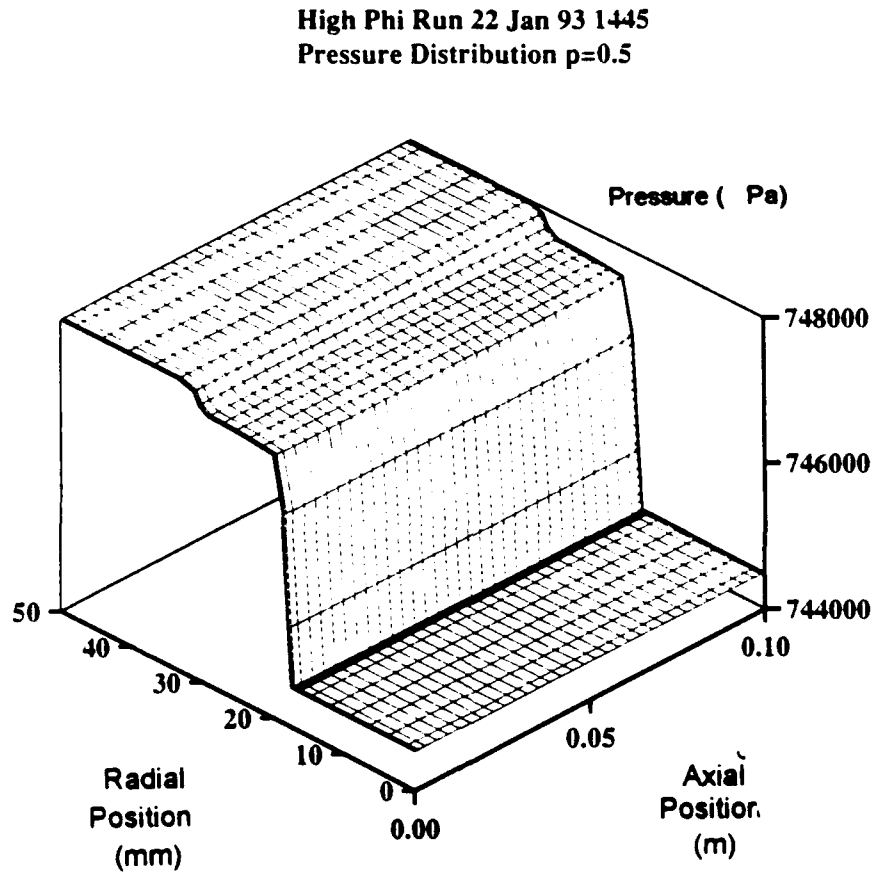


Figure G.3.27 SIMBED Run with Bed Porosity =0.6 (Temperatures)

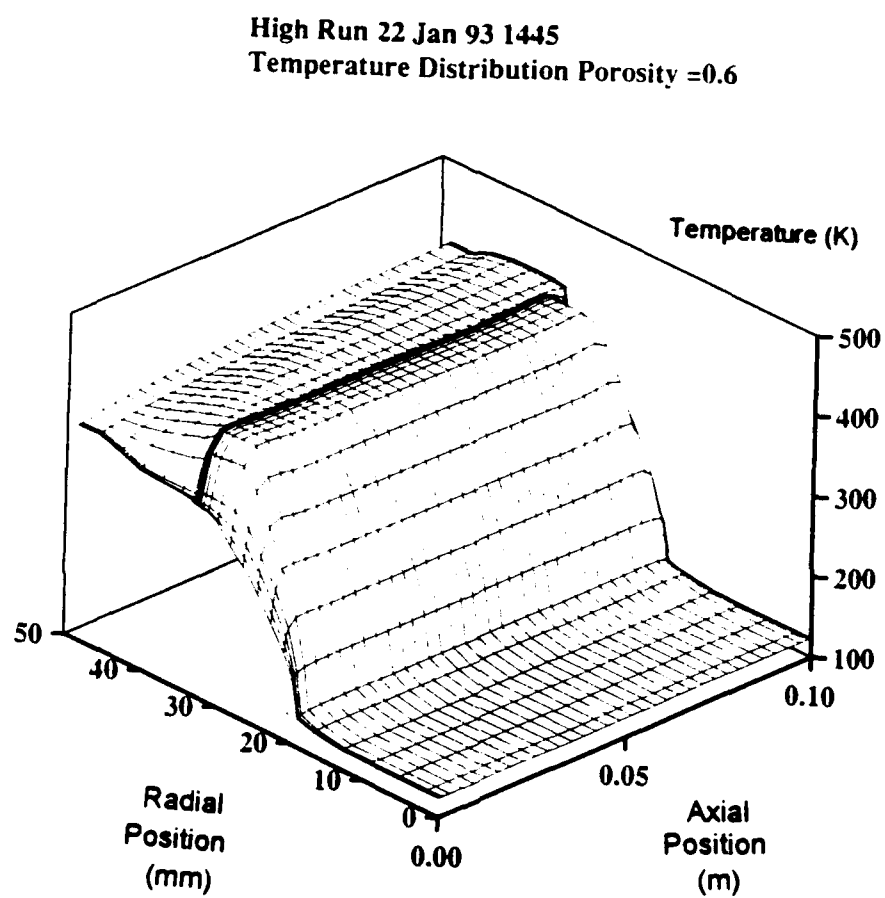


Figure G.3.28 SIMBED Run with Porosity =0.6 (Pressure Drop)

High Phi Run 22 Jan 93 1445
Pressure Distribution Porosity =0.6

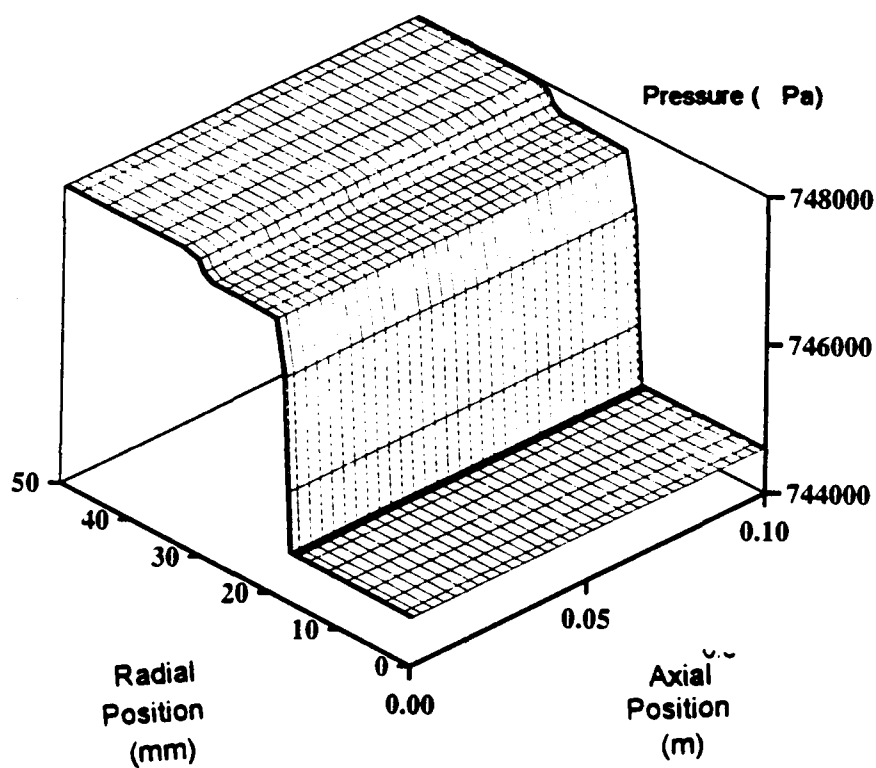


Figure G.3.29 SIMBED Run with 0.0464 cm Particle Diameter (Temperatures)

High Phi Run 22 Jan 93 1445

Temperature Distribution for Particle Diameter = 0.04064

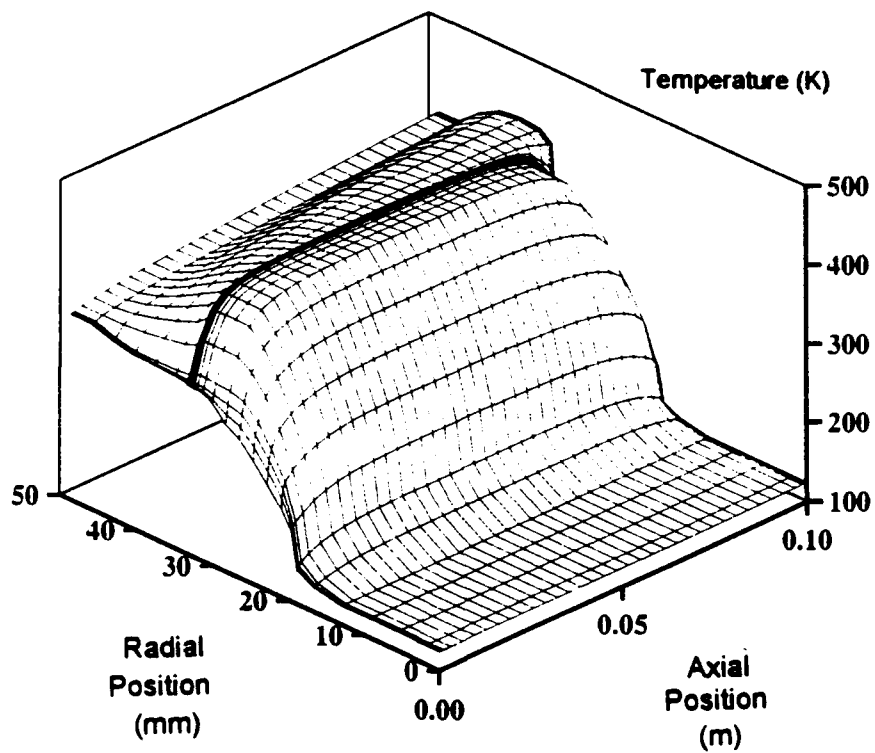


Figure G.3.30 SIMBED Run with 0.0464 cm Particle Diameter (Pressure Drop)

High Phi Run 22 Jan 93 1445

Pressure Distribution for Particle Diameter = 0.04064

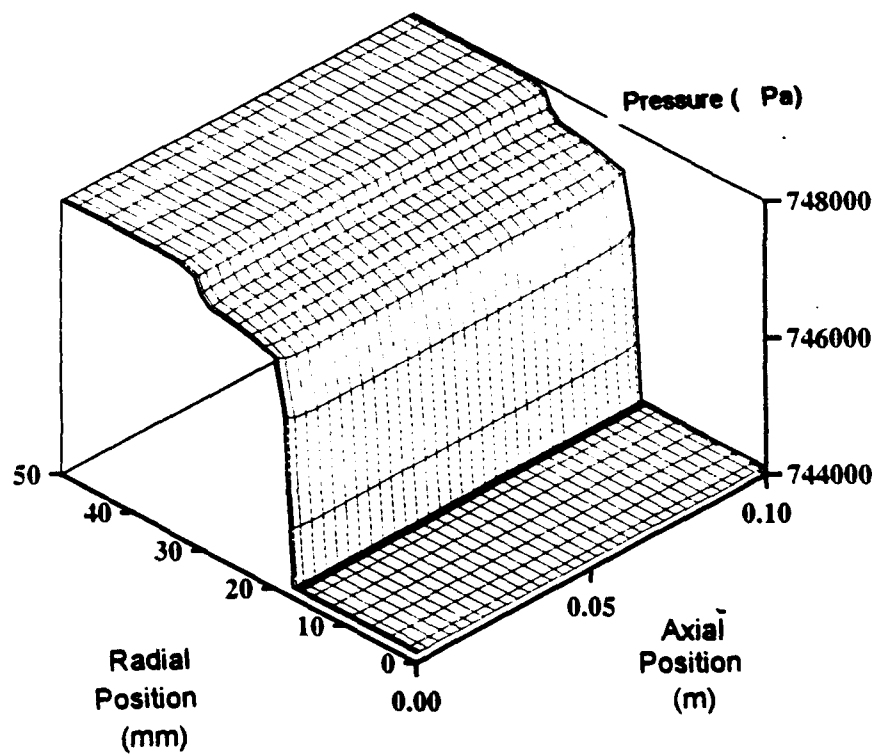


Figure G.3.31 SIMBED Run with 0.04318 cm Particle Diameter (Temperatures)

High Phi Run 22 Jan 93 1445

Temperature Distribution for Particle Diameter ≈ 0.04318 cm

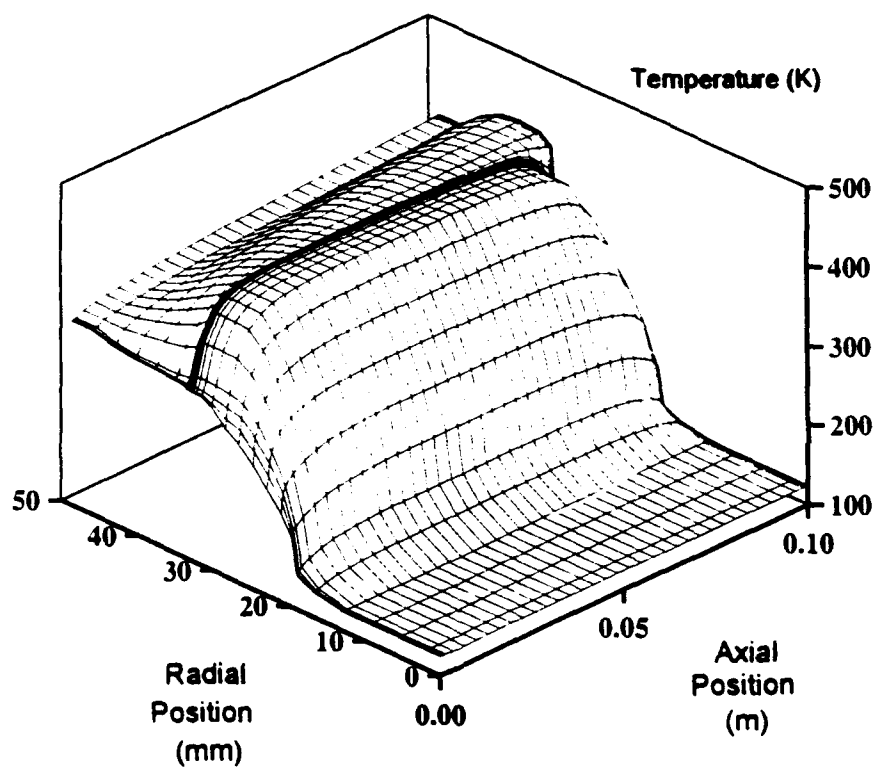
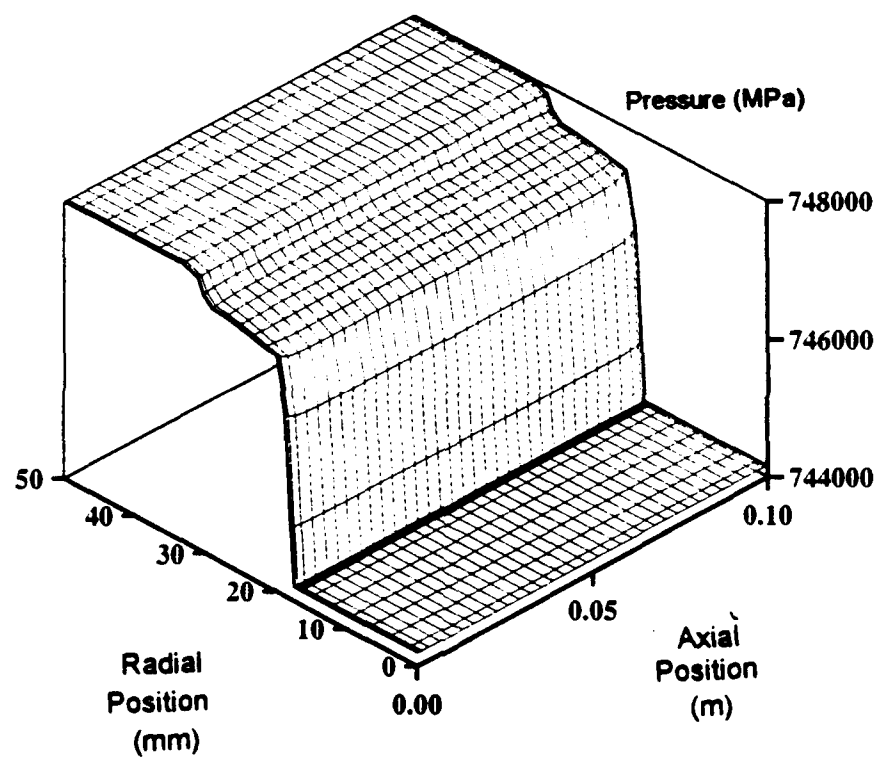


Figure G.3.32 SIMBED Run with 0.04318 cm Particle Diameter (Pressure Drop)

High Phi Run 22 Jan 93 1445

Pressure Distribution for Particle Diameter = 0.04318 cm



APPENDIX H

GLOSSARY

Table H.1 Table of Acronyms

Acronym	Definition
PBR	Particle Bed Reactor
BNL	Brookhaven National Laboratory
ACRR	Annular Core Research Reactor
PIPE	Packed Bed Element Experiments
ICBM'S	Intercontinental Ballistic Missiles
OTV	Orbital Transfer Vehicle
NERVA	Nuclear Engine for Rocket Vehicle Applications
Re	Reynolds Number
RTV	Room Temperature Vulcanizing
s. s.	Stainless Steel
lpm	Liters Per Minute
SUNY	State University of New York
T. C.	Thermocouple
SCFM	Standard Cubic Feet Per Minute
PBRFMP	Particle Bed Reactor Find Mass and Pressure
TRITRAN	Triple Transient
1DSS	One Dimensional Steady State
Prop2Ph2	Subroutine that calls NASA NBS Properties written by J. Walton at NASA Lewis
Spinel	$MgAl_2O_4$
CTE	Coefficient of Thermal Expansion
LN ₂ , LHe, etc.	Liquid Nitrogen, Liquid Helium
LO _x /LH ₂	Liquid Oxygen and Liquid Hydrogen that are used in combustion to propel a rocket
NTO/MMH	Hypergolic Nitrogen Tetroxide and Monomethyl Hydrazine are storable propellants used in combustion to propel a rocket
HePh2	Modification of Prop2ph2 in order to run He properties

Table H.2 Table of Symbols

Symbol	Definition	Units	Location
V, U	Velocities Used in Derivation of Rocket Equation	m/s	2.1.1
M	Mass used in Derivation of Rocket Equation	kg	2.1.1
P _{final} , P _{initial}	Momentum used in derivation of Rocket Equation	kg m/s	2.1.1
g ₀	Units conversion constant used in Rocket Equation Derivation	m/s ²	2.1.1
V _{rel}	V-U = Relative ejection mass velocity used in Rocket Equation Derivation	m/s	2.1.1
F _{rocket}	rocket vehicle thrust	kN	2.1.1
M _{initial}	Initial Rocket Vehicle Mass	kg	2.1.1
M _{final}	Final Rocket Vehicle Mass (Initial Mass - Propellant Burned)	kg	2.1.1
I _{sp}	Specific Impulse	s	2.1.1
T _E	Exit Gas Temperature	K	2.1.1
M _G	Mean Molecular Weight of Exit Gases	kg	2.1.1
q'''	volumetric heat generation rate	W/m ³	2.2.1
D _p	Particle or screen wire diameter	m	2.2.1, 5.3.2
A _s	superficial area	m ²	2.2.1, 5.3.2

\dot{m}	mass flow rate	kg/s	2.2.1 ,2.2.2 ,5.2.1, 5.3.2
dP/dx	Pressure Drop	Pa or kPa	5.2.1
ϕ, ϕ_i	$(T_{final} - T_{inlet})/T_{inlet}$	N / A	Chapters 1 - 6
β	Measure of Flow Regime	N / A	2.2.1
ϵ	Porosity	N / A	2.2.1 2.2.2 Chapter 3-4 Appendix C
U_m	Superficial Velocity	m / s	2.2.1, Appendix C
G	mass flow rate per unit area	kg/sm ²	2.2.1 Appendix C
f_E	friction factor	N / A	2.2.1
ρ	gas density	kg /m ³	2.2.1 5.3.2
w	mass flow rate	kg/s	2.2.2
h	enthalpy	kJ/kg	2.2.2
q	temperature rise	K	2.2.2
b_1, b_2, v	dimensionless quantities based on characteristics of bed and propellant	N / A	2.2.2
x	coordinate perpendicular to plane of bed	m	2.2.2
A, B	viscous and inertial terms for cold frit and hot frit resistances	Pa/kg ² s ²	5.2.2
\dot{m}	mass flow rate	kg/s	Appendix B, G
c_p	specific heat	kJ/kg K	Appendix B Chapter 4 , 5.2.1
L	flow length	m	Appendix C , 2.2.1
ρ_B	measured density	g/cm ³	Appendix C
ρ_G	known density of material	g/cm ³	Appendix C
P	porosity	N / A	Appendix C
u	Superficial velocity	m / s	5.3.2

Q	power	W	5.2.1 Appendix B Chapter 4
t	time	min: s	Chapter 4, 5
R _{TOTAL}	total resistance	Pa/kg ² s ²	5.2.2